Development of masterbatches for poly (ethylene terephthalate) with improved resistance to CO_2 permeation

Steven John Moloney

A thesis submitted in partial fulfilment of the requirements of Nottingham Trent University for the degree of Doctor of Philosophy

August 2008

Copyright statement

Abstract

This research has investigated nanocomposite based masterbatches as routes to improve the CO_2 retention properties of PET bottles. Masterbatches of different types of polyamide/clay, PET/clay, PET/nano-silica flakes and PET/divalent layered metal phosphonates (DLMP) were produced by melt compounding and evaluated.

In the case of polyamide based nanocomposites PA6 was found to produce the best dispersed nanocomposites followed by PA-MXD6, PA-6I/6T and PA-6-3-T. It was concluded from the results that surfactant/polymer compatibility and thermal stability play some role, but the most significant factor in effecting good dispersion was the polarity of the polymer and its ability to directly interact with the clay surface.

The CO_2 retention of PET/PA blends showed MXD6 to offer by far the greatest improvement (100% increase) but the use of PA-MXD6 nanocomposite did not result in further improvement. It was concluded that transfer of exfoliated clay platelets from the PA phase to the PET phase had not occurred. In order to address this issue and disperse the filler effectively through both polymer matrices several novel new processes were developed and the use of a catalyst was investigated. Overall, the novel PET/MXD6/clay blends had reduced CO_2 retention compared to the direct PET/MXD6 blend due to significant degradation of the polymers in the extrusion stage prior to bottle manufacture.

Nanocomposites produced by direct melt mixing of PET and organoclay were always intercalated in nature (with the exception of C30B and hexadecyl pyridinium surfactant where the layered structure collapsed due to degradation of the surfactant). A consistent interlayer spacing of ~3.15-3.25nm was observed for all these materials and it was concluded that a stable PET crystal structure had formed as the distance between layers corresponds to three repeats of the c dimension of the crystal unit cell. It is proposed that the stable equilibrium forms due to insufficient direct interaction between the polymer and the clay surface. Despite relatively poor dispersion modest improvements in CO_2 barrier were achieved (up to 25%).

The use of novel nano-silica flakes resulted in improved CO_2 retention, particularly with the 100nm thickness grade (30% improvement) despite

considerable breakage of the nano-silica flakes during melt compounding. In the case of DLMP the dispersion of the fillers was found to be poor and no improvement in CO_2 barrier was obtained.

It was also observed that all the fillers applied acted as nucleating agents for polymer crystallisation in the polymer systems to which they were applied.

Dedication

This thesis is dedicated to my wife Gaynor and my daughter Jessica who have provided support and inspiration throughout.

Acknowledgements

I would like to express thanks to Dr Fengge Gao my supervisor for his advice and guidance during this research. In addition I would also like to thank him for interesting and thought provoking discussion throughout.

In addition I would like to thank ColorMatrix Group for providing me the opportunity to conduct these studies. In particular I would like to thank my industrial supervisor Dr Adrian Charmichael and also Dr David Kemish, particularly for help in reviewing this thesis.

Finally I would like to thank my wife Gaynor for taking care of me and our beautiful daughter Jessica – I am sure I would never have finished without your support.

List of Abbreviations

PET	Polyethylene terephthalate
PA6	Polyamide 6
MXD6	Metaxylene diamine polyamide
G21	Polyamide 6/terephthalate/isophthalate polyamide
T5000	trimethyl hexamethylene terephthalic acid polyamide
PVP	Polyvinyl pyrolidone
CNa^+	Cloisite Na^+ unmodified clay
C10A	Cloisite 10A organoclay
C15A	Cloisite 15A organoclay
C30B	Cloisite 30B organoclay
C93A	Cloisite 93A organoclay
G105	Nanomer unmodified clay
I28	Nanomer I28 organoclay
BHC	Bentone HC unmodified clay
B2010	Bentone 2010 organoclay
N106	Nanofil 106 unmodified clay
N2	Nanofil 2 organoclay
N3010	Nanofil 3010 organoclay
NaPVP	Polyvinyl pyrolidone modified Cloisite Na^+
CPBr	Cetylpyridinium bromide
CPCl	Cetylpyridinium chloride
C30BE	Epoxy modified Cloisite 30B organoclay
XRD	X-ray diffraction
DSC	Differential scanning calorimetery
TGA	Thermo-gravimetric analysis
POM	Polarised optical microscopy
SEM	Scanning electron microscopy
BIF	Barrier improvement factor

List of Figures

9

13

List of schemes

List of Tables

Table of contents

21

1 Introduction

1.1 *Background of the research*

Poly (ethylene terephthalate) (PET) is a widely used thermoplastic material which finds usage in a variety of applications. Since its discovery by J.R. Whinfield and J.T. Dickson of Calico Printers Association [1] it has become a very important polymer for the production of fibres (Terylene, Dacron) and to a lesser extent films (Melinex, Mylar). Later, with the development of solid state polymerisation processes (SSP) the molecular weight could be elevated to such an extent that the production of injection moulded articles and extruded products became possible. Soon after this development DuPont turned their attention to the development of injection stretch blow moulded (ISBM) containers and were finally able to issue a patent on biaxially stretched PET bottles in 1973 [2]. This new process utilised the basic properties of PET which allowed amorphous preforms to be injection moulded due to the high T_g (80ºC) and slow crystallisation rate. The amorphous preforms can then be heated above T_g (but below T_m, usually at about 100ºC) and blown under high pressure to the desired shape. This development led to the widespread usage of PET as a packaging material for liquids i.e. PET bottles, and in particular carbonated beverages. The usage of PET has increased rapidly over the past decades to the point where 12.5 million tonnes of PET was used in packaging applications in 2006 (bottle and film applications) [3]. Of this 12.5 million tonnes 9.5million tonnes were used in bottles (only 200,000 tonnes was used for beer bottles).

The success of PET as a packaging material for beverages, and in particular carbonated beverages has in large part been due to its inherent properties including good resistance to gas permeation (particularly O_2 and CO_2), slow rate of crystallisation, strength and toughness, transparency and its ability to be readily formed into complex shapes at temperatures above T_g but below T_m.

Despite the success of PET as a packaging material for beverages its gas barrier properties do limit its usage for the most sensitive applications such as beer, wines, teas and some juices. These beverages are generally those which have a particular sensitivity to oxidation or CO_2 loss which results in an impairment of the taste. One of the most obvious solutions to this problem is to increase the

wall thickness but this is un-economic and wasteful from an environmental view point.

To address these problems many techniques have been devised with varying levels of success. For example the use of oxygen scavengers has become widespread in some oxygen sensitive beverage applications, and they have proved particularly effective despite their propensity for reduced clarity and usually a degree of yellowing over time as the scavenging component oxidises. Several companies currently have patented oxygen scavenging technologies such as Oxbar^{TM} and Amosorb^{TM}.

Alternatively some companies such as Sidel, PPG and Dupont have developed bottle coating systems for the reduction of both O_2 and CO_2 permeation. These systems can be applied externally or internally and give un-paralleled reduction in the gas permeability of PET. Despite this their usage remains relatively low due to the added level of processing complexity involved and the danger of the coating cracking under impact resulting in catastrophic failure of the gas barrier properties and contamination of the beverage in the case of internal coatings.

A further method devised to address this problem is the use of multi-layer structures whereby a thin layer of a higher barrier polymer, such as Poly (ethylene naphthalate) (PEN), poly (vinyl alcohol) (EVOH) or metaxylene diamine PA (MXD6) is inserted between an inner and outer layer of PET. This is accomplished either by co-extrusion, co-injection or over-moulding. This method is effective for the control of both O_2 and CO_2 permeation but similarly to coating technologies suffers from the addition of an added degree of processing complexity. In addition delamination of the barrier layer is known to be a problem with multi-layer systems. It is also known for these so called barrier resins to be used in blends with PET to improve the barrier properties. While improvements can be achieved they are generally lower than multi-layer structures and the impact on transparency and colour is greater. In addition to the individual problems outlined all these solutions tend to impact negatively on the recycling of PET. Mitsubishi, EMS grivory and Nanocor are among the companies developing such technologies.

Thus despite all the progress made so far in the control of gas permeation in PET a simple cost effective solution which has minimal impact on the optical properties of the PET, causes minimum changes in PET properties, is readily

24

compatible with conventional processing equipment and has a minimal impact on the recycle stream still proves elusive. If such a solution can be developed there are considerable benefits to be reaped by the beverage and packaging industry. For instance a simple mono-layer solution meeting the criteria described above would pave the way for widespread use of PET as a packaging material for beers. This alone offers many potential benefits such as improved safety (less breakage), increased consumer choice (wider range of pack sizes), reduced transport costs through reduced weight per unit. In addition, beverages such as carbonated soft drinks (CSD) could be packaged in lower weight packs with equivalent shelf life resulting in reduced polymer usage and hence environmental benefits. Overall there is a considerable need for PET with improved gas barrier properties.

1.2 Aims and objectives

The overall aim of this project is to develop novel technologies which will allow the development of monolayer packages using masterbatch nanotechnology. These new masterbatches will enable increased utilisation of PET for the most sensitive beverages by providing a two-fold improvement in CO_2 barrier.

In order to achieve this aim several objectives were addressed. The first objective was to fully understand the current difficulties in PET/clay nanotechnology. In short we investigated the role of surfactant compatibility and thermal stability on the dispersion of clays in PET and attempted to develop strategies to overcome these issues. If these problems could be overcome and exfoliated PET nanocomposites could be produced the aim of this project would be tantalisingly close to realisation.

A second objective of the project was to use the comparatively well understood technology of polyamide nanocomposites where exfoliation had been achieved previously and to use these materials as a masterbatch for the delivery of exfoliated clay platelets into PET. This would require the screening of a variety of polyamide polymers in order to find the best compatibility with PET and the development of new processing techniques to allow the transfer of exfoliation from the polyamide into the PET matrix.

The final objective was to develop processes for the utilisation of new novel nano-fillers for application in PET.

1.3 Scope of the work

In order to achieve the aims and objectives of this project several distinct phases of work were required. Firstly various polyamide/clay nanocomposite systems were investigated as possible exfoliants for clay in PET applications. This allowed familiarisation with the techniques and processes required for clay/polymer nanocomposite research. Following this initial stage a detailed investigation of direct intercalation of PET with commercially available organoclays was undertaken to understand the effects of different surfactants, how dispersion is effected and the resultant barrier and crystallisation properties. New clay modifications were also investigated in order to improve the current situation in clay polymer nanocomposites. The next major phase of work involved the analysis of nylon assisted exfoliation. Consequently novel new processes for processing hybrid materials were explored. The final phase of work was to gain an understanding of the effectiveness and prospect of new novel nanofillers as barrier materials in PET.

The properties and behaviour of different organoclays from both commercial sources and those produced in our own laboratory are discussed in relation to their thermal stabilities and potential compatibilities with the polymers used in these studies. Following the analysis of the clay materials an investigation of polyamide based clay/polymer nanocomposites was undertaken. Aspects of clay dispersion were investigated with particular attention to the effect of clay/polymer compatibility and thermal stability of the organoclays. The potential for the polyamides studied to act as carriers for exfoliated clay in PET was studied and the best materials for this approach and novel processing techniques were developed. In addition to the study of polyamide/clay nanocomposites as masterbatches for PET the direct intercalation of PET into organoclay was also investigated using both commercial organoclays and those developed in our laboratory. Finally the properties of novel fillers and PET nanocomposites produced from these fillers were investigated.

1.4 Literature Review

The literature review for this study initially covers pertinent background information on the materials studied. Attention is paid to the polymers including a brief history of their synthesis, properties and uses. A similar approach is taken to the fillers investigated whereby a history of the usage of the filler and its properties are discussed. The third portion of the literature review concentrates on clay/polymer nanocomposites. A review of the methods used for the synthesis of clay/polymer nanocomposites with reference to the advantages and disadvantages of each technique is discussed. Following discussion of the different synthesis techniques some examples of commercial clay/polymer nanocomposites are discussed with particular reference to polyamides and polyolefins where commercialisation has proved most successful. Particular attention is paid to the properties of these materials and how they have solved problems due to their enhanced properties. Clay/polymer nanocomposites produced from PET are discussed next according to their synthesis methods. The extent of clay dispersion of these materials is discussed in detail along with gas permeation properties where presented. The effects on other properties are noted and discussed where relevant. The blending of polymers is discussed with particular reference to polyester/polyamide systems and the resultant properties of such blends. The final portion of the literature review looks at some models that describe the permeation of gasses in filled polymers.

1.5 Fundamental knowledge on the polymers studied

Polymers can be broadly defined as large macromolecules formed from a repeating smaller unit. Polymer materials can be both naturally occurring (such as some proteins), or synthetic (such as polyethylene). For the purposes of these studies and for use as packaging materials for beverages thermoplastic polymers (polymers that can be heated to form a liquid or melt and then cooled to a solid state) are generally used. The two main types of thermoplastic are glassy amorphous materials (typified by polystyrene) and semi crystalline materials (e.g.

high density polyethylene). In general the amorphous glassy materials tend to have a less regular structure (due to features such as branching or pendant groups) and also exhibit less intramolecular attractions than semi-crystalline polymers.

1.5.1 Polyamides

The early development of polyamide materials was predominantly due to the seminal work of W.H.Carothers and his colleagues into the condensation polymerisation of polymers [4-5]. This initial work first centred on aliphatic polyesters but due to a lack of commercial success Carothers soon turned his attention to polyamides. Their extensive studies led to the synthesis of nylon 6,6 and the issue of the first patents in 1938[6]. In general the aliphatic polyamines are produced via the condensation of a diol and diamine. The choice of starting materials is consequently very large and a wide range of polyamides are commercially important including PA11 (from the polycondensation of aminoundecanoic acid); PA12 (via hydrolytic ring opening of laurolactam); PA4,6 (from polycondensation of butane diamine and adipic acid); PA6,9 (from polycondensation of hexamethylene diamine and azelaic acid); PA6,12 (from the polycondensation of hexamethylene diamine and dodecanoic acid); and also blends containing PA6,6/6,10 and PA6,6/6,10/6. These materials are termed aliphatic polyamides and are characterised by their high level of intermolecular attraction. This results in semi-crystalline polymers with high T_m (usually about Tg $^+200$ºC). The polyamides are tough, resistant to solvent and also known to be prone to adsorption of high levels of water (up to 10% for PA-6). These aliphatic polyamides find extensive usage in fibre forming, moulded articles, films and extruded profiles.

A second class of polyamides are those based on non-aliphatic monomers (i.e. aromatic or cycloaliphatic) and those produced with combinations of monomers (copolymers). Overall these materials can be classified into 3 groups.

- Copolymers with high Tg which are amorphous and glassy
- Crystalline polymers used as plastics
- Crystalline polymers for fibres, including some liquid crystal polymers.

These materials generally exhibit some superior property to those seen for aliphatic polyamides and hence find niche application fields where aliphatic polyamides have insufficient properties. Overall the polyamide family exhibit a combination of different properties that make them suitable for a wide range of applications. Such properties include good abrasion behaviour, high heat deflection temperature (particularly filled grades), high tensile strength, good insulation, excellent toughness and good chemical resistance. In the subsequent sections, some commercial materials relevant to this particular project will be discussed.

1.5.1.1 Polyamide-6

Polyamide-6 (PA6) is the exception to the general rule of polyamides being formed from the condensation reaction of a diol and a diamine. It is manufactured from the ring opening polymerisation of caprolactam and was developed as a direct competitor for polyamide 66 by Paul Schlack and co-workers at IG Farben in order to circumvent the patent on that material [7].

Commercial production methods may vary slightly but in general pure caprolactam is heated to around 260ºC under nitrogen in the presence of sodium hydride initiator for around 4-5hrs. This causes breakage of the ring structure at the peptide bond with the two active groups created forming new bonds as they become part of the backbone chain of the polymer (illustrated in Scheme 1.5.1.1-1).
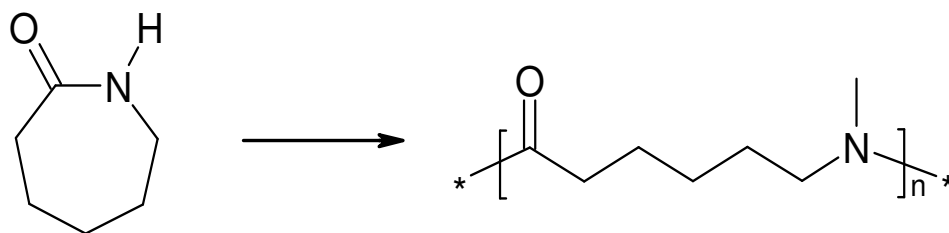
Scheme 1.5.1.1–1 Ring opening of caprolactam to form PA6

In general PA6 is considered as a tough semi crystalline polymer capable of considerable moisture uptake. The earliest uses were as a fibre forming material

but the use of solid state polymerisation (SSP) (as detailed in 2.1.2) has enabled PA6 to be produced in a wide range of relative molecular mass (RMM) grades with differing properties suitable for different applications. Today PA6 is still an important polymer for fibre production but is now commonly used to produce extruded articles (such as pipe and other profiles), packaging films, extrusion blow moulded articles (such as fuel tanks) and a wide range of moulded articles, particularly when filled with glass fibre (producing polymer with increased stiffness and reduced softening point – i.e. heat distortion temperature (HDT)). In general the higher the molecular weight of the PA6 the more likely it is to be used for extruded products while lower molecular weight grades are predominantly used for injection mouldings and fibre production.

1.5.1.2 Mitsubishi MXD6

In this project, this material enabled the effect of aromaticity on the nanocomposites formation to be studied and compared to aliphatic PA-6.

Poly-m-xylene adipamide (MXD6), is a semi-crystalline aromatic polyamide used as a plastics material and was first disclosed by Lum et al in 1956 [8, 9]. Despite the development of laboratory samples, commercialisation did not occur until the early 1970's when Mitsubishi Gas Chemical Company began production of para-xylene diamine free meta-xylene diamine. It is formed by the condensation of m-xylene diamine with adipic acid as outlined in Scheme 1.5.1.2-1. A generalised synthesis would involve low steam pressure (~400 – 700 kPa) addition of meta-xylene diamine to molten adipic acid (mp 153ºC) until the ratio of functional groups approaches one. This simple procedure is enough to produce resins of a reasonable molecular weight although higher molecular weight materials can be produced through post polycondensation SSP.

Initially these materials were emphasised as replacements for aliphatic polyamides where increased rigidity and good surface finish are desirable properties in injection moulded articles. Other applications involve the use of fillers (typically glass fibre at up to 50wt %) which allows the substitution of metals due to the high mechanical strength, modulus and heat resistance [10]. In more recent times greater attention has been paid to the gas barrier properties of MXD6. In 1974 Mantsunami et al produced the first patent on high gas barrier

flexible MXD6 films [11], followed by Okudaira et al [12] who were able to issue a patent on multi-layer, stretch blow moulded bottles in 1983. Further work on MXD6 has shown that in the presence of small quantities of cobalt compounds MXD6 acts as an oxygen-scavenging compound [13] and that blending of polyamides with PET can also produce packaging materials with improved gas barrier properties [14].

MXDA

Adipic acid

Nylon MXD6
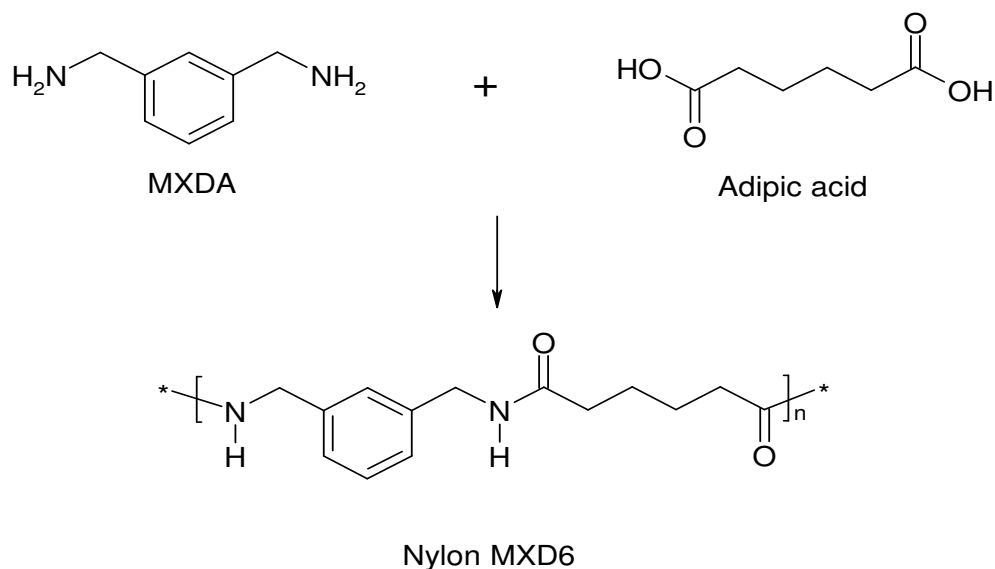
Scheme 1.5.1.2-1 Reaction of meta-xylene diamine and adipic acid to form MXD6 polyamide

Due to the wide processing window for MXD6, manufacture of such multi-layer and blend materials is relatively simple and results in doubled shelf life with a 5wt% barrier layer. In addition to simple MXD6 multi-layered structures Mitsubishi have collaborated with Nanocor on the development of a nanocomposite grade of MXD6 called Imperm. This material offers an additional one hundred percent increase in the gas barrier properties of multilayer bottles compared to standard PET [15]. Blending of MXD6 with PET has also achieved some commercial success in improving the barrier properties but the results are much more modest. Polyshield™ produced by Invista offers CO_2 permeation reduction of 15% in conjunction with oxygen ingress of less than 1ppm per year due to combined passive barrier and scavenging [16].

Overall the use of MXD6 as a barrier material for PET packaging offers many possibilities but so far some limitations have prevented its widespread usage. These limitations include difficulty in recycling, reduced transparency and yellowing. For multilayer packages in particular there is the added issues surrounding increased manufacturing complexity and possible delamination of the layers.

1.5.1.3 EMS Grivory G21

EMS Grivory G21 is an amorphous polyamide based on hexamethylene diamine/isophthalic acid (PA6I) and hexamethylene diamine/terephthalic acid (PA6T) in a 70/30 ratio [17]. The structure of Grivory G21 is shown in Figure 1.5.1.3–1.
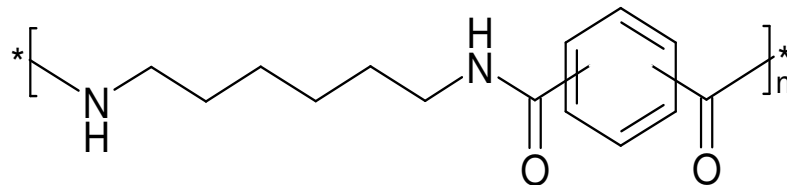
Figure 1.5.1.3-1 Chemical structure of PA6I/T

From the available data it appears that polymer is produced from simultaneous polymerisation of all three monomers. The amorphous nature of the polymer is due to the incorporation of the second aromatic monomer as both PA6I and PA6T would be expected to crystallise. Regardless of the exact processing and composition it is evident that the Grivory G21 polymer exhibits structural similarities to both PET and MXD6 and hence it is hoped that it will show good compatibility with PET.

Grivory G21 finds greatest usage in film applications where extremely high gloss and transparency are required. It is also known for the material to be used in multi-layer film and bottle applications as a barrier layer where its improved gas barrier properties compared to aliphatic polyamides result in improved gas barrier properties [18].

No reports were found in the open literature concerning the formation and properties of clay/polymer nanocomposites produced from Grivory G21 polymer hence it will provide valuable information on how slight structural variations and amorphous nature compared to crystalline materials behave in nanocomposites formation and gas barrier applications.

1.5.1.4 Degussa Trogamid T5000

Trogamid T5000 from Degussa is a high temperature engineering PA formed from the monomers trimethyl hexamethylene diamine and terephthalic acid and is described by the acronym PA6-3-T. The synthesis is shown in Scheme 1.5.1.4-1
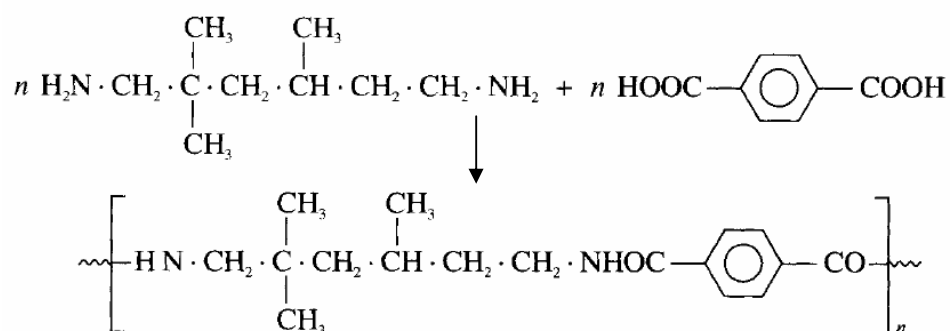
Scheme 1.5.1.4-1 Reaction of trimethyl hexamethylene diamine and terephthalic acid to form PA6-3-T

In practice a 1:1 ratio of 2, 2, 4 - /2, 4, 4 - trimethyl hexamethylene diamine is used to ensure an amorphous polymer. It is described as having excellent gloss and transparency and is deemed suitable for a wide range of injection moulding, extrusion and blow moulding applications such as battery seals, gear wheels and racks, pump cases, inspection glasses and guide rails. The general properties can be summarised as crystal clear optical transparency, high mechanical stability, high thermal stability, good chemical resistance, good electrical properties and low shrinkage [19].

So far there are few reports on its use in nanocomposites formation, nor with regard to its gas barrier properties. In this project, this material allows the study of an amorphous polyamide with greater thermal stability than the Grivory G21 that exhibits some structural similarities with PET and hence potentially some compatibility.

1.5.2 Poly (ethylene terephthalate)

The initial development of PET by Whinfield and Dickson centred on the simple condensation reaction of monoethylene glycol and terephthalic acid (Scheme 1.5.2-1). The material produced in the early days of PET was used specifically for the production of synthetic fibres, and still is to this day [20]. Further developments continued in the 1950's with the development of highly sophisticated drawing and heat setting processes to allow biaxial orientation of amorphous sheet to produce films for such items as audiotapes and food-packaging films. More recently in the 1970'the work of Wyeth at Dupont resulted in the development of three-dimensional hollow bodies with orientated structure. The bottles produced by this fledgling injection stretch blow-moulding (ISBM) process exhibited exceptional strength and excellent gas barrier properties and revolutionised the polyester and packaging industries.
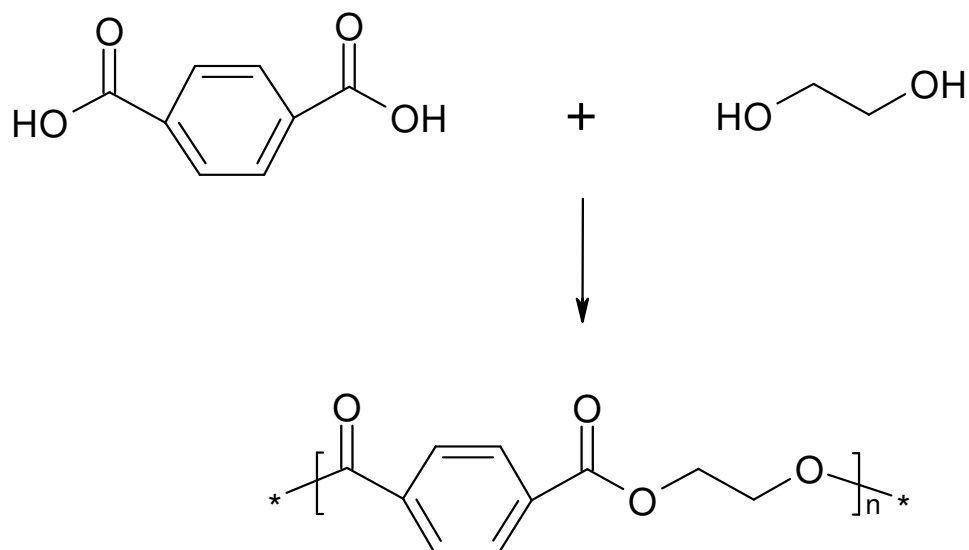
Scheme 1.5.2-1 Condensation of terephthalic acid and ethylene glycol to form PET

For large scale commercial synthesis of PET the initial starting materials and route can vary. One such route is the ester interchange reaction of dimethyl terephthalate with monoethylene glycol; a second route would be the direct esterification of terephthalic acid with monoethylene glycol and a third route would involve the reaction of ethylene oxide with terephthalic acid to form bis hydroxyethyl terephthalate (BHET) monomer. In the final method BHET requires extraction and purification prior to polycondensation and is therefore very rarely used in practice. The first two routes described may undergo polycondensation without further purification and are hence much more common commercial routes to PET. The polycondensation reaction requires high temperatures (250ºC – 290ºC), and most often is undertaken under vacuum to ensure efficient removal of water and free ethylene glycol in order to push the reaction to the product side of equilibrium. Polymerisation catalysts are used in order to ensure product of useful molecular weight is produced and are often antimony, germanium or titanium compounds. The PET in the melt phase is prone to degradation reactions (such as the generation of acetaldehyde [21,22]) and discolouration and hence small quantities of melt stabilisers such as phosphoric acid are often added.

The final molecular weight of the PET is generally found to be in the region of 15000 – 25000 (Mn) and would generally be deemed suitable for the production of staple fibre. The materials used today for packaging applications (i.e. sheet extrusion and ISBM) tend to have higher molecular weight, usually in the region 25000–33000 (Mn). This requirement has led to the development of solid state polymerisation (SSP) processes.

In the SSP process the pelletised polycondensation product of relatively low RMM is heated with agitation to a temperature of around 160ºC under dry nitrogen gas thus effecting primary crystallisation. In the next stage the pellets temperature is raised to about 210ºC, still under agitation and nitrogen gas flow enabling further crystallisation to occur (up to around 48%). These conditions are then maintained (or slightly higher temperature applied) for a sufficient period for the transesterification/ polycondensation and esterification [23-27] reactions to occur (as shown in Scheme 1.5.2-2 and 1.5.2-3). After the required reaction time polymer of different RMM can be recovered e.g. 300000 for ISMB or 35000 for extrusion blow moulding (EBM).

One of the major developments in PET chemistry was the introduction of copolymer materials to suit specific purposes. Although SSP allowed the RMM of PET to be increased sufficiently for bottles to be produced the increasingly demanding processing conditions and end user requirements stimulated significant effort into improving the polymer processing and properties. The most common copolymers are produced using the co-monomers cyclohexane dimethanol (CHDM), isophthalic acid (IPA) and naphthalene 2,6 dicarboxylic acid (NDCA) (Figure 1.5.2-4). Various loadings of co-monomer are used depending on the desired properties e.g. for processing in unfavourable environments (high humidity) around 1-2% wt/wt would be used while 3% wt/wt co-monomer would typically be used in re-fillable bottles with thick walls where the second monomer reduces the rate of crystallisation allowing amorphous preforms to be manufactured. There are some speciality copolymers available with even higher co-monomer levels, in the range of 3-15% wt/wt. These materials often have naphthalene 2,6 dicarboxylic acid as the co-monomer and have been shown to give improved gas barrier but are more expensive and difficult to dry and process. The final class of copolymers have very high co-monomer levels (about 35%) and are amorphous materials called PETG. They exhibit excellent clarity and are used in injection moulding and extrusion applications and are known to be difficult to dry.
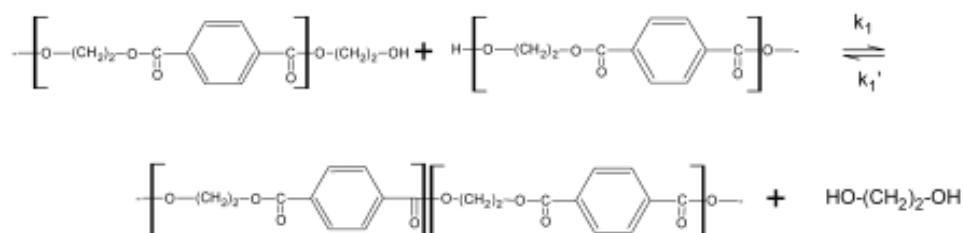
Scheme 1.5.2-2 Transesterification/polycondensation during SSP
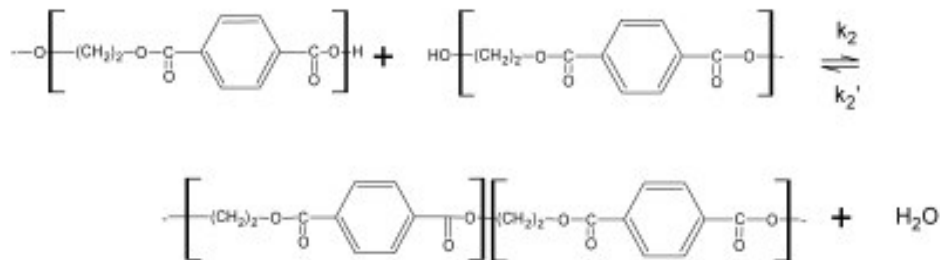
Scheme 1.5.2-3 Esterification reaction during SSP

The structure of PET due to its repeat unit governs the subsequent properties of this unique material. PET can exist in both amorphous and semi crystalline forms and its morphology has been well described by the chain folded model (Figure 1.5.2-5). Due to its high T_m (~250°C) and relatively low T_g (~60°C) PET can be readily quenched from the melt to produce amorphous articles.

Cyclohexane dimethanol
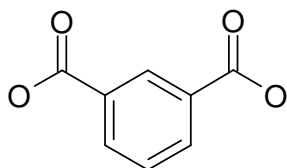
Isophthalic acid
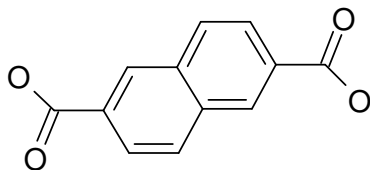
Naphthalene 2,6 dicarboxylic acid

Figure 1.5.2-4 Examples of co-monomers typically used in PET copolymer synthesis

One of the main properties of PET is its ability to be readily orientated. The performance on stretching is related to factors such as temperature, molecular weight, strain rate, crystallisation, moisture, and copolymer type and composition [28-36]. The best stretching behaviour for the formation of bottles is obtained at

T_g plus about 20ºC (i.e. about 100ºC) with polymer RMM of approximately 25000 – 33000. The presence of crystallinity can hinder orientation and stretching due to embrittlement and excessive modulus and often manifests as delamination. Moisture generally behaves as a plasticizer making the polymer more ductile and easier to orientate but may also cause hydrolytic degradation. Copolymers can also influence the stretching behaviour of PET, changes being dependant on the type of additive and the quantity added. Co-monomers such as long chain glycols and aliphatic diacids tend to reduce T_g of the polymer and hence improve flow whereas co-monomers such as NDCA tend to increase the stiffness of the polymer and thus inhibit stretching.

Figure 1.5.2-5 Chain folded model of crystallisation of polymer chains

PET bottles containing carbonated beverages are stored under continuous stress/strain for extended time periods and hence the creep properties of PET are important. Studies by Bonnebat et al [33] have shown that PET is quite resistant to creep at low temperatures but, as temperature approaches T_g the level of creep increases significantly as modulus falls. Increased creep can negatively impact barrier properties and is often tackled by increasing the crystalline content of the material or increasing the orientation.

For classification purposes PET is generally referred to by its intrinsic viscosity (IV) which is related to the molecular weight of the material by the Mark-Houwink equation (Equation 1.5.2-1) where ή is the IV, M is the molecular

weight and k and a are constants. IV is measured by dissolving the polymer in solvent and measuring flow time at different concentrations. Many solvents have been used but the most commonly accepted solvent system is a 60:40 phenol and tetrachloroethane mixture, and is the industry standard.

$$[\,\acute{\eta}\,] = k * M^{\alpha}$$

Equation 1.5.2-1 Mark-Houwink equation relating solution IV and molecular weight

The crystallisation behaviour of PET is also significant in the characterisation of different grades. In general it is observed that lower IV (i.e. molecular weight products) crystallise more easily as the polymer chains are more mobile due to the reduced number of entanglements. Such materials therefore, are unsuitable for thick walled preforms where cooling of the inner portion of the preform wall is slow. It would be expected that higher molecular weight grades would solve this problem but the high molecular weight imparts difficult flow properties in mould filling and bottle blowing hence copolymers are generally used to circumvent this issue. The co-monomer disrupts the close packing of parts of the polymer chain hence increasing the time taken for crystallisation to occur. Overall, in most applications a suitable delay is required in the onset of crystallisation from the melt in order that amorphous articles such as film or preforms can be produced. The second major feature is the temperature at which cold crystallisation occurs on heating prior to stretching processes. When orientation of PET is required the material must be heated above T_g to enable sufficient molecular motion of the polymer chains, hence it must be ensured that the temperature of cold crystallisation is not so low it occurs during orientation as crystallisation at this stage of processing is a significant cause of delamination. It is important to note that polyesters in general, including PET are highly hygroscopic in nature and can very quickly adsorb moisture up to saturation point. The total amount that can be adsorbed is dependant on the proportion of amorphous and crystalline material in the sample. It has been shown that entirely amorphous PET adsorbs water in a manner directly proportional to water vapour pressure [37] and obeys Henry's law. Crystallinity in the polymer has the effect of reducing the level of moisture present and the relationship between moisture

saturation and amorphous/crystalline content has been determined as has the temperature dependence.

Table 1.5.2-1 Summarised barrier properties of PET and PET copolymers (after Jones PET packaging, Sheffield academic press 2002)

Polymer type	O_2 cc · mil/100 inch^2 · 24 h · Atmos	CO_2* cc · mil/100 inch^2 · 24 h · Atmos	N_2 cc · mil/100 inch^2 · 24 h · Atmos	H_2O g · mil/100 in^2 · 24 h · Atmos
Gas barrier properties at 30°C				
PET homo/low copolymer				
Amorphous	9	54	2.4	4
Oriented	5	40		2.5
Crystalline	4	33	1.2	2
PET medium copolymer				
Amorphous				
10% IPA	8	40		
10% PETN	8.2	53		
20% IPA	6.5	35		
20% PETN	8	47.5		
PET high copolymer				
Amorphous				
PETG	19	109	5.5	8
50% IPA	4	16		
50% PETN	6.3	39		
100% IPA	2.3	6		
100% PEN	3	18	0.4	

The gas barrier properties of PET are essentially good. For packaging materials the crystalline content is critical as it is considered essentially impermeable. In addition to the level of crystallinity the orientation of the crystals in relation to the direction of flow of the permeant gas is also important. In PET packaging applications such as biaxially orientated PET sheet and ISBM bottles the stretching process ensures alignment of the crystals perpendicular to the flow of gas and hence maximises the gas barrier properties. In addition to the level of crystallinity the level and type of copolymer can also influence gas barrier and it has been shown that co-monomers such as isophthalic acid and naphthalene 2,6 dicarboxylic acid can have a positive influence on the gas barrier [38, 39]. Some of the important gas barrier properties as described are illustrated in Table 1.5.2-

1 and show that orientation and crystallisation improve the gas barrier as does the incorporation of various co-monomers.

1.6 Fundamental properties of the fillers studied

1.6.1 Montmorillonite based organoclay

The major filler used in this study is montmorillonite (MMT). MMT is part of the broader group of layered minerals known as phyllosilicates or more generally clay minerals. There are broadly four types of clay within this group, namely Kaolins, Illites (clay mica's), Chlorites and the Smectite clays. All of these clays are termed crystalline clays and are composed of fine plate shaped crystals with a thickness of around 1nm. The platelets vary in composition but are generally built on Si tetrahedron and Al or Mg octahedron building blocks (Figure 1.6.1-1). In the literature there is sufficient material regarding the structural characteristics of these materials.
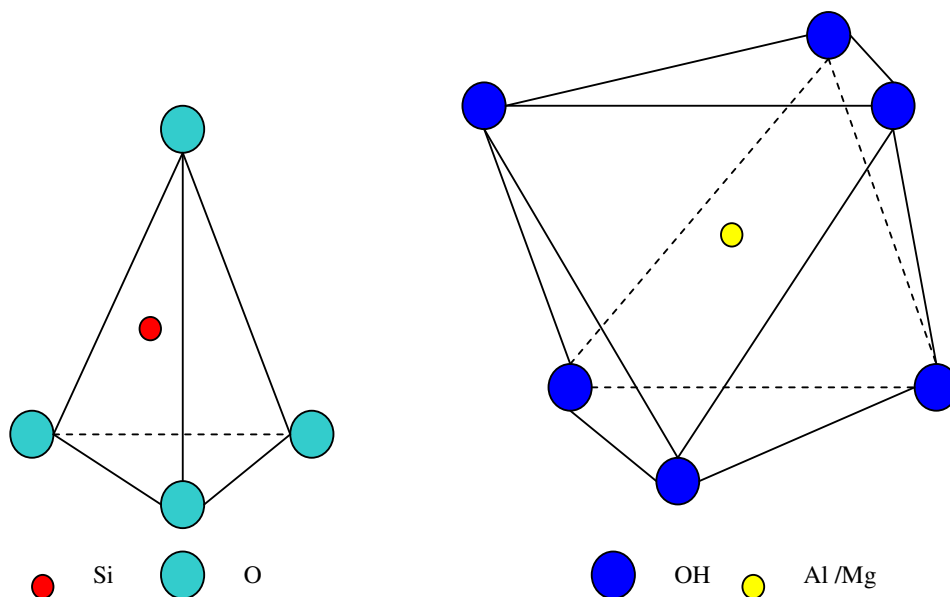
Figure 1.6.1–1 Silica tetrahedron and aluminium/magnesium octahedron

MMT belongs to the smectite sub-group and is the major component of bentonite clay (~80%). It was first identified in 1896 near Montmorillonite in France from where its name is derived. MMT is the most commonly used clay for polymer nanocomposites and is found distributed throughout the world. The raw bentonite clay is mined and then put through numerous grinding, sieving and purification and ion exchange steps until the sodium form of MMT is obtained. It is usually cream to light brown in colour and supplied as a powder of nominal particle size 8μm, hence each particle is made up of smaller agglomerated particles, each of which is made of thousands of individual clay layers.

The montmorillonite platelets are made up of a 2:1 sandwich structure consisting of two silica tetrahedral layers separated by an octahedral metal oxide layer (Figure 1.6.1-2).
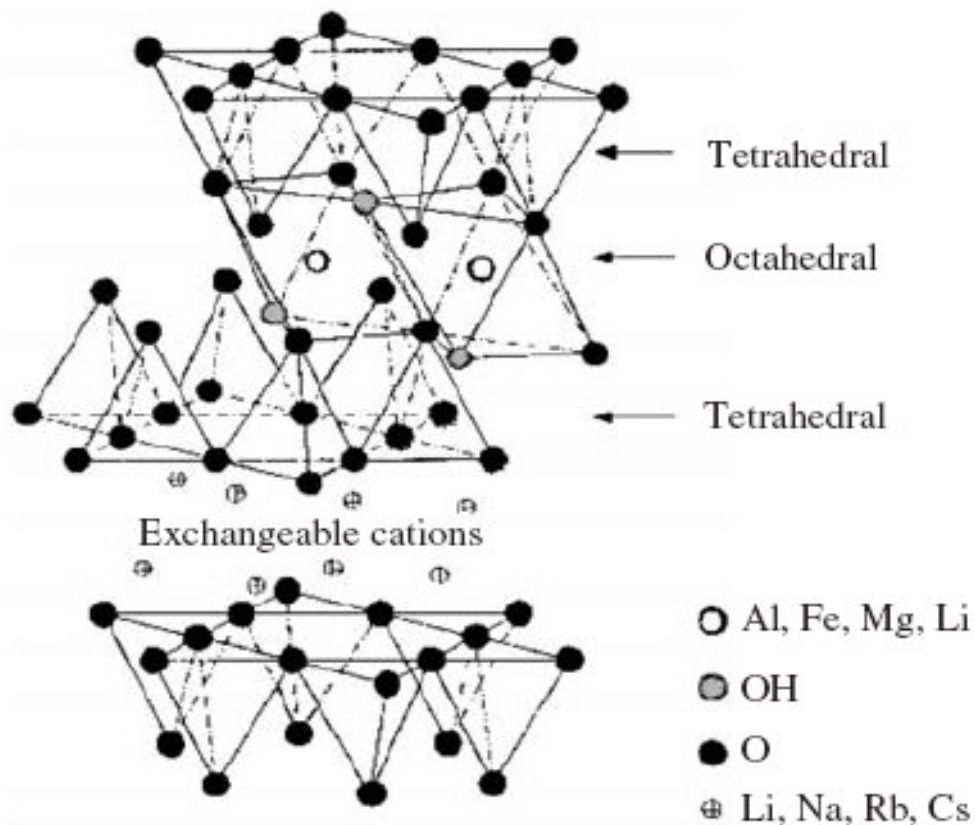
Figure 1.6.1–2 Structure of montmorillonite layers (from S.S. Ray and M. Okamoto; Prog. Polym. Sci. 28; 1539 (2003)

Each layer is separated by a Van der Waals gap referred to as the interlayer. Due to a certain amount of substitution of Mg for Al in the octahedral sheet an overall negative charge is developed which is balanced by the presence of an alkaline metal or alkaline earth metal cation such as sodium [40].

The presence of the sodium cation in the clay gallery and hence positive charge results in a very hydrophilic environment. The hydrophilic nature of the clay interlayer results in poor compatibility with most polymers hence the need for chemical modification of the clay interlayer (shown schematically in Figure 1.6.1–3).

Successful surface modification of montmorillonite has been conducted by cation exchange reactions and ion-dipole reactions using alkyl ammonium salts, alkyl imidazolium salts, alkoxy silanes, polysiloxanes and water-soluble polymers such as poly (vinyl pyrolidone) (PVP) and poly (ethylene oxide) PEO [41-48]. Current commercially available organoclays are without exception modified with alkyl ammonium salts.
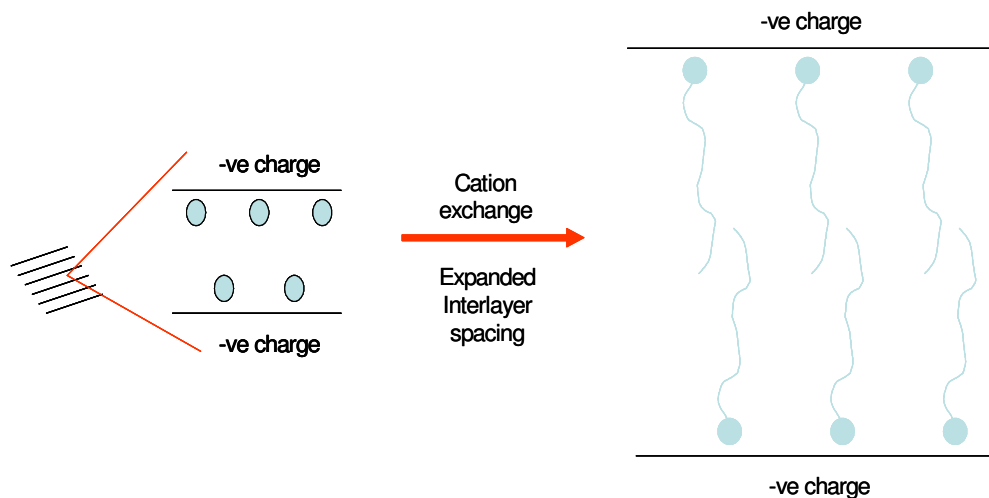
Figure 1.6.1–3 Chemical modification of the clay interlayer

1.6.2 Nano – Silica flakes

Nano-silica flakes are a recent development based on novel proprietary technology. Traditional glass flake manufacture involves blowing the molten glass into a thin tube and then pulverising the tube into small fragments. Silica

flakes produced by this technique generally have thickness of 1 - 5μm and lengths up to 1mm. Silica flakes have been used extensively as filler in polymeric coatings since the 1950's as they have been found to improve wear resistance, prevent cracking and peeling, have good chemical resistance and overall extend the life of the coatings [49]. In addition to these properties silica flake filled coatings have also been found to exhibit exceptional barrier properties to oxygen and moisture due to the tortuous pathway effect (as per Fig. 1.11.2-1). In recent years, through developments in the silica flake industry more and more flake grades have become available for thermoplastic moulding application and offer benefits including increased tensile/flexural strength and modulus, reduced shrinkage and warping, improved dimensional stability, increased liquid and vapour permeation, improved wear properties and increased heat distortion temperature [50]. Further potential applications for silica flakes include denture bases [51] and gas barrier films [52]. The main reason for the wider application of these materials is due to improved glass bubble stability which allows the manufacture of significantly thinner silica flakes and the development of new proprietary processes for the manufacture of ultra-thin flakes (as low as 100nm thickness).

1.6.3 Divalent metal layered phosphonates (DMLP)

The use of metal phosphonates as a layered nano-filler is a relatively new application despite metal phosphonate chemistry being researched from the mid 1970's. Recently much greater interest in the chemistry of these materials has been apparent due to their ability to form inorganic/organic hybrids at low temperatures thus allowing the incorporation of organic functionality without disturbing the inorganic portion of the layers. Also by varying the organic chemistry it is possible to build up structure with controlled pores or to build structures layer by layer to produce thin films. Much of the work so far has been focused on zirconium systems and these are well reviewed by Clearfield [53].

More recently more attention has been paid to the synthesis and characterisation of divalent metal phosphonates such as calcium phenylphosphonate [54] and nickel phosphonate materials [55], and these structures have been well characterised. In addition, Grebier et al [56] have investigated the synthesis of

amine intercalated zinc phosphonates. In their work amines are added to the phosphonate phase allowing the authors to increase the variety of the intercalants and their incorporation.

In addition to ongoing development of layered phosphonate some authors have investigated their use as nano-fillers for polymers. Wang et al [57] have synthesised polyacrylamide gamma-zirconium phosphate nanocomposites by an in-situ polymerisation method. X-ray diffraction (XRD) confirmed an increase in phosphonate interlayer spacing from 1.22nm to 1.64nm for intercalation of monomer and the subsequent polymer was found to have an exfoliated structure. Epoxy alpha-zirconium phosphonate nanocomposites have also been reported [58, 59] with good dispersion of the phosphonate.

Other reported applications of layered phosphonates in polymer materials include their use in fuel cells [60] and also in the work of Rule [61] and Loye et al [62] as a gas barrier additive for PET. In the work conducted by Rule [61] the various phosphonate additives are added to PET by melt processing techniques and the resultant level of dispersion estimated by the increase in SSP time due to the barrier effect of the materials to crystallisation. Modelling work indicates potential barrier improvements but actual measured data is not provided. An idealised structure of a phenyl modified phosphonate such as that described by Rule is shown in Figure 1.6.3-1.
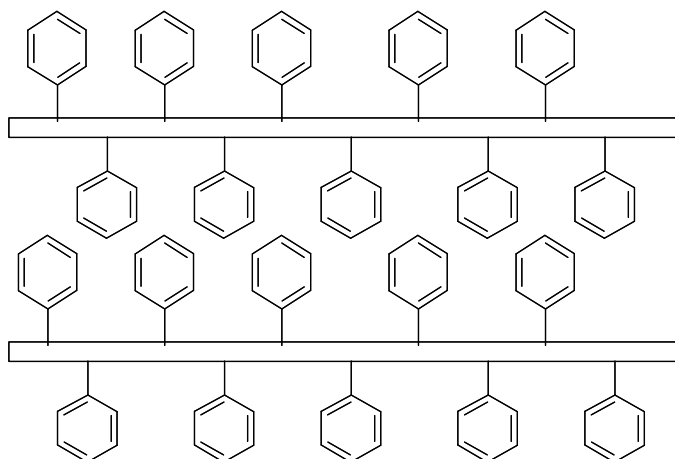
Figure 1.6.3–1 Divalent layered metal phosphonate with phenyl group in the interlayer

1.7 Nanocomposite formation

Nanocomposites, in the most general sense, are formed by the incorporation of a nanoscale particulate (referred to as the filler) into a macroscopic sample (known as the matrix). Through the incorporation of filler on the nanoscale rather than the microscale it has been shown that the properties of a polymer matrix can be greatly enhanced at lower filler concentrations than observed with microscale fillers. Many matrices have been investigated with numerous fillers such as clays, graphite, carbon nanotubes, metal oxides, nitrides and polyhedral oligomeric silsequioxanes. Over the past two decades considerable research effort in both academia and industry has been directed towards the development of nanocomposites and in particular, the development of clay polymer nanocomposites. This interest in polymer/clay nanocomposites was instigated by the pioneering work conducted by the Toyota group into PA6 nanocomposites [63]. The Toyota group's method was to intercalate clay with a suitable organic modification followed by mixing the organoclay with a monomer (i.e. carpolactam) and possibly catalyst and/or activator. The mixture is then heated to the prescribed polymerisation temperature. The resultant nanocomposite exhibited improvements in mechanical strength without the embrittlement associated with microcomposites and additional improvements in high temperature properties. Following on from this work many researches investigated the technology using numerous polymers until finally; in 1995 Allied Signal patented a new method for the manufacture of nanocomposites [64]. In this method the inventive step was to use a silane in conjunction with alkyammonium intercalants to induce sufficient affinity between the organoclay and the matrix polymer (PA6) to exfoliate the clay in melt compounding (e.g. twin-screw extruder). It was noticed that the nanocomposites produced had a considerable portion of γ-crystals (obtained by rapid cooling from the melt) which were resistant to conversion to the more thermodynamically stable α-crystal (obtained from slow cooling from the melt). The nanocomposites had improved rigidity and water resistance while retaining toughness, surface gloss and abrasion resistance. The final method used for nanocomposite synthesis is from solution and has been attempted with many polymers, but so far has not

achieved the commercial success of in-situ polymerisation and melt processing methods due primarily to the copious quantities of solvent required.

In terms of polymer/clay nanocomposites the ultimate goal is to produce a matrix containing individually dispersed clay layers as illustrated schematically in Figure 1.7-1.
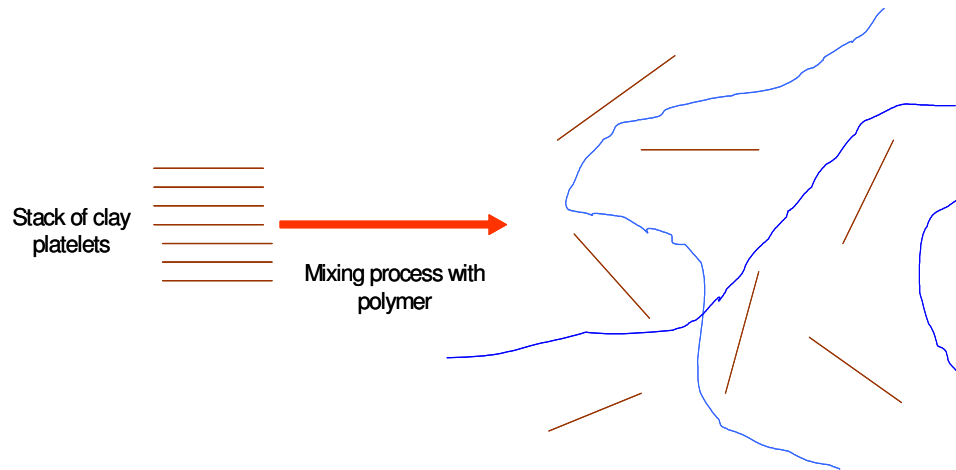
Figure 1.7-1 Schematic representation of exfoliated clay platelets

The dispersion of the clay as individual layers within the polymer matrix allows significant increases in properties such as strength and stiffness (without a detrimental effect on impact properties), heat distortion temperature and gas barrier at low filler concentrations while maintaining good optical properties/transparency.

1.7.1 Formation of nanocomposites from solution

In the formation of nanocomposites from solution the process is relatively simple. First the clay is dispersed in the appropriate polarity media e.g. water for hydrophilic clay or organic solvents for organoclay. The second step is to dissolve the polymer in the same, or an alternative compatible solvent. Care should be taken that the clay can be readily dispersed in the solvent used for the polymer. The clay dispersion and polymer solution are then mixed and the polymer displaces solvent molecules within the swollen clay layers. The solvent is removed and an intercalated/exfoliated composite is produced (as shown schematically in Figure 1.7.1–1).

Historically many water soluble polymers such as PEO [65], poly (vinyl alcohol), PVA [66] and PVP [67] have been used to intercalate clay galleries by this method. For PEO systems produced by varying routes, thin films of intercalated nanocomposites have been produced but were prone to cracking [65].

Organic solvents have also been used to produce nanocomposites by the solution method. In one such example Jeon et al [68] produced HDPE nanocomposites by dissolving HDPE in a xylene/benzonitrile mixture with dispersed organoclay. The nanocomposite was recovered by precipitation and washing in THF and found by XRD and TEM to contain well dispersed tactoids and some individual clay layers. Further examples include the synthesis of syndiotactic PS nanocomposites [69], polyimide [70], poly(dimethylsiloxane) [71] amongst others.

Overall the solution method shows significant promise as a technique to produce high quality nanocomposites but is unlikely to ever achieve significance in industry due to the large quantities of solvent required. It is likely that this technique will remain useful in academia for smaller scale research projects without ever becoming a commercial process.
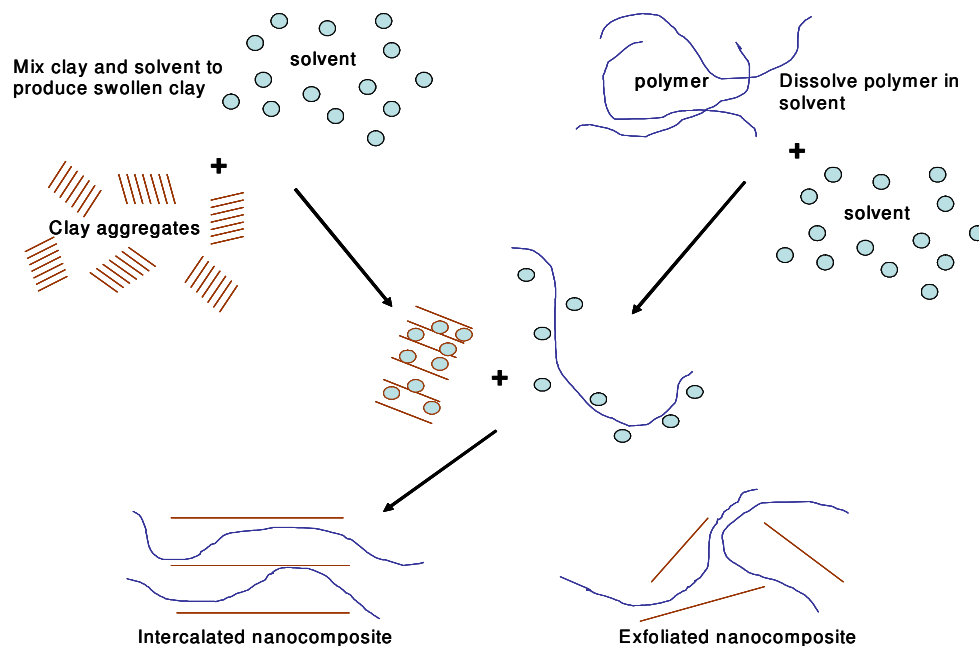
Figure 1.7.1–1 Schematic showing solution synthesis route to nanocomposite formation.

1.7.2 Formation of polymer nanocomposites from in-situ polymerisation

The Toyota research group pioneered the in-situ polymerisation approach for nanocomposites. In essence the appropriate clay materials are dispersed in the monomer (or monomers) with other additives as required (e.g. catalyst, stabilisers, antioxidants etc.). This mixture is then brought to the required temperature and pressure to affect polymerisation resulting in polymerisation of the monomer that has been intercalated in the clay layers. The growing polymer chains force the clay platelets apart affecting dispersion of the clay in the growing polymer matrix (as shown schematically in Figure 1.7.2–1.
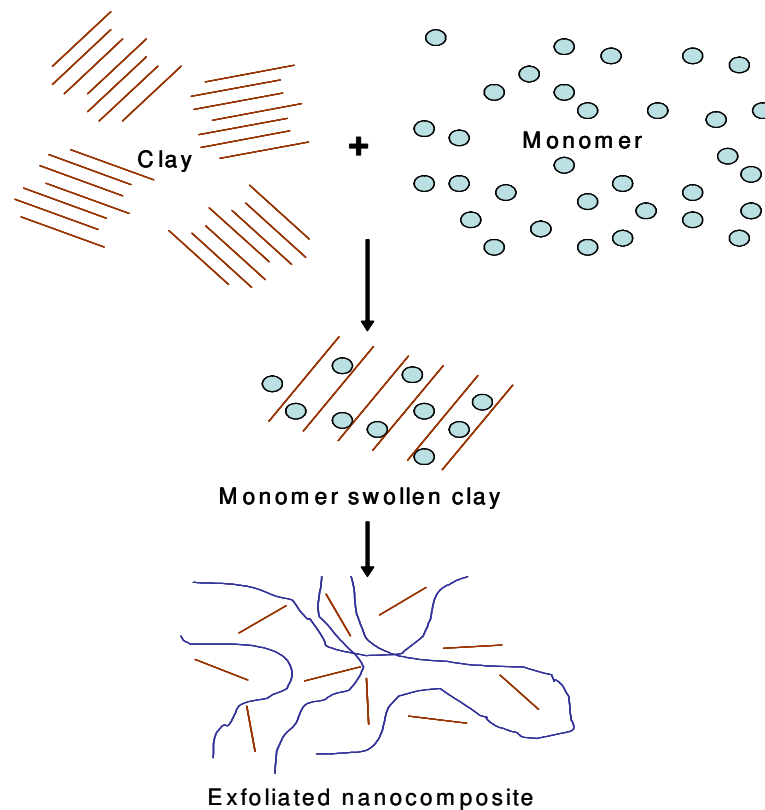
Figure 1.7.2–1 Schematic representation of in situ polymerisation

As mentioned previously the ground breaking work conducted in this field was by Deguchi et al [63] in their synthesis of PA6 nanocomposites. Further research in the Toyota research group has led to considerable refinement of the process. In

the work conducted by Usuki et al [72] in the early 1990's, focusing on the modification of sodium form clay with α ω-amino acids of varying CH_2 chain length. The modified clays were then swollen in ε-carpolactam at 100ºC. The mixture was then brought to the required polymerisation conditions to produce a nanocomposite. The authors confirmed a high degree of exfoliation in the resultant nanocomposite. This method has been extended and used for other polymers such as poly (propylene) (PP) [73], poly ε-carpolactone [74] and poly (methylmethacrylate) (PMMA) [75] amongst others. In general given considered choice of clay surfactant in order to maximise polymer/clay interactions, nanocomposites with a high level of dispersion can be produced using this technique.

1.7.3 Formation of nanocomposites from polymer melts

The formation of nanocomposites from polymer melts, has perhaps received the most attention of all the possible routes to polymer/clay nanocomposite synthesis. The main factors stimulating interest in the technique is flexibility in formulation, economic favourability and the technique requires only commonly used compounding and fabrication equipment. In general terms polymer and clay are added to a melt mixer (e.g. twin-screw extruder). The mixing and resultant shear generation breaks down agglomerated silicate particles into stacks of clay platelets which, are in turn broken down further into smaller tactoids. Diffusion of polymer chains coupled with shear generated in the extruder is thought to peel apart the remaining platelets in the clay platelet stacks to improve dispersion further (as illustrated in Figure 1.7.3–1).

Several factors have been found to be significant in optimising the melt mixing process and producing the highest level of dispersion possible. Studies conducted by Paul et al [76] have illustrated the importance of clay treatment in conjunction with differences in extruder type and screw configuration on the dispersion of PA6 nanocomposites. In addition this study also elucidated the importance of extruder residence time indicating longer residence times to be beneficial in producing the best dispersed nanocomposites. In addition to these factors it has also been determined that high melt viscosity [77] and the location of organoclay addition [78] can also play an important role in determining the extent of

exfoliation, and the final nanocomposite properties. Despite these practical guidelines nanocomposite quality can not be guaranteed and other factors such as organoclay thermal stability and clay/polymer compatibility may have greater influence in determining the quality of nanocomposite.
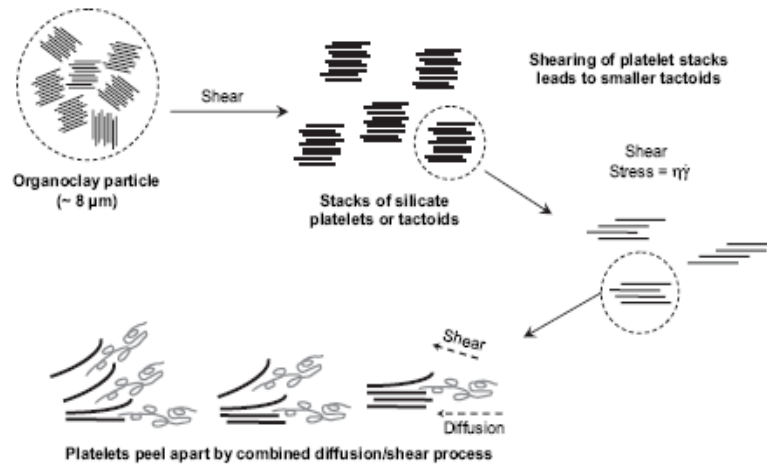
Figure 1.7.3–1 Schematic representation of the mechanism of clay dispersion and delamination of individual clay platelets in melt processing (from Ref [77]).

Over the past decade a huge amount of data has been published on the synthesis of nanocomposites by melt compounding hence individual cases cannot be discussed in detail here although a detailed discussion of PET nanocomposites from melt compounding will follow in section 2.5.

1.8 Commercial applications of nanocomposites

Despite the considerable research efforts expended on clay polymer nanocomposites both in academia and industry, commercialisation of nanocomposites products has been relatively slow. Several factors have influenced the slow development of the commercial market for nanocomposites, including identification of specific markets, increased cost compared to other filled systems (such as glass fibre filled PA6) and regulatory issues. Regardless of the problems associated with the commercialisation of polymer clay nanocomposites there have been some successful products developed.

The first commercial nanocomposite product was PA6 based and developed by Toyota Motor Company for timing belt covers [79]. The use of these materials has also been extended to the Toyota Camry [80]. A further PA6 based automotive engine application has been developed by Unitika for engine covers for Mitsubishi GDI engines [79, 81]. In addition to automotive applications PA6 has also been developed by Honywell as a barrier layer for multilayer bottles [79].

In addition to PA6 nanocomposites, PA-MXD6 has also been developed into a commercial nanocomposite through the collaboration of Mitsubishi Gas Chemical Company and Nanocor [79]. The resulting material is an excellent CO_2 barrier in multilayer bottles and has been used by the Miller Brewing Co. in the USA.

In addition to polyamides, polyolefins have also seen some significant commercialisation particularly in automotive applications. Basel and General Motors jointly developed a thermoplastic polyolefin for use in door panels of the Chevrolet Impala and have followed this with the development of a step assist component used in GMC Safari and Chevrolet Astra vans [82-83]. More recent developments by Honda Acura in conjunction with Noble polymers have seen the commercialisation of another thermoplastic polyolefin for structural seat backs [84].

From the types of applications described it is clear that nanocomposites have the potential to thrive in applications where the unique properties exhibited such as strength and stiffness with comparable density to the unmodified polymer and improved gas barrier add value to the product.

1.9 PET nanocomposites

So far there has been no commercialisation of a PET nanocomposite despite the high rewards for technical success. The following sections will detail the efforts made in the development of PET nanocomposites and the properties of these materials.

1.9.1 PET nanocomposites from solution

Due to the problems associated with handling large quantities of solvent it is not surprising that few researchers have investigated the possibilities of using solution techniques to form PET nanocomposites. In addition, solvent systems for PET are generally composed of difficult to handle solvent mixtures containing phenol, tetrachloroethane, chloroform and 1,1,3,3-hexafluoro-2-propanol amongst others. Despite this some interesting studies have been carried out using this technique such as the work of Ou et al [85]. In this study cetyltrimethyl ammonium chloride was used to modify the clay. Nanocomposites were formed with varying loadings (1, 5, 10 and 15wt%) from a 3/1 (w/w) ratio mixture of phenol and chloroform. The morphology of the nanocomposites was investigated using XRD and TEM and found to be a mixture of exfoliated platelets and small intercalated tactoids with a generally good dispersion even at 15wt% clay. DSC analysis was conducted and the clay was found to be an effective nucleating agent with optimum nucleation and acceleration of crystallisation rate occurring in the 10wt% clay nanocomposite. In an almost identical paper by the same authors similar experiments were conducted on clay containing a cetylpyridinium modified clay [86]. The morphology of these nanocomposites was found to be similar to those obtained for the cetyltrimethyl ammonium surfactant although XRD peaks were much stronger indicating a more intercalated structure than in the previous case. The DSC experiments revealed a heterogeneous nucleation effect and TGA revealed improved thermal stability with the temperature of maximum weight loss increasing (about 5ºC) in all cases for the nanocomposite compared to the pristine polymer sample.

The group of researchers led by Moore [87-89] have also produced several papers on solution based nanocomposites utilising a sulfonated PET ionomer in order to improve polymer clay compatibility. In one paper [87] composites were produced from PET and PET containing 2, 6 and 10 mol% sulfoisophthalic acid from a 1:1 v/v mixture of 1,1,3,3-hexafluoro-2-propanol and chloroform mixture with 5wt% Cloisite 30A organoclay (bis-2-hydroxyethyl methyl octadecyl ammonium surfactant). XRD analysis of the nanocomposites revealed a mixture of intercalated clay and pristine clay in the PET while ionomer based composites showed a much broader flatter peak in the range of 2-4º indicating intercalation

and some exfoliation of the clay particles. Again a nucleation effect was observed which became more pronounced with increasing ionomer content. These results are confirmed in a further paper [88]. A further paper [89] explored a comparison between C30A and CNa^+ clays and the resulting effect on crystallisation behaviour. Nanocomposites were produced in identical fashion to that described previously with 5wt% clay and ionomer contents of 2 mol% and 6 mol%. Cloisite 30A was found to be the more effective nucleating agent despite the expectation that CNa^+ would offer larger nucleation sites due to less dispersion.

One final paper pertaining to the synthesis of PET nanocomposites from solution concentrates on a high co-monomer PET containing 2.6 naphthalene dicarboxylic acid [90]. The composites were produced with varying contents of hexadecylamine modified clay from N,N-dimethylacetamide solvent. In all cases up to a loading of 6wt% organoclay a clear (001) peak was observed for the clay indicating full exfoliation had not occurred but that an intercalated nanocomposite had been produced. Supporting TEM indicates a predominantly intercalated structure with a few individual platelets.

The work conducted by this technique for PET indicates good dispersion of the clay can be achieved given maximisation of clay/polymer interactions but fully exfoliated nanocomposites were not obtained. The above studies did not include any evaluations of barrier properties.

1.9.2 PET nanocomposites from in situ polymerisation

The synthesis of PET nanocomposites has some distinct advantages over the solvent assisted process as large quantities of solvent are not required and there is potential for PET resin manufacturers to produce nanocomposite materials with very little modification of existing plant facilities. As would be expected with these advantages there is a larger body of literature pertaining to PET nanocomposites synthesised by this route.

In addition to clay based nanocomposites, it is of note that researchers have produced PET nanocomposites with alternative nano-fillers such as silica [91-93], calcium carbonate [94], barium sulphate [95] and alumina [96]. These studies

examine factors such as dispersion of the filler, influence on crystallisation behaviour and wear rate.

For PET/clay nanocomposites Zhang et al [97] modified MMT with hydroxypentyl trimethyl ammonium iodide (HPTA) and hydroxyethyl isonicotinamide (HENA) and polymerised with BHET to produce composites with polymer anchored to the clay (as shown in Figure 1.9.2–1).
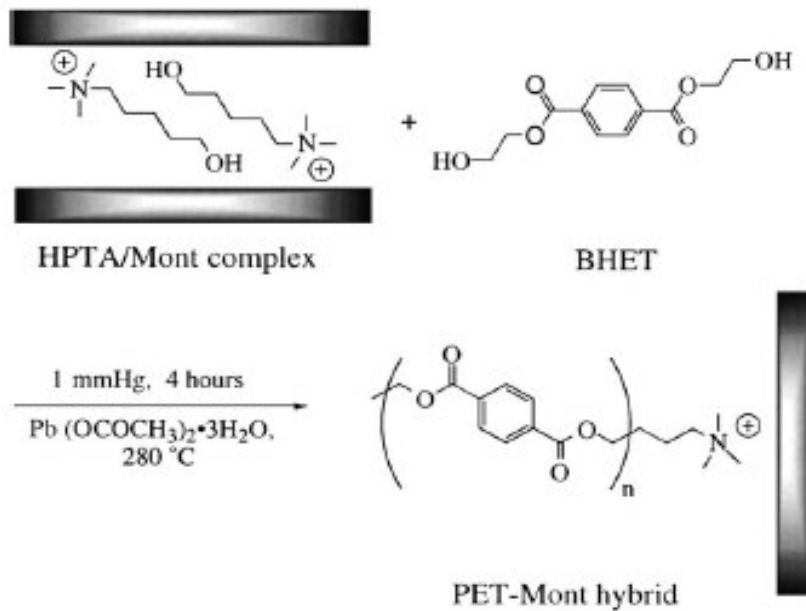
Figure 1.9.2-1 Polymerisation of BHET in the presence HPTA to form anchored nanocomposite (from ref [97])

Nanocomposites with 5wt% and 10wt% were produced and XRD revealed a high level of clay dispersion with the (001) peak almost disappearing for both clay types. Films containing 10wt% clay were found to be transparent further confirming a high level of clay dispersion although some yellowing was observed, particularly with HENA modified clay. In addition it was found that tensile strength of the HPTA nanocomposite was improved by 58% compared to the standard PET.

In the work of Ke and Yongping [98], clay was modified with a quaternary ammonium with carboxylic acid functionality and dispersed in ethylene glycol. Polymerisation was carried out by ester interchange of dimethyl terephthalate

and ethylene glycol/clay slurry to produce nanocomposites with 1, 2, 3 and 4wt% clay. XRD and TEM were used to investigate the nanocomposite morphology and it was found that the clay had dispersed evenly in the matrix to produce a mixed structure of exfoliated platelets and small tactoids (about 5 clay layers per tactoid estimated from TEM). Other tests on the nanocomposites showed that the clay acted as a nucleating agent for cold crystallisation and that a 50% reduction in oxygen transmission of films could be achieved with 3wt% of clay. In the work conducted by Ke and co-workers [99, 100] polymerisation of PET monomers was conducted in the presence of a proprietary modified clay and also clays modified with ethanolamine, cetyl trimethylammonium salt, laurilamine and hexanediamine. Resulting morphological investigation revealed an intercalated nanocomposite had formed with an interlayer spacing of approximately 3.4nm and some large agglomerations of clay. As per previous examples the clay acted as a nucleating agent and improvements in tensile strength and HDT (up to 50ºC increase) were also observed.

The previous papers have focused on ammonium based surfactant for clay which may degrade at PET polymerisation temperatures. It is believed that poor thermal stability of surfactant and subsequent degradation may lead to reduced clay dispersion and hence lower quality nanocomposites. In order to overcome this problem Imai and co-workers have produced novel phosphonium based surfactants [101-103] and used high purity synthetic clay (expandable fluorine mica). Nanocomposites were produced from the polymerisation of a BHET/organoclay mixture and the resultant nanocomposites had an intercalated structure with an interlayer spacing of about 3.2 – 3.3nm. It is of note that despite producing novel surfactants with increased affinity for PET and thermal stability exfoliation was not achieved.

In addition to the work of Imai, Chang et al [104] have also investigated phosphonium based surfactants in in-situ polymerised nanocomposites. In their procedure clay was modified with dodecyltriphenyl phosphonium and mixed with ethylene glycol and dimethyl terephtalate and polymerised. The resultant materials were drawn into fibres and the morphology and tensile modulus was investigated. The nanocomposites were found to have an intercalated structure with a distance of 1.72nm calculated from XRD. This is less than that observed for other intercalated PET structures and is probably due to the high orientation

56

of the PET chains due to the fibre forming process. Increasing the draw ratio of the fibre appeared to improve the clay dispersion as evidenced by the disappearance of the (001) peak in higher draw ratio samples but stacks of clay platelets were clearly evidenced by TEM. The tensile modulus of the fibres was found to increase significantly for 3wt% clay but the effect was reduced as the fibre draw ration was increased.

In other work Tsai and co-workers have developed a novel approach to in situ polymerisation [105-107]. In this work a new process for in-situ polymerisation has been developed called the 'driving force concept'. In this process sodium form clay is modified by a surfactant with functional group (either hydroxyl or carboxylic acid) and a catalyst or initiator which is then swollen in BHET prior to polymerisation. The authors have continued to develop improved clays and released impressive results in 2006 [107] including increased flexural strength, increased HDT, reduced transmission of UV light and most significantly reduced CO_2 barrier (from 0.304 to 0.04 cc/m^2/day) in bottles with no haze. In another novel approach to in-situ polymerisation Kim et al [108] produced a polymeric organoclay by first dispersing the clay in ethylene glycol and then esterification was carried out with 1,2,4-benzenetricarboxylic anhydride. The novel clay was added to the polymerisation of ethylene glycol and terephthalic acid to produce nanocomposites with varying clay loading. Characterisation of the morphology was conducted and a good dispersion of the clay had been obtained at the sub-micron level without achieving full exfoliation.

Other authors such as Hao [109], Lee [110] and Choi [111] have also developed novel approaches to the sythesis of PET nanocomposites via in-situ polymerisation. The work of Choi [111] is of particular interest as it is one of the few reports on PET nanocomposites to include some data from gas barrier testing. In this work the authors modified sodium form clay directly with chlorotitanium triisopropoxide catalyst in THF to produce clay supported polymerisation catalyst. The clay supported catalyst was used to produce nanocomposites with 1, 2 and 5wt% clay. The films produced from these materials were found to be intercalated with a (001) spacing of 1.52nm. Despite exfoliation not occurring significant improvements in O_2 transmission were observed from 857cc/m^2/day to 55cc/m^2/day for 5wt% clay. The transparency of the nanocomposite films was found to diminish as the clay content was increased.

The in-situ polymerisation method of producing PET nanocomposites indicates some very high levels of dispersion can be achieved. Significantly improvements in the gas barrier properties have also been demonstrated in nanocomposites produced by this technique yet commercialisation has not yet occurred.

1.9.3 PET nanocomposites from melt processing

The melt processing route to clay polymer nanocomposites is particularly attractive as it allows researchers in both academia and industry considerable control and flexibility in nanocomposites formation. In addition, melt processing can be carried out with traditional industry processing equipment such as twin-screw extruders, two-roll mills and internal mixers. It is therefore not surprising that the largest body of material pertaining to PET nanocomposite is focused on their synthesis by melt compounding techniques.

In an early paper on melt processed PET nanocomposites by Sanchez-Solis et al [112] PET was processed with Cloisite 15A organoclay (dimethyl dihydrogenated tallow ammonium salt surfactant) which is highly hydrophobic. The authors recognised that compatibility was likely to be poor with PET and included maleic anhydride and dipentaeurithritol to improve the compatibility of the PET and the clay layers. The resultant nanocomposites had (001) spacing of approximately 3.15nm measured by XRD. This value is similar to that of the unmodified clay indicating exfoliation had not occurred. The resultant nanocomposites did show a nucleating effect and increased strength indicating an intercalated nanocomposite had been produced. In another early study by Boesel and Pessan [113] nanocomposites were produced using a dialkyl dimethyl modified sodium clay and two commercial clay grades (Viscogel and Impaltone). In each case XRD analysis coupled with TEM indicated an intercalated structure with an interlayer spacing of about 3.3nm. It is of note that the Impaltone grade of commercial clay exhibited particularly good dispersion with tactoids reduced to only 4 or 5 clay layers in most cases. No further tests were conducted on the nanocomposite samples.

In papers by Pendse et al [114] and Phang et al [115] the crystallisation behaviour of PET nanocomposites is investigated. In the former paper the nanocomposites were intercalated in nature with an interlayer spacing of

approximately 3.39nm and the clay significantly nucleated crystallisation of the PET. In the latter paper no analysis of the nanocomposite morphology was undertaken but it was confirmed that the clay acted as a nucleating agent for both cold crystallisation and crystallisation from the melt. Studies conducted by Calcagno et al [116] concentrate on the effect of surfactant on the dispersion and crystallisation behaviour of PET nanocomposites. The authors observed a similar interlayer spacing of approximately 3.3nm for different polarity clays and observed that the (001) peak was absent for unmodified clay. TEM revealed a predominantly intercalated morphology for all the modified clays. The sodium clay appeared well dispersed from the TEM presented despite its hydrophobic nature and the authors propose exfoliation was achieved on the basis of direct polymer/clay interaction. This result is surprising and has not been previously observed nor further explained. Other authors who have experienced difficulty in obtaining exfoliated nanocomposite include Wang et al [117], McConnel et al [118], Pendse et al [119] and Pegoretti et al [120].

Surprisingly few papers are available dealing with the gas barrier properties of PET nanocomposites produced by the melt compounding method. One such example is detailed in the work of Garcia-Rejon et al [121]. This paper is of particular interest as it details barrier properties of bottles rather than film samples. The authors produced PET nanocomposites via twin-screw extrusion with 3wt% loading of Cloisite 6A organoclay (hydrophobic grade modified with dimethy dihydrogenated tallow ammonium). It was noticed that during further processing to produce bottles the PET nanocomposites could be injected at lower pressures and blown at lower pressures with the authors speculating that the nanoparticles may act as an internal lubricant although it is much more likely that degradation had occurred during processing and the phenomenon observed is attributable to reduced molecular weight. The resultant bottles were found to have a more uniform distribution of polymer in the bottle wall for the nanocomposites although the overall wall thickness was lower by about 12%. Top load resistance for the nanocomposites was found to improve at room temperature and the resistance to deformation was also improved for the nanocomposite bottles. The appearance of the nanocomposite bottles indicated some degradation may have occurred due to the distinct amber discolouration and the bottles also exhibited significant haze. Despite some positive property

enhancements the oxygen permeability improvement for the nanocomposite was quite modest (P = 0.35 cf P = 0.28 for the nanocomposite) which indicates that the overall dispersion of the clay was probably low despite these properties not having been reported.

In the work of Sahu et al [122] the properties of nanocomposite films were examined and some improvements were observed although biaxial stretching and fatigue resulted in reduced properties compared to the PET control. Sanchez-Garcia and co-workers [123] have also investigated the permeability behaviour of PET nanocomposites produced from the melt. Nanocomposites were produced from NanoBioMatters Nanoter 2000 organoclay (5wt%), which contains an undisclosed surface modification. The resultant nanocomposite was investigated to determine morphology, crystallisation properties and barrier properties to oxygen, water and limonene. Their investigation of the morphology concluded that the nanocomposite structure was predominantly exfoliated with some limited small tactoids while the crystallisation properties were found to be largely unaffected. The barrier property was improved to all the permeants tested (50% reduction in oxygen permeation) further confirming good dispersion of the clay and development of a tortuous pathway.

From these published results it is evident that there is potential to improve the properties of PET by the addition of clay nanoparticles but to achieve exfoliation certain factors need to be addressed such as the poor thermal stability of commercial organoclays at the PET processing temperature (270º - 300ºC generally) and the poor compatibility of these organoclays with PET [124].

The thermal stability of commercial organoclays and other quarternary ammonium modified clays has been explored in the literature [125, 126] and it is clear that degradation of the surfactant occurs at temperatures well below the processing temperature of PET. In order to address this fundamental deficiency in commercial organoclays considerable research time has been invested. In the work conducted by Davis et al [127] it was found that bromide-containing impurities from the dimethyldioctadecyl ammonium surfactant accelerated the thermal decomposition of the surfactant. The authors were able to demonstrate that by careful solvent extraction using hot ethanol followed by tetrahydrofuran (THF) the offending bromide compounds could be successfully removed thus improving the thermal stability of the organoclay. Other research activities have

centred on the synthesis of more thermally stable onium salts such as phosphoniums [128 – 130] and imidazoliums [131]. These materials have been found to exhibit significantly improved thermal stability compared to ammonium based surfactants.

Several authors have directly investigated the relationship between organoclay thermal stability and the dispersion quality of the nanocomposites produced. In one such paper Davis et al [132] investigated the performance of dimethyldioctadecyl ammonium surfactant in comparison to 1,2-dimethyl-3-hexadecyl imidazolium surfactant. PET nanocomposites were produced by twin screw extrusion under varying conditions of screw speed and varying residence time. The nanocomposites were processed at 290ºC with 5wt% clay added. The ammonium modified clay nanocomposite was quickly found to be extremely discoloured due to degradation of the clay surfactant. On the other hand the imidazolium modified clay produced nanocomposites with good colour. The best dispersion was found for the nanocomposite with low screw speed and residence time indicating that even with a more thermally stable clay surfactant reducing the time spent at high temperature was beneficial. The overall quality of clay dispersion was deemed to be good with a mixture of small tactoids (about 4 clay sheets) and individual delaminated platelets observed. In another study conducted by Costache et al [133] novel thermally stable surfactants based on quinolinium and a vinylbenzyl-ammonium copolymer were used in the melt synthesis of PET nanocomposites. Despite the increased thermal stability the nanocomposites produced had an intercalated morphology and full exfoliation was not achieved.

In a more recent paper Stoeffler et al [134] have studied the influence of organoclay surfactant on the morphology and crystallisation behaviour of PET nanocomposites. The authors synthesised four organoclays with ammonium, pyridinium, phosphonium and imidazolium based surfactants and also unmodified sodium form clay, the thermal stability was measured using TGA-MS. All the organoclays were found to have thermal stability greater than 290ºC (based on 5% weight loss) but it was noted that gasses are evolved at significantly lower temperatures indicating some degradation is occurring at temperatures lower than the PET processing temperature. The authors noted that the sodium form clay did not exhibit any diffraction peak but concluded that this

is typical of sodium form clay in microcomposites form. Contrary to the findings of Colcagone et al [116] the authors directly observed significant micro-scale particles through optical microscopy in the sodium clay case. For the ammonium, phosphonium and imidazolium based clays intercalated/partially exfoliated nanocomposites were produced with an interlayer spacing of approximately 3.3nm in each case. In contrast the pyridinium based clay exhibited a very wide diffraction peak and TEM revealed a mixture of microscale particles and small tactoids consisting of approximately 4–10 clay layers. These tactoids were found to have variable interlayer spacing from 1.7nm–2.8nm. It was also shown that the crystallisation kinetics were influenced both by the dispersion and the clay polymer interface properties.

In the paper of Lai et al [135] ammonium and phosphonium modified clays are directly compared and although the overall dispersion was improved in the phosphonium organoclay both nanocomposites exhibited a predominantly intercalated structure with some exfoliated platelets.
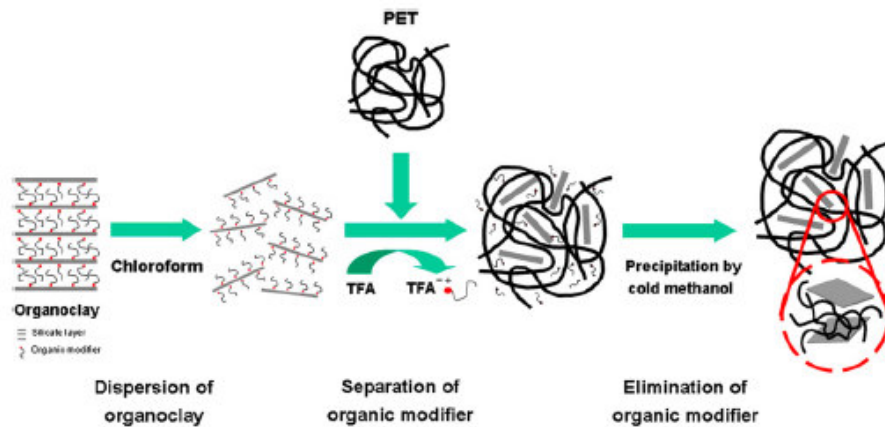
Figure 1.9.3-1 Schematic representation of selective surfactant removal (after [136])

The final paper concerning the influence of thermal stability by Chung et al [136] explores a novel new approach to obtaining thermally stable exfoliated PET nanocomposites. In this process (shown schematically in Figure 1.9.3-1) the organoclay was dispersed in chloroform and then after thorough mixing the clay/chloroform dispersion was added to trifluoroacetic acid and stirred. PET

was then added to this solution and mixed for a further hour until dissolved. Two further samples were produced, the first with the surfactant removed and the latter with the surfactant included. This was achieved, in the former by adding drop-wise to methanol to precipitate the PET clay and then isolating the filtrate and drying while in the latter case the solvent was removed by fume hood extraction over 48hrs then dried. These mixtures were blended with dry PET by twin-screw extruder to produce the nanocomposite samples. The resultant melt mixed samples exhibit a peak free XRD pattern and the accompanying high resolution TEM images confirm an exceptionally high degree of dispersion. Films produced from this method had excellent clarity and no discolouration. Overall this technique exhibits excellent potential but requires the solvent based pre-melt mixing stage which may prove a barrier to commercialisation.

In contrast to those authors dealing directly with the issue of organoclay degradation and its effect on PET nanocomposite properties other authors have chosen to tackle the issue of PET/clay compatibility. In one such work Thellen et al [137] investigated the effect of using maleic anhydride (MA) coupling agent on the properties of PET nanocomposites. The authors investigated both hydrophobic (Cloisite 20A) and hydrophilic (Cloisite 30B) clays with and without the MA and found that intercalation of the organoclays occurred and that the hydrophilic clay had slightly better dispersion based on TEM data. The authors observed that the dispersion was not improved by the addition of the MA and this did not influence the crystallisation behaviour of the nanocomposites produced either. In another study Yuan et al [138] produced a hexadecyltrimethyl ammonium clay and also similar clay modified with both hexadecyltrimethylammonium and poly (ethylene glycol). The resulting nanocomposites indicated better dispersion in the PEG/ammonium modified clay although the morphology was intercalated rather than exfoliated based on the XRD data and TEM. It is of note that the HDT and flexural modulus of the nanocomposites increased compared to the unmodified PET and that the increase was most significant in the case of the PEG modified clay. This indicates that the PEG has indeed improved the affinity of the PET for the clay compared to the ammonium based organoclay but the compatibility is not such that complete exfoliation occurred.

In a paper by Lai and Kim [139] a PET/PEN copolymer (8mol% PEN) and epoxy modified organoclays were investigated. The authors further modified Cloisite organoclays C20A and C30B with diglycyidyl ether of bisphenol A and then produced PET nanocomposites by twin screw extrusion. The XRD and TEM analysis indicates that the intercalated nanocomposites have been produced for both C20A and C30B although the peak intensity from XRD for C30B is much diminished indicating improved dispersion compared to the C20A, which is confirmed by TEM. The authors propose that the epoxy is able to react with the hydroxyl group of C30B and provide a high compatibility for PET in the clay interlayer. It is further proposed that the epoxy can further react with polymer chain ends resulting in considerable clay/polymer interaction (as shown schematically in Figure 1.9.3-2). In addition to evaluation of the mechanical properties of the resultant C30B based nanocomposites the authors also investigated the oxygen transmission of compression moulded films and observe values of permeability coefficient of ~6.5 for PET/PEN copolymer, ~3.5 for PET/PEN copolymer with 4wt% clay and ~0.5 for PET/PEN copolymer with 4wt% epoxy clay indicating significantly improved dispersion of the clay and development of an extensive tortuous pathway for permeant molecules.
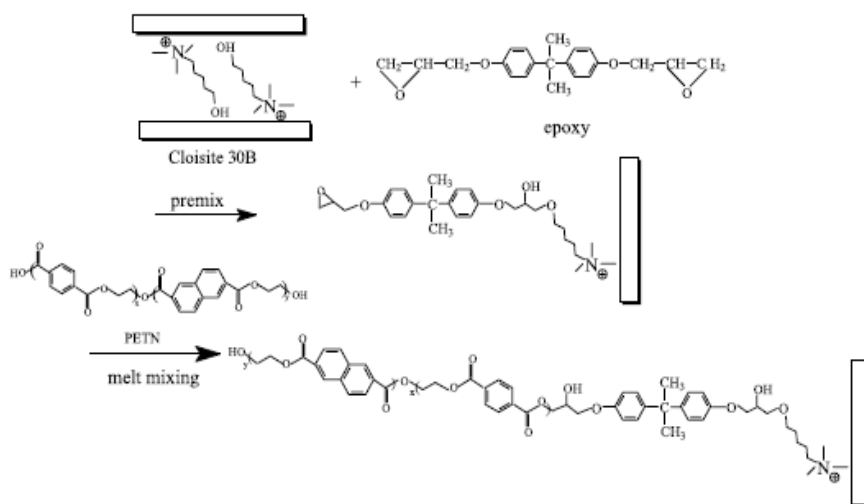
Figure 1.9.3-2 Schematic of epoxy modified clay and further reaction with PET/PEN copolymer (from [139])

64

A second approach taken by some researchers to improving compatibility between PET and clay is to modify the polymer rather than add coupling agents or modify the clay. In the work of Barber et al [140, 141] PET ionomer is used to increase the polarity of the polymer and hence improve compatibility with the clay surfaces. The ionomer is synthesised by replacing a small quantity of terephthalic acid with sulfoisophthalic acid to give copolymers with ionic content as depicted in Figure 1.9.3-3.

$x = 1.8, 3.9,$ or 5.8 mole%
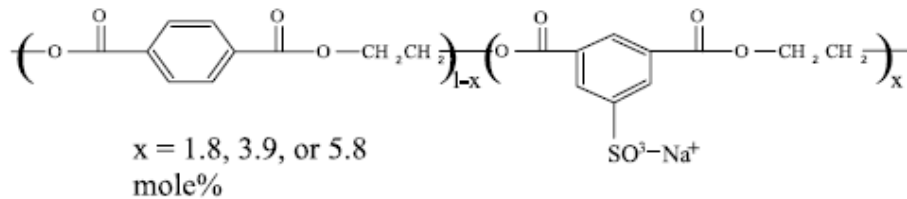
Figure 1.9.3-3 Structure of PET ionomers (from [141])

The authors have been able to demonstrate that the compatibility of PET with clay can be considerably improved by the incorporation of small quantities of the ionomer moiety and that the dispersion improves further as the ionomer content increases. The explanation of these phenomena is that the ionomer is able to interact strongly with the clay platelet edges, and this assists the dispersion during shearing in melt processing to improve the dispersion (Figure 1.9.3-4). The authors have shown that improvements can be obtained with various organoclays and even unmodified sodium clay.

More recently a novel approach to the use of PET ionomers has been suggested by Ammala et al [142]. In this study AQ55 polyester ionomer from Eastmann Chemical company is dispersed in water with the required quantity of clay (Cloisite 10A montmorillonite, Somasiff MEE and Somasif ME100 modified and unmodified synthetic fluorine mica), also dispersed in water. This mixture was then poured onto PET and the water removed by mechanical agitation and heat to leave coated PET pellets which were then processed using conventional melt processing techniques. The authors observed improved dispersion for ionomer treated clays compared to the nanocomposites containing untreated clays. From XRD data peaks were observed in all cases but for the ionomer treated clay

nanocomposites the intensity of these peaks was reduced indicating more delaminated clay particles, which was confirmed by TEM.
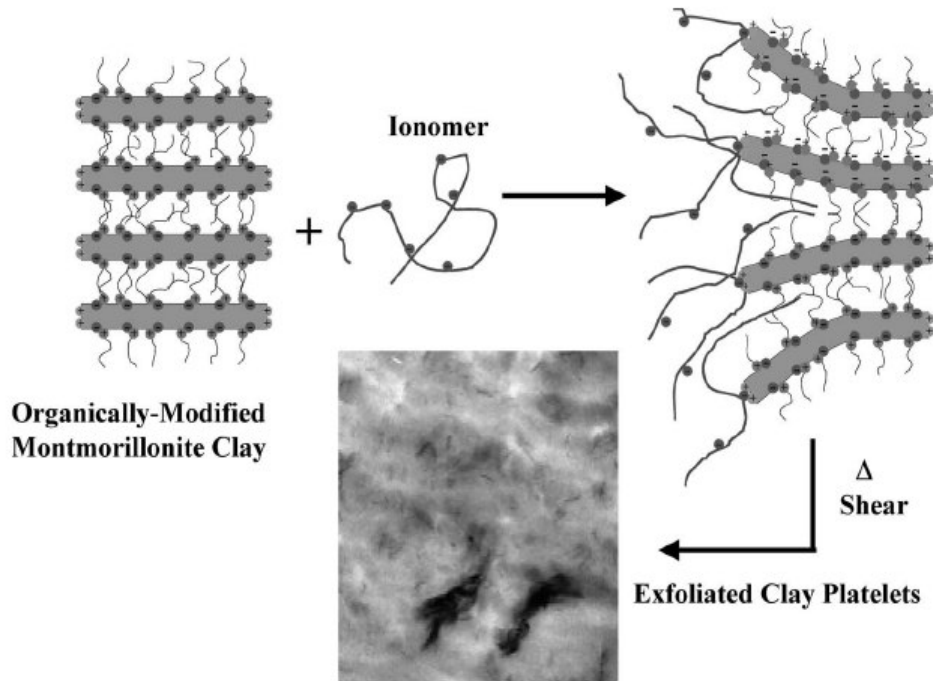
Figure 1.9.3-4 Schematic representation of the interaction of ionic groups with the clay platelets leading to improved clay dispersion (from [141])

1.9.4 Summary of PET nanocomposites

Overall the literature pertaining to PET based nanocomposites illustrates the difficulty in obtaining exfoliation of the clay due to poor compatibility of the PET/clay and the poor thermal stability of the commercial organoclays available. The synthesis of PET nanocomposites from solution and from in-situ polymerisation indicates that slightly better dispersion is obtained due to the lack of thermal history in the solvent assisted process and due to the polymerisation of the polymer in the clay layers facilitating clay platelet dispersion in the case of the in-situ technique. The melt mixing technique on the other hand requires considerable processing of the polymer and clay at temperatures where degradation of the surfactant may occur. From the literature it is evident that considerable research effort has been spent in an attempt to address this problem

and it has been shown that improving the thermal stability of organoclay often results in improved clay dispersion. Despite these improvements full exfoliation has not yet been achieved, most likely due to poor compatibility with the polymer. When the compatibility of the polymer and clay has been directly addressed again improvements in clay dispersion have been observed without full exfoliation of the clay. Overall this indicates that the full potential of PET/clay nanocomposites has yet to be realised.

When looking at the properties of the resultant nanocomposites it is clear that the presence of the clay has a nucleating effect and allows crystallisation to occur at higher temperatures when cooling from the melt and lower temperatures for cold crystallisation. In addition it has been shown that properties such as tensile modulus can also be significantly improved, further indicating that the dispersion of clay in PET can be of benefit. One of the more disappointing aspects of the literature available on PET nanocomposites is that very few reports deal with gas barrier properties. Of those that do, it is evident that even in systems where the dispersion of the clay platelets is not optimised improvements in gas barrier can be obtained and illustrates the attractive nature of PET nanocomposites technology to packaging applications.

1.10 Polymer Blending

Due to the comparatively advanced nature of polyamide/clay based nanotechnology and its potential to be used as a masterbatch for PET aspects of the compatibility and potential for blending various polyamides with PET are important to these studies. The following section outlines some of the salient points regarding polymer blending of importance to this study.

The blending of polymers is a particularly useful technique that allows the improvement of the bulk polymer properties by imparting some of the properties of the second. Blending is often the preferable method for obtaining the desired polymer properties rather than the synthesis of an entirely new polymer due to the significant reduction in research and development costs. There are two types of polymer blend, those that are miscible and those that are immiscible.

Miscible polymer blends are those which do not separate during processing or cooling to give a dispersed phase. This type of polymer blend is rare and there are few examples. One such example is blends of polyphenylene oxide and polystyrene (sold under the trade name Noryl by GE polymers) which is a very stable one phase blend. In contrast immiscible polymer blends are much more common place and commercially important. In such blends the smaller volume fraction polymer phase separates and forms a dispersed phase of predictable morphology within the higher volume fraction polymer. To maintain the predictable morphology of the dispersed phase compatibilisation is generally required.

Compatibilisation of the two phase system is generally achieved by incorporating block copolymers or graft polymers. These block copolymers (diblocks and triblocks) and graft polymers (multigraft and single graft) reside at the dispersed/bulk phase interphase (as depicted in Figure 1.10-1).

diblock

triblock

multigraft

singlegraft
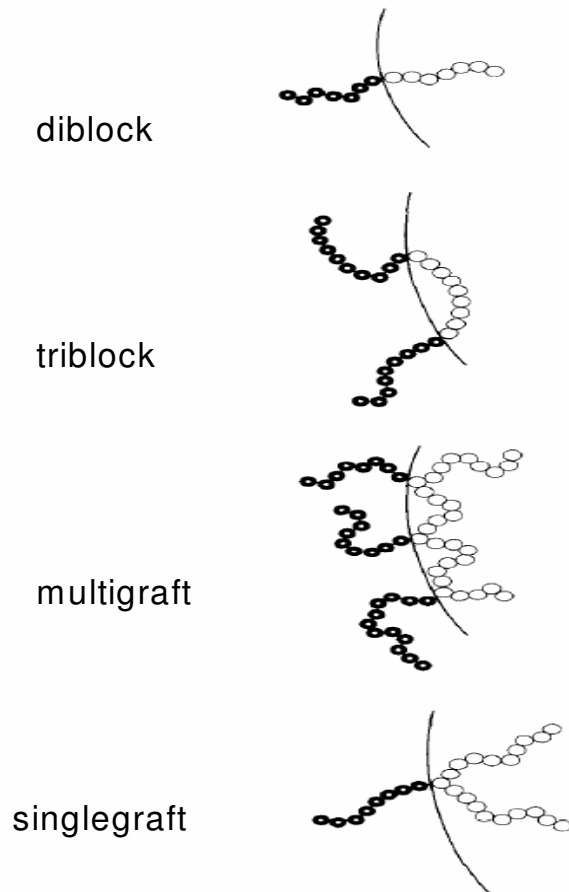
Figure 1.10-1 Block copolymers used for compatibilisation of the interface in polymer blends

The most common methods employed to produce the block copolymer compatibilisers are the addition of pre-made block copolymers, addition of reactive polymers, addition of low molecular weigh chemicals that can act as coupling agents for polymers and interchange reactions between reactive polymer groups [143, 144].

Blends of PET with polyamides are immiscible, and generally of little importance commercially. Early work focused on the use of polyamides to modify the impact properties and as nucleating agents for PET which enabled increased rate of crystallisation and reduced spherulite size [145]. Due to the well-characterised discolouration observed for PET/PA blends [146] these materials have not been a commercial success. More recently researchers have appreciated the possible improvements that can be made in gas barrier properties by blending PET with polyamides of higher gas barrier. The work of Hu et al [14, 147] has demonstrated, for instance, that MXD6 polyamide can improve the gas barrier properties of PET considerably in blends. For these types of materials, compatibilisation is not actively considered and generally occurs through end group reaction to produce block copolymers and interchange reactions that produced branched block copolymer in-situ.

1.11 The permeation of gases in polymers

The permeation of gasses in polymers occurs due to the process of diffusion, which, in turn occurs due to natural processes that tend to equal out the concentration of a species in a given environment. The diffusion coefficient of one material through another (D) is defined by Fick's first law (Equation 1.11-1).

$$F = -D \frac{\partial c}{\partial x}$$

Equation 1.11-1 Fick's first law describing diffusion of one material through another

F is the weight of the diffusing material crossing a unit area of the other material per unit time (i.e. the flux), and the differential is the concentration gradient. This permeation can also be simply described as a three stage process involving the

solution of small molecules (i.e. gas) into the polymer, followed by diffusion through the polymer (governed by the concentration gradient) and finally the emergence of the small particle on the outer surface (desorption). On the basis of this mechanism the permeation can be described in terms of diffusion and solubility thus, when the solubility obeys Henry's law (Equation 1.11-2)

$$P = DS$$

Equation 1.11-2 Relationship between permeation, solubility and diffusion

In the above equation P is the permeability, D is the diffusion and S is the solubility coefficients thus solubility and diffusion are the over-riding factors that influence the rate of permeation in polymers. As the solubility of the permeant in and its diffusion through the polymer matrix follow Henry's and Fick's laws respectively, the type and concentration of the permeant and the molecular state of the polymer (i.e. above or below Tg) are important. In the simplest case where the permeant is a fixed gas and the polymer is above the Tg, the passage of the permeant through the polymer is proportional to the Fick's diffusion constant, the Henry's solubility coefficient, and the pressure difference divided by the sheet thickness. The permeability coefficient (i.e. the product of the Fick and Henry numbers) measures relative permeation behaviour and enables comparison of the permeability of different polymers. The permeation of a gas through a polymer is dependant on the polymer, the permeant and the environment.

From the polymer point of view, given that permeation occurs due to permeant molecules passing through voids and gaps in the polymer, the state of the polymer is the first factor of significance. For example, rubbers exist as rubbery amorphous materials above Tg at room temperature and as such there is considerable free volume and chain mobility in these materials and hence considerable permeation. On the other hand glassy amorphous materials such as polystyrene are below the Tg at room temperature hence free volume and chain mobility is less than in the rubbery amorphous phase thus these materials exhibit lower permeation. In the case of semi-crystalline polymers there is considerably more molecular order and the crystal lamellae can be considered as essentially impermeable. For semi-crystalline polymers the level of permeation is much

reduced as the permeation can only occur in the amorphous regions (Figure 1.11-1) of the polymer and the extent of the permeation is governed by the level of crystallinity.
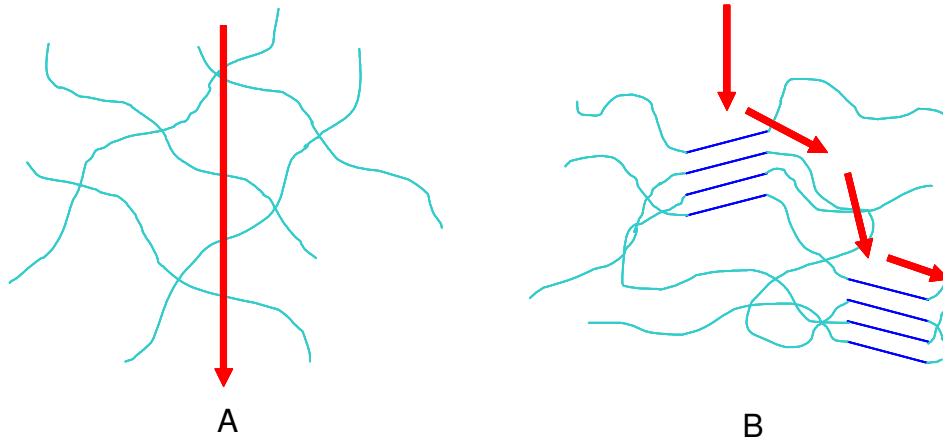
Figure 1.11-1 Schematic showing the relatively un-impeded permeation path through A, rubber compared to that of B, semi-crystalline polymer.

In addition to the morphology of the polymer, structural features can also significantly influence the rate of permeation through a polymer sample. Polymers exhibiting bulky pendant groups (e.g. polystyrene) tend to have reduced barrier performance compared to materials with no pendant groups where the polymer chains are able to closely pack (e.g. PET). In addition, the tacticity of the polymer can also inhibit the extent of close packing.

The permeation of gas through a material is also significantly influenced by the nature of the penetrant as the rate of passage through the polymer is governed by its solubility in the polymer and the size of the molecule. It is important to note that the interaction of polymer and penetrant is important as these properties could give rise to low permeability of one penetrant and high permeability of another. One such example of this behaviour is highly polar polymers containing hydroxyl groups such as poly(vinyl alcohol) (PVA) which has excellent barrier properties to gases but is a poor barrier to moisture vapour.

The final factor that can influence the permeability is the environmental conditions. Both temperature and humidity affect the permeation. In the case of polar polymers such as PVA gas barrier properties are significantly affected by humidity as PVA is plasticized by the moisture. In addition it has been observed

that a 30 – 50% increase in the permeation can be expected for every 5ºC rise in temperature.

1.11.1 Gas barrier properties of PET.

Due to it use as a packaging material the gas barrier properties of PET have been studied extensively over the years. Early works by Michaels and Brixler [148] has revealed that sorption and diffusion of gases in PET occurs exclusively in the amorphous phase hence orientation of polymer chains through stretching is advantageous to the gas barrier properties. In addition Michaels et al [149, 150] also produced two papers examining the solution and diffusion of different gases in PET over a range of temperature and these are now well characterised. More recently McGonigle et al [151] have investigated the permeability of a number of gases in biaxially orientated films and examined the dependence on free volume. The authors found that overall the orientation and distribution of crystallites plays the dominant role in determining the gas permeation behaviour in PET. Based on this the permeation of gases in PET is reduced by an increased tautness of the chains through orientation coupled with alignment of the crystalline regions thus increasing the tortuosity of the diffusion pathway [152].

1.11.2 Modelling of gas barrier properties in filled polymers.

The gas barrier properties of PET are known to be dependant on increasing the permeation pathway through increased tortuosity thus a semi crystalline polymer would be expected to have improved gas barrier compared to an amorphous rubber (as shown in Figure 1.11-1). In addition to crystallites acting as impermeable barriers to permeation, fillers can be used to increase the tortuous pathway. It has been observed that the correct morphology of filler and the correct alignment of the filler in the finished article will influence its effectiveness as a gas barrier. The most effective fillers to reduce permeation are those with a high aspect ratio thus plate-like filler particles have greater efficacy in barrier improvement than rod shaped or spherical shaped fillers (as depicted in Figure 1.11.2-1).

Due to the interest in improving and controlling the barrier properties of polymers several authors have attempted to model the permeation behaviour of filled polymers. The most well known models are those by Nielsen [153], Cussler [154], Fredrickson-Bicerano [155] and Gusev [156] although much work has also been conducted by Barrer [157], Bharadwaj [158], Xu [159] and Lu [160].

A   **B**   **C**
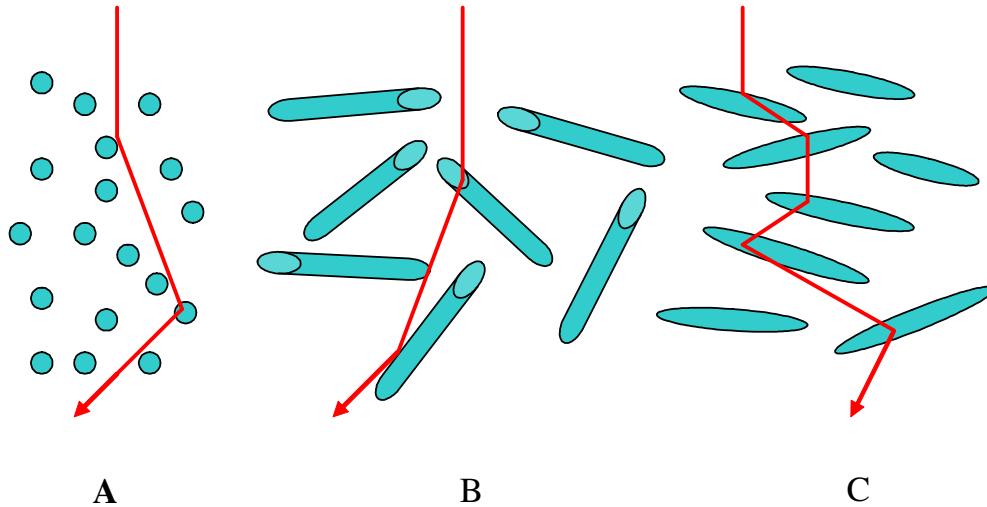
Figure 1.11.2-1 Schematic illustration of the effect of particle shape (A – spheres, B – rods and C – discs) on the diffusion pathway of a permeant through a filled polymer.

The Nielson model [153] is based on the argument of increased tortuosity and simply describes the permeability of gas in filled polymers where the particles (clay) are fully exfoliated and uniformly dispersed in the preferred orientation (i.e. parallel to the film surface. A detour pathway was thus calculated as per Figure 1.11.2-2. The development of this tortuous pathway theory allowed Nielsen to develop the model shown as Equation 1.11.2-1.

$P/P_0 = (1 - f)/(1 ^+ x/2)$

Equation 1.11.2-1 Neilsens model of permeation in filled systems

In this formula P/P_0 is the permeability coefficient (filled/unfilled system), f is the platelet volume fraction and x is the product of aspect ratio and the volume fraction.
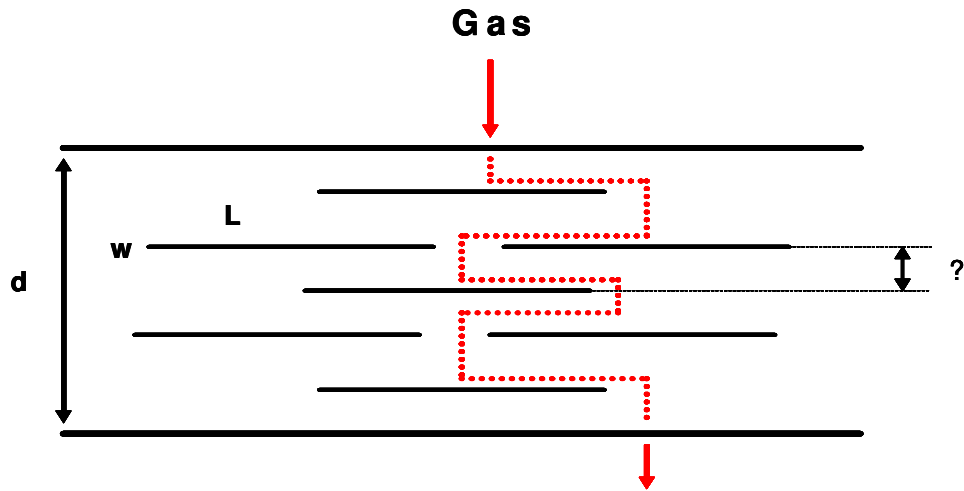
Figure 1.11.2-2 tortuous pathway proposed by Nielsen [153]

Later, Cussler observed that the Neilsen model was two-dimensional in nature and developed his own expression for permeability in a three-dimensional disordered system typical of the nanocomposites situation. This alternative model is presented in Equation 1.11.2-2.

$$P/P_0 = 1/(1 + \mu x2)$$

Equation 1.11.2-2 Cusslers 3D model for permeation in filled systems

In this expression the geometric factor μ is $\pi^2/[8 \ln(a/2)]^2$ where a is the platelet aspect ratio. The models of Neilsen and Cussler have been widely used to describe the permeation of gasses in nanocomposites but only provide a qualitative description due to their over simplification and purely geometric nature.

$$P/P_0 = [1/(2 + a_1\chi x) + 1/(2 + a_2\chi x)]2$$

Equation 1.11.2-3 Fredrickson-Bicerano model for permeation in filled systems

Fredrickson further developed and extended these models by examining the disorder and polydispersity aspects and produced Equation 1.11.2-3 which is valid over a much greater concentration. Here $a_1 = (2-2^{1/2})/4$, $a_2 = (2^+2^{1/2})/4$ and $\chi = \pi^2/\ln(a/2)$.

Finally Gusev has employed finite element analysis for the design of barrier properties for nanocomposites and developed equation 1.11.2-4.

$$P/P_0 = \exp[-(x/x_0)^\beta]$$

Equation 1.11.2-4 Gusev model for permeation in filled systems

In the Gusev formulation $\beta = 0.71$ and $x_0 = 3.47$. The models described will be used in the analysis of results in order to better understand the behaviour of the nanocomposites produced in this study. In addition, by examining a number of different models an indication as to how well the permeation behaviour is described by each of the models could be obtained.

1.11.3 Summary of the literature review

The literature review reveals that the area of clay/polymer nanocomposites has been extensively researched since the early 1990's. Polyamides have enjoyed significant focus, especially PA6 where highly exfoliated nanocomposites have been reduced. It is evident that other polyamides such as the partially aromatic MXD6, G21 and T5000 have received significantly less attention. These studies will provide improved understanding of the effects of polyamide structure and the resultant compatibility of the organoclay on nanocomposite formation and resultant nanostructure. Improvements in gas barrier of PET obtained by blending polyamides with PET are well researched in the MXD6 case but much less so for the other materials and hence new knowledge on the permeation of PET/PA blends will be obtained.

Nanocomposites produced form PET and clay have also been investigated by many authors but it is apparent that the proportion of work conducted detailing gas barrier properties is comparatively small. This study will benchmark the performance of many commercially available organoclays and also organoclays

synthesised in our laboratory in terms of gas barrier performance. In addition, further understanding of the effects of clay polymer compatibility and the effect of organoclay thermal stability will be obtained. Novel new fillers that are previously un-reported in the literature were also studied enabling new areas of research to be explored and further improving the current understanding of the gas barrier properties of PET.

2 Materials and experimental methods

2.1 *Materials studied*

The following section details the materials used in this study for the fabrication of polymer nanocomposites. In addition methods of processing and characterisation will be discussed with suitable background where required.

2.1.1 Polymers applied to nanocomposite formation

PET used throughout this study was Eastman 9221W carbonated soft drink grade PET. This grade of PET is a copolymer PET with approximately 2mol% cyclohexane dimethanol (CHDM) co-monomer added to reduce the rate of crystallisation. The material has an intrinsic viscosity of 0.79dl/g measured in a mixture of 60:40 dichloromethane/phenol solvent. Detailed technical data on properties of films and injection-moulded samples is contained in the product data sheet [161].

In this study, PA6 materials of differing viscosity (i.e. molecular weight) were obtained from several different suppliers. In Table 2.1.1-1 some of the important properties of these materials are summarised. From the data in the table it appears that the main difference in properties is the viscosity (i.e. molecular weight) and that this does not significantly affect the other properties of the polymer.

MXD6 polyamide used in this study was obtained from Mitsubishi Gas Chemical Company Inc. MXD6 is available in three different molecular weight/viscosity grades, MX6001, MX6007 and MX6012. MX6007 is generally used for packaging products and is used in these experiments and is referred to simply as MXD6 throughout. Detailed polymer properties are available in the literature [162].

Grivory G21 is described as a high viscosity amorphous co-polyamide suitable for many applications, and in particular blow moulding and film applications. Full details of properties can be found in the relevant technical literature [18].

T5000 polyamide was supplied by Degussa and is characterised by its permeant transparency and high chemical resistance. In addition, due to its amorphous nature it has low shrinkage and warpage. Detailed material properties are available in the product brochure [19].

Table 2.1.1-1 Properties of PA6 polymers studied

Supplier	DSM	BASF	DSM	EMS Grivory
Grade	F223D	UB3	F136C	F50
Application	Injection moulding	Injection moulding	Extrusion (film)	Extrusion (various)
Density (kg/m^3)	1130	1130	1130	1183
Water absorption (saturation %) (50% RH %)	10 3	9.5 3	9.5 2.5	9 3
Tensile (ISO 527) (dry/cond) Modulus (MPa) Strength @ yield (MPa) Elongation @ yield (%)	3300/ - 85/ - 4/ -	3000/1000 85/45 - / -	- / - - / - - / -	2900/750 80/40 4/15
Charpy Impact (notched) 23ºC dry (kJ/m^2) 23ºC conditioned (kJ/m^2)	11 -	5.5 60	- -	6 no break
Melting Temperature (ºC)	220	220	220	222
HDT 1.8MPa (ºC) 0.4MPa (ºC)	60 180	65 -	- -	55 130
Zero shear viscosity (Pas)	240	360	2500	5300

2.1.2 Montmorillonites

Organoclay grades from Southern Clays, Nanocor, Sud Chemie and Elementis were investigated thus covering a wide range of clay sources and organic

modifications. A summary table of the grades, supplier and organic modification (where known) are presented in Table 2.1.2–1.

Table 2.1.2–1 Summary of clay grades and chemical modification

Supplier	Grade	Surfactant	Structure
Southern Clays	Na^+	Unmodified	Sodium counter ion
Southern Clays	C10A	dimethyl, benzyl, dihydrogenated tallow	$CH_3\text{–}N^+(\text{HT})(CH_3)\text{–}CH_2\text{–}C_6H_5$
Southern Clays	C15A	dimethyl, dihydrogenated tallow	$CH_3\text{–}N^+(\text{HT})(\text{HT})\text{–}CH_3$
Southern Clays	C30B	methyl, tallow, bis-hydroxyethyl	$HOCH_2CH_2\text{–}N^+(\text{T})(CH_3)\text{–}CH_2CH_2OH$
Southern Clays	C93A	methyl, dihydrogenated tallow	$CH_3\text{–}N^+(\text{HT})(\text{HT})\text{–}H$
Nanocor	G105	Unmodified	Sodium counter ion
Nanocor	I28		Not known Aliphatic quarternary ammonium
Sud Chemie	N106	Unmodified	Sodium counterion
Sud Chemie	N2	dimethyl, benzyl dodecyl	$C_{11}H_{23}\text{–}N^+(CH_3)(CH_3)\text{–}CH_2\text{–}C_6H_5$
Sud Chemie	N3010	dimethyl, benzyl, stearyl	$C_{17}H_{35}\text{–}N^+(CH_3)(CH_3)\text{–}CH_2\text{–}C_6H_5$
Elementis	HC	Unmodified	
Elementis	B2010		Not Known

* HT – hydrogenated tallow (65% C18, 30% C16 amd 5% C14)

From Table 2.1.2–1 it can be seen that Cloisite clays provide a broad range of clay materials from highly hydrophilic (CNa^+) to highly hydrophobic (C15A). In addition it can be seen from the structure of the surfactants that there are significant differences in terms of the number of alkyl chains (e.g. 1 for C10A and C30B and 2 for C15A and C93A) and the additional substitute groups (e.g. benzyl for C10A and hydroxyethyl for C30B). For the Nanocor clays and the Elementis clays the unmodified clay is supplied and also an organoclay with unspecified surfactant. In the case of Sud Chemie clays natural clay is supplied in addition to N2 and N3010 which both have benzyl group with differing alkyl chain length. These clays were chosen due to their differing modification and general availability.

2.1.3 Nano-silica flakes

In addition to the multi-layered structured clay, single-layer nano-silica flakes were applied to this study. The materials used in this study were provided by GlassFlake Ltd. The flakes are manufactured from corrosion resistant C-glass and samples were provided with thickness of 100nm and 350nm.

Table 2.1.3 – 1 Summarised technical data for nano-silica flakes

Grade	Code	Composition	Particle size	Density (g/cm^3)	L/D
GF100nm 100nm thickness	S1	SiO_2 64-70%; Al_2O_3 3-6%; CaO 3-7%; MgO 1-4%; B_2O_3 2-5%; Na_2O 12-13%; K_2O 0-3%, TiO_2 0-3%; ZnO 1-5%	> 1000μm 0% 1000-300μm <10% 300-50μm >65% < 50μm <25%	2.60	1750
GF350nm 350nm thickness	S3	SiO_2 64-70%; Al_2O_3 3-6%; CaO 3-7%; MgO 1-4%; B_2O_3 2-5%; Na_2O 12-13%; K_2O 0-3%, TiO_2 0-3%; ZnO 1-5%	> 1000μm 0% 1000-300μm <10% 300-50μm >65% < 50μm <25%	2.60	500

Full details of these materials are given in Table 2.1.3-1. Aspect ratio i.e. L/D, due to the variable particle size of the material is estimated as the mid point of the 50µm - 300µm range (i.e. 175µm) as this makes up the bulk of the sample.

2.1.4 Divalent metal layered phosphonates

The divalent metal phosphonates synthesized for this study were produced using readily available raw materials. Starting materials were obtained directly from Sigma Aldrich and were used without any further modification. The materials used were:

Zinc acetate tetrahydrate
Calcium acetate monohydrate
Calcium nitrate tetrahydrate
Magnesium acetate tetrahydrate
Phosphorous acid
Phenylphosphonic acid.

2.2 Experimental methods

In this section, relevant methods detailing materials preparation and processing are discussed. In addition the characterisation techniques applied and theoretical background (where applicable) is discussed.

2.2.1 Determination of Hansen Solubility parameters

Hansen solubility parameters were developed by Charles Hansen in 1966 as a method of predicting the solubility of solvent mixtures. The method is additive and breaks down the total Hildebrand solubility parameter into a dispersive component, a polar component and a hydrogen bonding component. The three component nature of the model allows the components to be determined as fractions and plotted in triangular axis graphs (TEAS plots) allowing

visualisation of the potential compatibility of different materials. Detailed theory and methods are readily available in the literature [163].

2.2.2 Preparation of organoclays

The surface modification of MMT is extensively explored in the literature (chapter 2.2.1) as is the significance of processing parameters. The following sections detail the specific methods utilised in the synthesis of the organoclays used in this study.

2.2.2.1 Modification of Cloisite Na$^+$ with PVP

To modify Cloisite Na$^+$ (CEC 92meq/100g), 20g of the pristine clay powder was mixed with 500ml of deionised water in a large beaker for one hour while the temperature was raised to 50ºC. A further solution of 50wt% (10g) PVP with deionised water was also mixed for one hour while raising the temperature to 50ºC. After one hour the two mixtures were combined and the temperature was raised to 90ºC with stirring for approximately three hours. After mixing a large proportion of the water was removed and a thick paste like material remained. The resultant clay/PVP organoclay mixture was poured onto flat aluminium trays and the moisture was allowed to evaporate for a period of two weeks. The dry clay was ground using a mortar and pestle and further dried for 24hours under vacuum.

2.2.2.2 Modification of Cloisite Na$^+$ with cetyl pyridinium (Br/Cl)

Cloisite Na$^+$ (CEC 92meq/100g) was modified with both cetyl pyridinium bromide and cetyl pyridinium chloride at one and a half times the CEC of the clay to ensure good coverage of the clay interlayer. The procedure used was to disperse 40g of the Cloisite Na$^+$ in 1l deionised water for one hour while increasing the temperature to 50ºC. Meanwhile the required quantities of cetyl pyridinium chloride and cetyl pyridinium bromide were calculated as follows and dispersed in 500ml deionised water.

Cation exchange capacity (CEC) Cloisite Na$^+$ = 92meq/100g

1.5 X CEC = 138meq/100g

RMM CPBr 384.44 therefore 1meq = 0.384g

RMM CPCl 339.986 therefore 1meq = 0.340g

Therefore

52.992g CPBr/100g clay = 21.197g/40g clay @ 1.5 X CEC

46.920g CPCl/100g clay = 18.768g/40g clay @ 1.5 X CEC

After one hour the two mixtures were combined and the mixture was stirred for 24hrs at 50ºC. After 24hrs the solid was separated by centrifuge and washed with 50/50 mixture of deionised water/ethanol. The centrifuge procedure and washing procedure was repeated three times. The final wet clay was dried for 24hours at 90ºC under vacuum to remove the excess water after which the material was ground using a mortar and pestle and then further dried for 24hrs at 90ºC under vacuum.

2.2.2.3 Modification of Cloisite 30B with epoxy

Cloisite 30B was modified with epoxy using a method similar to that described by Lai and Kim [135]. Initially 30g of Cloisite 30B was dispersed in 1l of deionised water to which 100ml of ethanol was added. The clay/water/ethanol mixture was stirred for one hour and the temperature raised to 50ºC. The diepoxide diglycidyl ether of bisphenol A (15g) was added to 150ml of acetone and the mixture was also stirred for 1hr while raising the temperature to 50ºC. After one hour the two mixtures were combined and mixed further while increasing the temperature to 80ºC. Once a significant portion of the liquid had been evaporated (4hrs) the remaining slurry was poured into an aluminium tray and dried in a vacuum oven at 100ºC for 24 hours.

2.2.3 Preparation of divalent metal layered phosphonates

All the DMLP's were prepared using the methods described by Rule [61] hence only brief experimental details are included.

Zinc (phosphite-co-phenylphosphonate) (ZPcP) was made by the reaction of zinc acetate tetrahydrate (0.2M) with phosphorous acid (0.1M) and phenylphosphonic acid (0.1M). In practice 43.8g zinc acetate tetrahydrate was added to 200ml of hot (70ºC) deionised water and stirred for ten minutes. Separately 8.2g phosphorous acid and 15.8g phenylphosphonic acid were added to 200ml of hot (70ºC) water and stirred for 10minutes. The zinc acetate solution was then added drop wise to the phosphorous acid/phenylphosphonic acid solution and the resultant mixture stirred for two hours at 75ºC. A white precipitate was removed by filtration and washed three times with deionised water. The ZPcP was then dried for 24hrs at 80ºC under vacuum. 27.49g of product was recovered.

The synthesis of calcium (phosphate-co-phenylphosphonate) (CPcP) was achieved through the reaction of calcium acetate monohydrate (0.27M) with phosphorous acid (0.08M) and phenylphosphonic acid (0.12M). Experimentally 40g of calcium acetate monohydrate was stirred into 300ml of deionised water. Into a separate container 19g of phosphorous acid, 6.6g phenyl phosphonic acid and 300ml of deionised water were stirred. The two mixtures were combined by adding the calcium solution drop wise and the temperature raised to 75ºC The mixture was maintained at 75ºC for two hours with stirring. The resultant precipitate was then filtered, washed and dried as described for ZPcP. After drying 19.85g of the CPcP was recovered.

For the synthesis of calcium bis phenylphosphonate (CP) calcium nitrate tetrahydrate (0.125M) was reacted with phenylphosphonic acid (0.125M). In practice 29.5g of calcium nitrate tetrahydrate and 39.5g phenylphosphonic acid were each dissolved separately in 125ml each of hot (70ºC) deionised water. The calcium solution was added drop wise and the resultant mixture was mixed for six hours at 80ºC. The resultant filtrate was recovered and washed and dried as per the previous examples. In total 28g of the product was recovered.

The synthesis of the final DMLP, magnesium (phosphite-co-phenylphosphonate) MPcP was conducted by reacting magnesium acetate tetrahydrate (0.2M) with phosphorous acid (0.1M) and phenylphosphonic acid (0.1M). A solution of 42.8g

magnesium acetate tetrahydrate in 250ml hot (70ºC) deionised water was added drop wise to a solution of phosphorous acid (8.2g)/phenylphosphonic acid (15.8g) also in 250ml hot deionised water. The resultant mixture was heated for two hours with stirring under reflux after which the usual filtration, washing and drying procedures were applied. After drying 28g of the product was recovered.

2.2.4 Melt processing of nanocomposites

Melt processing of the nanocomposites was conducted on a 16mm Thermosprism intermeshing co-rotating twin-screw extruder capable of extruding at both 40/1 and 24/1 L/D ratio. Figure 2.2.4-1 shows the screw profile including mixing sections and a photograph of the equipment.
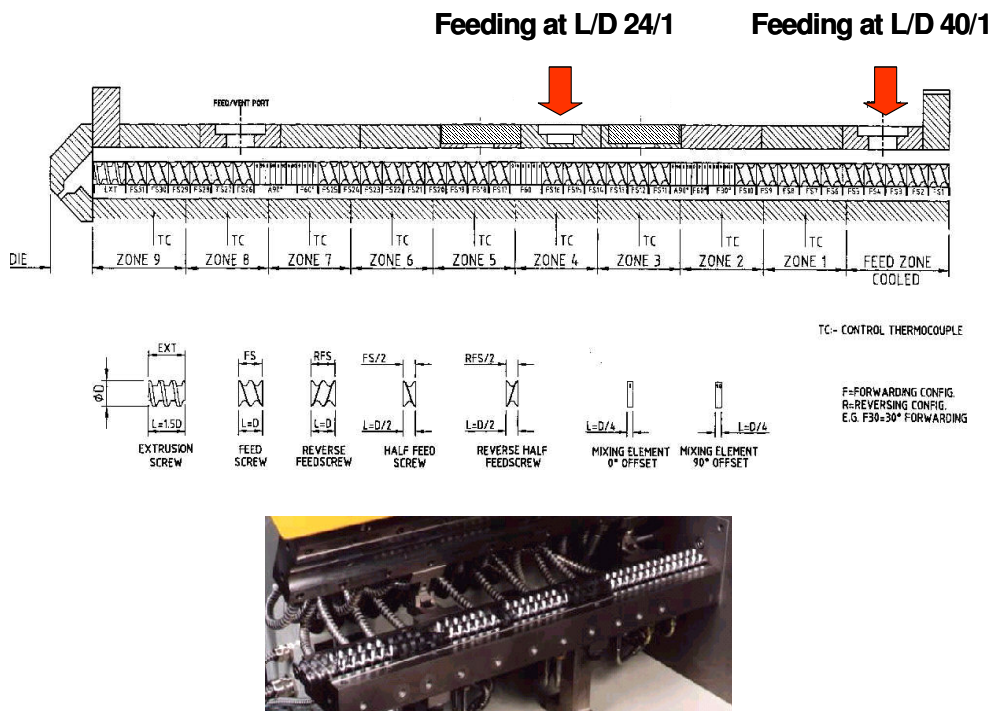
Figure 2.2.4–1 Screw profile for Prism 16mm twin-screw extruder

All experiments within this study were conducted on 24/1 L/D ratio similar to previous authors as it was felt that 40/1 L/D would induce un-necessary degradation of polymer and clay especially considering the high processing temperatures required for many of the polymers used in this study. Prior to extrusion all the polymers were dried under vacuum for the appropriate time

under the appropriate temperature as indicated. In addition the fillers were also dried. Details of the drying procedures are set out in Table 2.2.4-1.

Due to the differences in the materials processing conditions were altered to suit the parameters of the particular polymer. The conditions employed for each polymer for direct formation of nanocomposites are shown in Table 2.2.4-2.

In addition to the polymer/filler nanocomposites produced a number of blends were also made. These blends were made with MXD6 and have variation in polymer ratios, different filler loadings and with and without catalyst. These further materials and the processing conditions are shown in Table 2.2.4–3.

The main parameter where adjustment was required was the polymer feed rate. This was adjusted to allow extrudate with sufficient stability for stranding and pelletising to be carried out.

Table 2.2.4–1 drying conditions for materials prior to extrusion

Code	Description	Drying temperature (°C)	Drying time (hrs)
F223D	PA6	80	12
UB3	PA6	80	12
F136C	PA6	80	12
F50	PA6	80	12
MXD6	Barrier Nylon	100	12
G21	Barrier Nylon	100	12
T5000	Engineering Nylon	100	12
PET	CSD grade	160	8
Montmorillonite	Raw/organoclays	100	12
GF	Nano-silica	160	8
DMLP	Phosphonates	80	24

Table 2.2.4-2 Processing conditions for Polymer/filler nanocomposites

Polymer	Filler	Wt% Filler	Barrel temperature (°C)	Screw speed (rpm)	Feed rate (%)	Extruder Torque (%)
PA6	Clay	5	230	350	15	50-60
MXD6	Clay	5	250	200	15	30-40
G21	Clay	5	250	200	15	60-75
T5000	Clay	5	270	200	20	50-70
PET	Clay	5	270	200	15	45-75
PET	Nano-silica	1 2	270 270	300 300	15 15	45-90 60-70
PET	DMLP	2.5	270	200	10-15	60-70
PET	DMLP ext 2	2.5	270	200	18	50-90

Table 2.2.4-3 Composition and processing conditions for PET blends

MXD6 wt%	Clay (wt%)	Catalyst (wt%)	Barrel temp (°C)	Screw speed (rpm)	Feed rate (%)	Extruder torque (%)
5	-	-	270	200	15	40-60
5	0.5	-	270	200	20	50-65
5	0.5	0.2	270	200	25	60-80
5 -	- 0.5	- -	270 270	200 200	20 25	60-80 60-70
5 -	- 0.5	0.2 -	270 270	200 200	20 25	60-80 60-70
20	2	-	270	200	15	35-50
20	2	0.5	270	200	15	35-45
20 -	- 2	- -	270 270	200 200	15 20	40-60 40-50

MXD6 wt%	Clay (wt%)	Catalyst (wt%)	Barrel temp (°C)	Screw speed (rpm)	Feed rate (%)	Extruder torque (%)
20	-	0.2	270	200	15	40-60
-	2	-	270	200	20	40-50
20*	-	-	270	200	20	55-75
20*	-	0.2	270	200	20	55-75

*MXD6 has been previously blended with 10wt% C93A organoclay.

2.2.5 Characterisation techniques

A wide range of characterisation techniques were employed to investigate the properties of nanofillers and the polymer/filler nanocomposites. Various microscopy techniques were employed to examine the morphology of the fillers in conjunction with XRD experiments whilst TGA was utilised to investigate the thermal stability and degradation of the fillers. For the polymer/filler nanocomposites XRD and microscopic techniques were again employed to investigate the dispersion of the nanocomposites. DSC was utilised extensively to investigate the effect of nano-fillers on the crystallisation behaviour of the nanocomposites. The final major technique employed was the determination of CO_2 loss from bottles. Other techniques such as melt capillary rheometry were employed for rheological assessment as required. All the methods employed are described in the following sections.

2.2.5.1 X-Ray Crystallography (XRD)

X-ray scattering techniques are a powerful tool for investigating crystal structures and other long range morphological characteristics of many materials. Theoretical aspects of XRD are adequately discussed by many authors [164] hence only a brief description of the technique is included. A simple illustration of XRD set up is shown in Figure 2.2.5.1–1.
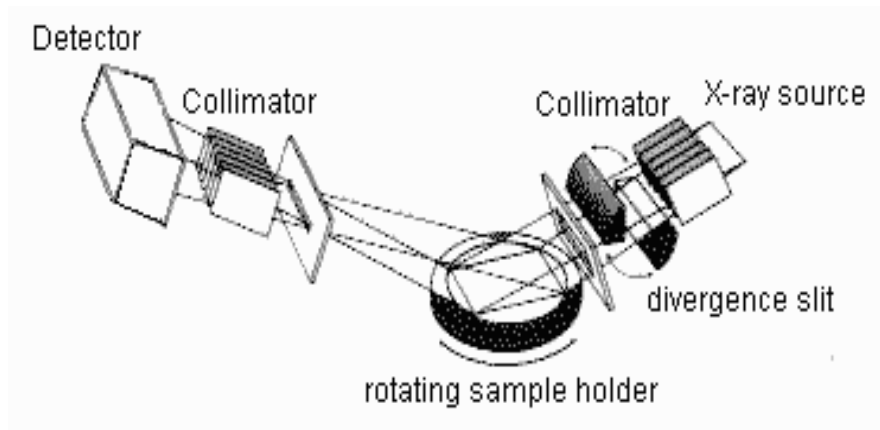
Figure 2.2.5.1–1 Illustration of XRD set up

In general the x-rays are fired from the source onto the sample and the diffracted x-rays are collected in the detector. This data is measured and intensity peaks at particular diffraction angles can be used to ascertain information on particular spacial arrangements within a material sample. For polymer nanocomposites XRD has proved particularly useful for the determination of interlayer spacing in clays and resultant nanocomposites via Bragg's equation (Equation 2.2.5.1-1)

$$n\lambda = 2d\ \sin\Theta$$

Equation 2.2.5.1–1 Braggs equation for calculation of distance between adjacent clay layers

The term n represents an integer, λ is the wavelength of the incident x-ray beam and d is the variable distance between atomic layers in a crystal (or between clay layers).

In addition to the interlayer spacing of materials, XRD can also be used to elucidate details on the crystal domain size using Scherrer's Equation (Equation 2.2.5.1-2) [164]

$$\text{Crystallite size} = K\lambda/FW\cos\theta$$

Equation 2.2.5.1-2 Scherrer's equation for calculation of crystal size

In the equation K is the crystal shape factor (usually between 0.85 and 0.99), λ is the wavelength, FW is the peak width at half height and $\cos\theta$ is the Bragg angle. Using this equation the crystallite domain size for a specific peak can be determined giving a size for a preferred crystal axis. In order to gain a more general idea of crystallite domain size it is common to analyse multiple peaks. It is important to note that the crystallite size is the size of repeating crystalline units and therefore does not represent the particle size of the material hence this method has not been employed in these studies as good approximations of particle size have been obtained through microscopy and literature sources.

In addition to information that can be obtained from Bragg's and Scherrer's equations, much can also be learned from the XRD traces themselves. For instance when XRD scans of clay and resultant nanocomposite are compared and there is no significant change in the diffraction angle or intensity (Figure 2.2.5.1-2) it can be surmised that the clay has not been dispersed in the clay and exists as a micro dispersion in the polymer matrix. In contrast when the clay has been intercalated by the polymer without significant reduction in the particle size (i.e. reduction of the number of clay layers per clay particle) an XRD trace similar to that observed in Figure 2.2.5.1-3 would be expected. In this case, the peak position has shifted indicating a change in the clay interlayer distance but the intensity of peak is not significantly reduced.
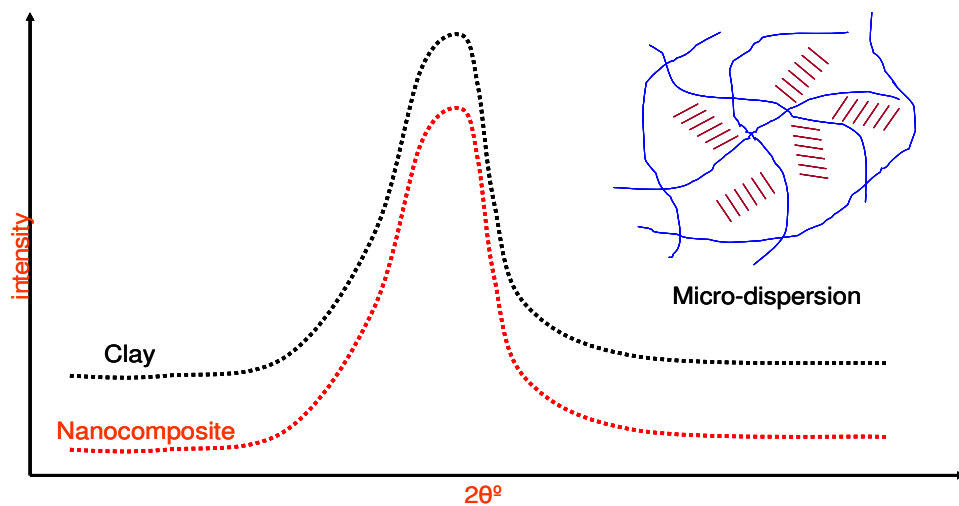
Figure 2.2.5.1-2 Schematic representation of clay micro-dispersion in a polymer matrix

90
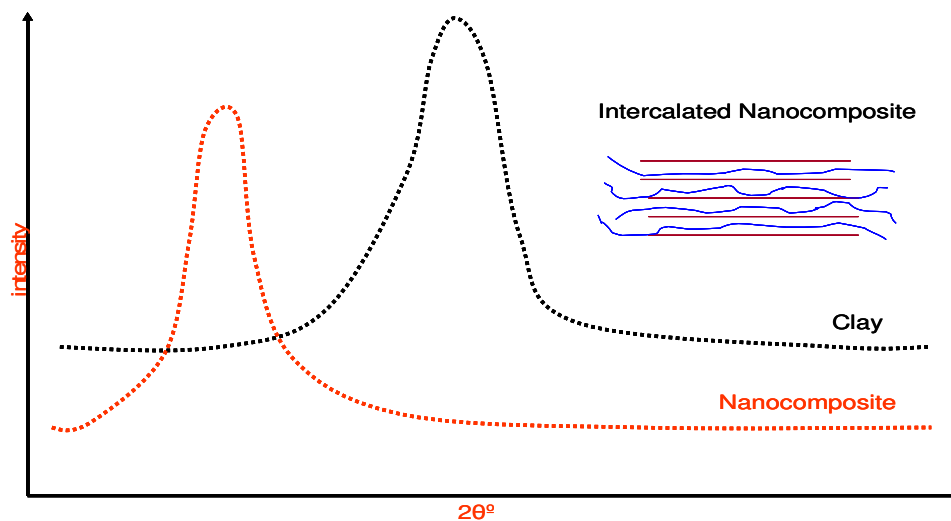
Figure 2.2.5.1-3 Schematic of polymer intercalated clay

The final type of commonly seen XRD diffraction pattern is observed for an exfoliated composite and is generally a trace without any peak evident in the low two theta angle region (Figure 2.2.5.1-4). In this case it is generally accepted that the absence of a diffraction peak indicates delamination of the clay layers and that the clay is highly dispersed in the polymer matrix.

One final common feature of XRD spectra that is often observed is that of differences in the number of orders of a reflection that are observed (Figure 2.2.5.1-5). In this case, a large number of (00) reflections are present indicating a highly regular and repeatable layered structure is present. In contrast where only a (001) reflection is observed the layered structure may be more disrupted.
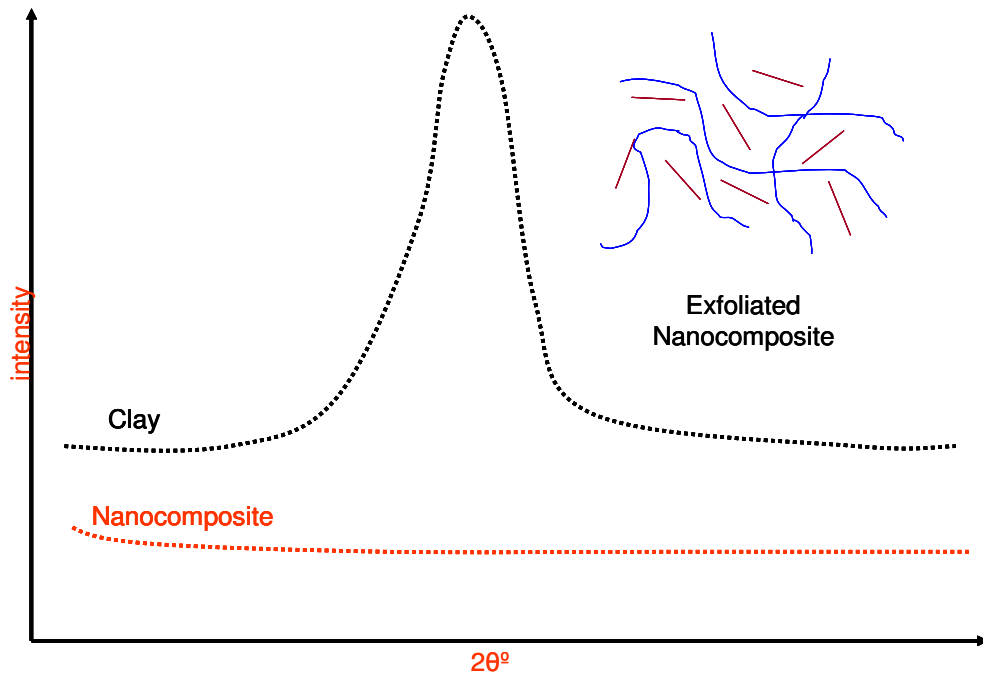
Figure 2.2.5.1-4 Schematic of exfoliated polymer clay nanocomposite

In addition to the quite well defined XRD spectra that are readily interpreted other types of spectra are also common such as that shown in Figure 2.2.5.1-6
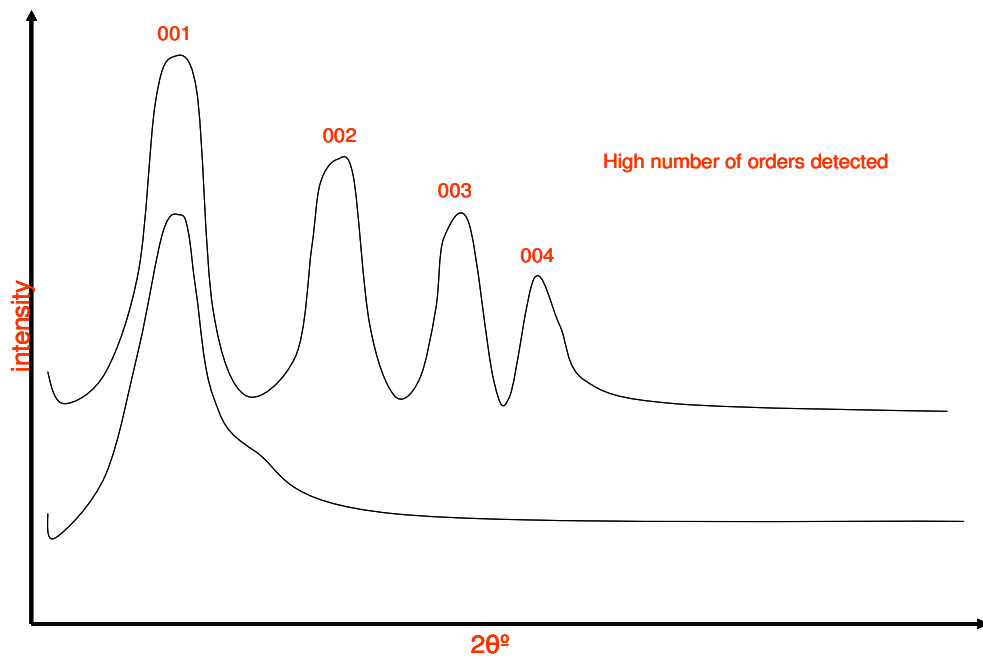
Figure 2.2.5.1-5 Schematic comparing high number of (00) orders

.
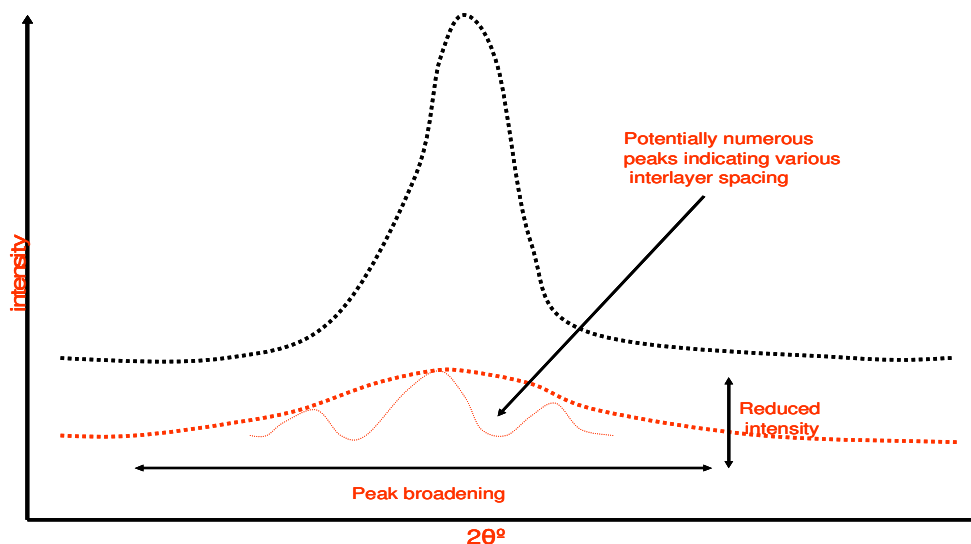
Figure 2.2.5.1-6 Schematic of peak broadening and intensity reduction

Here the peak position has remained constant but the peak width is significantly increased. In addition to the broadening of the peak the intensity is also reduced. In a case such as this several features of the nanocomposite morphology could be responsible. For instance the reduction of peak intensity could be due to a low concentration of species, possibly due to a chopping down of the number of clay layers in each clay particle. A second explanation could be that the peak has broadened due to a variable spacing of the interlayer i.e. that the broad peak hides many small peaks hence the low intensity and large width of the peak or the size of the crystal domains is small.

A second example of scans with difficult to interpret shape is shown in Figure 2.2.5.1-7. Here there is a gradual increase in the intensity without the resolution of a clear peak. Overall this type of XRD response may be indicative of the presence of some structures with regular structure over a larger distance or, similar to the previous case a number of different species with similar spacings.

Overall, the scan types illustrated in Figures 2.2.5.1-6 and 2.2.5.1-7 indicate that care needs to be taken when analysing XRD data as significant features of structure may be hidden and not readily apparent.
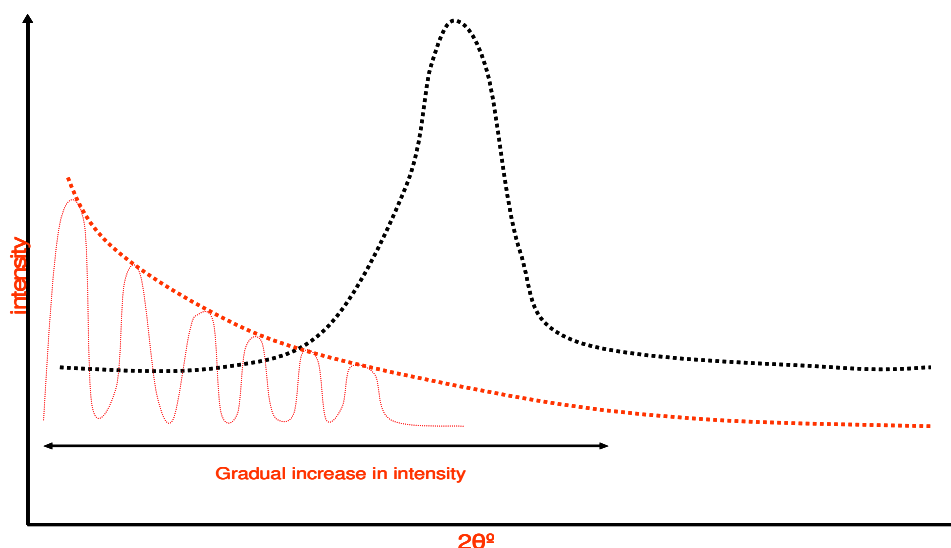
Figure 2.2.5.1-7 Schematic of intensity increase without defined peak

In these experiments 2 diffractometers were used. The initial polyamide samples were all tested using a Philips X-ray diffractometer set to 30mA current and 40kV voltage with 1º/min scanning rate at 0.02º per step. Chromium was used as the radiation source and has wavelength, $\lambda = 0.229$nm to allow the determination of higher interlayer distances than with Cu X-ray source on equipment limited to a minimum two theta angle of 3º. All experiments were conducted on plate shaped samples of dimension 30mm x 30mm x 3mm which had previously been produced using a manual injection moulding machine. Samples of clays, novel blends and PET nanocomposites were tested on a Pananalytical X'pert Pro x-ray diffractometer set to 35mA current, 45kV voltage with a scan step size of 0.008 and a time per step of 30.48 seconds. Copper x-ray source was used with wavelength, $\lambda = 0.154$nm as this equipment allowed a minimum angle of 1º to be scanned.

2.2.5.2 Microscopic techniques

2.2.5.2.1 Polarised light optical microscopy (POM)

Optical microscopy was used to investigate the dispersion of clay in the polymer matrices on a micro-scale. All optical microscopy was conducted on a Zeiss Axio Image M1m microscope equipped with filters for crossed polarised light and

integrated software and camera. The microscope was attached to a computer with incorporated software for image analysis and scaling. All of the samples were prepared simply by cutting sections from blown bottle walls.

2.2.5.2.2 *Scanning electron microscopy (SEM)*

Scanning electron microscopy was utilised to provide higher resolution images of micro-structure where required. Scanning electron microscopy was conducted on a Jeol JSM-840A scanning electron microscope with 6×10^{-8} amps probe current and 10kV accelerator voltage.

2.2.5.3 Differential scanning calorimetery (DSC)

DSC was the principle method used in these studies to examine the crystallisation behaviour of nanocomposites compared to their parent polymer. Briefly DSC entails the measurement of the change of heat capacity in a sample compared to that of a reference sample and allows the determination of thermal transitions such as Tg, Tc and T_m. A simple schematic of DSC apparatus is shown in Figure 2.2.5.3-1 while detailed theoretical information regarding DSC is readily available in the literature [165].
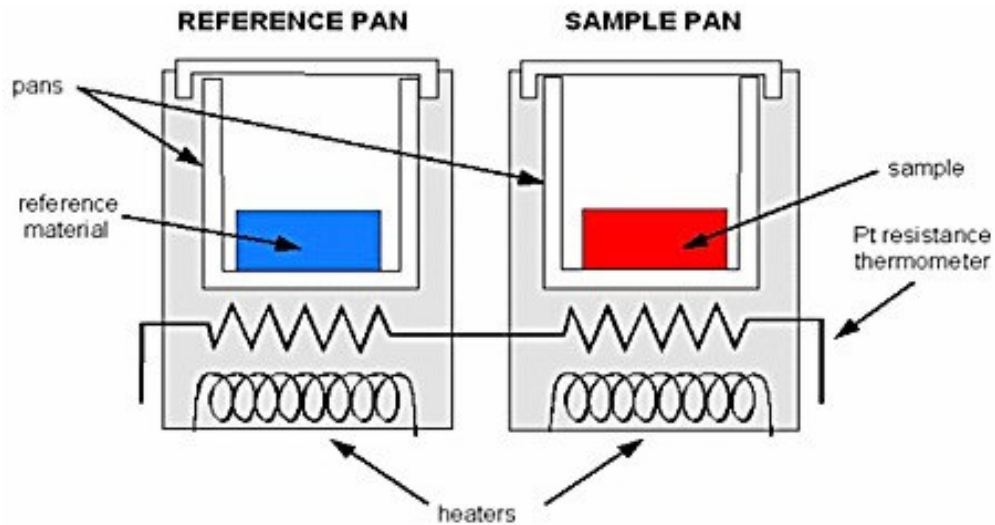
Figure 2.2.5.3–1 Schematic showing DSC equipment

95

In addition to pinpointing thermal transitions the data provided by DSC can also be used to calculate the crystallinity of a sample using equation 2.2.5.3-1 [165].

$$X = (\Delta H_m - \Delta H_c)/\Delta H_m^{\theta} \, x100\%$$

Equation 2.2.5.3-1 Calculation of crystalline content from DSC

In the equation χ is the percentage crystallinity, ΔH_m and ΔH_c are the respective enthalpies of melting and crystallisation and ΔH_m^{θ} is the enthalpy of melting for a one hundred percent crystalline sample of the polymer (obtained from the literature).

Tests were conducted using a heat cool heat cycle whereby an initial heating scan is conducted to give information on the effect of processing on the materials followed by a hold period to ensure all previous thermal history is removed from the sample. Next a controlled cooling stage is employed to enable a comparative study of crystallisation when cooling from the melt. The final stage of the DSC experiment is the second heat where the melting behaviour of the material can be studied. The DSC analysis was conducted over a suitable temperature range for the polymer under investigation (e.g. PA6 50ºC – 250ºC, PET 50º - 300ºC) with a heating and cooling rate of 10ºC/minute and 3minutes hold after each heating or cooling procedure.

The equipment used in these studies was a Perkin Elmer DSC7 differential scanning calorimeter. The calorimeter was calibrated using Indium as a standard with a heating rate of 10ºC/minute. It is acknowledged that DSC experiments for polyamides were conducted at a higher heating rate (20ºC/minute) and also that no allowance was made for the cooling hence there is likely to be a slight offset in the results. Nevertheless it was decided that this slight offset could be tolerated in view of the fact that it would not affect the conclusions and that there were a large number of samples to test.

2.2.5.4 Thermo gravimetric analysis (TGA)

Thermogravimetric analysis (TGA) is commonly used technique used to analyse the changes in weight of materials over a range of temperatures. As per other characterisation techniques employed the theoretical aspect of TGA are well discussed in the literature [166] therefore only a brief description of the technique and the relevant experimental details are included.

The TGA analyser consists of high precision balance with pan that can be loaded with sample. The pan and sample are placed in a small electrically heated furnace fitted with a thermocouple and the temperature is increased in a controlled manner as per individual testing requirements. A computer is used to plot the resulting weight loss against temperature curve. The furnace is purged with the required gas (usually air or nitrogen). A simple schematic of a typical TGA set up is shown in Figure 2.2.5.4 - 1.
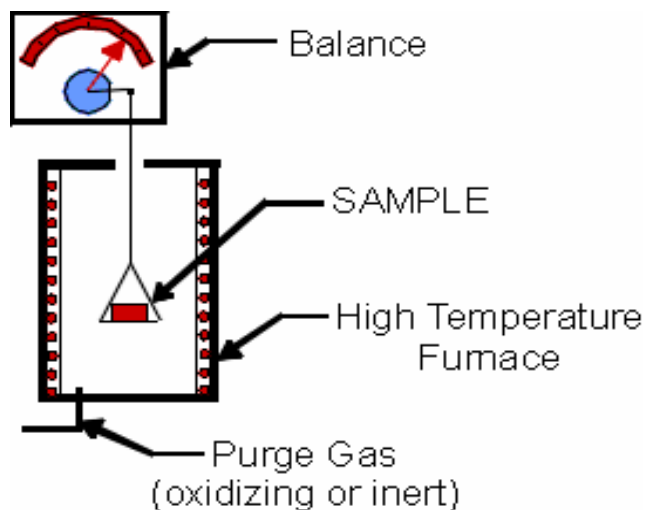
Figure 2.2.5.4 – 1 Schematic diagram of typical TGA set up

TGA experiments in this study were carried out on a Perkin Elmer Pyris 1 TGA. Tests were carried out in both air and nitrogen atmospheres with a heating rate of 20ºC per minute over a temperature range of 50ºC to 800ºC. Perkin Elmer software was used to calculate derivative curves to enable the determination of peak weight loss temperatures.

2.2.5.5 Melt rheology

Capillary rheometer measurements on PA6 samples were carried out on Malvern capillary rheometer at 230ºC (i.e. the same temperature as nanocomposite processing). The tests where carried out over a shear rate range of $50s^{-1}$ to $3000s^{-1}$. The PA6 samples were dried overnight in a vacuum oven prior to the melt rheology measurements.

2.2.5.6 Fabrication of plaques for PET/PA compatibility evaluation

Plaques were produced by moulding PET with 5wt% of the relevant polyamide using a BOY 30M injection moulding machine. The machine was fitted with a plaque mould of 60mm x 40mm x 2.5mm and samples were produced using standard processing parameters for PET moulding retained in the computer memory of the machine.

2.2.6 Measurement of CO_2 loss

For the purpose of this study, CO_2 loss measurements were conducted on finished product (i.e bottles) rather than film in order that the materials under investigation could be assessed under processing conditions as close to application as possible. The following sections outline the experimental details for the production and testing of bottles for CO_2 egress.

2.2.6.1 Fabrication of test samples

The production of bottles for CO_2 egress testing was carried out by a two-stage process consisting of firstly injection moulding of bottle preforms followed secondly by stretch blow moulding of bottle preforms into bottles.

Injection moulding of bottle preforms was carried out on a Husky GLS160 injection moulding machine fitted with a hot runner system and two cavity, 35g, 1l preform tool. The machine was used under standard operating conditions established for the production of preforms using this tooling. Prior to moulding

all materials required pre-drying. Pristine PET used in this study was dried at 160ºC for at least 4hrs prior to use using Con Air drying equipment. Nanocomposite masterbatches and compound materials were dried in a convection oven at 160ºC for at least 12hrs prior to injection moulding. Prior to injection moulding nanocomposites and pristine materials were pre-blended in the dry state using 5l buckets with sealable lids. The proportions of masterbatch and pristine PET were modified in order to give final clay weight of 0.75% in the composite. This figure was calculated on the inorganic content and adjustment of the nanocomposite masterbatch loading was made based on the surfactant level in the clay as determined from TGA. Nano silica flake loadings were pre-determined from the extrusion process while loadings of DMLP were fixed at 1500ppm (i.e. 0.15wt%). In the case of blends the dry pre-blend mixture was formulated so that a final bottle composition of 94.5% PET, 5% MXD6 and 0.5% organoclay was obtained.

Injection stretch blow moulding of the preforms to produce bottles was carried out without further treatment of the preforms. The preforms were blown into bottles on a Sidel SB-01 electronic stretch blow moulding machine fitted with a petaloid base 1l carbonated sort drink bottle mould. The machine ovens were set to a standard profile for blowing this design of bottles while the output of the ovens was adjusted in order to give a preform temperature of 102ºC $^+$/- 3ºC prior to blowing. The machine was set to run at 1200 bottles per hour.

2.2.6.2 Permeation testing

The CO_2 loss measurements were conducted on the bottles using a simple weight loss method. In this method the bottles were filled with an accurately weighed (to four decimal places) quantity of dry ice (approximately 7g). The bottles were then sealed with bottle caps containing an ethylene vinyl alcohol barrier insert. The bottles were then weighed periodically using a four-place balance in order to determine the weight loss of CO_2 from the package over time. All bottles were stored under ambient conditions hence a control was required for each test set.

The results are expressed as the barrier improvement factor which is the ratio of the CO_2 egress rate of a control bottle compared to that of the barrier bottle under investigation.

3 Characterisation of clays

The clays used in this study were characterised for the purpose of investigating the effects of organoclay/polymer compatibility on nanocomposite formation. In addition TGA analysis enabled the effect of organoclay thermal stability on the nanocomposite formation to be investigated.

3.1 Morphological characterisation of clays

3.1.1 Micro–morphology from SEM

The micro–morphology of the clays can be investigated using SEM to show the particle size of agglomerates and their shape and give indication of any other features of note. In each case the parent unmodified clay is examined (i.e. Cloisite Na^+, Nanomer G105, Nanofill 106 and Bentone HC). In Figure 3.1.1-1 low magnification SEM micrographs of each of the raw clays are shown for comparison.
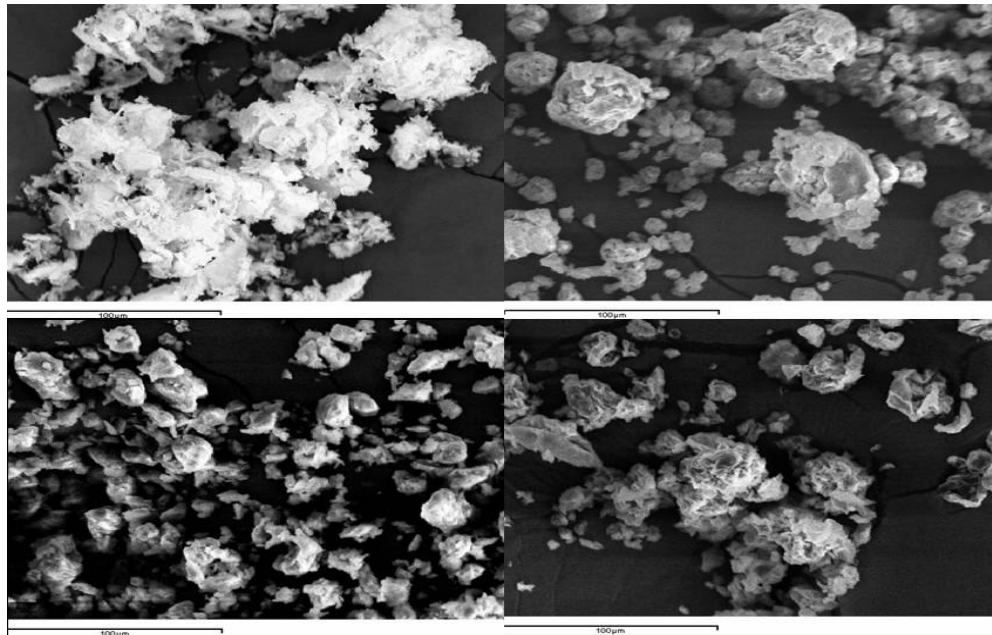
Figure 3.1.1-1 Low magnification (100µm scale bar) SEM images of (A) CNa⁺, (B) G105, (C) N106 and (D) Bentone HC raw clays

From the SEM micrographs it is evident that CNa^+ is more angular in nature than the other clays and consists of very loose agglomeration of particles in the region of 10-20μm in size. In the case of the other clays the particles have a much more rounded shape and appear more loosely agglomerated. The Nanomer G105 has most particles in the range of 10μm with some small agglomerations up to 50μm while the N6 has a generally more even particle size of about 10μm. The final clay, Bentone HC has a more loosely agglomerated structure akin to CNa^+ but with the more rounded particles similar to G105 and N106. In Figure 3.1.1-2 SEM images with higher resolution are shown.
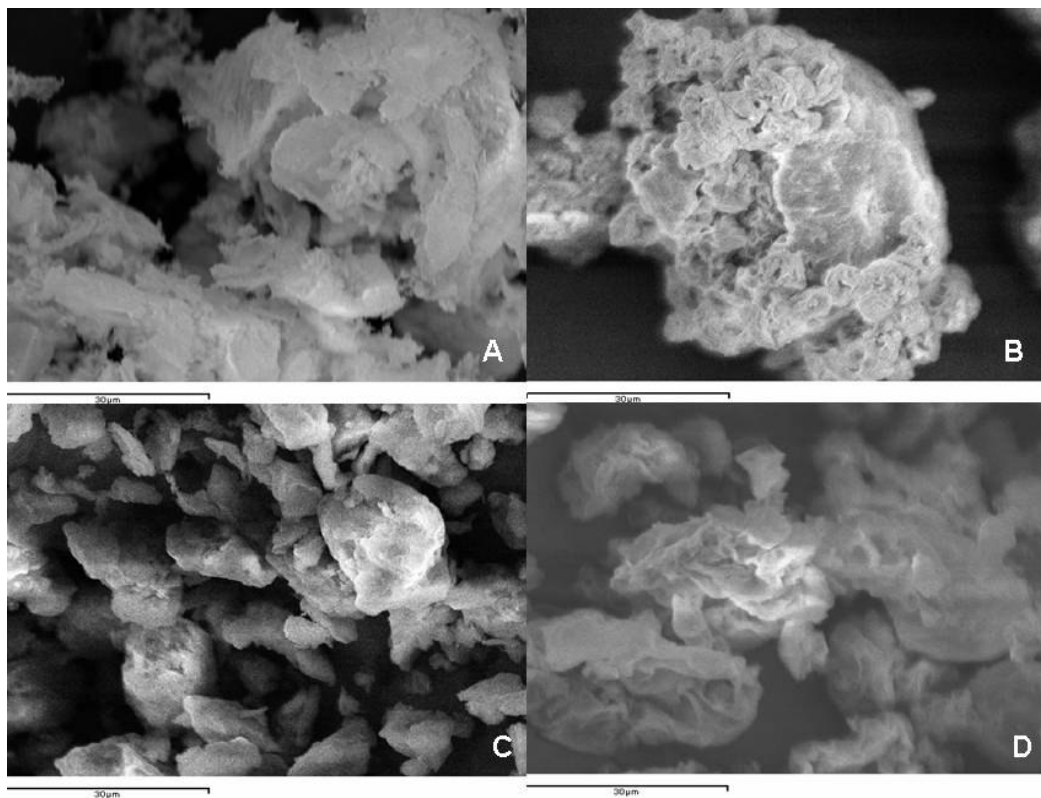
Figure 3.1.1-2 Medium magnification (30μm scale bar) SEM images of (A) CNa^+, (B) G105, (C) N106 and (D) Bentone HC raw clays

From the higher magnification SEM micrographs the agglomerated structure of the clays particles is more clearly evident. In addition it can be observed that the CNa^+ is much more angular and irregular in shape and size compared to the other clays.

3.1.2 Nano – morphology from XRD

The nano-morphology of the raw and organoclays was studied using XRD as described previously. The main purpose of these investigations was to determine the original (001) basal spacing. This allows a more detailed interpretation of the nano-structure of the nanocomposites to be made.

3.1.2.1 Commercial clays

A wide range of commercial clays was investigated from a number of suppliers. Southern Clays provided a selection of their Cloisite materials with varying hydrophobicity. The XRD scans for these materials are included below as Figure 3.1.2.1–1.
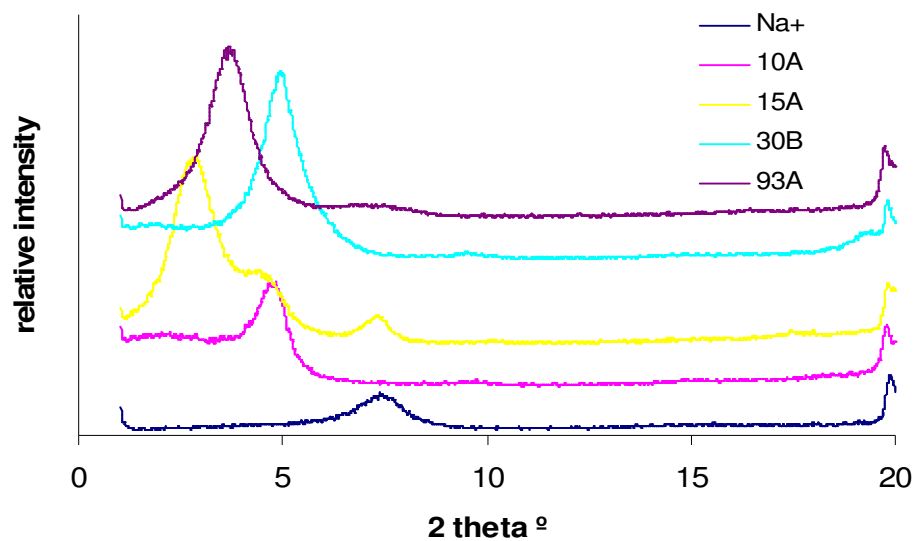
Figure 3.1.2.1–1 XRD spectra for Closite clays produced by Southern Clays Inc.

It is immediately evident that the (001) peak position is variable dependant on the organic modification applied to the clay. The position of this peak provides us with the (001) d spacing i.e. the distance between two adjacent clay layers via Braggs equation. Thus calculated (001) d values for these materials are 1.178nm (Na$^+$), 1.846nm (C10A), 3.065nm (C15A), 1.760nm (30B) and 2.356nm (C93A). These figures indicate that the distance between the clay layers is dependant on

the surfactant used in the case of modified clays. In the case of CNa^+ the distance of 1.178nm is the (001) distance for unmodified clay. When a surfactant is added the space between adjacent layers is increased to accommodate the new molecule and hence a larger (001) spacing is observed. The extent of the increase is largely dependant on the size and quantity of the new molecule, although polarity of the surfactant may also play a role. In the case of C15A and C93A for example the main structural difference is the incorporation of a second alkyl tail group and an increased surfactant concentration. These differences result in a considerably larger d spacing for C15A compared to the C93A. In the case of C30B the alkyl chain is of similar length to C93A with concentration slightly lower. The resultant d space is smaller indicating that the polar ethyl hydroxyl groups have some influence over the final d spacing.

In Figure 3.1.2.1-2 the XRD scans for Nanocor clays G105 (unmodified sodium clay) and I28 organoclay are shown.
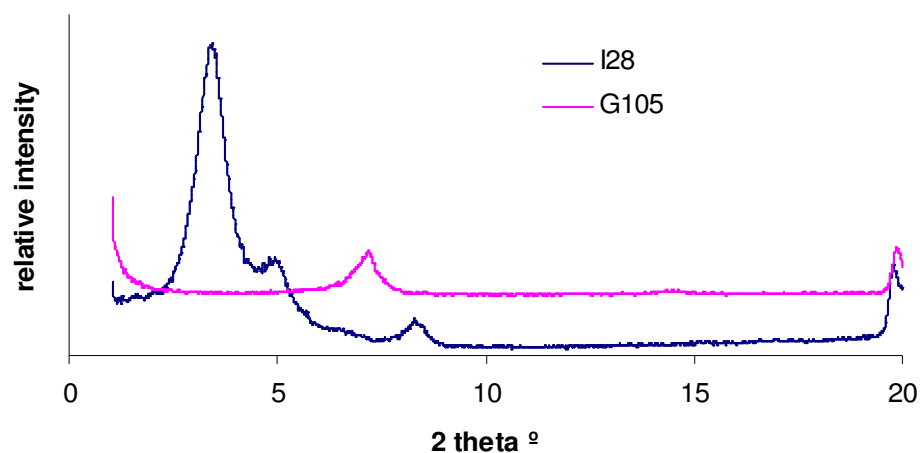
Figure 3.1.2.1–2 XRD Spectra for Nanomer clays produced by Nanocor Inc.

The recorded (001) spacing for the Nanocor clays are 1.215nm (G105) and 2.542nm (I28). The spacing for G105 is similar to the CNa^+ material indicating similar (001) spacing can be expected for unmodified clay independent of the source of the MMT. Secondly from our understanding it is thought that I28 organoclay contains an aliphatic quarternary ammonium surfactant. The presence

of (002) and (003) peaks in the I28 scan would indicate a more perfect layered crystal structure than that observed for the C93A

Further clay samples were investigated from Sud Chemie and also from Elementis. The XRD scans for these materials are shown in Figure 3.1.2.1-3 and Figure 3.1.2.1-4.
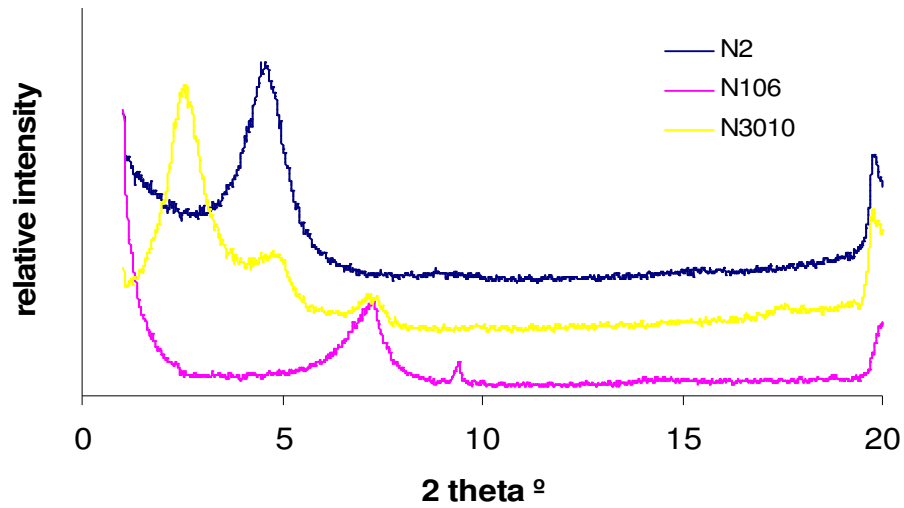
Figure 3.1.2.1–3 XRD spectra of Nanofill clays produced by Sud Chemie GHMB.
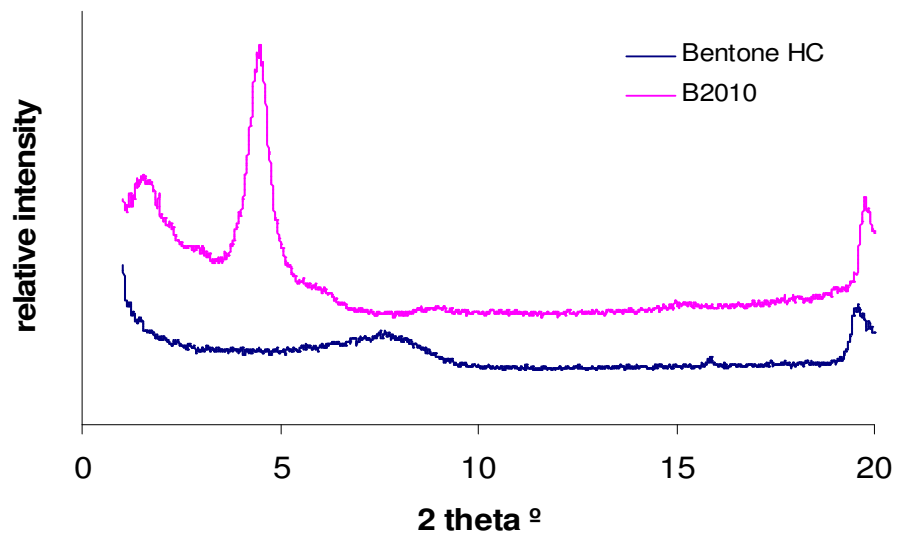
Figure 3.1.2.1–4 XRD spectra of Bentone clays produced by Elementis plc.

The N106 clay from Sud Chemie and the Bentone HC from Elementis are the respective unmodified sodium forms of clay from these suppliers and are analogous to CNa^+ and G105. As such they would be expected to have similar (001) spacing to the previous unmodified clays and this turns out to be the case. N106 has (001) spacing of 1.208nm and Bentone HC has (001) space of 1.139nm. Thus overall unmodified sodium form MMT has very similar nanostructure regardless of the source of the material.

The organoclays from Sud Chemie have (001) spacings of 1.897 and 3.335 respectively for N2 and N3010. N2 is known to have similar surface modification to C10A and this is reflected in the identical (001) spacing. N3010 has a large (001) spacing of 3.335nm. The surfactant is similar to that used for the N2 but the alkyl chain is longer hence the larger interlayer spacing. The final organoclay, B2010 has an interesting XRD pattern with a peak evident at 1.61° 2Θ and a second peak positioned at 4.5° 2Θ. These peaks correspond to spacings of 5.490nm and 1.965nm respectively. If the peak at 1.61° is taken as (001) using Braggs equation a (002) peak would be expected at 4.780nm, which corresponds closely to the second peak found. This explanation would ordinarily seem sufficient but the 4.50° peak appears much sharper and more defined than that observed at 1.61° possibly indicating that some bilayer surfactant structure has formed due to a surfactant loading in excess of the cation exchange capacity of the clay. Comparison with TGA data may help to further elucidate the situation as it may also be a result of the use of two surfactants for this clay.

3.1.2.2 In house modification of clay

In addition to commercially available organoclays a number of in house modified organoclays have also been investigated. All of these clays are based on CNa^+ which is included in the figures for reference.

The first modification was PVP which was added as described in section 3.2.1. Figure 3.1.2.2-1, shows the resulting structure of the organoclay formed. It is clearly evident that the (001) spacing of the clay has increased with the addition of PVP. This has resulted in an increase in the (001) spacing from 1.178nm (CNa^+) to 2.490nm with PVP modification. This confirms that the PVP has successfully penetrated into the interlayer of the clay.
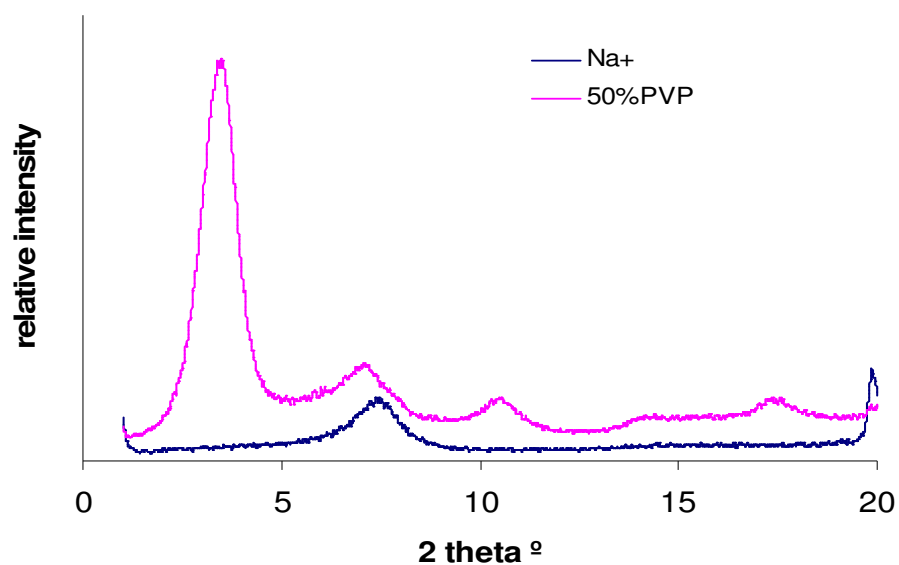
Figure 3.1.2.2 – 1 XRD spectra of CNa$^+$ and PVP modified CNa$^+$

The second material used for the modification of MMT was cetyl pyridinium. Both Bromide and Chloride analogues were investigated for this project and the resultant diffractograms are presented in Figure 3.1.2.2-2 with CNa$^+$ shown for comparison.
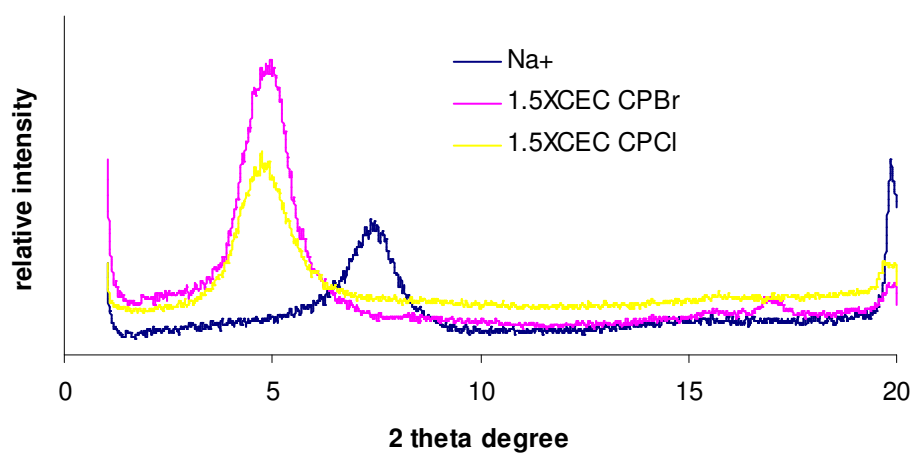
Figure 3.1.2.2–2 XRD spectra of CNa$^+$ and CNa$^+$ modified with CPBr and CPCl

The first feature of note is the change in two theta angle of the (001) peak of the pyridinium modified clays compared to the CNa^+. This indicates successful intercalation of the pyridinium into the clay interlayer. Peaks are observed at 5.04º and 4.94º for the cetyl pyridinium bromide and chloride respectively. The interlayer basal spacing was thus calculated to be 1.75nm for the bromide analogue and 1.79nm for the chloride material. As would be expected given the similarity these two values of (001) spacing are approximately identical.

The final in house developed clay was C30B modified with epoxy as described 3.2.1. The diffractogram in Figure 3.1.2.2-3 shows a comparison with its parent clay C30B.
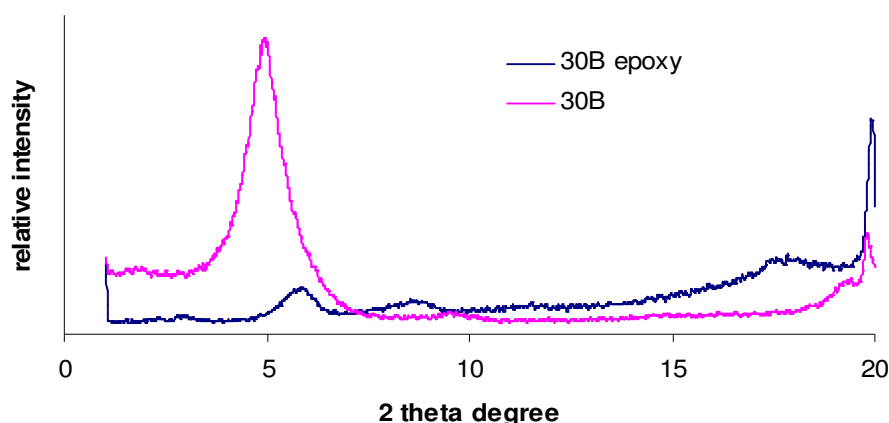
Figure 3.1.2.2–3 XRD spectra of C30B and epoxy modified C30B

For the epoxy modified Cloisite 30B (C30BE) the first peak is rather weak and located at 3.04º. This corresponds to an interlayer spacing of 2.91nm. The corresponding (002) peak is observed much more clearly at 5.97º and this value fits well with the theoretical prediction. This result indicates that the epoxy has intercalated the clay layers resulting in an increased (001) d spacing compared to the parent C30B clay.

3.1.2.3 Summary of XRD data

The XRD data obtained for the clays clearly shows that intercalated structures are formed when organic surfactants are added to the clay (as evidenced by the

increased (001) spacing compared to the unmodified clays). In some cases such as C15A, I28 and PVP higher order reflections are evident indicating that these clays exhibit a particularly ordered layered structure which may make them more difficult to disperse in the eventual host polymers. Overall the results obtained are as would be expected for clay materials.

3.2 Thermal stability of organoclays

The thermal stability of the organoclays was investigated using TGA. The thermal stability under air and nitrogen atmospheres is compared and the temperature of peak weight loss is analysed. Finally the surfactant loading is investigated.

3.2.1 Thermal stability of commercial organoclays

The TGA data for the commercial organoclays is summarised in Table 3.2.1-1 below.

Table 3.2.1–1 Summarised TGA data for commercial clays

Clay	5% loss air ºC	5% loss N_2 ºC	Peak wt loss air ºC	Peak wt loss N2 ºC	% surfactant
C10A	226	232	250	250	40.73
C15A	279	294	339	381	43.01
C30B	279	302	366	463	30.50
C93A	335	355	335	434	36.69
I28	323	310	364	438	38.16
N2	245	247	314	326	33.54
N3010	266	284	346	385	42.91
B2010	239	242	261	262	38.98

If the current opinion of nanocomposites formation were true it would be expected that thermal stability along with composite/surfactant compatibility are

of the utmost importance. From the table above it is evident that the commercial clays investigated exhibit variation in thermal stabilities and a significant dependence on test environment i.e. whether tested under air or under nitrogen. As would be expected when the materials are tested under a nitrogen atmosphere there is an increase in the temperature required for the onset of degradation. Correspondingly the temperature of the peak weight loss also increases when the clays are tested under an inert atmosphere. Overall this is indicative of the susceptibility of the organoclays to thermo oxidative degradation. Damaging degradation of the surfactants could occur during processing with some of the polymers used in this project. In particular PET and T5000 which are processed at 270ºC in nanocomposite formation may cause unwanted organoclay degredation.

The wide range of thermal stabilities observed (from 216°C in air for C10A to a maximum of 323°C in air for I28) indicates that the thermal stability is directly influenced by the chemical structure of the surfactant. In the case of C10A it is evident that if the benzyl or methyl bonds that connect the group to the nitrogen atom break a significant portion of the surfactant is degraded and this will result in significant weight loss in TGA experiments. In contrast the breakage of a single bond in the aliphatic alkyl type surfactants (such as C93A) may only result in the loss of one methyl group hence the rate of weight loss is slower than observed for the C10A. In addition the presence of reactive functional groups (such as the hydroxyl groups present in C30B) may contribute to un-wanted degredative reactions and hence the degredation temperature is lower.

3.2.2 Thermal stability of in house modified organoclays

From the commercial materials available, only C93A and I28 showed thermal stability suitable for all the polymer materials under investigation, and in particular for PET (processing temperature circa 285°C – 300ºC). It is hoped that by modifying standard base clay (Cloisite Na$^+$) with carefully selected chemicals it may be possible to increase the thermal stability of organoclay and, in conjunction with improved compatibility towards PET produce composites with greatly improved clay dispersion.

The first of these clays is PVP modified and TGA thermographs are shown in Figure 3.2.2-1.

The data obtained from the TGA experiment indicates that 5wt% loss occurs at 120ºC in air and 272ºC in Nitrogen. This would indicate that the PVP modified clay has thermal stability no better than many of the standard commercial clays. On direct viewing of the thermographs however, it is evident that this mass loss is gradual and most likely attributable to loss of moisture from the clay or moisture associated with the PVP. The main mass loss under both air and nitrogen atmosphere can be observed at about 430ºC indicating that PVP modified clay has considerably improved thermal stability compared to commercial clays. This is confirmed by the peak mass loss which was determined to be at 472ºC in both atmospheres and is expected based on the thermal stability of PVP.
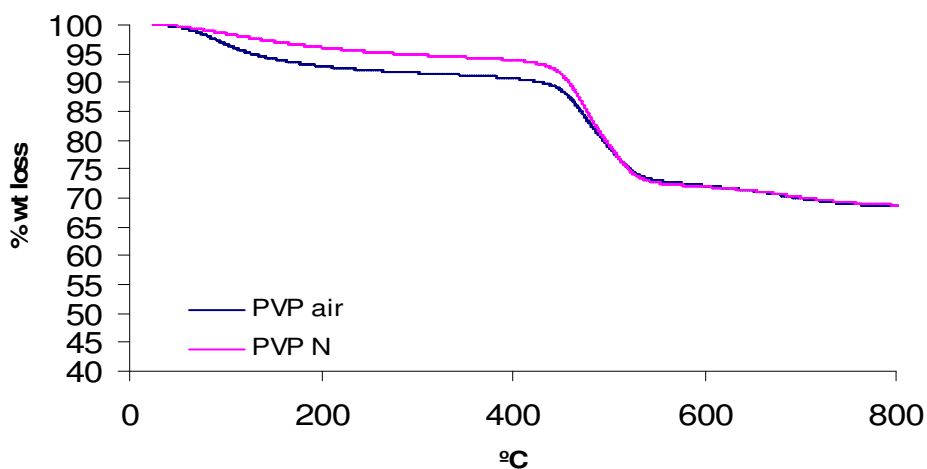
Figure 3.2.2–1 TGA comparison of PVP modified CNa$^+$ in air and nitrogen atmosphere

The second clay modification identified was cetyl pyridinium. It is hoped that the ring structure will provide increased thermal stability compared to standard quarternary ammonium based surfactants. In this case both bromide and chloride analogues of cetyl pyridinium were used to ascertain if counter ion affects the thermal stability.
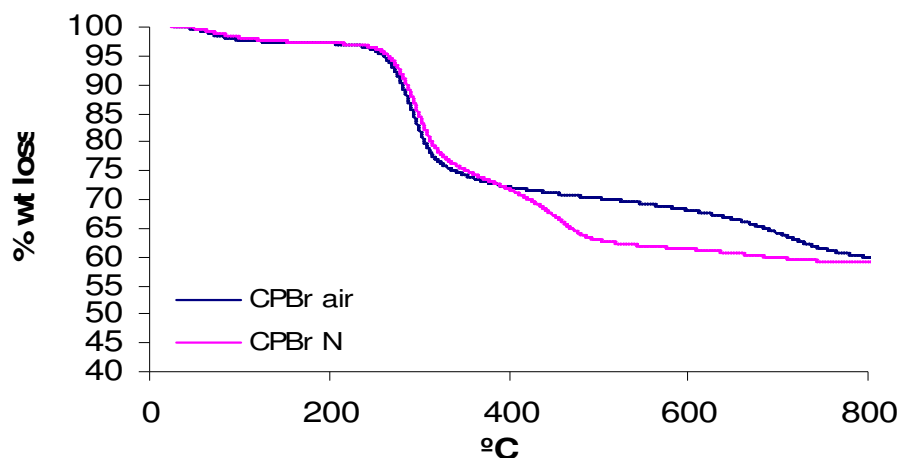
Figure 3.2.2–2 TGA comparison of CNa$^+$ modified with CPBr in air and nitrogen atmosphere

From the TGA curves (Figure 3.2.2–2) it is clear that thermal stability has not been raised to a very high temperature for the bromide analogue with 5wt% loss at 265ºC and 270ºC for air and nitrogen atmospheres respectively. The peak weight loss temperature determined from the derivative weight loss was found to be unchanged regardless of the test environment (298ºC for air and 300ºC for nitrogen). The overall surfactant loading was found to be 41.98%. Overall this modification does not offer any real benefits over the commercial organoclays studied.
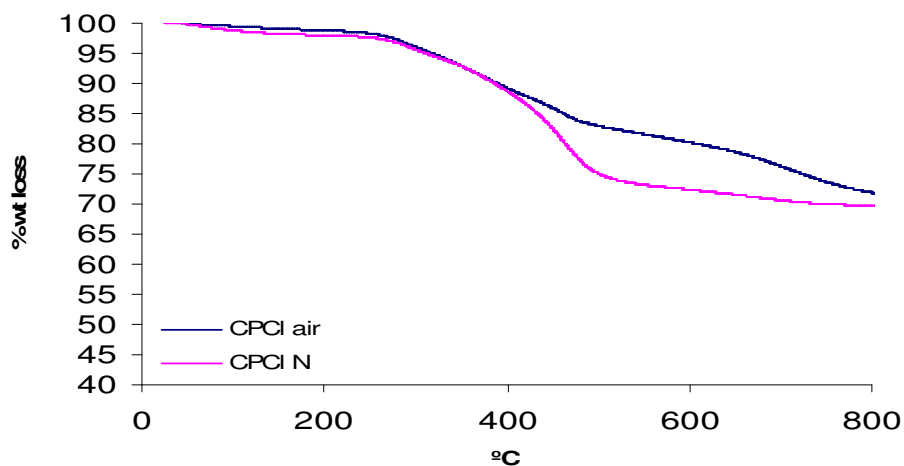
Figure 3.2.2–3 TGA comparison of CNa$^+$ modified with CPCl in air and nitrogen atmosphere

In addition to the cetyl pyridinium bromide analogue the chloride analogue has also been investigated. The TGA curves for this material are also presented in Figure 3.2.2–3.

From the results presented it is evident that the thermal stability of the chloride analogue is greater than that observed for the bromide. In this case 5wt% loss was determined to be 323ºC in both air and nitrogen atmosphere. The peak heat loss temperatures also show considerable increase compared with the bromide additive with values of 462ºC and 467ºC respectively for air and nitrogen. The total surfactant loading was determined to be 30.31% indicating that either some bi-layer coverage has occurred for the bromide derivative or that incomplete cation exchange has occurred for the chloride derivative.

Overall this indicates that the bromide derivative is less thermally stable, probably due to some bi-layer structure of surfactant. In addition, counter-ion residues (i.e. Br^- and Cl^-) may affect the thermal stability with bromide affecting the thermal stability more [127].
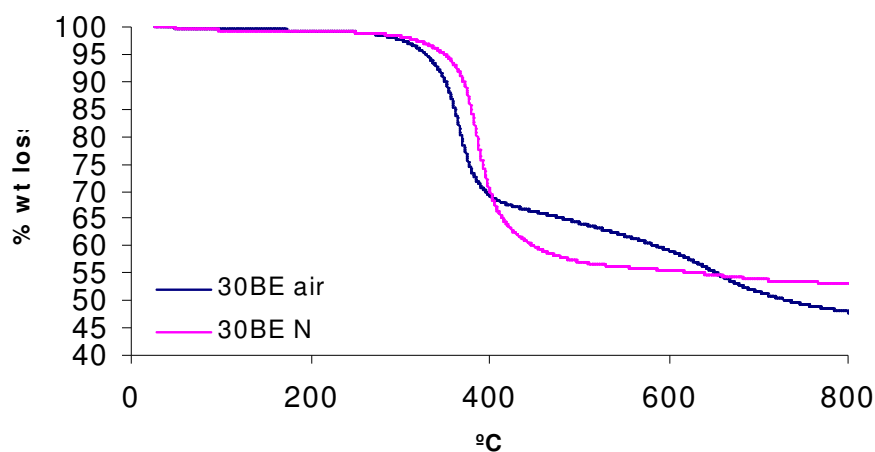
Figure 3.2.2–4 TGA comparisons of C30B and epoxy modified C30B in air and nitrogen atmospheres

The final in house modified clay investigated was C30B modified with Bisphenol A epoxy of diglycidyl ether. It is hoped reaction of epoxide end groups with hydroxyl groups on the C30B will both improve thermal stability and compatibility with PET. Thermograms for C30BE are included as Figure

3.2.2-4. It is evident from the TGA experiments conducted that the thermal stability of the clay is improved considerably compared to the original C30B clay. For C30BE tested in air the 5wt% loss has increased from 279ºC up to 331ºC and for tests conducted in nitrogen the 5wt% loss value has increased from 302ºC to 349ºC. New derivative weight loss values show peak weight loss to be reached at 369ºC and 387ºC respectively for air and nitrogen atmospheres. This compares favourably with the previously reported values for 30B in air but the value for nitrogen atmosphere is reduced. Overall this indicates that the new degradation mechanism is controlled by the epoxy component rather than the quarternary amine component of the organoclay. The total loading of surfactant (i.e. quarternary ammonium and epoxy was found to be 47.48% indicating approximately 17% of the surfactant detected in TGA is epoxy.

3.3 Compatibility of organoclays with polymers

The organoclays and polymers, where structural detail is known have been analysed using Hansen solubility parameters to give an indication of potential compatibility between surfactants and polymer. The absolute solubility parameter (δ total) of the materials is shown in Table 3.3-1 along with the dispersive (δd), polar (δp) and hydrogen bonding (δh) component.

From the table it can be seen that there is a broad range of solubility parameter represented within the materials. PA-6 for instance, would appear to be most compatible with Cloisite 30B (out of the clays used in PA-6) but there is a considerable difference in the component fractions. Although the dipole contribution is similar the remainder of PA-6 is equally distributed between polar and hydrogen bonding contribution. In contrast the C30B has further contribution almost exclusively from the hydrogen-bonding component (as its structure would suggest as it contains 2 hydroxyl groups). This illustrates that the actual compatibility between polymer and clay may not be governed by the total solubility parameter alone but rather its make up in terms of dipole, polar and hydrogen bonding component. To further illustrate this point a triangular plot of the fractional contribution to total solubility parameter of PA6 and the clays used (with known structures) is shown below (Figure 3.3-1). The axes correspond to

113

dispersive fraction (fd), polar fraction (fp) and the hydrogen-bonding fraction (fh).These plots provide an excellent tool to aid in the visualisation of the compatibility between two materials. In essence the closer two materials appear on the chart the greater their compatibility. In this case it confirms that C30B is the most compatible of the clay used. In addition it can be seen that C10A and C15A, as used with PA-6 show poor compatibility.

A similar method can be used to examine the other polymer/clay systems tested. Figure 3.3-2 above is a TEAS plot for MXD6 with organoclays. Similar to PA-6 C30B is the most compatible clay surfactant. In this case the MXD6 is more compatible with the other clay types than the PA6 as it lies closer on the TEAS plot. This indicates that the MXD6 material is less polar than PA6.

For G21 compatibility is very similar to that observed for MXD6 due to the similarity in the solubility parameter for MXD6 and G21 (Figure 3.3-3).

Table 3.3–1 Hansen solubility parameter data for polymers and clays

Material	δ total	δd	δp	δh
PA-6	22.7	19.6	8.7	7.5
MX6007	20.9	18.8	5.6	7.1
G21	19.9	17.9	5.3	6.9
T5000	16.4	15.2	1.2	6.3
PET	21.3	17.9	6.9	9.1
C10A	19.8	19.8	0.3	0
C15A	17.8	17.8	0	0
C30B	21.6	18.8	1.9	10.4
C93A	17.6	17.6	0	0
I28	-	-	-	-
N2	20.1	20.1	0.4	0
N3010	19.8	19.8	0.3	0
B2010	-	-	-	-
PVP	21.7	15.9	12	8.7
Cetyl pyridinium	16.3	16.6	0	0
30B epoxy	18.3	16.9	2.8	6.4
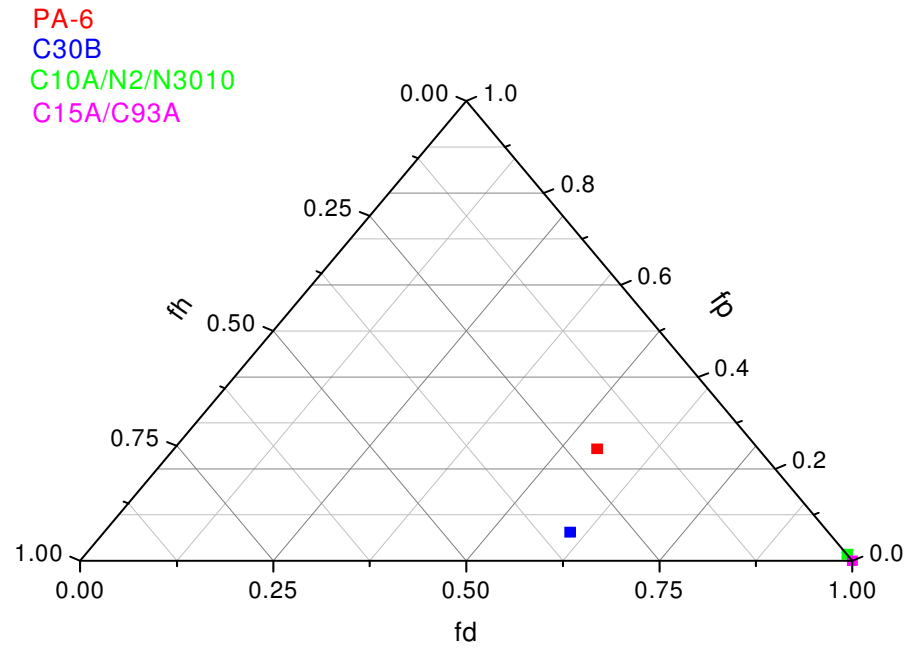
Figure 3.3–1 TEAS plot showing compatibility of organoclays with PA6
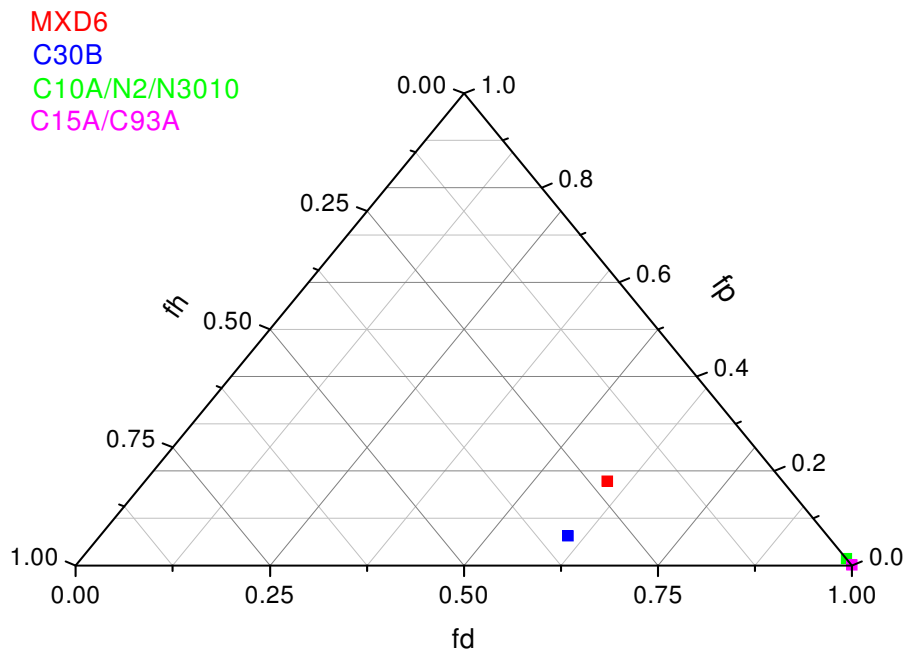
Figure 3.3–2 TEAS plot showing compatibility of organoclays with MXD6
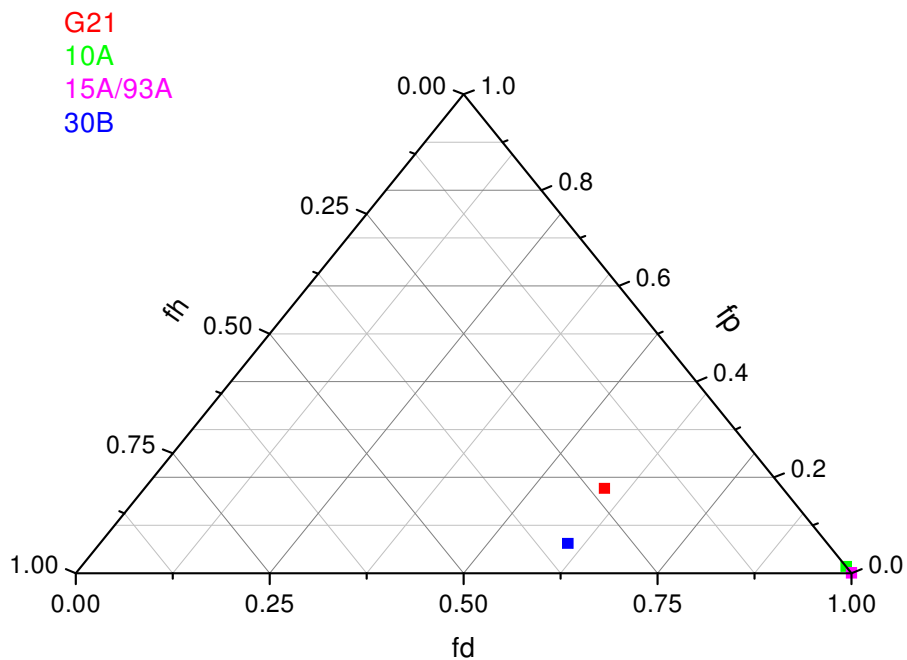
Figure 3.3–3 TEAS plot showing compatibility of organoclays with G21
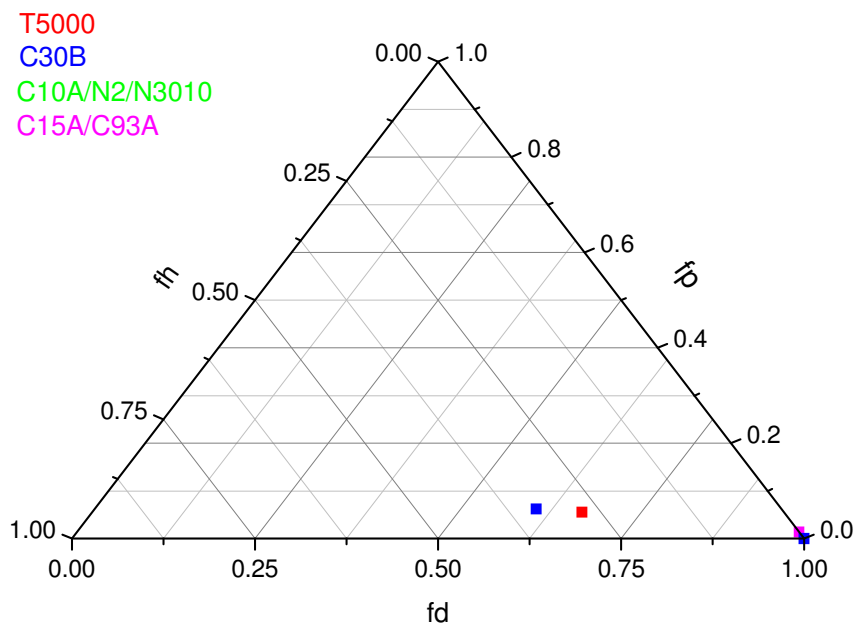
Figure 3.3–4 TEAS plot showing compatibility of organoclays with T5000

A similar situation is observed for T5000 amorphous polyamide (Figure 3.3-4) whereby C30B offers the closest compatibility to the polymer. The T5000 is also positioned closer to the other clays than either the PA6 or the MXD6 polyamides indicating lower polarity than the other polyamides as this axis corresponds to zero contribution from polar or hydrogen bonding contributions.

PET
C30B
C10A/N2/N3010
C15A/C93A/Cetyl pyridinium
PVP
Epoxy 30B
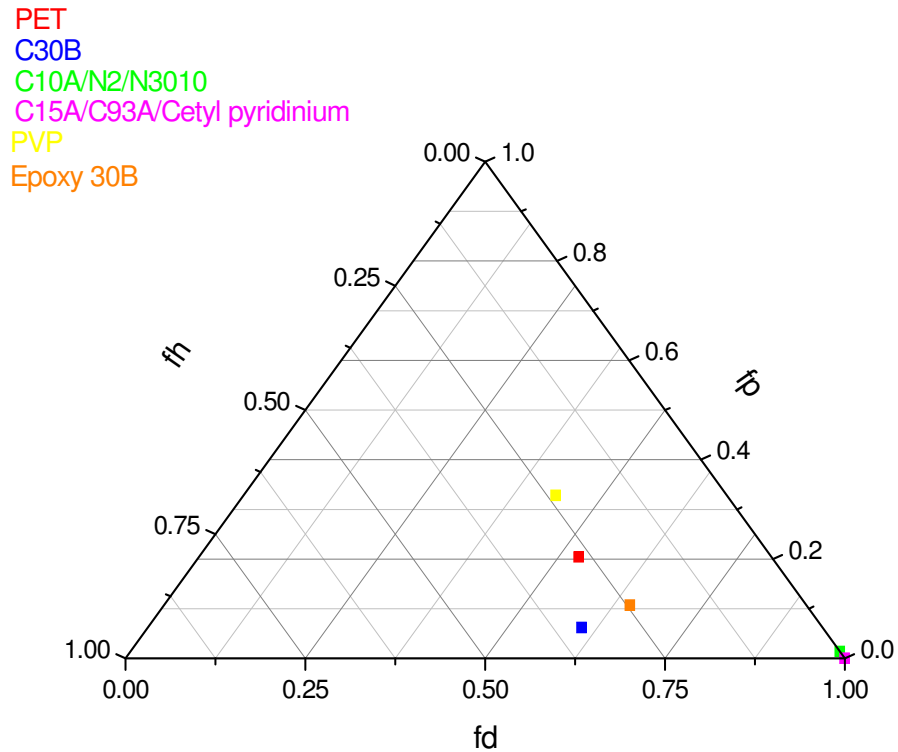
Figure 3.3–5 TEAS plot showing compatibility of commercial and in-house modified clays with PET

The compatibility of PET with both commercial and in house modified clays is illustrated in the TEAS plot below (Figure 3.3-5). As is the case for the polyamide materials the C30B proves to be the most compatible with PET while the other commercial clays and cetyl pyridinium modified clay exhibit 'poor' compatibility based on the TEAS plot. Modification with PVP has produced clay with improved compatibility toward PET compared to those which are

commercially available due to its greater polarity. Similarly the use of Epoxy to modify C30B improves the compatibility of the clay compared to commercial clays.

3.4 Summary

The SEM images of the unmodified commercial clays indicate that there are significant differences in the MMT structure based upon the source of the Bentonite mineral. Generally speaking the SEM has illustrated that Southern Clays material is more angular in nature and less agglomerated than the other commercial clays investigated. It is possible that these differences in micro-structure may influence the quality of the dispersion of clay in polymers since clay exfoliation involves both separation of micro-structured particles and nano-exfoliation.

The nanostructure of the commercial clays illustrated a dependence of (001) spacing on the size of the surfactant molecule. Large surfactant molecules such as dimethyl dihydrogenated tallow quarternary ammonium used in C15A produced large interlayer spacings and smaller molecules such as dimethyl benzyl hydrogenated tallow used in C10A resulted in a smaller interlayer. It is unclear if the initial interlayer spacing will significantly affect the intercalation of polymer into the clay galleries but it is evident that a small interlayer could hinder diffusion controlled intercalation. The compatibility of these organoclays with the target polymers was found to be poor in many cases. For instance hydrophobic clays such as C15A or C93A would be expected to have poor compatibility with the polar nylons and PET used in these studies. In addition to the compatibility issues many of the clays under test exhibit poor thermal stability for processing with many of the polymers under investigation (i.e. MXD6, G21, T5000 and PET). This lack of thermal stability infers that degradation of the organoclay may occur during processing. The nano-structure of the nanocomposites produced will provide valuable insight into the mechanisms responsible for producing the most highly dispersed clay polymer nanocomposites and the influence of compatibility of surfactant and polymer and its thermal stability.

In addition to the commercially available organoclays several in-house modified clays were produced so the effect of improved compatibility and increased thermal stability can be assessed in relation to PET. PVP modified clay shows both improved compatibility towards the PET and improved thermal stability compared to the commercial clays investigated. Cetyl Pyridinium modified clays produced exhibit generally poor compatibility and thermal stability but offer an interesting choice due to their food approved status. The PVP modified clay and epoxy modified C30B may prove much more interesting as they have comparable thermal stability to the most thermally stable commercial clays such as C93A and I28 but offer better PET compatibility than any of the commercially available materials. If the prevailing wisdom were correct it would be expected that these materials would produce much improved nanocomposites compared to the commercial materials.

4 Evaluation of polyamides for exfoliation transfer of clay into PET

One of the possible solution routes to the problem of improving CO_2 retention in PET beverage containers is to use well established exfoliation technology such as that of polyamides. The exfoliation of MMT in polyamides is well studied and highly exfoliated composites have been produced via melt processing. This chapter evaluates a range of polyamide/clay nanocomposites in order to gain understanding of the best polymer clay combinations, and also to identify optimum combinations for blending with PET to maximise gas barrier. In Table 4-1 a summary of the polymer/clay combinations evaluated and their processing temperatures is provided.

Table 4–1 Table of PA/clay combinations and processing temperature

Polymer	Designation	Clay	Processing Temperature (ºC)
PA-6	F223D	C93A	230
	UB3	C93A	230
	F136C	C15A	230
	F136C	C30B	230
	F136C	C93A	230
	F136C	I28	230
	F50	C15A	230
	F50	C30B	230
	F50	C93A	230
	F50	I28	230
PA-MXD6	MXD6	C10A	250
	MXD6	C15A	250
	MXD6	C30B	250
	MXD6	C93A	250
	MXD6	I28	250
PA-6I/6T	G21	Na^+	250
	G21	C10A	250
	G21	C15A	250
	G21	C30B	250
	G21	C93A	250
PA-6-3-T	T5000	Na^+	270
	T5000	C10A	270
	T5000	C15A	270
	T5000	C30B	270
	T5000	C93A	270

Using the samples in Table 4-1 the effects of different polyamide structures can be investigated and the effects of various polymer/clay compatibilities in addition to the effects of different processing temperatures.

4.1 Polyamide-6/organoclay nanocomposites

PA-6 nanocomposites were the first to be scrutinised due to the relatively large body of literature available on the subject. The first aspect investigated was the influence of the PA-6 viscosity, as evidence suggests that higher viscosity is more effective in clay exfoliation due to the increased shear during processing. The second major factor investigated was the effect of different surfactants and their potential compatibility with PA6 on the dispersion of organoclay and the resultant nanostructure and crystallisation behaviour.

4.1.1 Morphological characterisation of PA-6 nanocomposites

4.1.1.1 Influence of PA-6 viscosity

The four PA-6 materials studied, F223D, UB3, F136C and F50 were subjected to rheological evaluation using capillary rheometery as described in section 3.2.4.5.2. The resulting viscosity/shear rate curves are presented in Figure 4.1.1.1-1
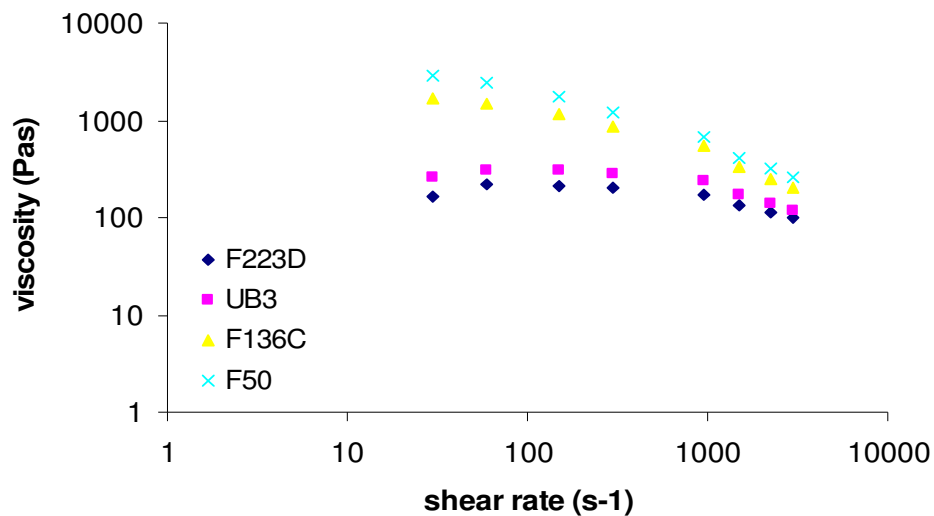
Figure 4.1.1.1–1 Viscosity curves for PA6 materials with differing molecular weight

From the above data zero shear rate viscosity was determined by extrapolation of the data points back to the viscosity axis. Zero shear viscosity values of 240Pas, 360Pas, 2560Pas and 5300Pas were determine for F223D, UB3, F136C and F50 respectively, thus a wide range of polymer viscosity is investigated.

Nanocomposites of these PA-6 materials were compounded with 5wt% C93A for comparison of the effect of rheology on the nanostructure of the resultant composites. This particular clay was chosen because it produces better dispersed nanocomposites in PA-6 according to a previous study conducted in this laboratory [167].

The XRD pattern for F223D/C93A composite is shown in Figure 4.1.1.1-2 with the unmodified polymer and the organoclay for comparison purposes.
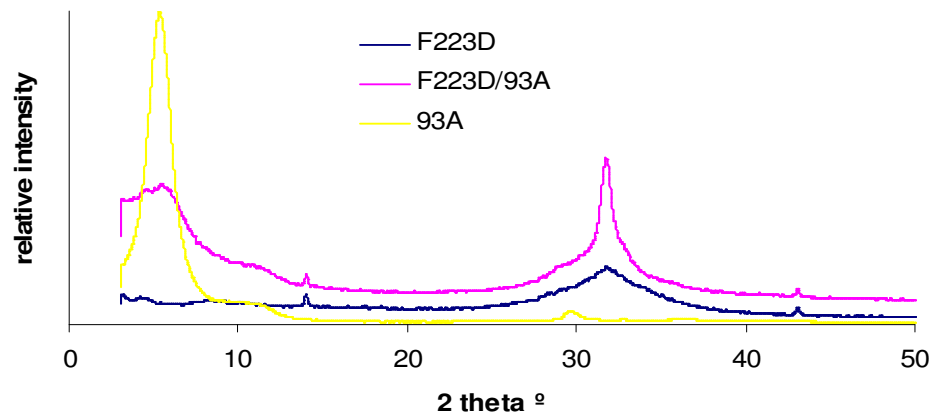
Figure 4.1.1.1–2 XRD spectra of F223D, F223D/C93A nanocomposite and C93A clay (Cr x-ray source)

For the F223D polymer there is a small peak at 4.6°. The association of this peak is not known but it may represent some additive that is incorporated into the base polymer such as a lubricant or stabiliser. There is a peak at 32.4° which corresponds to the crystal structure of the PA-6. With the incorporation of the clay a new peak is evident at 5.28° which correspond to a (001) spacing of 2.485nm. From the x-ray patterns it is evident that this is very similar to the peak position and spacing for the raw C93A clay (5.48° and 2.395nm (001) spacing). It appears that the clay dispersion process occurs in chopping down the height of

the layered-structure of clay particles due to shear forces in the extruder rather than layer-by-layer exfoliation.

In addition to the nanostructure a change in the crystal structure can be observed. The peak at 32.4º now shows increased intensity and there is also an additional shoulder present at 29.1º. This indicates that the presence of the clay has resulted in a more ordered crystal structure and the formation of a small amount of an alternative crystal structure.

The UB3 composite showed different behaviour than the F223D composite as there was a shift of the (001) peak to 4.12º (Figure 4.1.1.1-3). This corresponds to a new (001) spacing of 3.185nm and is indicative of an intercalated nanocomposite structure. Again the peak intensity is reduced indicating reduced particle size Similarly to F223D/C93A composite there is also a change in the crystal structure as the peak intensity at 32.4° is again increased and an additional shoulder is again present at 29.1º.
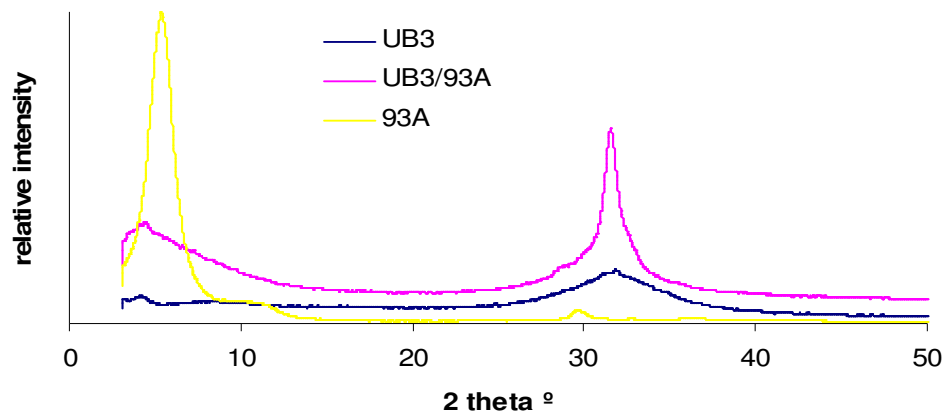
Figure 4.1.1.1–3 XRD spectra of UB3, UB3/C93A nanocomposite and C93A clay (C5r x-ray source)

The two high viscosity PA-6 materials studied exhibit very similar behaviour and their x-ray patterns are shown in Figures 4.1.1.1-4 and 4.1.1.1-5. The first feature of note is the absence of (001) peak for these materials. This is indicative of a high degree of clay dispersion/exfoliation of the organoclay. In both cases a small peak is evident at 4.6º which corresponds to the small peak evident in the

unmodified polymer. Similar to the F223D and UB3 there is an identical change in the crystal structure of the nanocomposites compared to the base polymer.
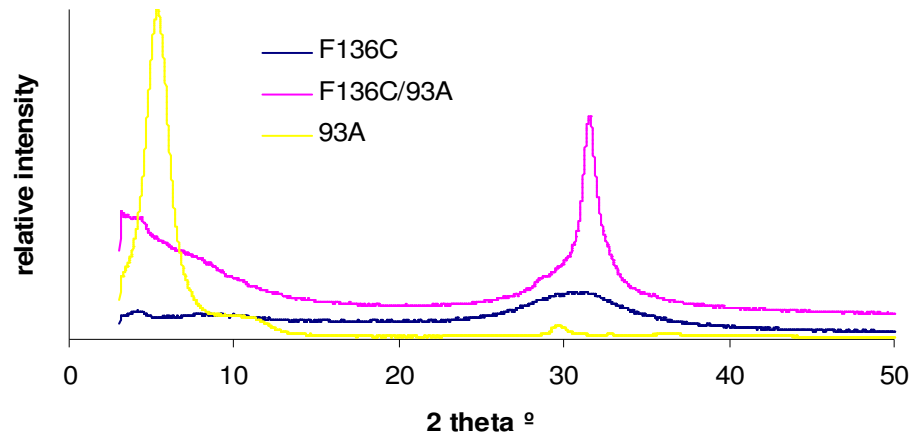
Figure 4.1.1.1–4 XRD spectra of F136C, F136C/C93A nanocomposite and C93A clay (Cr x-ray source)
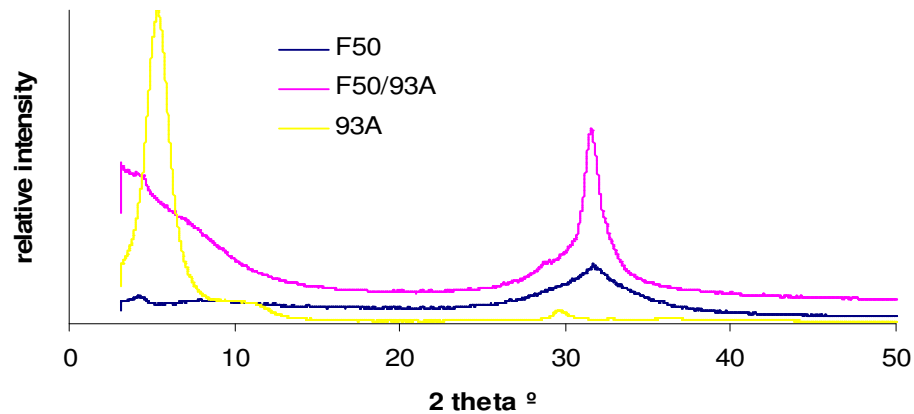
Figure 4.1.1.1–5 XRD spectra of F50, F50/C93A nanocomposite and C93A clay (Cr x-ray source)

Overall these results suggest that higher viscosity of PA-6 is favourable for the fabrication of highly dispersed/exfoliated nanocomposites from the melt as suggested in the literature. We are in agreement that this effect is due to the additional shear stresses generated by the high viscosity materials during processing. It is also likely that reduced thermo-oxidative degradation of the

polymer during processing is helpful in maintaining high viscosity during processing – i.e. that the molecular weight reduction due to degradation in processing has less effect due to the higher starting RMM.

4.1.1.2 Influence of surfactant

To investigate the influence of surfactant on the dispersion of clay in PA6 four commercial organoclays were chosen. The clays selected were C15A (highly hydrophobic), C30B (hydrophilic and recommended by the manufacturer Southern Clays), C93A (hydrophobic and best for PA6 based on our experience [167]) and I28 (again hydrophobic but with a different clay structure). Each of these materials was added to PA6 at 5wt% via the extrusion process described previously. Both high and ultra high viscosity PA6 (i.e. F136C and F50) were evaluated as they have the greatest potential to exfoliate compared to low and medium viscosity materials. The XRD patterns obtained for F136C are shown in Figure 4.1.1.2-1.
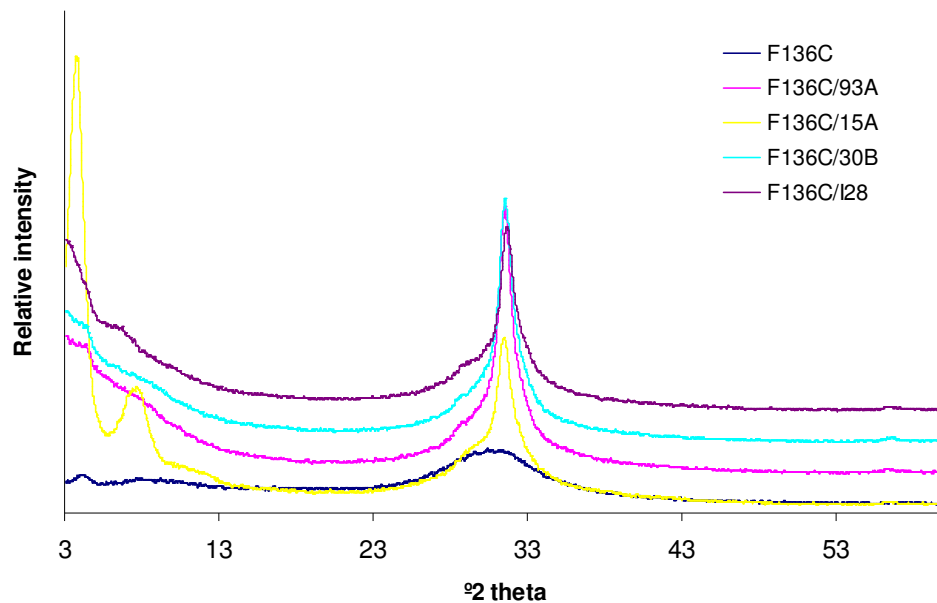
Figure 4.1.1.2–1 XRD Spectra of F136C and nanocomposites produced with different organoclays (Cr x-ray source)

In the case of C15A there is a clear (001) peak positioned at 3.88º and a (002) peak positioned at 7.76º. The (001) distance calculated from this peak angle is 3.382nm compared with 3.065nm for the original clay. This data suggests that there has been some intercalation of polymer chains into the clay galleries due to the increase in (001) basal spacing but that a high level of dispersion has not been attained as the clear (001) and (002) peaks indicate the layered structure of the clay is largely intact. In the case of C30B and C93A there is no defined peak at low angle (excluding the small peak at 4.22º which is present in the unmodified polymer) indicating a high level of clay dispersion. It would be expected that some exfoliation has occurred or an intercalated structure with (001) spacing greater than 4.374nm. To the best of our knowledge an intercalated structure with such a large (001) spacing has not been produced in PA-6 materials previously, therefore it would be expected that the nanocomposites produced with C30B and C93A are predominantly exfoliated. For I28 there is evidence of a peak just within the limit of this test at 3.23º and a second peak at 7.16º. These are the (001) and (002) peaks for the clay and correspond to a (001) spacing of 3.940nm. This would indicate considerable intercalation of the clay ((001) for raw clay is 2.542nm) but the overall layered clay structure is retained.

The final features of note are the peak centred at approximately 32º and the small shoulder observed at 29.5º. These peak positions are known to be representative of the PA6 gamma and alpha crystalline forms respectively [168]. As such it can be surmised that the gamma crystal form dominates due to the processing method employed but that the presence of clay promotes the formation of alpha crystals also. In essence a change in the crystal form of the samples has occurred with the incorporation of clay.

The second high viscosity PA-6 used for assessment of the effect of surfactant on nanocomposites formation is F50 ultra high viscosity PA-6. Figure 4.1.1.2-2 presents the XRD scans obtained from these materials.
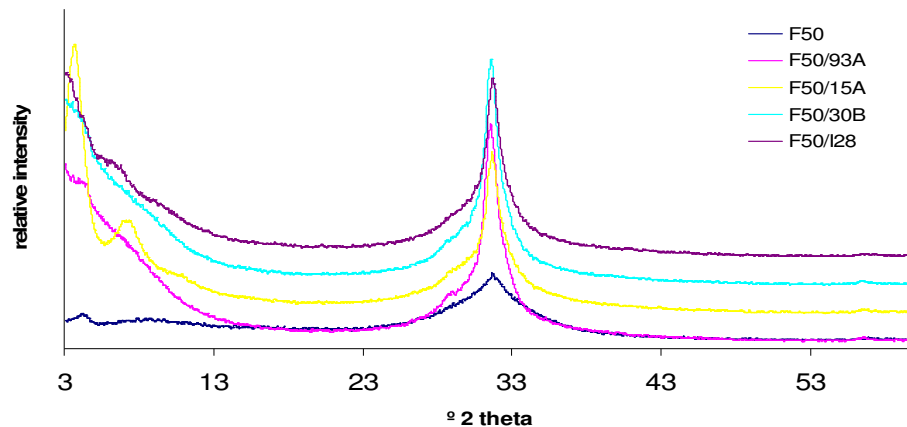
Figure 4.1.1.2–2 XRD Spectra of F50 and nanocomposites produced with different organoclays (Cr x-ray source)

In the case of the F50 material the behaviour of the different types of clay is identical to that observed for F136C, as is the crystallisation behaviour indicating that the RMM has a significant influence on the nanocomposite formation

4.1.1.3 Summary of PA6 Nanocomposite XRD data

From the XRD spectra obtained several of the features noted in Section 2.2.5.1 are in evidence for PA6 nanocomposites. Such features include peak broadening and reduced intensity (for low RMM PA6) due to both reduced concentration of the clay (5wt% of the composite) and also due to reduction in the number of clay layers per particle. In addition the highly hydrophobic clay C15A continues to show a very ordered structure (multiple (00) orders evident) even after melt processing with the polymer indicating very little dispersion of the clay due to poor compatibility. One final feature of note is that although all the high RMM PA6 nanocomposites (with the exception of (C15A) could be considered highly dispersed there is a rise in intensity at low angles. This may indicate some structural features with regularity over larger distances that can not be resolved by XRD techniques. Further work could be conducted using SAXS/SANS to further elucidate these features.

4.1.2 Crystallisation behaviour of PA-6 nanocomposites

The crystallisation behaviour of the PA-6 nanocomposites, as investigated by DSC is discussed in this section. Briefly samples were heated then held at temperature to remove thermal history then subjected to further cooling and heating. These scans were recorded.

Low viscosity PA-6 and medium viscosity PA-6 (F223D and UB3 respectively) with C93A clay were investigated first. The DSC cooling scans for these materials are included below as Figure 4.1.2–1. It is evident that the inclusion of clay in these materials results in a shift in the crystallisation temperature to higher temperature than that seen for the unmodified material. In the case of F223D, T_c has increased from 161ºC to 184ºC and the crystallisation peak is much sharper indicating rapid nucleated crystallisation. Thus it appears that the clay, when in a micro dispersed form (as in this composite case) acts as a nucleating agent. Similar phenomenon can be seen for the medium viscosity PA-6 UB3. A similar shift to higher temperature for T_c has occurred (from 160ºC to 177ºC) in this case also along with a distinct sharpening of the crystallisation peak. Overall this indicates that in an intercalated nanocomposite the clay also acts as a nucleating agent.
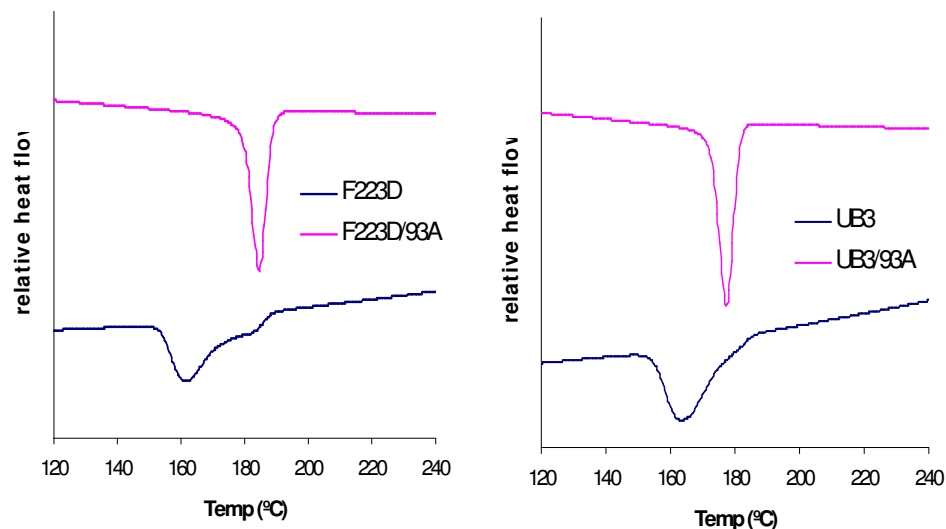
Figure 4.1.2–1 DSC cooling of low RMM/viscosity PA6 and nanocomposites

The F136C composites showed a similar trend in terms of clay acting as a nucleating agent. In this case the unmodified polymer has a T_c of 155ºC whilst the nanocomposites have T_c 177ºC C15A, 176ºC C30B, 174ºC C93A and 177ºC for I28 polymer clay nanocomposite. As for the low and medium molecular weight nanocomposites there is a considerable shift of T_c to higher temperature and a sharpening of the crystallisation peak. It also appears that T_c is slightly depressed for exfoliated nanocomposites (i.e. C30B and C93A) compared to the intercalated nanocomposites (i.e. C15A and I28). The DSC cooling scans for F136C clay nanocomposites are shown in Figure 4.1.2–2.

The high viscosity/molecular weight PA-6, F50 showed a similar tendency to that observed for high viscosity PA-6 F136C. The unmodified polymer exhibited T_c of 154ºC compared with 155ºC for the F136 material. The nanocomposites also followed a similar trend. Exfoliated nanocomposites C30B and C93A had T_c of 174ºC and 173ºC and intercalated nanocomposites C15A and I28 both had T_c of 176ºC. Overall the trend shows that like other PA-6 materials studied there is a tendency towards significant nucleation of the PET and that the effect is more pronounced when the nanocomposite is of intercalated form rather than exfoliated. The DSC traces for F50 cooling are shown in Figure 4.1.2–3.
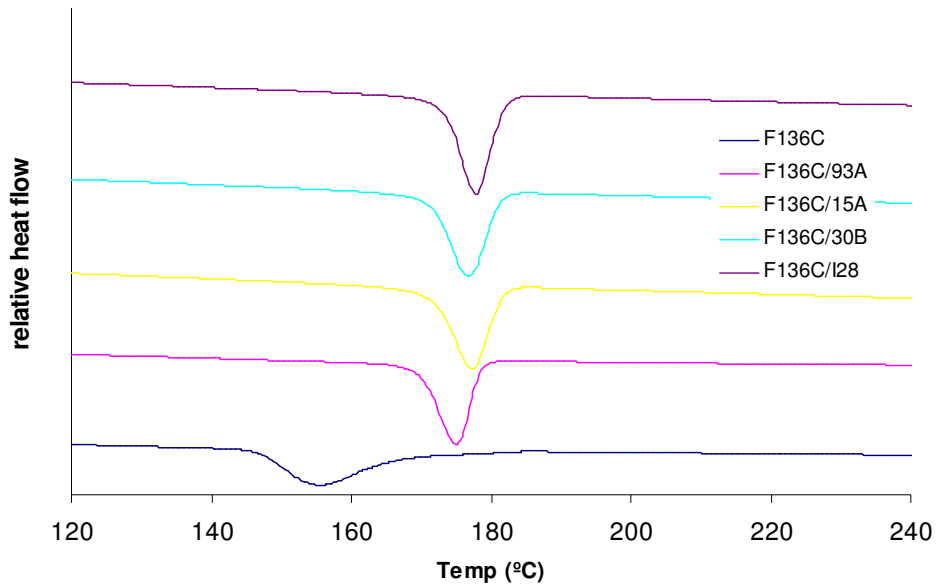
Figure 4.1.2–2 DSC cooling of F136C PA6 and F136C nanocomposites
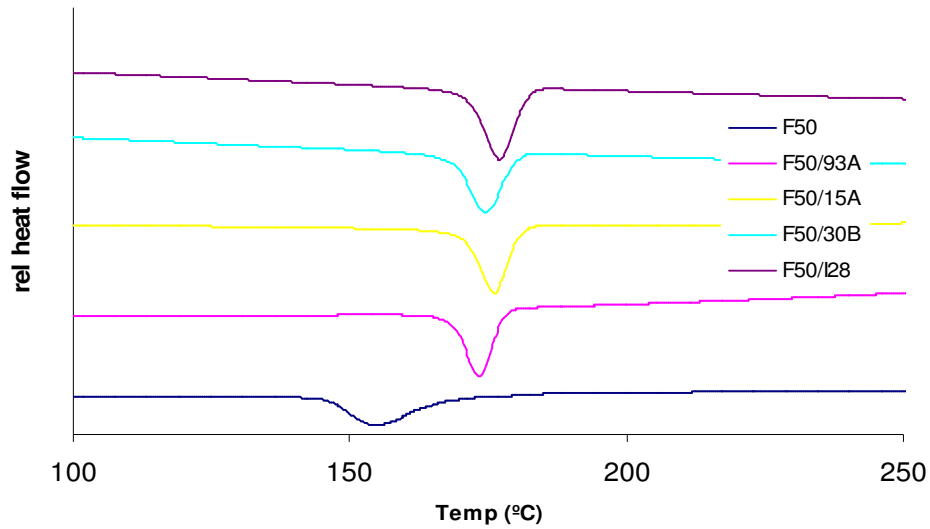
Figure 4.1.2 – 3 DSC cooling of F50 PA6 and F50C nanocomposites

Table 4.1.2-1 below provides a summary of the crystallisation behaviour of the PA-6 nanocomposites.

Table 4.1.2–1 Summary of the effect of nanocomposite type on crystallisation on cooling from the melt

PA-6	Clay	$T_{c(on)}$ °C	T_c °C	Nanocomposite structure
F223D	-	187	160	-
UB3	-	183	161	-
F136C	-	168	155	-
F50	-	167	154	-
F223D	C93A	190	184	Micro dispersion
UB3	C93A	183	177	Intercalated
F136C	C15A	181	177	Intercalated
F50	C15A	180	176	Intercalated
F136C	C30B	181	176	Exfoliated
F50	C30B	180	174	Exfoliated
F136C	C93A	178	174	Exfoliated
F50	C93A	177	173	Exfoliated
F136C	I28	181	177	Intercalated
F50	I28	181	176	Intercalated

Overall there are two main trends observed in the data presented regarding crystallisation from the melt. First, there is a viscosity/molecular weight effect whereby crystallisation onset is at higher temperature with low molecular weight materials compared to higher weight materials. This is a well known phenomenon and is due to increased chain mobility of low molecular weight materials due to their lower number of chain entanglements. The second feature of interest is that the nucleation effect is reduced for exfoliated nanocomposites compared to intercalated counterparts. In essence it appears that when clay platelets are highly dispersed as single layers they restrict the growth of crystals due to the large amount of volume they occupy. When the composite is intercalated there is less total volume and hence greater numbers of crystals are able to nucleate and grow thus allowing a greater nucleation effect.

The second feature of PA-6 nanocomposite crystal behaviour investigated was the crystal melting behaviour. DSC second heating traces for F223D/C93A nanocomposite and UB3/C93A nanocomposite are shown below in Figure 4.1.2-4 with their respective neat resins for comparison.
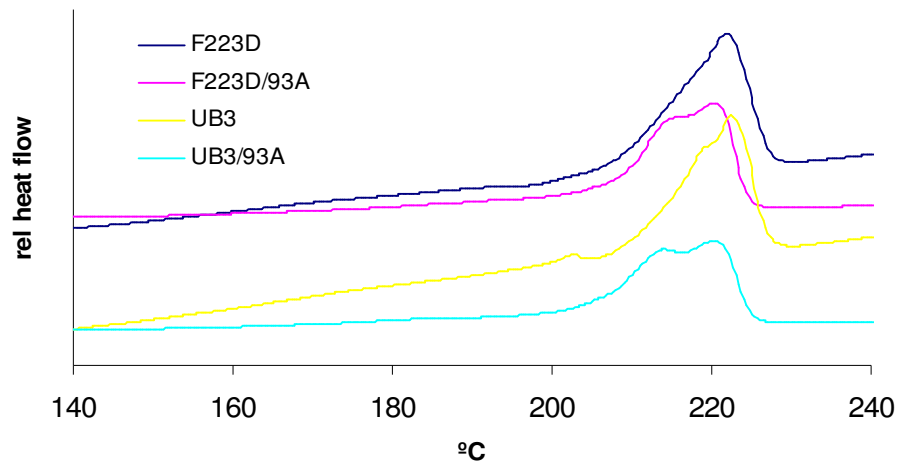
Figure 4.1.2–4 DSC crystal melting of low RMM/viscosity PA6 and nanocomposites

Both unmodified PA-6 materials have a single large melting peak centred at 222ºC. This corresponds to melting of the alpha crystal form for PA-6. Interestingly with the addition of clay, regardless of the type of nanocomposite formed there is a distinct change in the crystal melting peak, which becomes split

between peaks at 214ºC and 221ºC. The first peak at 214ºC corresponds to the crystal melting temperature of gamma crystals in PA6 (as indicated in XRD analysis) while the 221ºC represents the alpha crystal melting. Therefore it is evident that the presence of the clay results in the formation of a significant level of gamma crystals in PA-6. Due to their lower melting temperature it can be assumed that these crystals exhibit less perfection than their alpha crystal counterparts indicating that the presence of clay inhibits the formation of the largest, most perfect crystals.
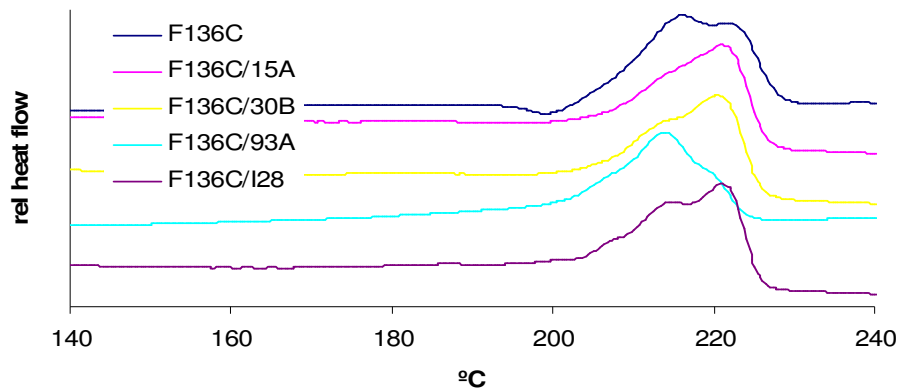
Figure 4.1.2–5 DSC crystal melting of F136C PA6 and F136C nanocomposites

In the case of F136C high viscosity PA6 there is also a change in the melting behaviour of the nanocomposites compared to the unmodified material (Figure 4.1.2-5).

In the case of F136°C the melting peak of the unmodified polymer shows that both gamma and alpha crystal structures exist. There is a slight tendency towards gamma crystallites. This indicates that the formation of the largest, most perfect crystals is restricted in F136C. The most likely explanation for this behaviour is the high molecular weight results in a high degree of chain entanglements which restrict the formation of the largest, most perfect alpha crystals. Interestingly all the nanocomposites produced, with the exception of F136C/C93A, show an alpha crystal dominant structure with some gamma crystal content. This would seemingly indicate that formation of the more perfect alpha crystal structure was promoted by the presence of clay, contrary to the situation seen in the low molecular weight PA-6 samples. One possible explanation for the phenomena

may be that due to the higher molecular weight of F136C initial crystal are larger and hence slower to melt. This could result in the melting crystals acting as nucleation sites for re-crystallisation during melting which may explain the formation of a large portion of more perfect alpha crystals i.e. they are predominantly formed due to re-crystallisation during the melting phase. The case of F136C/C93A composite is again interesting. In this case the melting peak indicates almost exclusively gamma crystal formation. It is possible that the dispersion of the clay in the PA-6 and the subsequent high level of interaction between the clay and polymer results in a restriction in chain mobility. The reduction of the chain mobility may prevent the polymer chains conforming to the most stable and perfect alpha crystal conformation. In addition the highly dispersed clay platelets may also act as a physical barrier to the formation of alpha crystal structures.

The DSC melting scans for ultra high viscosity PA-6 (F50) with and without clays are presented in Figure 4.1.2-6. This data again raises many interesting questions regarding the crystallisation processes in PA-6 nanocomposites and the influence of nanocomposite nature and PA-6 molecular weight.
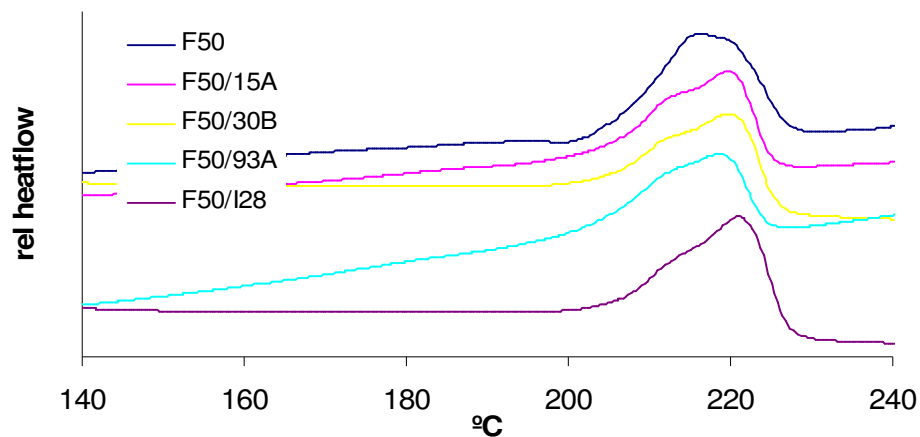
Figure 4.1.2–6 DSC crystal melting of F50 PA6 and F50 nanocomposites

As in the previous case for F136C high viscosity PA-6 the tendency for F50 is towards a greater extent of gamma crystallites. This result may be expected if we are to believe that the main influence in the crystallisation behaviour of the unmodified polymer is due to the chain entanglements which inhibit mobility and

hence the polymers ability to adopt the required crystal conformation within a given time period at a given temperature. The clay nanocomposite materials produced with the F50 PA6 all show a predominance of alpha type crystallites. Given the evidence from the unmodified polymer that the molecular weight influences crystal type it seems reasonable that re-crystallisation during melting explains this phenomena as the mobility of the molecular chains is much increased during melting hence the polymer can form more complex and perfect crystals – i.e. the alpha crystal structure.

4.2 MXD6/organoclay nanocomposites

The investigation on MXD6/organoclay nanocomposites is discussed in the following sections. It is expected that due to the materials structure (i.e. the presence of an aromatic ring) there will be significant differences between the behaviour seen for PA-6 and that of MXD6.

4.2.1 Structural characterisation of MXD6 nanocomposites

For the investigation of PA-MXD6 the MX6007 grade was utilised. Other rheology grades are available (MX6002 and MX6012) but MX6007 is known to be used and recommended for packaging applications.
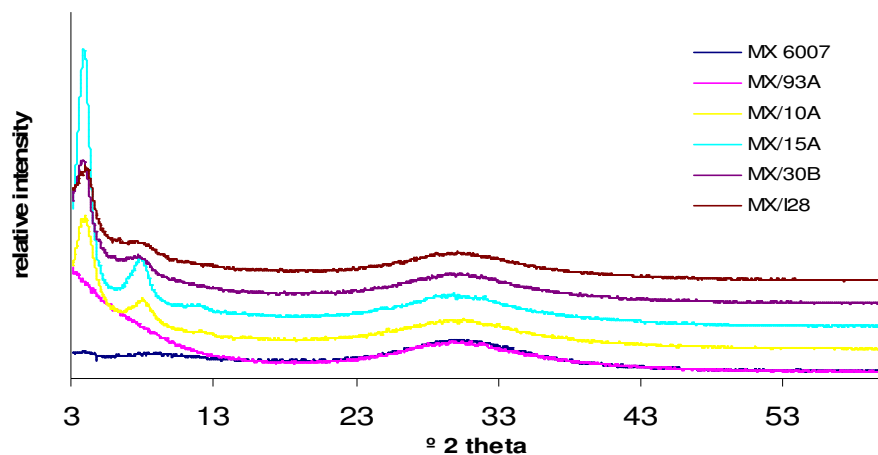
Figure 4.2.1–1 XRD spectra of MXD6 and MXD6 nanocomposites (Cr x-ray source)

The clays used in this study to provide a range of surfactants were C10A, C15A, C30B, C93A and I28. Compatibility with the polymer based on solubility parameter behaviour was determined to be in the order C30B > C10A > C15A > C93A (the surfactant structure of I28 is not known but it is expected that the compatibility will be similar to that of C15A and C93A). The processing of MXD6 nanocomposites was conducted at 250ºC and as such thermal stability of the surfactants may also have an important role in the development of nanocomposites. The five clays tested have thermal degredation temperature of 226ºC (C10A), 279ºC (C15A), 279ºC (C30B), 335ºC (C93A) and 323ºC (I28) based on five percent weight loss determined in air via TGA. It is assumed that compatibility and thermal stability are of the utmost importance for the formation of nanocomposites, thus it would be expected that C30B would offer the best hope of producing a highly exfoliated nanocomposite due to its better compatibility with MXD6 and only minimal degradation occurring at the processing temperature (i.e. the 5% weight loss temperature is above the processing temperature).XRD analysis of the unmodified polymer and the nanocomposites is included in Figure 4.2.1–1.

For the unmodified polymer there is no (001) diffraction peak as would be expected. There is however a broad peak centred at 30.5º which corresponds to weak crystallisation behaviour. Unlike the PA-6 based composites whereby there was an increase in both peak sharpness and intensity for nanocomposites there is no effect on this peak through the addition of clay. This would indicate that the clay has had little effect on the crystalline behaviour for the samples prepared for XRD analysis.

Based on the compatibility and thermal stability of clays it was expected that C30B would produce the best nanocomposite but in this study only an intercalated composite could be formed with this polymer/clay combination ((001) 3.56º 2 theta with spacing 3.69nm). In addition C10A, C15A and I28 produced only intercalated nanocomposites with (001) spacings of 3.26nm, 3.35nm and 3.20nm respectively. For all these clays there is a similar (001) spacing which suggests that the spacing is a feature of the polymer structure rather than the surfactant and also that the polymer replaces the surfactant in the interlayer. Of the surfactants tested only MXD6/C93A exhibited a highly dispersed structure with no (001) diffraction peak evident within the range of the

scan. This indicates that the (001) spacing is greater than 4.37nm. As it is very rare to find ordered clay structures with such a high (001) spacing it is assumed that at the very least this polymer/clay combination has produced a highly dispersed nanocomposite with possible exfoliation of clay platelets.

It is interesting that as per PA-6, despite a poor compatibility with the polymer C93A produces highly dispersed nanocomposites. This may provide some evidence that primary interactions (such as dipole interaction or hydrogen bonding) between the polymer and the surfactant are less important in nanocomposites formation than previously thought therefore it appears that thermal stability of the organoclay is more important in this case.

In summary the XRD traces were as expected with the only question remaining being the increase in the intensity for the most dispersed nanocomposite (MX/93A) at low diffraction angles. It is possible that some order over greater distances is present but further research would be required to confirm this.

4.2.2 Crystallisation behaviour of MXD6 nanocomposites

Crystallisation and melting behaviour of the MXD6 and its nanocomposites was again investigated using DSC. The DSC cooling scans are shown in Figure 4.2.2-1
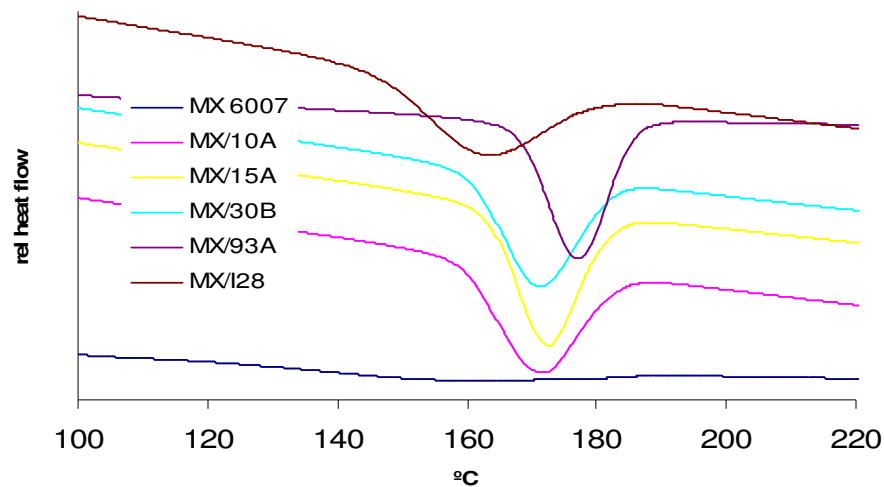
Figure 4.2.2–1 DSC cooling of MXD6 and MXD6 nanocomposites

136

The pure MXD6 polymer sample shows that the material has a tendency to crystallise very slowly under the test conditions used. It is difficult to isolate an accurate T_c crystallisation temperature as the peak is very wide and shallow. Based on the available data an approximation of 156°C has been used for comparison purposes.

The nanocomposite materials all exhibit a clear crystallisation peak compared to the unmodified material indicating the clay has had a significant nucleating effect on the polymer. From a T_c of 156°C for the polymer alone the T_c has increased to 171°C (C10A), 172°C (C15A), 170°C (C30B), 177°C (C93A) and 162°C (I28) with a significant sharpening and narrowing of the crystallisation peak. Several other interesting features of the melt crystallisation behaviour are also evident from the results. The behaviour of MXD6/I28 nanocomposite is interesting as this material has the lowest crystallisation temperature and is also the only clay of differing structure therefore it can be assumed that some aspect of the clay morphology (i.e. the more rounded and regularly shaped particles) results in a less pronounced nucleating effect than that observed for the Cloisite based nanocomposites. Of the three Cloisite clays investigated, C10A, C15A and C30B all had T_c around 170°C. Overall this means that all the intercalated nanocomposites had lower T_c than that observed for the only exfoliated nanocomposite in this series – MXD6/C93A which had T_c 177°C. This is interesting as in the case of PA-6 the nanocomposite with exfoliated structure had less of a nucleating effect than the intercalated nanocomposites. Overall the MXD6 exhibits behaviour similar to PA-6 in terms of clay nucleating crystallisation but opposite behaviour in terms of the nanocomposite structure which most effectively initiates nucleation – i.e. the exfoliated nanocomposite. This result is not fully understood at this time.

The data for melting behaviour of the MXD6 polymer and its nanocomposites is shown in Figure 4.2.2-2.
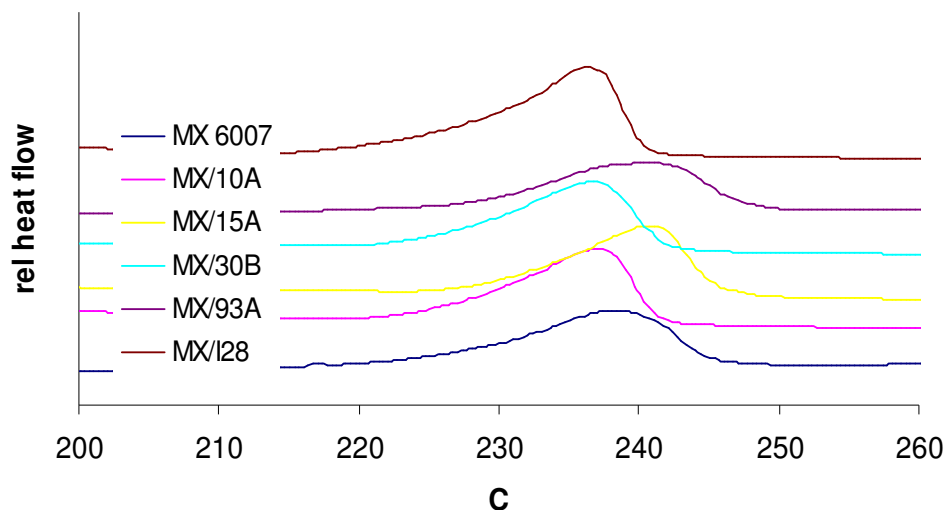
Figure 4.2.2–2 DSC crystal melting of MXD6 and MXD6 nanocomposites

The individual melting points are 239°C (MXD6), 238°C (10A), 242°C (C15A), 237°C (C30B), 240°C (C93A) and 237°C (I28). Although there are small differences there is no apparent pattern to them such as intercalated exhibiting lower T_m than exfoliated or vice versa. The differences may be due to difference in the lamellar thickness but from the results presented this can not be certain.

4.3 G21/organoclay nanocomposites

G21 is a copolymer of 70/30 composition of PA-6 terephthalate and PA-6 isophthalate and as such is amorphous in nature. This polymer will enable the effect of aromaticity and amorphous nature on the nanocomposites formation to be studied. It is hoped that this material can be an effective in dispersing clay and hence act as an exfoliation transfer agent for clay in PET. In addition the G21 PA allows us to widen our investigation into amorphous polyamide nanocomposites. As no previous literature was found concerning this material a screening of the commercial organoclays from Southern Clays were investigated. In addition to the sodium form of Cloisite (CNa$^+$), organoclays C10A, C15A, C30B and C93A were investigated.

138

4.3.1 Structural characterisation of G21 nanocomposites

The G21 amorphous PA is only available as one grade therefore an investigation of the effect of rheology for this material was not possible. As such an investigation of the effect of surfactant alone was conducted.

The XRD data for the G21 PA and it nanocomposites is shown in Figure 4.3.1-1.
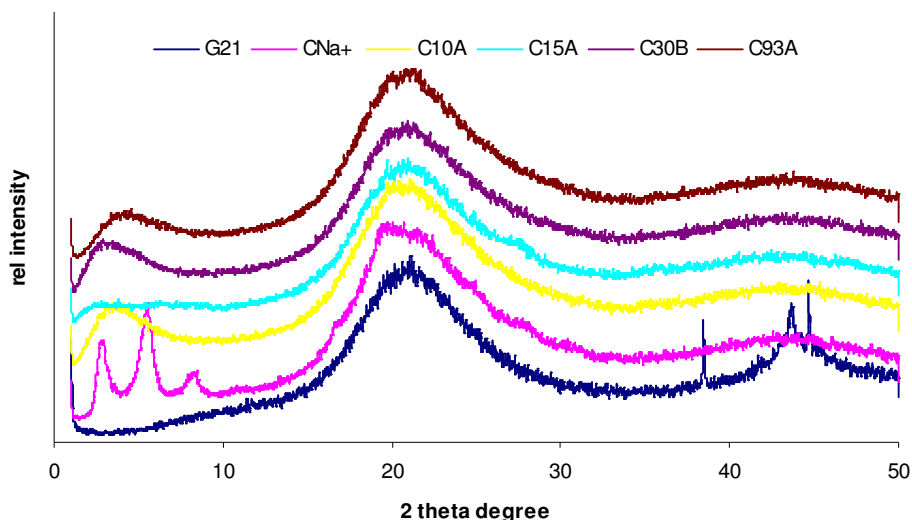
Figure 4.3.1–1 XRD spectra of G21 and G21 nanocomposites (Cu x-ray source)

For the G21 polymer there is clearly no peak in the low 2Θ degree range (i.e. less than 10º) but there is a broad ill defined peak centred at 21º 2Θ known as the amorphous halo. A second, sharp peak is evident at 38.44º and 43.73º 2Θ which corresponds to some unknown ordered aspect of the polymer structure. With the addition of CNa^+ there is a significant change in the diffraction pattern with 3 peaks evident in the low 2Θ degree range. The new peaks are found at 3.08º, 5.193º and 8.03º. These angles correspond to interlayer spacings of 2.87nm, 1.70nm and 1.03nm respectively and indicate that a multi structured material has been formed. In each case the peaks are sharp indicating that significant numbers of clay layers are retained in the clay platelet stacks.

The composite produced from C15A clay only exhibits a very slight shoulder at 2.91º 2Θ which corresponds to a (001) spacing of 3.037nm. This is identical to the raw C15A clay and would indicate that there has been no intercalation of this material by the G21 but the intensity of the peak is very low. This reduced intensity of the peak may indicate that the overall structure is a mixture of

139

exfoliated and pristine clay which would be a most unusual nanocomposite structure. The polymer structure as derived from the XRD data is similar to that observed for C10A

Cloisite 30B nanocomposite resulted in an intercalated nanocomposite structure. The (001) spacing of the clay increased from 1.786nm (pristine clay) to 2.63nm for the nanocomposite indicating significant penetration of the polymer chains into the clay galleries. The structure of the polymer is similar to that observed for the previous organoclays C10A and C15A.

The final G21 based nanocomposite produced with C93A clay resulted in a micro dispersed nanocomposite. The initial (001) spacing of the clay was 2.35nm while after melt processing the (001) spacing of the clay had reduced to 2.12nm. Overall this indicates that intercalation of polymer chains into the clay galleries had not occurred. And rather the clay exists as a micro dispersion in the polymer matrix. The polymer behaves as seen for previous organoclays with similar peaks. The overall shape of the XRD spectra obtained for G21 nanocomposites shows a significant broadening of the peak compared to the raw clay and may indicate that a number of structures with different spacing may be present.

4.3.2 Crystallisation behaviour of G21 nanocomposites

G21 and its nanocomposites were investigated by DSC and were found not to exhibit any peaks associated with crystallisation or crystal melting. This indicates that under similar conditions to those used for other PA's G21 is amorphous in nature with or without the presence of clay.

4.4 T5000/organoclay nanocomposites

Trogamid T5000 polyamide is a high temperature amorphous material generally used in applications where thermal stability and excellent optical properties are required. This material provided further opportunity to investigate nanocomposite formation with amorphous polyamides. In addition to its amorphous nature the T5000 also offers good potential for compatibility with

PET in exfoliation transfer approach for the improvement of CO_2 barrier properties.

4.4.1 Morphological characterisation of T5000 nanocomposites

As per the G21 polyamide T5000 is only available in one molecular weight/viscosity grade hence only an investigation of the effect of surfactant will be conducted. Similar to the case for G21 there is no known literature relating directly to the preparation and properties of nanocomposite with this material. The range of clays used previously in the investigation of G21 will again be employed to investigate this polyamide providing a direct comparison of the two amorphous types of polyamide with aromatic structure.

In Figure 4.4.1-1 XRD traces for T5000 and its nanocomposites formed with CNa^+, C10A, C15A, C30B and C93 are shown.

As would be expected the unmodified polymer does not exhibit any peaks in the low angle region where (001) peaks for clay are detected. There is a broad amorphous halo centred on 17° and also there are further small sharp peaks at 38.24° and 43.68° similar to those observed for G21. This indicates some small scale ordered structure and hints at some structural similarities between the two materials such as the aromatic ring.

The nanocomposite produced with unmodified sodium form clay (CNa^+) exhibits only a low broad peak at 7.38° corresponding to (001) spacing of 1.20nm. This value is similar to that observed for the raw clay and indicates that no intercalation of the clay has occurred. This would be expected given the highly hydrophilic nature of the raw clay interlayer as compatibility between polymer and clay will be very low. With the addition of clay the two T5000 peaks at 38.24° and 43.68° have disappeared and the large amorphous halo has shifted slightly and is now centred on 19.24° indicated some structural changes have occurred in the polymer due to the presence of the clay. The composite produced from T5000/C10A exhibits a (001) peak at 6.08°, corresponding to a basal spacing of 1.455nm. Similarly peaks for C15A and C30B are also found at this angle. This indicates that some intercalation of the polymer has occurred and that the interlayer cations have been replaced by the polymer as a combination of

polymer and surfactant would be expected to produce different (001) spacings dependant on the contribution of the surfactant. Overall this indicates that the interactions between the polymer and C10A, C15A and C30B are insufficient to produce exfoliated nanocomposites.

A slightly different picture emerges in the case of C93A. This nanocomposite exhibits a large broad peak with shoulders at 4.22° and 6.01°. These two peaks correspond to clay basal spacing of 2.095nm and 1.471nm respectively. It is possible the larger of the two spacings observed results from polymer and surfactant occupying the interlayer as C93A exhibits the highest thermal stability (335°C for 5% wt loss) compared to the other clays. All the clays tested resulted in the same change to polymer structure as described for CNa^+ indicating this phenomenon is directly related to the presence of the clay in the polymer.
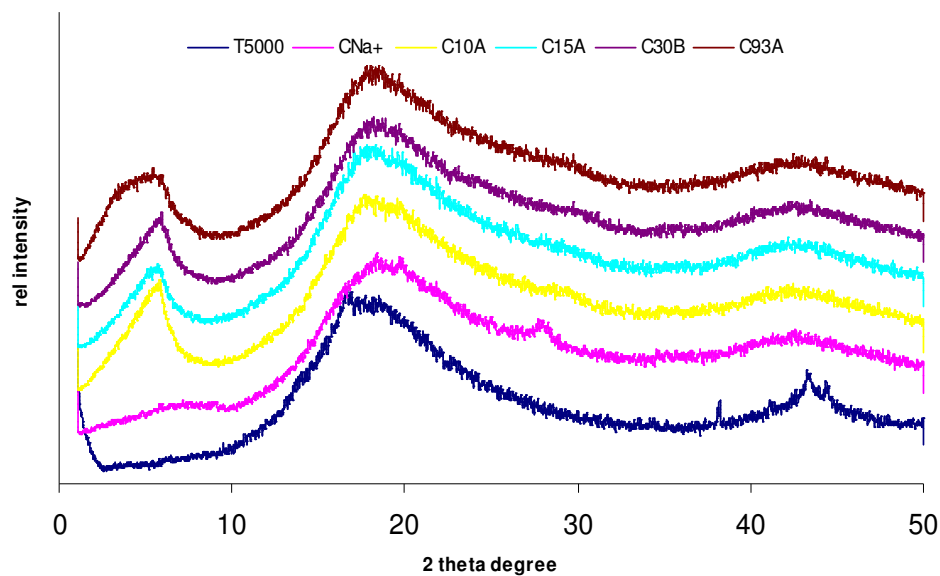
Figure 4.4.1–1 XRD spectra for T5000 and T5000 nanocomposites

The XRD scans obtained for T5000 are typical of those expected for intercalation although it is of note that the interlayer distance is reduced for the clay in this case.

142

4.4.2 Crystallisation behaviour of T5000 nanocomposites

Similar to G21, T5000 was investigated by DSC. No crystalline behaviour was observed indicating T5000 is an amorphous polymer under normal conditions.

4.5 Summary and Selection of materials for exfoliation transfer approach

The results obtained for polyamide nanocomposites indicates that there are several important factors which can influence the type of nanocomposite produced. These main factors are the polarity of the polymer (i.e. the concentration of amide groups), the molecular weight of the polymer (polymer viscosity), polymer surfactant compatibility and thermal stability of the clay surfactant.

Of the polyamides studied PA-6 has the highest concentration of amide groups. PA-6 is also the best material for producing highly dispersed nanocomposites with a (001) basal spacing of greater than 4.37nm observed for C30B, C93A and I28 organoclay indicating delamination of the clay layers. In the case of MXD6 a highly dispersed nanocomposite was only achieved with the C93A organoclay and this is the next most polar PA of those studied. In the G21 case only C15A produces a nanocomposite with a high level of dispersion, but in this case there is a weak (001) diffraction peak present indicating complete exfoliation has not occurred. Similarly the T5000 PA does not produce highly dispersed exfoliated type nanocomposites. The effect of polymer polarity on the exfoliation potential is summarised in Figure 4.5–1.

A second variable of importance to the exfoliation potential of the organoclay is the polymer viscosity. In the study of PA6 it was possible to investigate the phenomena by using a single clay to produce nanocomposites with four different viscosity PA-6 materials. The results clearly suggest that as viscosity increases exfoliation of clay platelets is more easily facilitated. Explanations provided in previous research indicating the importance of shear during the melt compounding process are expected to be responsible for the formation of nanocomposites with improved dispersion.
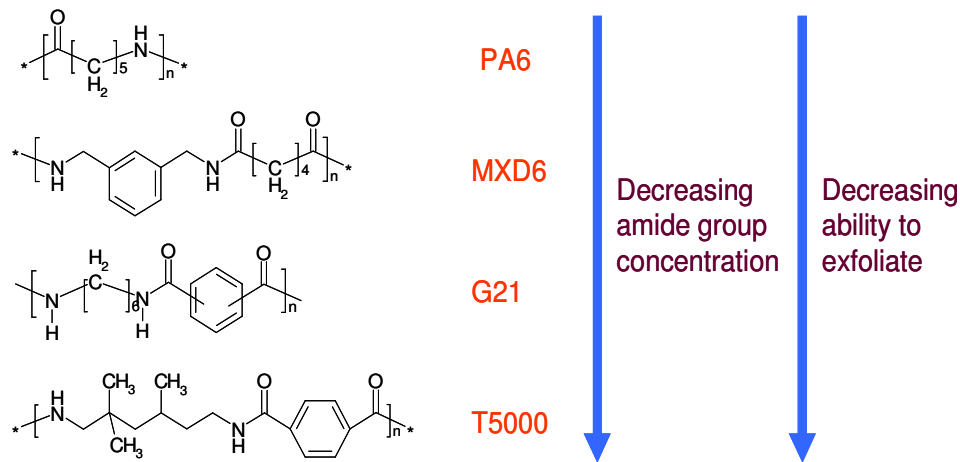
Figure 4.5–1 The effect of polarity on the ability of PA's to exfoliate clays

Surfactant polymer interaction are also believed to have some importance in promoting a high level of dispersion but our results show this effect is not as important as direct polar interactions between the polymer and the clay. It is our belief that the main function of the clay surfactant is to provide an environment that is initially sufficiently compatible with the polymer, and which increases the (001) basal spacing to such an extent that an initial diffusion of polymer chains into the clay interlayer is possible. In terms of the surfactants studied it is evident that those with greatest compatibility toward the polymer (such as C30B) do in fact promote dispersion but those with the least compatibility (C15A) seem to hinder the dispersion process (for the highly polar PA-6). The major deviation from this theory is the effectiveness of C93A as a surfactant for polyamides indicating that polarity of the polymer is important but also that the thermal stability of the organoclay is also important

The final factor which can influence the formation of the nanocomposites is the thermal stability of the surfactant. In the case of PA-6 the thermal stability of the commercial organoclays is sufficient to be ruled out as an important factor but for the higher temperature polyamides investigated (MXD6, G21 and T5000) degradation of the surfactant could be a significant issue due to degradation at the processing temperature. It is suspected that loss of surfactant from the clay surface inhibits the initial compatibility provided for intercalation and also causes

144

the clay interlayer to collapse further preventing diffusion of polymer into the clay galleries. This may explain the good performance obtained with C93A as its thermal stability is higher than the other clays investigated.

Based on these results materials have been selected for investigation as Polymers for the transfer of exfoliation into PET. Based on the level of exfoliation achieved PA-6 is a clear choice for further investigation. In addition the combination of MXD6 with C93A also offers a good choice for further investigation as it is the only MXD6 nanocomposite of exfoliated nature and MXD6 is well known to offer reasonable compatibility with PET. For G21 and T5000 no composites of a highly exfoliated nature were produced but as these materials offer potentially unique properties due to their amorphous nature and high compatibility with PET an initial study of their compatibility with PET and effect on CO_2 barrier properties will be conducted.

5 Exfoliation transfer blends of PA nanocomposites with PET

The overall aim of the work conducted in this chapter is to investigate the possibility of using the much better understood technology of polyamide nanocomposites to produce masterbatches that can be used to produce exfoliation of clay in PET. It is hoped by blending a pre-exfoliated polyamide based nanocomposite, transfer of the exfoliated clay platelets into the bulk of the PET matrix can be achieved. If this effect is achieved a significant improvement in CO_2 retention should be possible. Overall this effect will rely on the reaction of functional groups present in the chain ends of the PET and the PA's to produce in-situ block copolymers with resulting exfoliated clay as shown schematically in Figure 5-1.
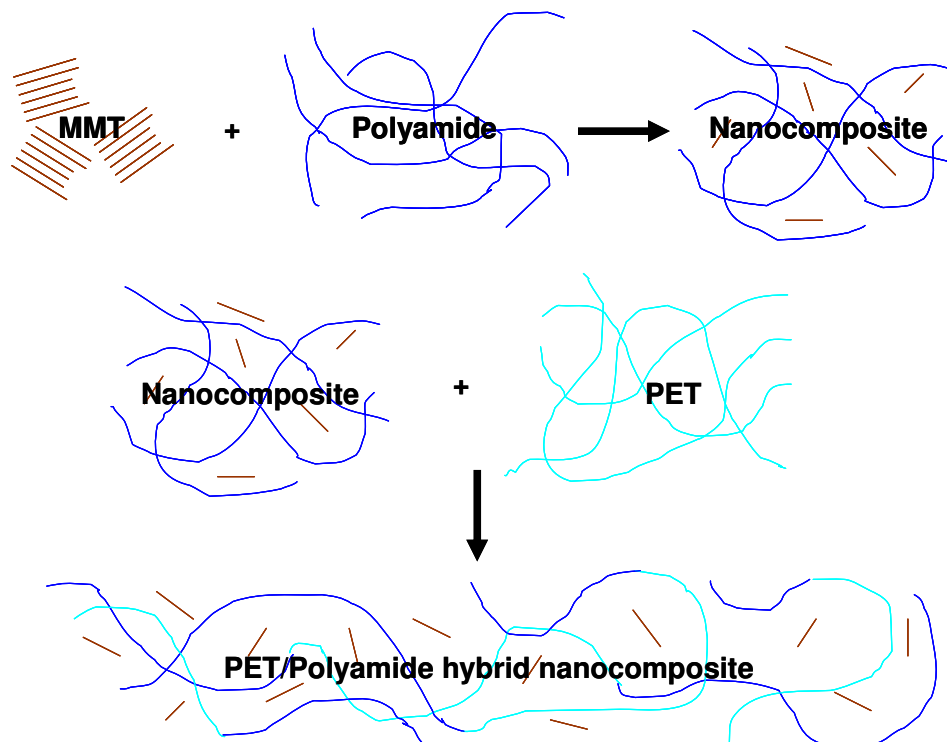
Figure 5–1 Schematic of exfoliation transfer through PET/PA blending approach

The data presented in the following chapter aims to establish if this approach can be used and which PET/Polyamide composites provide the best performance.

5.1 Blends of PET with PA's

The first step in assessing the potential of polyamides for an exfoliation transfer blending approach is to investigate the compatibility of the polyamide base polymers with PET. To this end simple physical blends of the polyamides at 5wt% are assessed by blending in a Boy injection moulding machine (as described in section 3.2.5.6). In addition, Hansen total solubility parameter and fractional Hansen parameters were calculated.

5.1.1 Compatibility of PET/PA blends

The Hansen solubility parameter data calculated for PET and the PA materials under investigation is presented in Table 5.1.1-1.

Table 5.1.1–1 Hansen solubility parameter behaviour for polymers

Polymer	δ total $\delta/\text{MPa}^{1/2}$	δd $\delta/\text{MPa}^{1/2}$	δp $\delta/\text{MPa}^{1/2}$	δh $\delta/\text{MPa}^{1/2}$
PET	21.3	17.9	6.9	9.1
PA6	22.7	19.6	8.7	7.5
MXD6	20.9	18.8	5.6	7.1
G21	19.9	17.9	5.3	6.9
T5000	16.4	15.2	1.2	6.3

The total solubility parameter data suggests MXD6 will offer the greatest compatibility with PET. Both PA6 and G21 are 1.4 $\delta/\text{MPa}^{1/2}$ in different from PET with PA6 above and G21 below. The T5000 is expected to be the least compatible based on the total solubility parameter. The dispersive components are all relatively similar (less than one unit difference) compared to PET with the exception of T5000. In addition, the polar component of the total parameter is much lower for T5000 than for the other polymers due to a lower amide group concentration. Overall the contribution due to hydrogen bonding is lower for the PA's than the PET. A TEAS plot of the fractional contributions is shown in Figure 5.1.1–1.

147
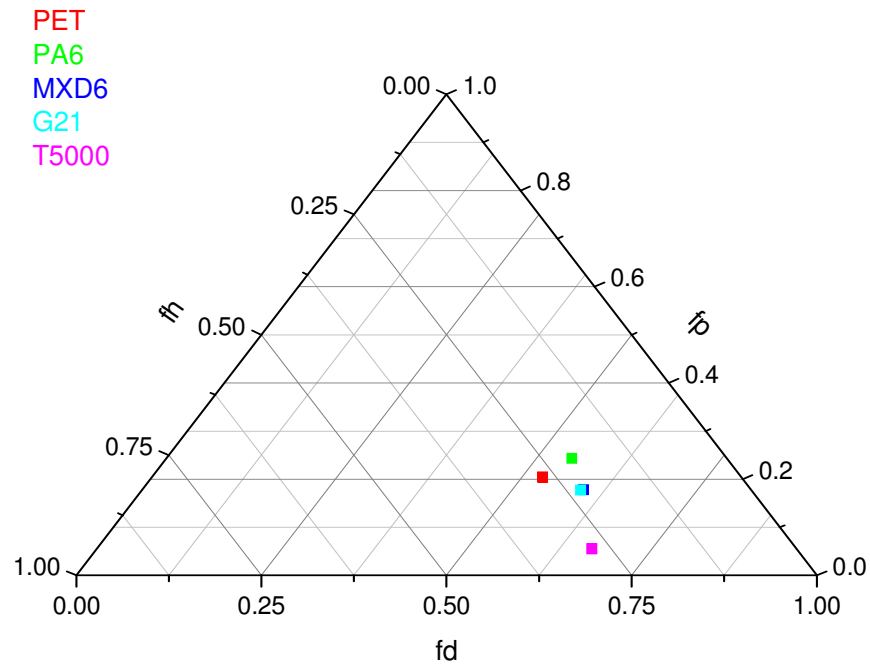
Figure 5.1.1–1 TEAS plot of polymer compatibility

Overall the TEAS plot reinforces the solubility parameter data and indicates all the polymers with the exception of T5000 should exhibit some element of compatibility with PET.

The plaques produced from the 5 wt% blend of PET with PA's are shown in figure 5.1.1-2. Of the polymers investigated PA6 has the least compatibility based on a visual assessment. Based on a simple like dissolves like approach to compatibility this would be expected as PET contains aromaticity while PA6 is aliphatic in nature. This indicates that structural factors can significantly affect the compatibility as Hansen solubility parameter data indicated that PET and PA6 may be compatible. G21 also exhibits poor compatibility from a visual perspective despite its closeness to PET in solubility parameter terms. This may be due to the increased length of the aliphatic chain compared to that in the PET (i.e. 6 carbon atoms compared to 2 for the PET).
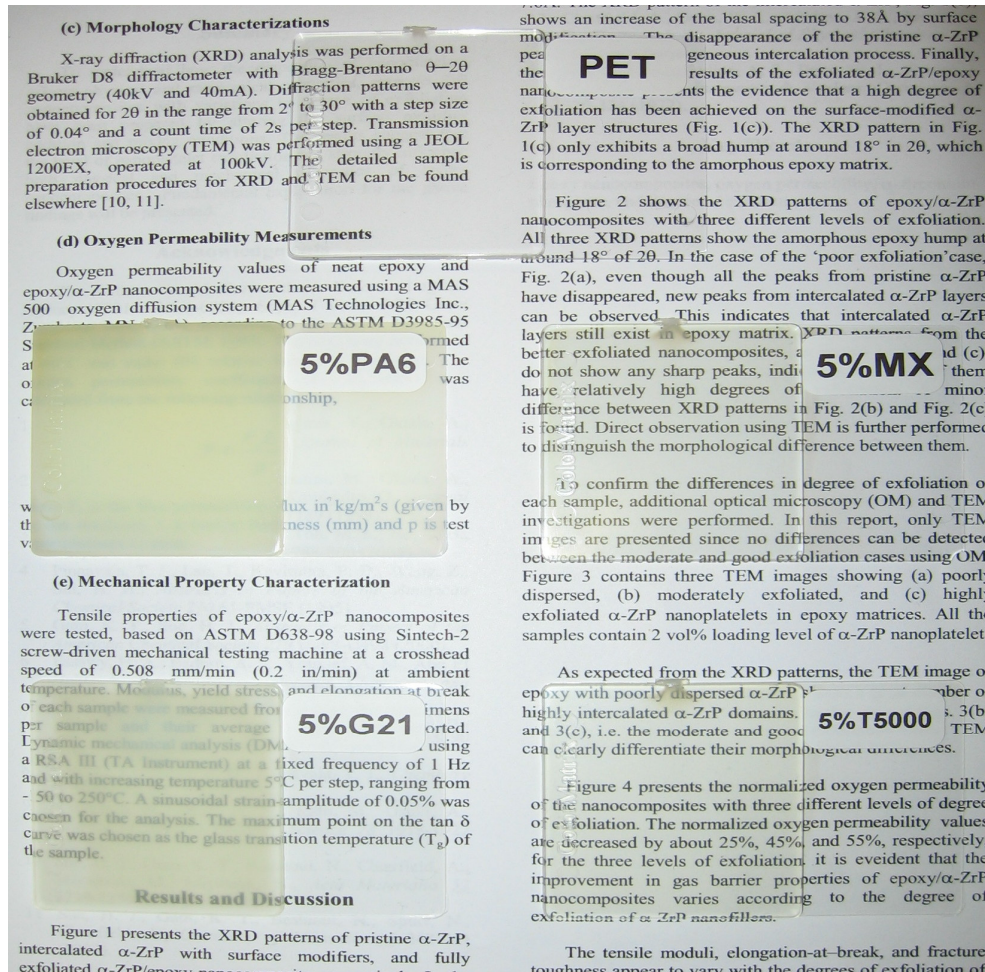
Figure 5.1.1–2 Comparison of haze for PET with 5wt% different PA's

The clarity of MXD6 and T5000, although not equal to the unmodified PET is very good. In the case of the MXD6 this is not surprising when considering the Hansen solubility parameter data and the obvious structural similarities. More surprising, is the very good clarity of the T5000/PET blend. Based on the solubility parameter data alone this would be expected to be the least compatible blend. The reasons for this behaviour are not clear.

5.1.2 Influence of polyamides on the crystallisation behaviour

DSC measurements were performed on samples removed from the plaques shown in Figure 5.1.1-2. The scans were conducted on a heat – cool – heat

programme as described in 3.2.5.3. The initial heating scans are shown in Figure 5.1.2–1.
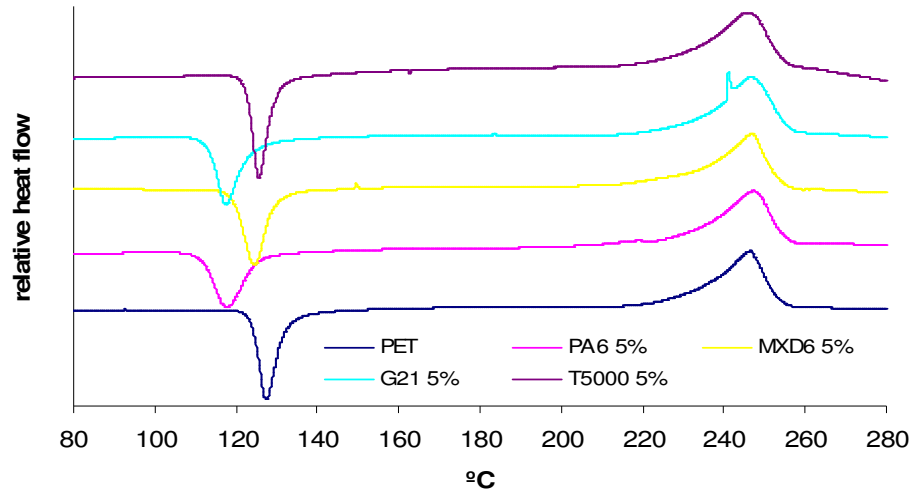
Figure 5.1.2–1 DSC heating scan of as extruded pellets comparing PET with 5wt% blends of PA's

From the DSC trace it is evident that the presence of clay has very little effect on the melting behaviour of blends but does significantly affect the cold crystallisation behaviour. The cold crystallisation temperature, T_c for PET is 127ºC and is reduced to 118ºC, 125ºC, 118ºC and 126ºC respectively for 5wt% blends with PA6, MXD6, G21 and T5000. For PA6 and G21 the reduction in T_c is particularly large and may result in difficulties in the bottle blowing process i.e. the onset of premature crystallisation as preforms pass through the bottle blower ovens prior to blowing. The crystallinity of the plaques was calculated as 9.35% PET, 11.03% PET/PA6, 9.13% PET/MXD6, 13.75% PET/G21 and 14.40% PET/T5000. The MXD6 blend has similar crystallinity to the PET standard and also has similar T_c indicating that overall this combination has the least effect on PET. From T_c and crystallinity data it is evident that the other nylons act as a nucleating agent.

The behaviour of the blends on cooling from the melt is shown in Figure 5.1.2–2.
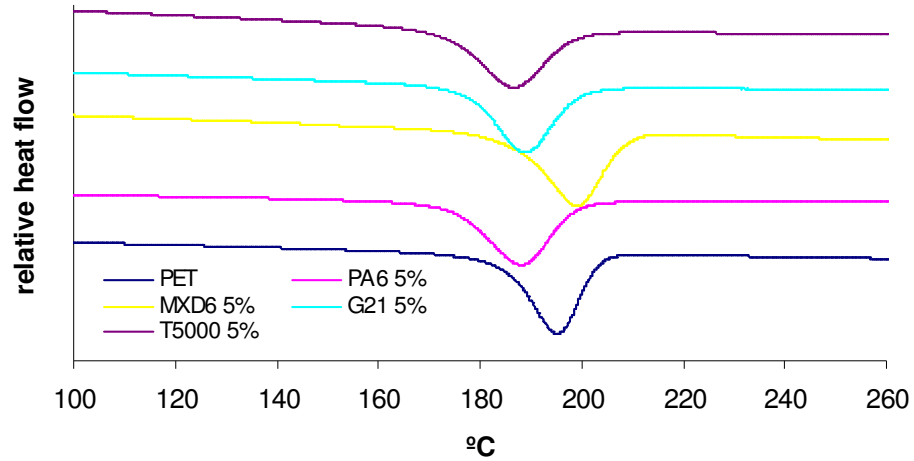
Figure 5.1.2–2 DSC cooling of PET and PET blends with 5wt% PA's

Interestingly, from the DSC traces it is evident that PA6, G21 and T5000 hinder nucleation from the melt resulting in reduced T_c (5-7ºC) compared to the PET and control and the PET/MXD6 blend. As per the initial heating scan the behaviour of the PET is most closely mimicked by the PET/MXD6 blend.

The second heat DSC traces for PET/PA blends are shown in figure 5.1.2–3.
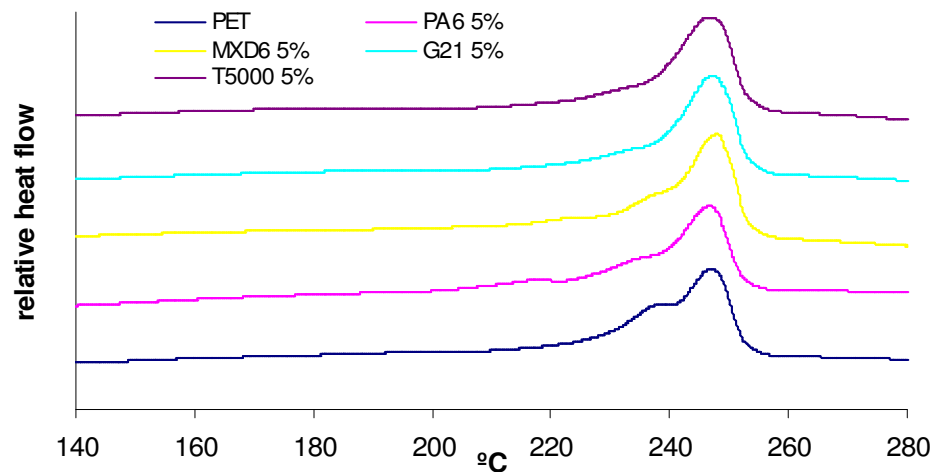
Figure 5.1.2–3 DSC crystal melting of PET and PET blends with 5wt% PA's

Overall the melting behaviour during the second heating scan is similar for PET and all the blend materials.

In summary the melting behaviour of the PET blends is the same as that of the base PET but the crystallisation behaviour is changed. In terms of the crystallisation behaviour MXD6 has the least impact on the PET retaining almost identical properties to the base resin. This is due to its ability to crystallise under similar conditions to PET and its similar processing temperature. The other polyamides have a nucleating effect during cold crystallisation but retard crystallisation when cooling from the melt. It is likely that when the material is cooled during the injection moulding process the PA forms large domains which, act as nucleation points on heating from cold. Conversely when cooling from the melt the inability of the PA's to crystallise/co-crystallise must inhibit the PET chains and prevent them crystallising as easily.

5.1.3 Gas barrier properties of PET/PA blends

To examine the gas barrier properties dry pellet blends of PET with high viscosity PA6, MXD6, G21 and T5000 were produced with 5/wt% of the polyamide. The process for producing preforms and bottles is described in section 3.2.6.1 in detail. As indicated in section 5.1.1 there is a considerable difference in the compatibility of the different polyamides with PET. A similar pattern was observed in the moulded preforms i.e. that PA6 and G21 produced preforms with a high level of haze while MXD6 and T5000 produced preforms with some yellowing but essentially transparent. When blow moulding was conducted it quickly became evident that the haze present in the PET/PA6 blend was due to crystallisation. The PA6 acts as a nucleating agent for the PET from a cold state resulting in premature crystallisation of the preform in the bottle blowing process. This indicates that PA6 is unsuitable for exfoliation transfer due to its nucleation properties. It was found that blends with MXD6, G21 and T5000 could all be blown easily into bottles for CO_2 testing. The PET/MXD6 bottle had the least haze while both G21 and T5000 produced bottles with significant haze. It is worthy of note that transparent preforms of T5000 produced hazy bottles. It is likely that although compatible with PET in the amorphous phase on orientation the developing crystals appear to have forced the T5000 domains to

152

coalesce into larger domains which, negatively impacts the optical properties of the bottle. Overall the only bottle of reasonable aesthetic properties is the PET/MXD6 blend.

The measured CO_2 retention properties of the 5 wt% blends of PET with MXD6, G21 and T5000 are shown in Figure 5.1.3-1
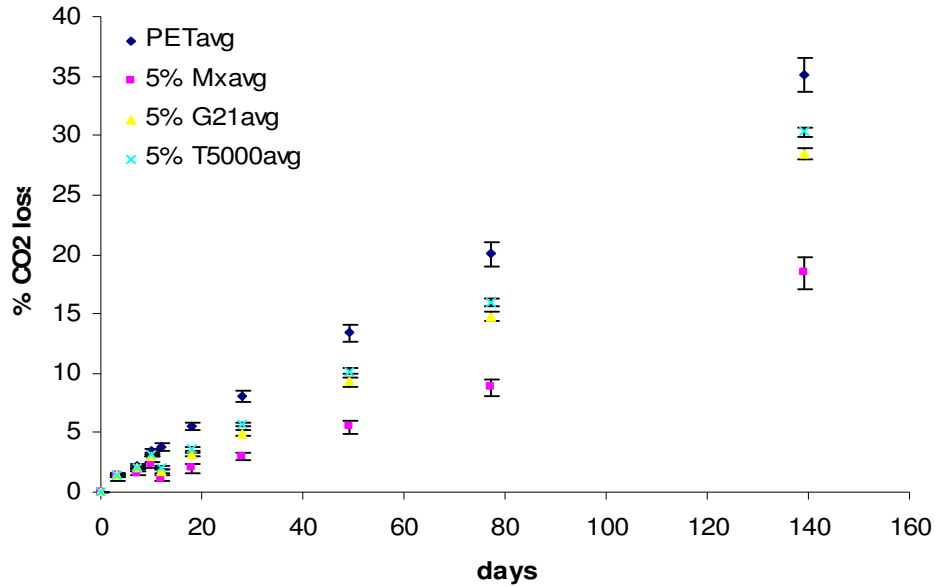
Figure 5.1.3–1 CO_2 loss from PET and PET blends with 5wt% PA's

From the results it is clear that the PET/MXD6 blend considerably improves the bottle CO_2 retention compared to the PET control, PET/G21 blend and PET/T5000 blend. The barrier improvement factor - BIF (ratio of the CO_2 of a standard bottle compared to that of a bottle containing a barrier) for this blend is 2.04 indicating that the shelf life of the package could be effectively doubled. Both PET/G21 blend and PET/T5000 blend exhibit improved CO_2 retention characteristics compared to the PET control but the improvement is not as significant as that noted for PET/MXD6 blend (BIF 1.29 and 1.20 respectively).The considerable improvement of the MXD6 blend compared to the other Nylons is in all likelihood due to its semi-crystalline nature in comparison to the other PA's which are amorphous. The amorphous nature of the G21 and T5000 prevent them from co-crystallising during the bottle blowing process thus the ultimate barrier performance is reduced compared to the PET/MXD6 blend.

5.1.4 PA nanocomposite/PET blends

From the initial investigation of PET blend CO_2 retention it is evident that PET/PA6 blends are unsuitable for nanocomposites blend approach due to the strong nucleating effect on PET. Previous results have shown that the presence of clay in PA6 considerably nucleates the PA6 hence it is clear that PA6 based nanocomposites would have an even stronger nucleating effect than PA6 alone. In addition the results have also shown that the CO_2 barrier properties of PET blended with both G21 and T5000 are inferior to PET/MXD6 blends. Due to these factors only MXD6/C93A nanocomposite has been selected for blending with PET and CO_2 barrier testing.

Preforms were produced from a dry blend of PET with 5/wt% MXD6 nanocomposite, which itself contained 5/wt% C93A organoclay. Immediately it was evident that the inclusion of clay in the MXD had changed the material significantly compared to the PET/MXD6 blend. The preforms were very hazy and it was quickly determined that they were crystalline and hence it would not be possible to produce bottles for CO_2 tests. This is not surprising as it was shown previously that the clay has a significant nucleating effect on the PET.
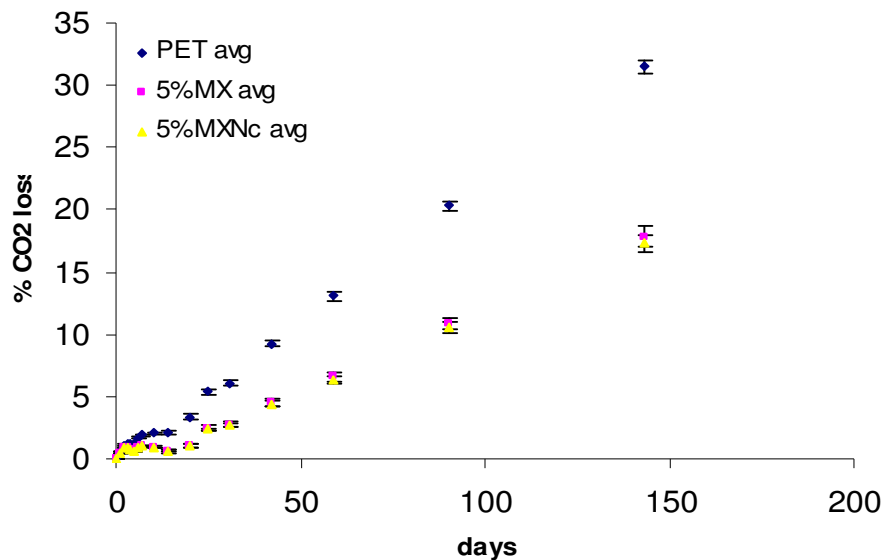
Figure 5.1.4–1 CO_2 loss for PET, PET/5wt% MXD6 and PET/5wt% MXD6 nanocomposite

The use of a 5wt% clay MXD nanocomposite was chosen to produce composites with 0.5wt% loading of organoclay in the final product. In order to overcome the

premature crystallisation hurdle a 1wt% clay MXD6 nanocomposite was produced. It was found that this material could be effectively blended with PET to produce bottle preforms that could be blown into bottles readily. The results of this nanocomposite blend along with a PET control and a PET/MXD6 blend are shown in Figure 5.1.4-1.

These results indicate that both the nanocomposite blend and the polymer blend improve the CO_2 retention characteristics of the PET considerably. BIF values of 1.90 for the nanocomposite blend and 1.85 for the polymer blend have been calculated. This indicates a slight improvement for the Nanocomposite blend compared to the polymer blend but error bars of one standard deviation indicate no real difference between these results. There are several possible explanations for this lack of efficacy for the organoclay in improving barrier. The most likely explanation would be insufficient clay content to significantly influence the CO_2 barrier properties, or alternatively, due to the clay being incorporated in the MXD6 there has not been transfer of the clay to the PET matrix – i.e. the clay is retained exclusively in the MXD6 phase.

5.2 Novel processing of PET/MXD6/organoclay hybrids

The results from blending PA nanocomposites with PET indicate that improved barrier properties are predominantly due to the presence of the polyamide and the clay has little influence. Due to nucleation of the PA by organoclay the PET itself was in turn nucleated resulting in only low levels of clay (0.1 wt%) in the final bottle. In addition, it is likely that the clay has remained incorporated in the PA domain due to low levels of ester-amide interchange as shown schematically in Figure 5.2–1.

In order to overcome these problems i.e. increase the clay loading and reduce the nucleating effect several new processing strategies were developed that involve the use of twin screw extrusion to blend the PET/PA and organoclay prior to any injection moulding. Three main process groups were compared, namely a compound approach whereby the material was processed with the correct proportions to allow bottles to be produced without the addition of virgin PET. Secondly a masterbatch approach was investigated whereby the blend

constituents are added at a ratio which allows the resultant masterbatch to be added at a fixed concentration to virgin PET in order to give a final product with similar loading to the compounding approach. Within these two processing approaches the effect of pre-blending the PET/PA component prior to addition of the clay compared to the effect of adding all the blend constituents together and the effect of catalyst addition is examined. A final approach is also undertaken where the clay is pre-extruded with the PA and then extruded with the PET as further step. This masterbatch can be added to virgin PET in the correct ratio to produce materials with similar final composition as the previous methods. This was done both with and without catalyst. The catalyst used in these experiments was Titanium iso-propoxide which has been shown to be an effective catalyst for esterification and ester-amide interchange reactions [170].

Dispersed MXD6 domains containing clay form tortuous pathway
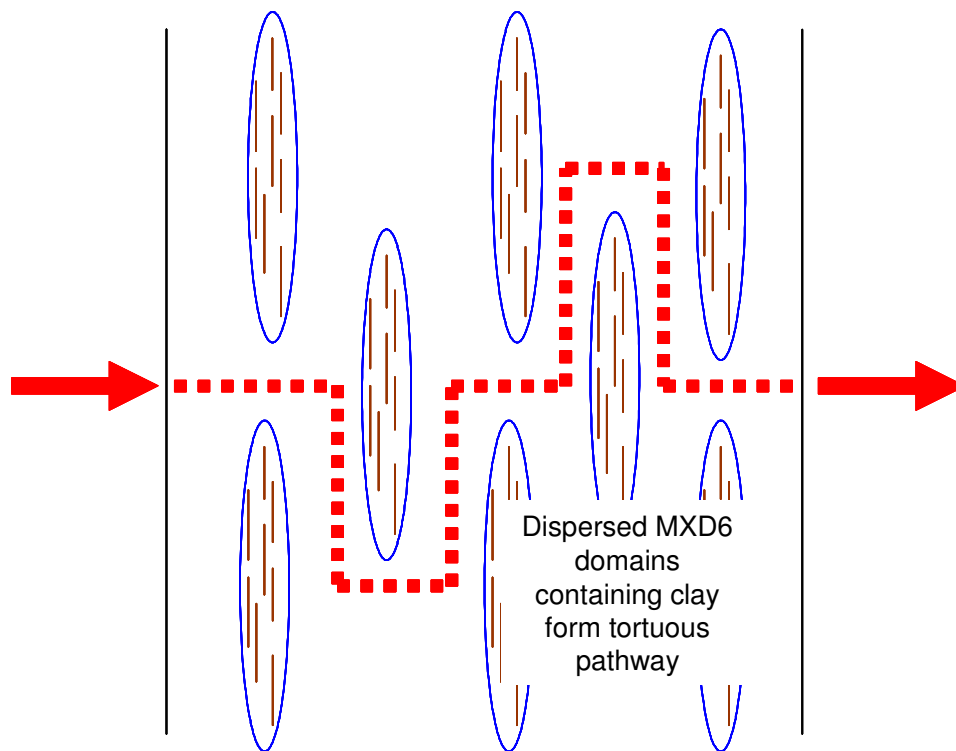
Figure 5.2–1 Schematic showing improvement in barrier due to PA rather than clay.

The composition and designation of each novel blend is shown in Table 5.2-1. Each blend is named by type of process (i.e. direct to mould – D, masterbatch –

M or PA nanocomposite – N). Where the PET and PA components have been pre-blended prior to addition a P follows the first letter. Inclusion of catalyst is indicated by the prefix c prior to the remaining product code. The novel nanocomposite blends were designed in order to produce novel hybrid bottles with 5 wt% MXD6 and 0.5 wt% organoclay

The make up of these blends also allows the PET to be made more polar, which potentially will make the polymer more polar thus, based on the results obtained for polyamides could improve the polymer clay affinity thus resulting in better clay dispersion. The use of a masterbatch approach allows the level of polar Polyamide to be greatly increased (i.e. 20% of polymer with greater polarity). In addition, the addition of catalyst may promote a much higher level of ester-amide reaction thus improving the PET/MXD6 compatibility.

Table 5.2-1 Novel blends designations, processing and compositions

Code	PET (wt%)	MXD6 (wt%)	C93A (wt%)	MXD6 Nc (wt%)	Ti catalyst (wt%)
D	94.5	5	0.5	-	-
c-D	94.3	5	0.5	-	0.2
D-P	94.5	5	0.5	-	-
c-D-P	94.3	5	2	-	0.2
M	78	20	2	-	-
c-M	77.8	20	2	-	0.2
M-P	78	20	2	-	-
c-M-P	77.8	20	2	-	0.2
N-M	80	-	-	20	-
c-N-M	79.8	-	-	20	0.2

5.2.1 Morphological characterisation of PET/MXD6/organoclay hybrids

The morphological characterisation of these novel hybrid PET/MXD6/clay hybrids will be studied using XRD and POM (polarised optical microscopy) techniques.

The XRD micrographs of the PET/MXD6/clay blends produced by the direct to mould approach are shown in Figure 5.2.1-1.
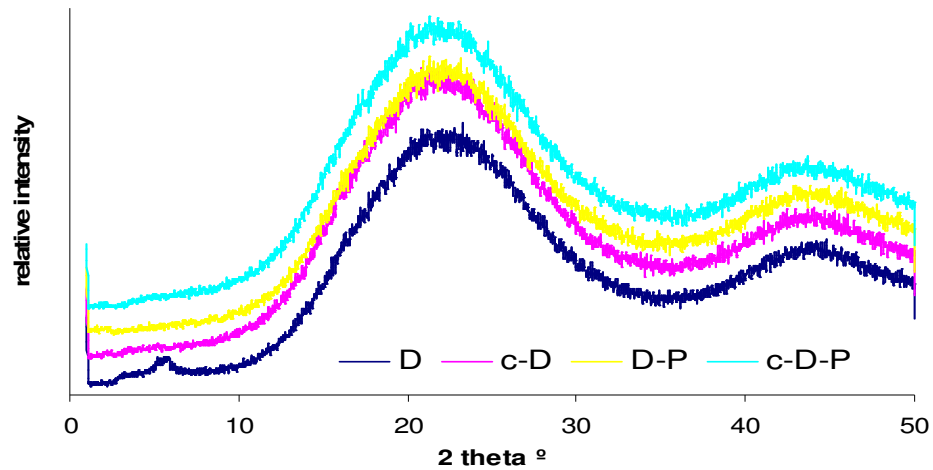
Figure 5.2.1–1 XRD spectra for novel blends produced as compound with final bottle composition (Cu x-ray source)

In the chart above the intensity of (001) peaks is low, as would be expected given the relatively low loadings present in the composites. For sample D where PET, MXD6 and clay have been blended in a single extrusion step two peaks are evident in the (001) region. The first peak is present at 3.47º which corresponds to an interlayer spacing of 2.548nm. This is very similar to the (001) spacing of the pure C93A clay of 2.356nm and indicates that no intercalation of the organoclays has occurred. The second peak positioned at 5.97nm correspond to (001) spacing of 1.48nm indicating that some of the organoclay may have suffered some degradation leading to the collapse of the (001) spacing. Sample c-D where the mix was prepared as sample D but with the addition of titanium catalyst no (001) peak is present indicating improved dispersion of the organoclay in the polymer blend.

Samples D-P and c-D-P where the PET and MXD6 have been pre-blended there are no peaks evident within the (001) peak region indicating improved dispersion of organoclay. Overall these results indicate that improving the compatibility of the PET and MXD6 component whether by the use of catalyst to promote ester amide change, physically pre-blending the polymers prior to the addition of the

organoclay or by a combination of both techniques can improve the clay dispersion in the polymer.
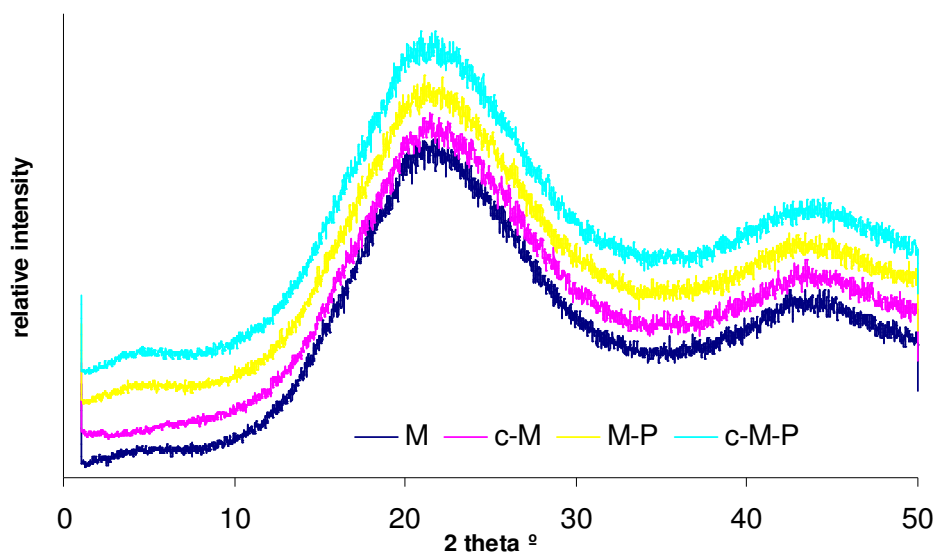
Figure 5.2.1–2 XRD spectra for novel blends produced as a masterbatch (Cu x-ray source)

Further novel blends produced via a masterbatch approach contained a much greater quantity of organoclay (2wt% compared to 0.5wt% for the direct to moulding masterbatches) and a much greater quantity of MXD6 PA (20wt% compared to 5wt% for the direct to mould blends). The XRD scans for the masterbatch blends are shown in Figure 5.2.1-2.

From the XRD scans it can be seen that sample M when PET, MXD6 and clay were directly blended a broad low peak can be observed at 4.83°. This corresponds to a (001) spacing of 1.831nm indicating that some degradation of the organoclay may have occurred. In the case of the catalysed analogue, sample c-M no (001) peak is visible indicating improved dispersion of the organoclay. This further strengthens the observation that the presence of catalyst can assist in the clay dispersion process. Samples M-P and c-M-P when the PET and MXD6 components are pre-blended with and without catalyst prior to clay addition both exhibit (001) peaks at 4.54° and 4.34° respectively. These values correspond to (001) spacings of 1.947 and 2.037nm, lower than the parent clay C93A. This

159

again indicates some degradation of the clay surfactant has occurred. It is possible that the presence of high levels of MXD6 in the blend and the effects of trans-esterification have resulted in reduced overall molecular weight of the polymer. Any reduction in molecular weight can hinder the potential for shear generation which can help clay dispersion. In addition the loading of clay for these mixes was higher and hence achieving a high level of dispersion is more difficult.

The final novel blends were again produced by a masterbatch approach but this time the clay component had been pre-blended with the MXD6 polymer. In order to provide a final clay loading of 0.5 wt% in the bottle the MXD6 nanocomposite had to be produced using 10 wt% clay. The XRD scan for the MXD6 nanocomposite containing 10 wt% clay is shown in Figure 5.2.1-3. For comparison purposes a further nanocomposite of MXD6 containing 5wt% clay was prepared and the original organoclay is included. From the result a very low broad bulge is visible for the MXD6 nanocomposite with 5wt% clay centred on 2.564º. This corresponds to a (001) spacing of 3.482nm but the intensity is very low suggesting a predominantly exfoliated nanocomposite with some intercalated clay present. Overall the nanocomposite has well dispersed organoclay. For the 10wt% organoclay nanocomposite the (001) reflection peak is much clearer. The peak is positioned at 2.589º corresponding to a basal spacing of 3.414nm. The 10wt% composite clearly has an intercalated nanostructure as the (001) distance has increased from 2.356nm for the pristine clay. It may be expected that the increased clay loading has prevented better dispersion simply due to a lack of space for the exfoliated platelets at such a high loading. This may hinder the exfoliation of the clay particles in the PET blending situation.
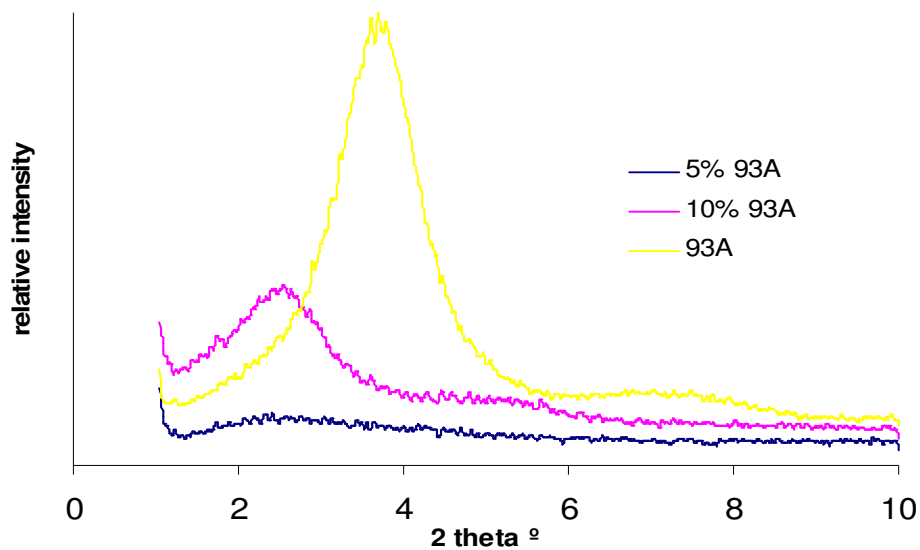
Figure 5.3.1–3 XRD spectra of MXD6/C93A nanocomposite with 5wt% and 10wt% organoclay (Cu x-ray source)
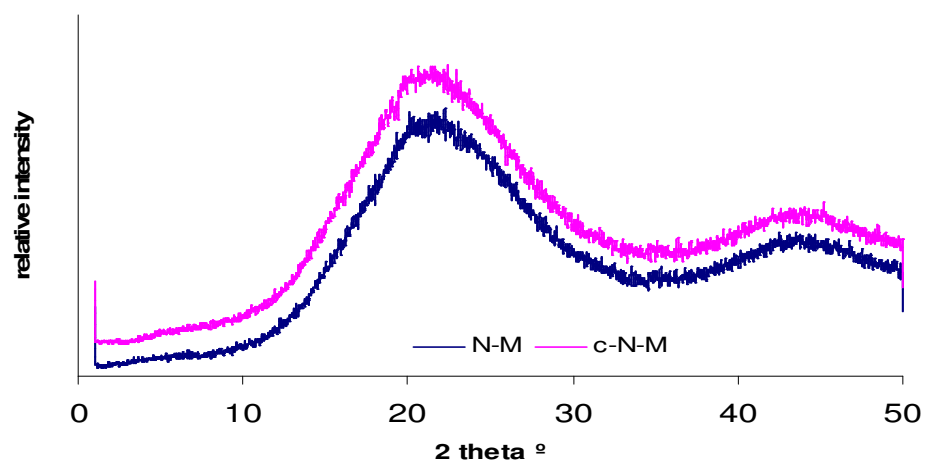
Figure 5.3.1–4 XRD spectra for novel blends using MXD6 nanocomposite (Cu x-ray source)

The XRD diffraction patterns for samples N-M and c-N-M that were produced by blending a 10wt% MXD6 nanocomposite with PET both with and without catalyst are shown in Figure 5.3.1-4. It can be seen that there is no (001) basal spacing present for either material indicating a good dispersion of the clay. As the nanocomposite portion of the blend had an intercalated structure it appears

that further melt mixing and dilution of the clay content has helped to improve the dispersion of the clay.

Overall the novel blends indicate that it is possible to process PET, MXD6 and clay by different methods with good dispersion. Lower MXD6 content (i.e. 5 wt% as in the compound samples) and the addition of catalyst and pre-blending of the MXD6 and clay appear to produce the best dispersed nanostructures.

5.2.2 Crystallisation behaviour of PET/MXD6/organoclay hybrids

DSC analysis was conducted on bottle wall samples to allow the effect of the organoclay on the bottle wall crystallinity and its behaviour under cooling from the melt to be investigated. In addition analysis of bottle wall ensures all the samples have a similar composition and like is compared to like i.e. 5% MXD6 with 0.5% C93A clay.

Table 5.2.2–1 Summary table of PET blends crystal melting behaviour

Sample	T_m on ºC	T_m ºC	T_m end ºC	ΔH_m j/g	%χ (bottle wall)
PET	239	248	254	47.39	33.8
5% MXD6	239	249	255	43.29	30.9
5% MXD6 ext	239	249	255	39.65	28.3
G21	240	250	255	43.15	30.8
T5000	239	250	255	47.42	33.8
D	239	250	255	43.82	31.2
c-D	240	249	255	38.40	27.4
D-P	239	250	255	34.26	24.4
c-D-P	240	249	254	44.12	31.4
M	239	250	255	44.43	31.7
c-M	238	250	255	46.22	33.0
M-P	238	250	255	47.06	33.5
c-M-P	238	250	255	45.75	32.6
N-M	238	250	256	44.46	31.7
c-N-M	238	250	255	43.40	30.9

Table 5.2.2-1 summarises the melting data for bottle wall samples and includes calculated crystallinity values. In general it can be seen from the T_m data that the melting temperature and range over which the melting occurs is unaffected by the incorporation of polymer and clay and remains stable regardless of the processing route followed. When the MXD6 is added to the PET there does appear to be a slight reduction in the overall level of crystallinity, possibly due to the dispersed domains of MXD6 acting as a physical barrier to crystallisation. As would be expected the effect is magnified when the PET/MXD6 have been pre-blended as the number of dispersed MXD6 phases will be increased due to reduced size and improved dispersion through the twin-screw extrusion process. When the materials are processed in combination with the clay to produce samples there is again a reduction in the overall level of crystallinity for reasons similar to those stated previously.

On cooling from the melt some differences in behaviour are observed. DSC cooling scans for PET in comparison to PET/MXD6 and PET/MXD6 (pre-extruded) are shown in Figure 5.2.2-1
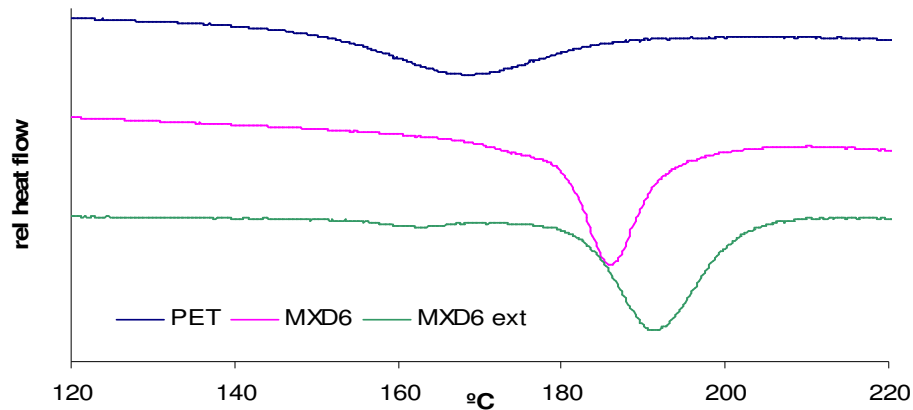
Figure 5.2.2–1 DSC cooling of PET and PET/MXD6 blends produced using different processing methods

As shown in previous scans for PET blended with MXD6 there is a nucleation effect and crystallisation from the melt is occurs at a higher temperature than for PET alone. For MXD6 blended in the injection moulder the T_c increases to 186ºC compared to 168ºC for the PET control indicating that the MXD6 acts as a

nucleating agent. The effect is greater when the PET/MXD6 are pre-blended using the twin screw extruder and the T_c is increased to 191ºC in this case. Two effects account for this greater increase than that observed for the injection moulder blend. Firstly the number of MXD6 nucleation points is increased in the extruded blend due to better mixing of the MXD6 and secondly there is potentially a reduction in molecular weight due to the added processing history resulting in easier crystallisation of the PET.

DSC cooling scans for novel blends produced as a compound with the correct material proportion for the final bottle are included in Figure 5.2.2-2
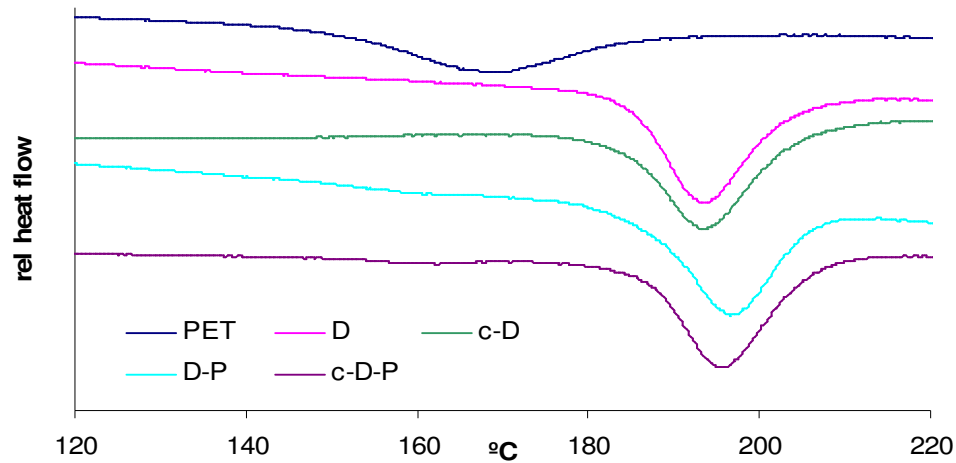
Figure 5.2.2–2 DSC cooling of novel blends produced with final bottle composition

Again the overall effect is nucleation of the PET. In this case samples D and c-D where the all the materials are added together in one extrusion an increase in T_c to 193ºC and 194ºC respectively was observed. This increase is slightly greater than that seen for the PET/polymer blends without the clay and indicates that the presence of the clay has a further nucleating effect. In addition it is evident that the use of catalyst has not affected the crystallisation properties of the samples.

DSC cooling scans are presented in Figure 5.2.2-3 for novel hybrids produced by a masterbatch approach.

164
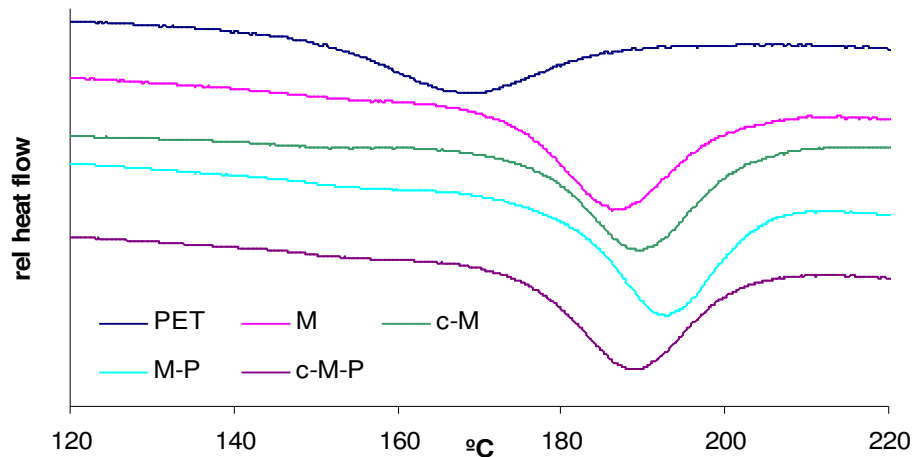
Figure 5.2.2–3 DSC cooling of novel blends produced as a masterbatch

Again as would be expected there is a significant nucleation effect compared to the standard unmodified PET. Interestingly the overall effect is lower than the materials produced as a compound probably due to the addition of virgin material in the bottle which is not degraded and hence of higher RMM and slower crystallising.
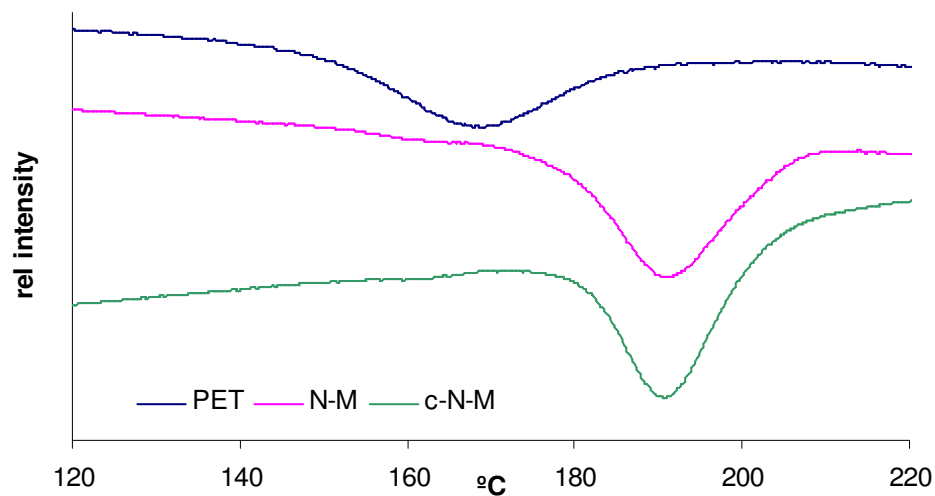
Figure 5.2.2–4 DSC cooling of novel blends produced using MXD6 nanocomposite

The final set of materials investigated was those produced using MXD6 nanocomposite. The DSC cooling scans are shown in Figure 5.2.2-4

As expected there is a nucleation effect but again it is not as significant as that observed for the compound materials. Both samples have T_c of 191ºC. This may be lower than the compounds due to the clay being encompassed in the MXD6 and hence only able to nucleate the MXD6 rather than the wider PET matrix.

The second heating scan further confirms that there is little effect on the melting properties of the PET due to the inclusion of MXD6 and clay with T_m onset values of 238ºC to 240ºC, T_m values of 248ºC to 250ºC and T_m end values of 255ºC to 257ºC.

5.2.3 Gas barrier properties of PET/MXD6/organoclay hybrids

The gas barrier properties of the novel nanocomposite blends were evaluated in comparison to control PET bottles. In addition to the novel nanocomposite blends MXD6 added at the injection moulding stage and MXD6 pre blended were also investigated and compared to PET. The CO_2 loss data for the MXD6 materials without clay are shown in Figure 5.2.3-1.
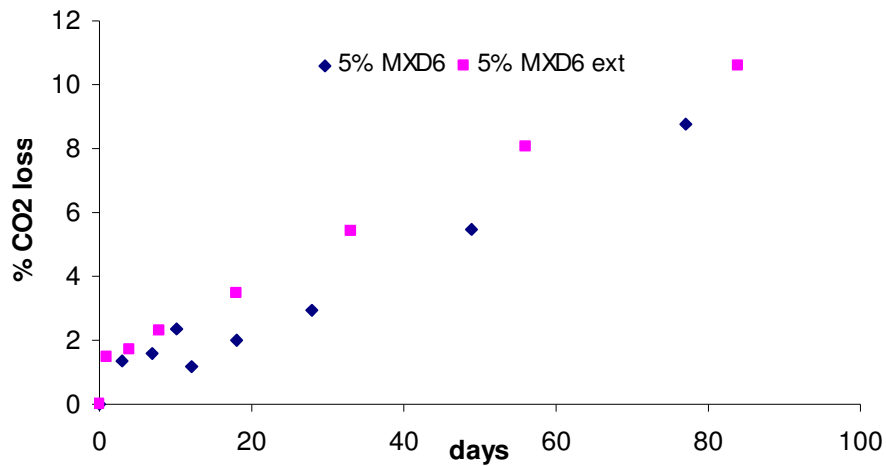
Figure 5.2.3–1 Comparison of CO_2 loss for 5wt% MXD6 blend via different processing route

This chart shows that there is a small loss of barrier property when the MXD6 is pre-blended by extrusion prior to the production of the bottles. The micrographs of bottle wall samples shown in Figure 5.2.3-2.
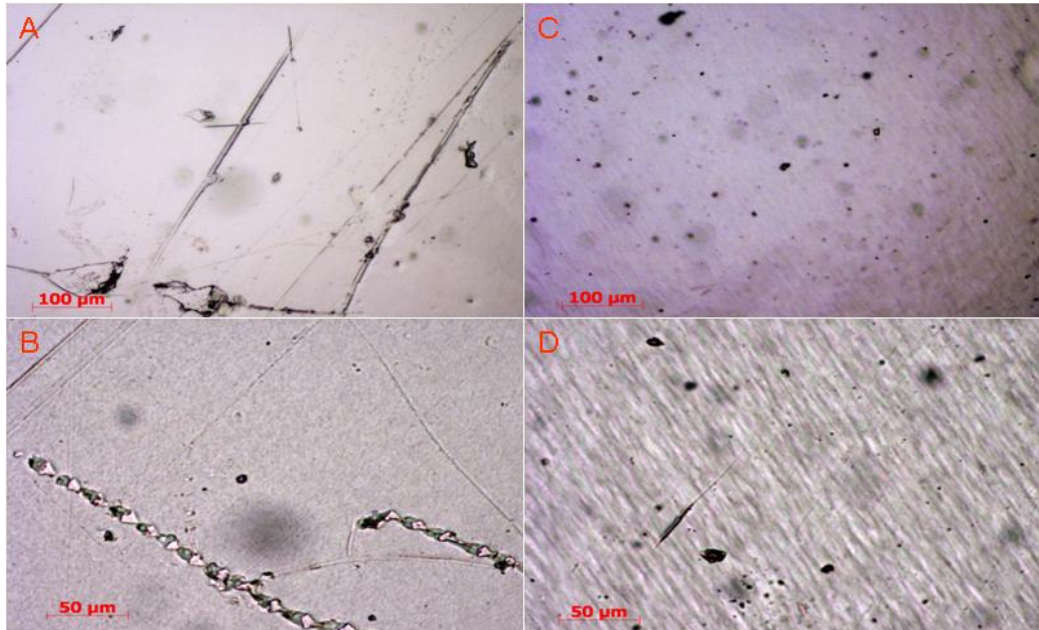
Figure 5.2.3–2 Micrographs of (A) 5wt% MXD6 low magnification, (B) 5wt% MXD6 higher magnification, (C) 5wt% MXD6 ext low magnification and (D) 5wt% MXD6 ext higher magnification with 100μm scale bars for low magnification and 50μm scale bars for higher magnification

In the figure A and B are micrographs of PET/MXD6 bottle wall produced at the injection moulder. The figure shows some artefacts are present in the bottle wall but these are mainly transparent. In contrast in the case of micrographs C and D there are a significantly greater number of black specs indicating increased degradation has taken place due to the increased processing history. Degradation of the polymer is very likely to reduce the overall barrier property of the bottle and explains this slight reduction compared to the injection moulder produced blend.

For the direct to moulding approach (Figure 5.2.3–3) it can be seen that there is little difference between the samples within error of 1 standard deviation. This indicates that when producing a hybrid material with the correct composition for the final bottle the order in which additives are added (i.e. all additives added to

the extruder together or PET/MXD6 pre-blended) does not influence the overall CO_2 barrier property. In addition, the use of catalyst to improve PET/MXD6 compatibility and hence polymer compatibility with clay does not have an influence on the overall gas barrier property. The BIF for these materials was calculated to be 1.66. This is a considerable improvement over the unmodified PET resin but is less than the BIF obtained for a physical blend of PET with 5wt% MXD6 produced on the injection moulding machine (BIF of 1.9 – 2.05 have previously been obtained) or one produced by extrusion pre-blending of PET/MXD6. It is likely that due to the added processing step degradation of the PET has taken place. This is supported by the considerable yellowing noted for these materials and this may influence the subsequent barrier properties. Examples of micrographs obtained for these materials are shown in Figure 5.2.3–4.
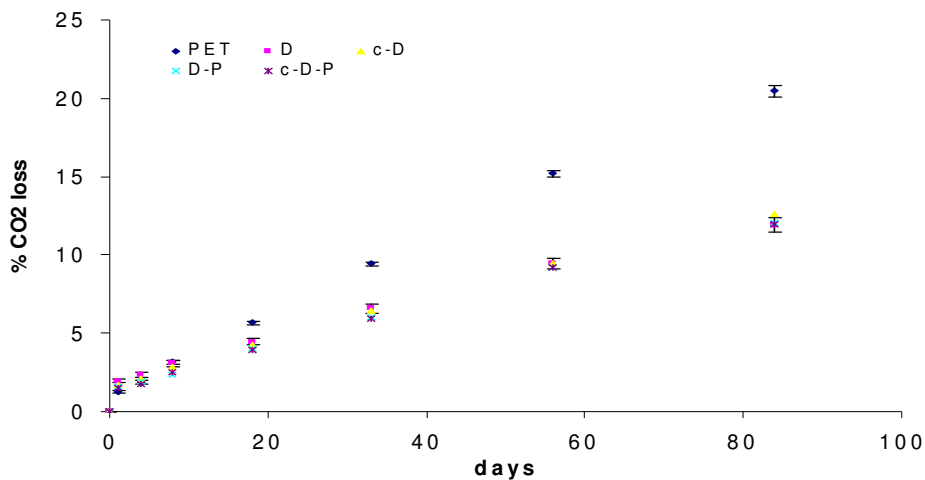
Figure 5.2.3–3 Comparison of CO_2 loss for novel blend produced to final bottle composition

A corresponds to D, B to c-D, C to D-P and D to c-D-P. It is clearly evident that the amount of artefacts is increased considerably compared to blends produced with MXD6 alone. The artefacts evident are most likely due to increased degradation and it appears the presence of clay increases this problem further. The materials with catalyst (prefix c-) appear to exhibit more degradation and resultant artefacts than their un-catalysed analogues while it also appears that

pre-blending (suffix –P) also has a detrimental effect due to the incorporation of yet another processing step. Thus despite an improvement in barrier properties it appears that increased degradation prevents optimisation of the barrier offered by both the MXD6 and the clay.
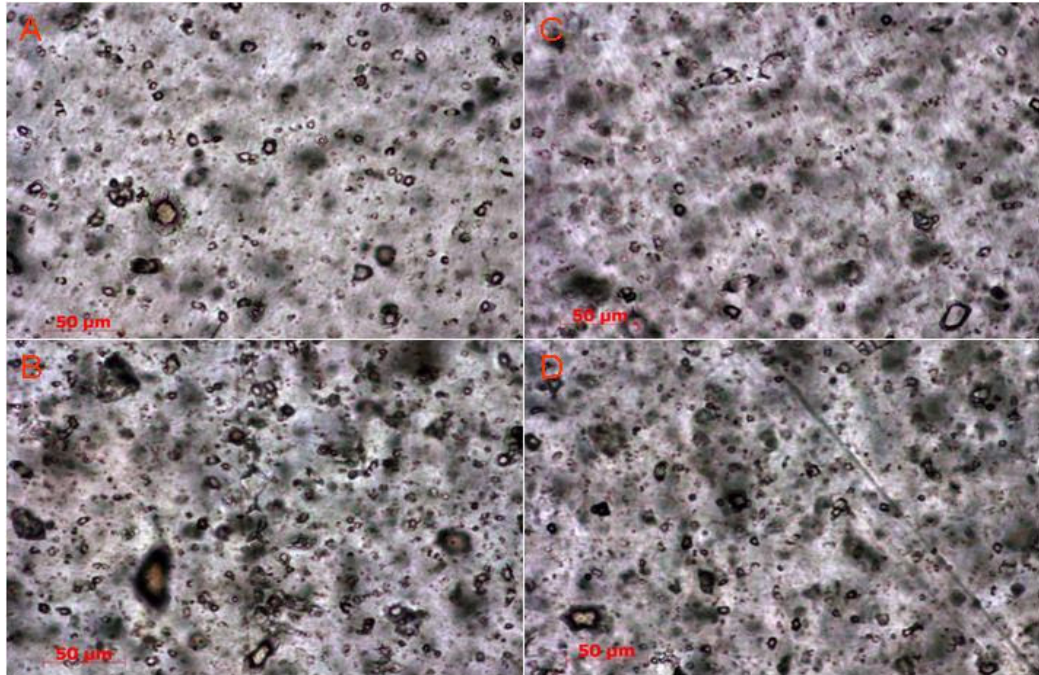
Figure 5.2.3–4 Micrographs of (A) direct to mould, (B) direct to mould (catalyst), (C) direct to mould (pre-blended PET/MXD6) and (D) direct to mould (pre-blended PET/MXD6 and catalyst) all with 50μm scale bar.

For the hybrid materials produced as a masterbatch to be added to virgin PET at 25% CO_2 loss results are shown in Figure 5.2.3-5. Similarly to the hybrids produced in proportions suitable for producing the final bottle those produced by differing masterbatch approaches do not show any major difference within experimental error. The presence of catalyst or the pre-blending of PET and MXD6 prior to addition of clay have no significant effect on the final CO_2 barrier properties. The overall BIF for these materials was determined to be 1.7, again much lower than that observed for a direct blend of PET and MXD6 produced via injection moulding. In addition it appears that a MB approach does not hold any advantages in terms of CO_2 barrier properties compared to a compounding

approach. When viewing the associated bottle wall micrographs it is again evident that significant degradation has occurred (Figure 5.3.2-6).
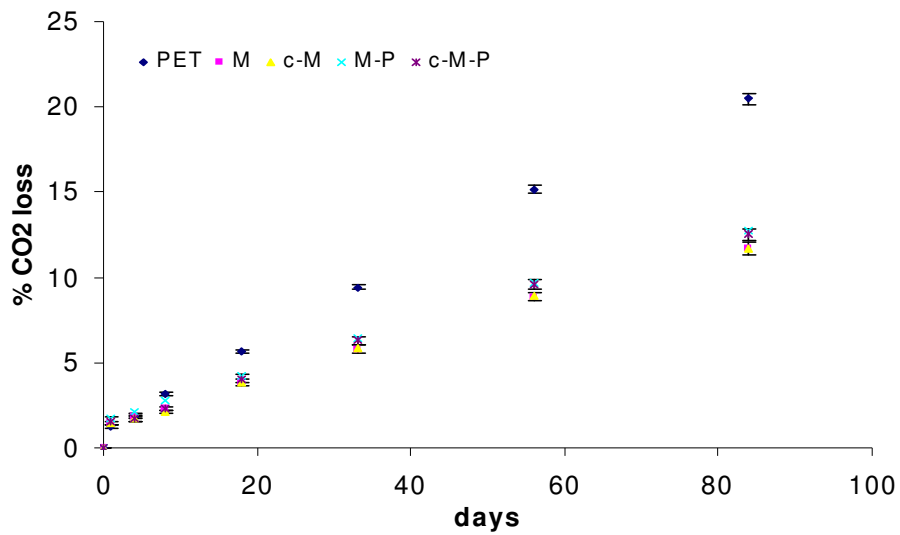
Figure 5.2.3–5 Comparison of CO_2 loss for novel blend produced as masterbatch
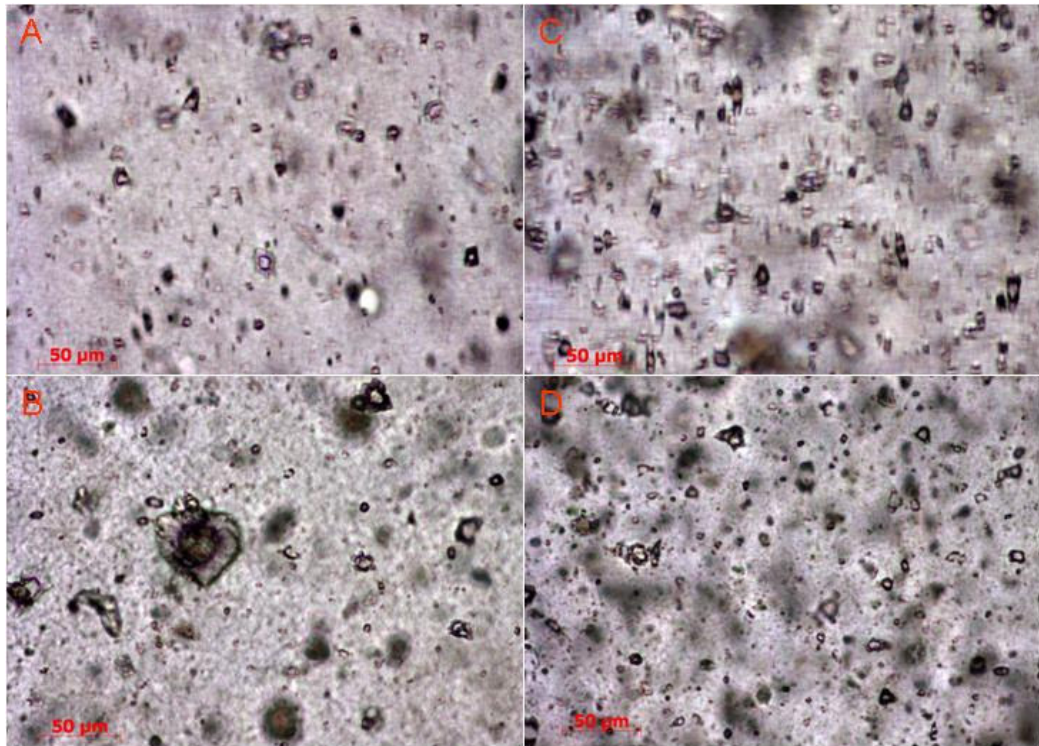
Figure 5.2.3–6 Micrographs of (A) masterbatch, (B) masterbatch (catalyst) , (C) masterbatch (pre-blended PET/MXD6) and (D) masterbatch (pre-blended PET/MXD6 and catalyst) all with 50µm scale bar.

As per the previous novel hybrid micrographs it is evident that the degradation is worsened by both the presence of catalyst and the addition of further processing steps.
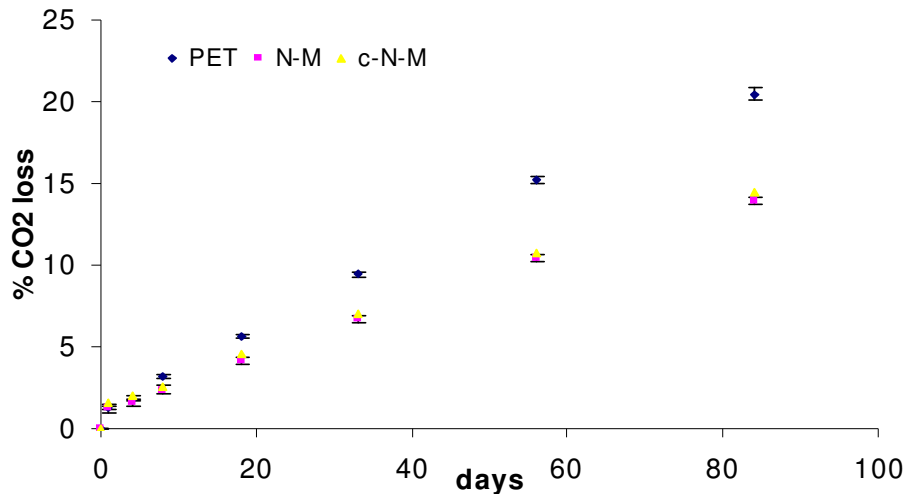
Figure 5.2.3 – 7 Comparison of CO_2 loss for novel blend produced with MXD6 nanocomposite

The final hybrid mixtures that were produced by blending nanocomposite with PET both with and without catalyst are shown in Figure 5.2.3-7. As per the previous hybrid materials there is no difference in the CO_2 retention property due to the use of catalyst. Interestingly the BIF for these materials was determined to be 1.4, much lower than that seen for direct to moulding hybrids and masterbatch hybrids. This could be due to the clay component being contained within the nylon phase and not being distributed through the whole matrix.

Micrographs of this novel blend are shown in Figure 5.2.3-8 and indicate that less degradation has occurred when the clay is added as part of an MXD6 nanocomposite. In addition the effect of the addition of catalyst does not have a significant effect. Overall this indicates that the presence of the clay and its direct combination with catalyst are the main causes of degradation.
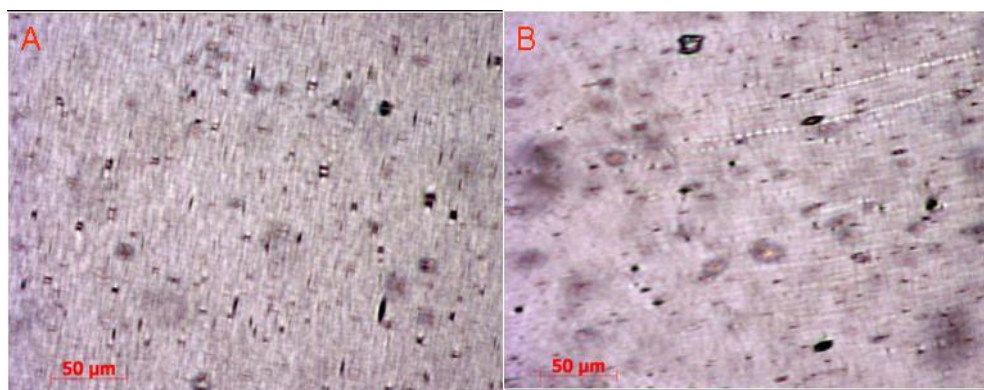
Figure 5.2.3-8 Micrographs of (A) nanocomposite blend, (B) nanocomposite blend (catalyst) with 50μm scale bar.

5.3 Summary of PET/PA blending approach to barrier improvement

The use of polyamides blended with PET has been demonstrated to improve the barrier properties considerably with a loading of 5wt%. The most effective materials of the polyamides investigated was clearly MXD6 which resulted in a barrier improvement factor of ~ 1.9, considerably higher than the BIF observed for the other nylon blends. Based on this result further blending experiments were conducted solely on variants containing MXD6 nylon. The first investigations were conducted on blends of PET with 5wt% MXD6 nanocomposite containing varying clay loadings. It is known from our earlier work that the incorporation of clay into MXD6 significantly nucleates the MXD6. We have also shown that the presence of MXD6 in PET also has a significant nucleating effect. It was therefore not surprising that reasonable loadings of clay (5wt%) in the MXD6 resulted in bottle preforms that were crystalline and hence it was not possible to blow them into bottles. A loading of 1wt% clay in the MXD6, when added to PET at 5wt% did allow the production of bottles but the barrier properties of these were only similar to those of a simple PET/MXD6 blend. This indicates that either the loading of clay is too low to impart significant barrier improvements (0.1wt% in the final bottle) or that the clay is not dispersed within the whole polymer matrix and is confined entirely to the MXD6 phase.

In order to try and overcome these problems and produce blends that utilise both the barrier properties of the MXD6 and the clay novel blend routes were devised. These novel blending routes overcame the problem of crystallisation of the bottle preforms and bottles with a final clay loading of 0.5wt% clay were readily produced. Unfortunately the barrier properties of these materials were not improved as significantly as the simple blend of PET/MXD6. On examination of bottle walls sections using POM it was found that significant degradation had occurred and it is surmised that this has led to the lower than hoped for barrier improvements. It is significant that the blends produced using an MXD6 nanocomposite had BIF lower than both compound and masterbatch material indicating that some benefit was obtained from the clay present. In addition it was found that no improvement was obtained by using catalyst in the hope of promoting ester amide interchange reactions and hence greater compatibility of the PET and MXD6.

Overall the addition of MXD6 at the injection moulding stage can significantly improve the CO_2 barrier of PET but when clay is incorporated no additional benefit is observed. Using novel processing techniques it was possible to increase the clay loadings but resultant degradation negated any benefits offered by the clay in terms of barrier improvement.

6 Evaluation of direct intercalation/exfoliation of clays in PET

In the literature to date, there has not been a complete assessment of all the important properties of nanocomposites produced from commercial clays or clays produced by various research groups. This chapter will discuss the varying morphologies produced and their influence on the crystallisation and CO_2 barrier behaviour of PET.

6.1 Morphological characterisation of PET nanocomposites

The morphological characterisation of PET nanocomposites can be neatly split into those produced using commercial organoclays and those produced using our own in-house modified clays. XRD was utilised to investigate the morphology.

6.1.1 Commercial organoclays

The predominant group of commercial clays investigated were the Cloisite range produced by Southern Clays. The range of materials is as per the polyamide investigations i.e. CNa$^+$, C10A, C15A, C30B and C93A in order that a range of polarity and hence potential compatibility can be investigated.

The XRD trace for PET with CNa$^+$ with the virgin polymer and the raw clay included for comparison is shown below in Figure 6.1.1-1 The measured (001) spacing for the raw clay was 7.52nm, in good agreement with published data. For the PET/CNa$^+$ nanocomposite a (001) spacing of 7.33nm was measured. As the value for the raw clay and the nanocomposite are similar it is expected that no intercalation or exfoliation of the clay has been achieved. The unmodified CNa$^+$ has a highly hydrophilic interlayer and it is expected that penetration of the less hydrophilic polymer chains will not occur due to poor compatibility between the polymer and the clay surface.
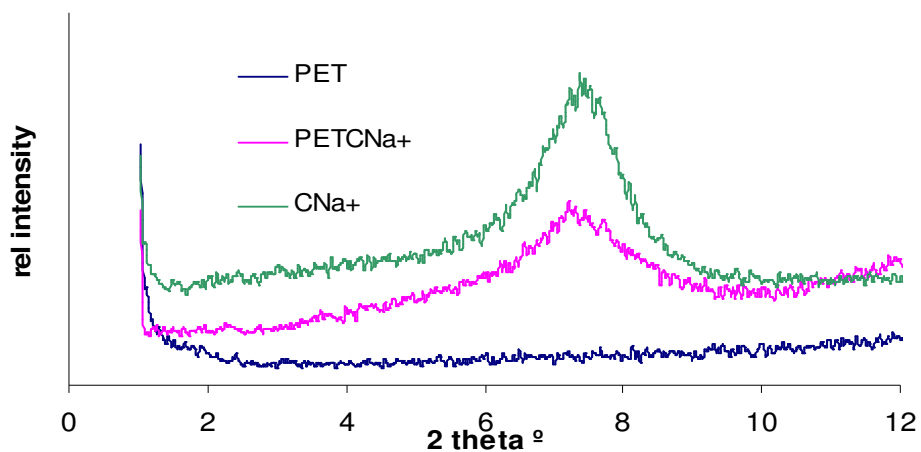
Figure 6.1.1–1 XRD Spectra for PET, CNa$^+$ and 5wt% PET/CNa$^+$ nanocomposite (Cu x-ray source)

For C10A the initial (001) spacing was measured at 1.83nm while the resultant nanocomposite had (001) spacing measured to be 3.11nm (Figure 6.1.1-2).The interlayer spacing has increased by 1.28nm indicating intercalation of the polymer chains into the clay interlayer. The presence of a clear (001) peak for the nanocomposite indicates that exfoliation has not occurred to any great extent hence the composite produced would be classed as an intercalated nanocomposite. The reduced peak intensity of the nanocomposite compared to the clay indicates that the number of clay layers per stack has been reduced. This further indicates that the mere incorporation of similar chemical groups in order to promote compatibility is not enough on its own to promote exfoliation of clay in polymer.
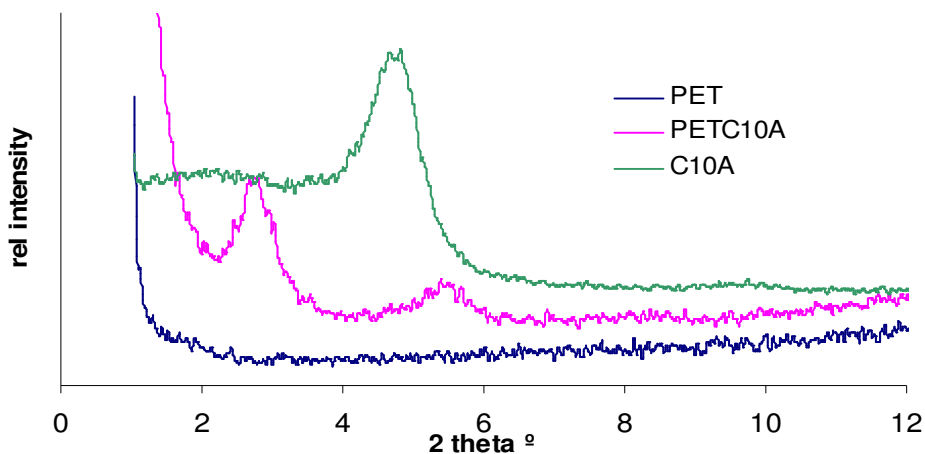
Figure 6.1.1–2 XRD spectra for PET, C10A and 5wt% PET/C10A nanocomposite (Cu x-ray source)

For C15A and its PET nanocomposite (Figure 6.1.1-3) (001) spacings of 3.04nm and 3.19nm respectively were obtained. The (001) spacing has increased slightly (by 0.15nm) and in combination with the presence of (002) and (003) peaks it would be expected that a highly regular intercalated nanocomposite structure has been formed. As the surfactant for C15A is highly hydrophobic low compatibility with the PET would be expected hence an intercalated nanocomposite would be expected rather than exfoliation of the clay.
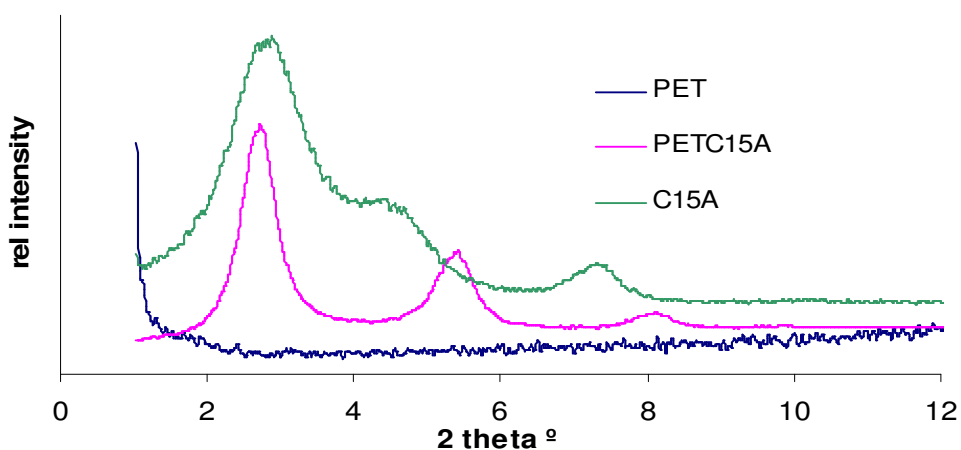
Figure 6.1.1–3 XRD spectra of PET, C15A and 5wt% PET/C15A nanocomposite (Cu x-ray source)

176

From the Hansen solubility parameter data C30B was expected to have the best compatibility with PET from the commercial organoclays tested and hence the greatest potential to produce highly exfoliated nanocomposites. The XRD scans are presented in Figure 6.1.1-4. The initial (001) spacing of the clay is 1.76nm while after processing with PET to produce nanocomposite the (001) spacing has reduced to 1.42nm (a reduction of 0.34nm). This indicates that no intercalation of the PET into the clay interlayer has occurred and that the surfactant has degraded to some extent resulting in the collapse of clay galleries. This result is somewhat surprising as C30B has similar thermal stability to C15A and much better thermal stability to C10A and may be due to reactions between the PET ester linkage or PET end groups and the surfactant hydroxyl group that are degradative in nature.
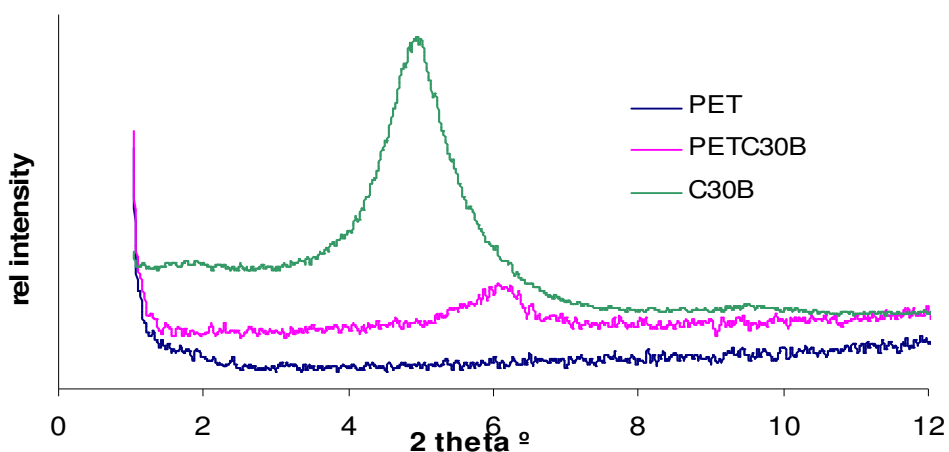
Figure 6.1.1–4 XRD Spectra of PET, C30B and 5wt% PET/C30B nanocomposite (Cu x-ray source)

The final Southern Clays material, C93A has (001) spacing of 2.37nm in its pristine form which increases by 0.75nm to 3.12nm (Figure 6.1.1-5). This increase is significant and confirms that a nanocomposite of intercalated nature has been formed.
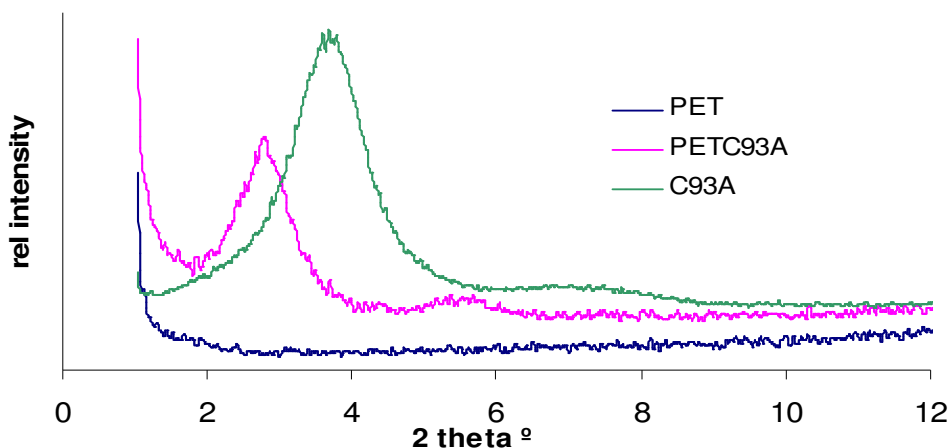
Figure 6.1.1–5 XRD spectra of PET, C93A and 5wt% PET/C93A nanocomposite (Cu x-ray source)

These southern clays materials provide a range of potential compatibilities with PET from hydrophilic (CNa^+), polar (C30B), similar chemical groups (C10A) through to hydrophobic materials (C15A and C93A). It is of note that intercalation occurred in the more hydrophobic clays but not in the polar clays as would be expected for a polymer such as PET that exhibits some polarity such as PET.

Further organoclays from alternative manufacturers (Sud Chemie, Elementis and Nanocor) were also investigated. Figures 6.1.1-6 and 6.1.1-7 show the XRD data obtained for the Sud Chemie clays N2 and N3010 which, are both relatively hydrophobic in nature but offer some compatibility in terms of similar structural groups (i.e. benzyl group). These two materials also allow an indication of the effect of the initial interlayer opening of the clay on the formation of the nanocomposite.

For N2 a change in interlayer spacing from 1.91nm (for the unmodified clay) to 3.09nm (for the nanocomposite) was observed, an increase of 1.18nm. This indicates the formation of an intercalated nanocomposite. When N3010 organoclay is used the (001) spacing changed from 3.37nm for the organoclay to 3.08nm for the nanocomposite. This constitutes an overall reduction in the (001) spacing of 0.29nm. Judging by the strong (002) and (003) peaks it is expected that an intercalated nanocomposite has been formed
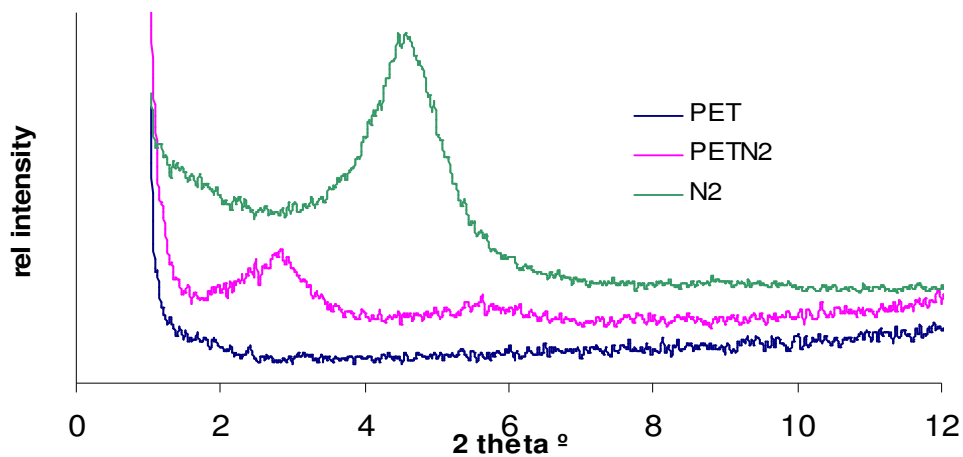
Figure 6.1.1-6 XRD Spectra of PET, N2 and 5wt% PET/N2 nanocomposite (Cu x-ray source)
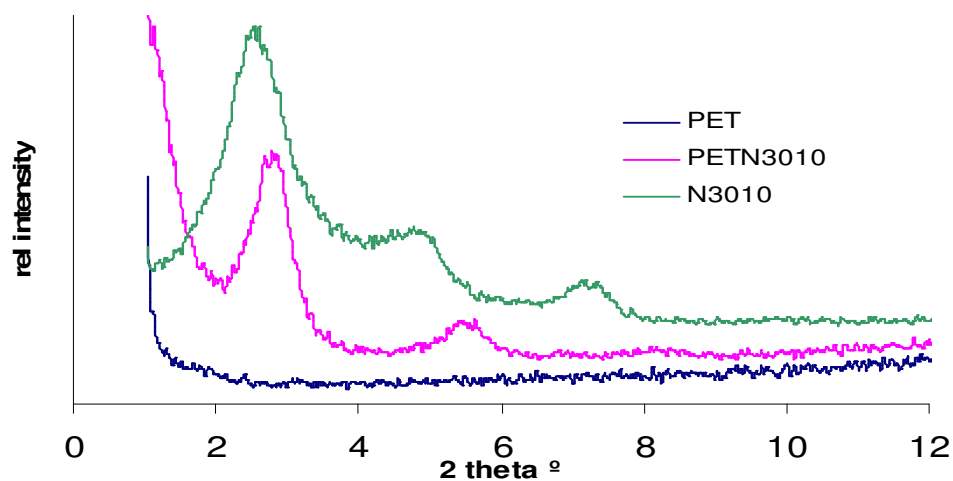
Figure 6.1.1–7 XRD spectra for PET, N3010 and 5wt% PET/N3010 nanocomposite (Cu x-ray source)

The N2 and N3010 clays are modified with the same surfactant except the length of the alkyl chain differs. This results in the greater (001) distance for the N3010 clay compared to the N2. From these results both nanocomposites had the same final (001) spacing indicating two things. Firstly the N3010 is indeed an intercalated nanocomposite and not merely the result of degradation of surfactant

and secondly that the initial distance between the clay layers does not have a major influence on the final nanocomposite structure.
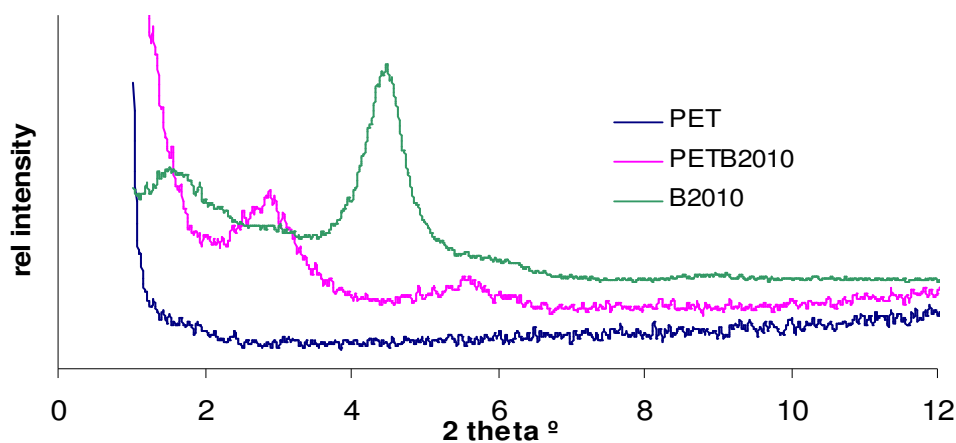
Figure 6.1.1–8 XRD spectra for PET, B2010 and 5wt% PET/B2010 nanocomposite (Cu x-ray source)

Bentone B2010 organoclay from Elementis has an interesting clay structure (Figure 6.1.1-8). A (001) peak is evident at both 1.61° and at 4.51° 2θ and on close inspection the relevant lower (00) reflections can be detected i.e. (002) at 3.13nm and (004) at 6.32nm for the 1.61° peak and (002) at 9.11nm for the 4.51nm (001) peak. The 4.51° (001) peak obscures the 4.83° (003) peak for the 1.61° (001) peak. Two main explanations for this behaviour are that there is some formation of a surfactant bi-layer or that two different surfactants are used. When the clay is processed with PET to produce a nanocomposite the final (001) spacing is 3.04nm indicating an intercalated nanocomposite has been produced. The final commercial organoclay investigated was Nanomer I28 from Nanocor (Figure 6.1.1-9). The interlayer spacing for this clay was found to be 2.54nm and the associated (002) peak is just evident as a slight bulge at 6.82nm. When processed the resultant nanocomposite has (001) spacing of 3.03nm, an increase of 0.49nm indicating the formation of an intercalated nanocomposite.
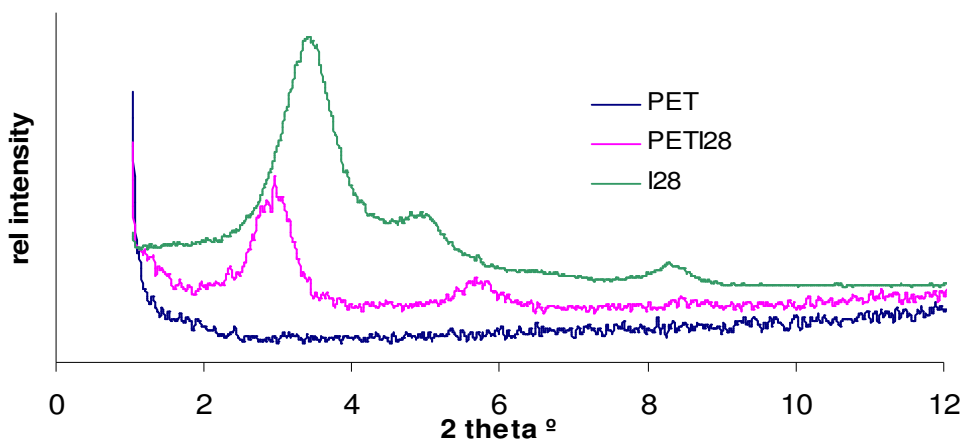
Figure 6.1.1–9 XRD spectra for PET, I28 and 5wt% PET/I28 nanocomposite (cu x-ray source)

In summary it appears that commercial organoclays are not suitable for the production of highly exfoliated nanocomposites in PET. Intercalated nanocomposites are readily produced with a range of the clays (i.e. surfactants) with a nominal interlayer spacing of 3.1nm independent of the surfactant. The exceptions are CNa^+ where no intercalation has occurred due to the highly hydrophilic nature of the clay and C30B where it appears that the surfactant has degraded to some degree.

6.1.2 In house modified clays

The first of the nanocomposites produced with in house modified clays examined was PET/PVP clay. The XRD scan for this material is shown in Figure 6.1.2–1. The clay had a 2 theta peak at 3.55º which corresponds to a (001) spacing of 2.49nm. When processed with PET the interlayer spacing of the resultant nanocomposite was found to be 2.56nm. This indicates that no intercalation of PET into the clay interlayers has occurred. It also indicates that the PVP has formed a very stable intercalant for the clay that is not adversely affected by the relatively high PET processing temperature. Based on the lack of intercalation of the PET into the organoclay it is unlikely any significant improvements in barrier would be observed for this material.
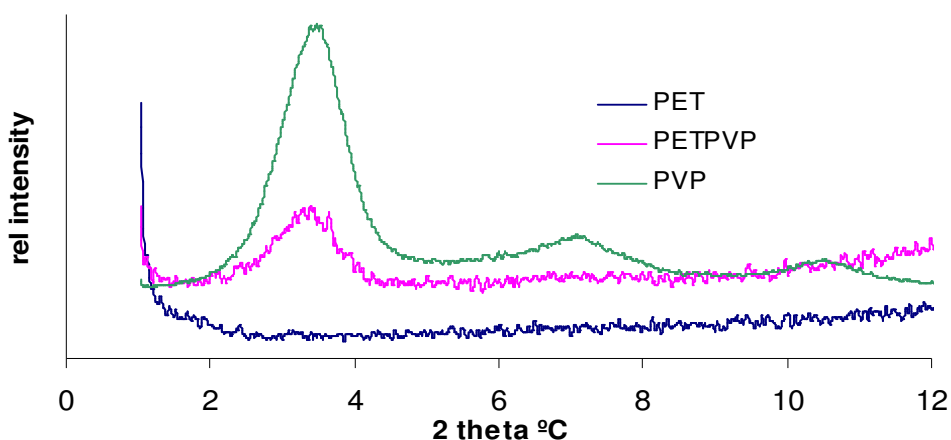
Figure 6.1.2–1 XRD spectra for PET, PVPNa$^+$ and 5wt% PET/PVPNa$^+$ nanocomposite (Cu x-ray source)

The XRD scans for sodium clay modified with CPBr are shown in Figure 6.1.2-2. In the case of CPBr modification the original modified clay exhibited a (001) spacing of 1.75nm. On processing with PET to form a nanocomposite, the (001) spacing was reduced to 1.47nm indicating that PET had failed to intercalate the clay. The reduction in (001) spacing is indicative of the CPBr intercalated clay structure undergoing some degradation. Again such a composite would not be expected to have significantly improved barrier properties.

Similar to CPBr modified clay the CPCl modified version also exhibited a reduction in the (001) spacing after processing with PET as shown in Figure 6.1.2–3. The initial CPCl clay had original (001) spacing of 1.80nm which was reduced to 1.50nm after nanocomposite processing. The (001) spacing is very close to that observed for the PET/CPBr composite and hence it can be presumed that similar degradation of the surfactant has occurred during processing.
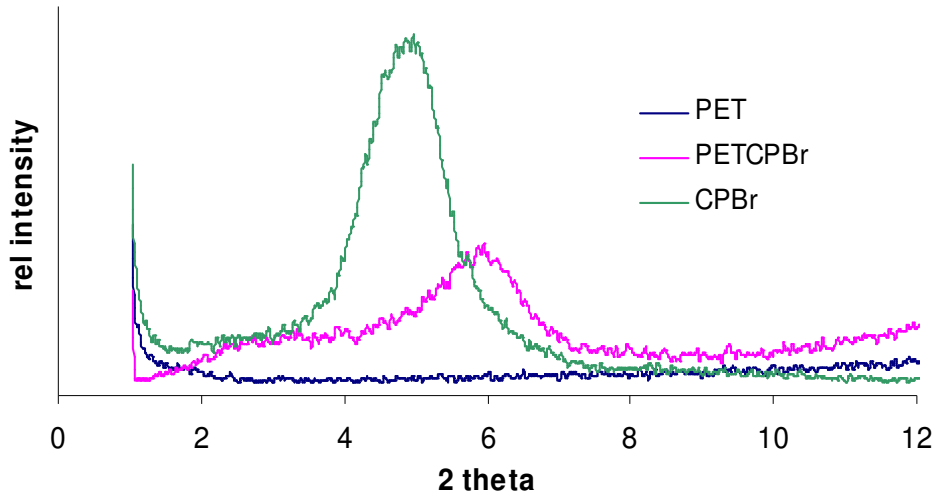
Figure 6.1.2–2 XRD spectra for PET, CPBr clay and 5wt% PET/CPBr nanocomposite (Cu x-ray source)
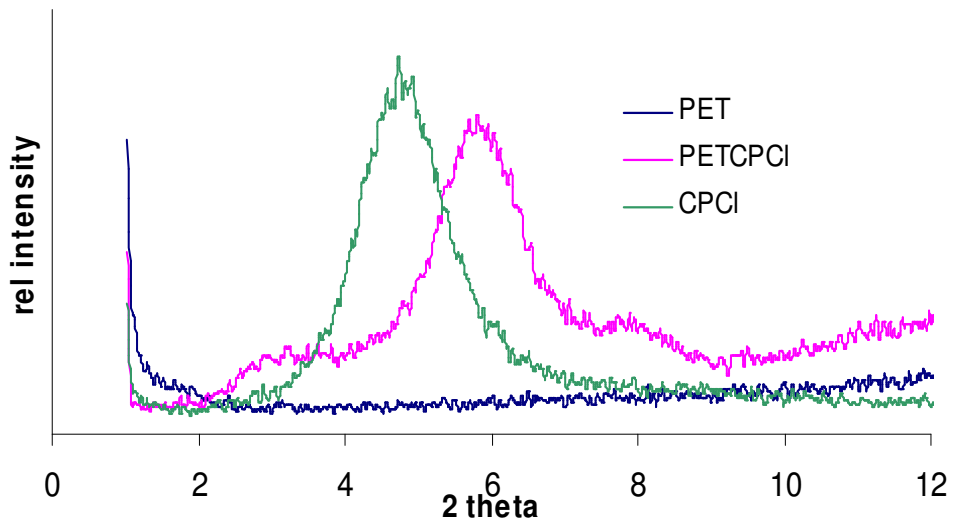
Figure 6.1.2 – 3 XRD spectra for PET, CPCl clay and 5wt% PET/CPCl nanocomposite (Cu x-ray source)

The final in house modified organoclay was epoxy modified Cloisite 30B. The relevant XRD scan is shown in Figure 6.1.2–4.
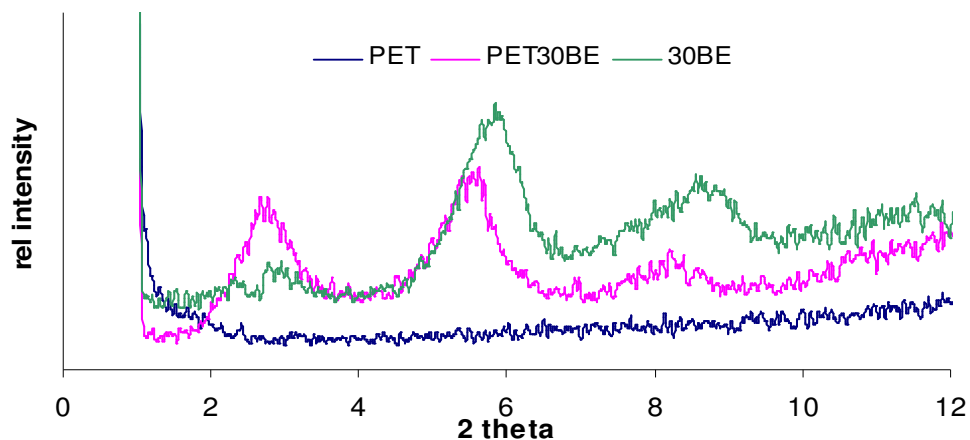
Figure 6.1.2–4 XRD spectra for PET, epoxyC30B and 5wt% PET/C30BE nanocomposite (Cu x-ray source)

In the case of 30BE the initial (001) spacing was 2.91nm.After processing with PET the (001) spacing had increased to 3.18nm indicating intercalation of PET into the clay galleries and some level of PET to clay interaction.

6.1.3 Summary of PET/clay morphologies

From the evidence provided by XRD it is evident that the intercalated nanocomposites were produced rather than exfoliated nanocomposites except for unmodified clays and those where significant degradation of the clay surfactant has occurred.

6.2 Crystallisation behaviour of PET nanocomposites

The influence of the clays on the crystallisation behaviour of the PET is reported in the following section. Tests were conducted on PET nanocomposite pellet samples by a heat cool heat regime as described in chapter 3.

6.2.1 Commercial organoclays

6.2.1.1 1ˢᵗ heat – behaviour on cooling from the extruder.

The DSC heating scans for PET and PET nanocomposites produced with Cloisite clays are shown in Figure 6.2.1.1-1
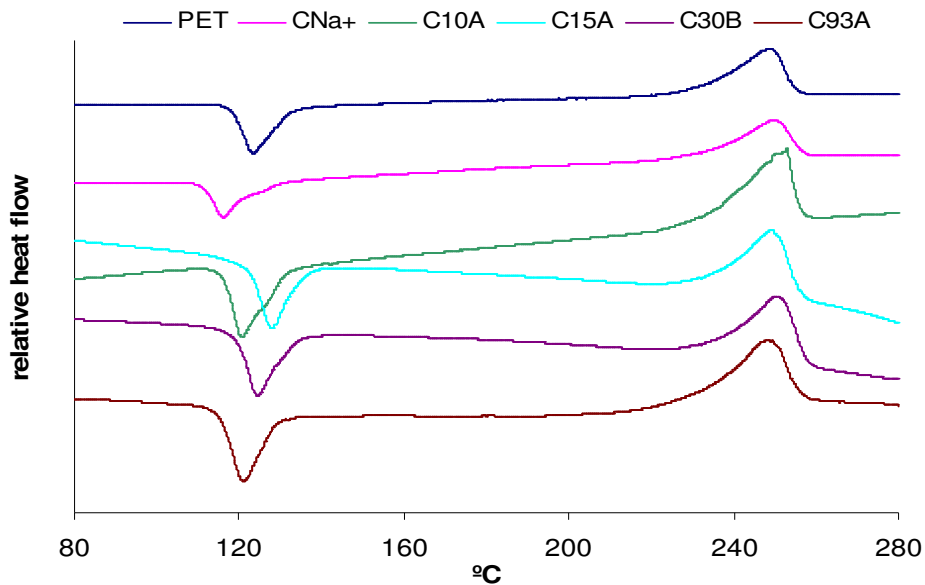
Figure 6.2.1.1–1 DSC initial heating for PET with Cloisite organoclays CNa⁺, C10A, C15A, C30B and C93A

From the scans it can be seen that the CNa⁺ clay significantly shifts the cold crystallisation temperature from 125ºC for PET to 116ºC for the nanocomposite. In contrast the cold crystallisation is affected less in the intercalated nanocomposites with T_c values of 121ºC, 128ºC, 125ºC and 121ºC respectively for clays C10A, C15A, C30B and C93A. Overall the changes are not significant in terms of their potential effect on bottle blowing as the T_c remains considerably above the temperatures used for blowing bottles (circa. 95ºC – 105ºC). In terms of the melting behaviour there is neither little change in crystal melting point nor the temperature range over which melting occurs.

The level of crystallinity was calculated as described in chapter 3 for the as produced nanocomposites in pellet form. The PET control and the PET/C93A composite exhibited the highest levels of crystallinity at approximately 14%

followed by C15A (12.5%), C30B (12%), C10A (9.5%) and CNa^+ (5%). Overall this indicates that the presence of clay reduces the overall level of crystallinity for Cloisite clays, probably due to the clay particles forming a physical barrier to the formation of the largest most perfect crystals. The extent to which the nucleation and growth of crystals is hindered may, in part be due to the size of clay particles after processing with PET. It can be expected that the largest particles are left in the CNa^+ nanocomposite where no intercalation of polymer chains has occurred. The resultant large clay particles would be expected to provide a large barrier to the formation of large crystals but also large and effective nucleation points for crystallisation resulting in lower T_c from cold crystallisation. Of the other clay materials C30B does not possess an intercalated structure but rather one where the interlayer structure has collapsed but does contain hydroxyl groups with reactivity towards PET. It is possible that the close compatibility of these materials has resulted in better dispersion of the clay, even without extensive intercalation of PET into the clay galleries. Of the other clays it would be expected that the order of dispersion of the clay would be C10A is less than C15A is less than C93A. All these samples resulted in intercalated structure implies interaction between the polymer and clay they would be expected to be better dispersed than the unmodified clay.

To further investigate a link between dispersion and the crystallisation behaviour POM was used to examine the dispersion of the clays in the bottle wall samples for the Cloisite clays (Figure 6.2.1.1-2). From the POM micrographs the inference that the dispersion affects the overall level of crystallinity can be taken as valid. The PET sample does show a limited number of artefacts but generally remains clear while the CNa^+ sample which has the lowest crystallinity shows extensive particles, some of which are clearly agglomerated together, up to a maximum size of almost 100μm. In the case of the C30B there are extensive particulates but the dispersion is good and the particle size is smaller than that observed for C10A (which it has greater crystallinity than). The micrographs also show the best dispersion for C15A and C93 that have the best dispersion and lowest particle size from the micrographs.
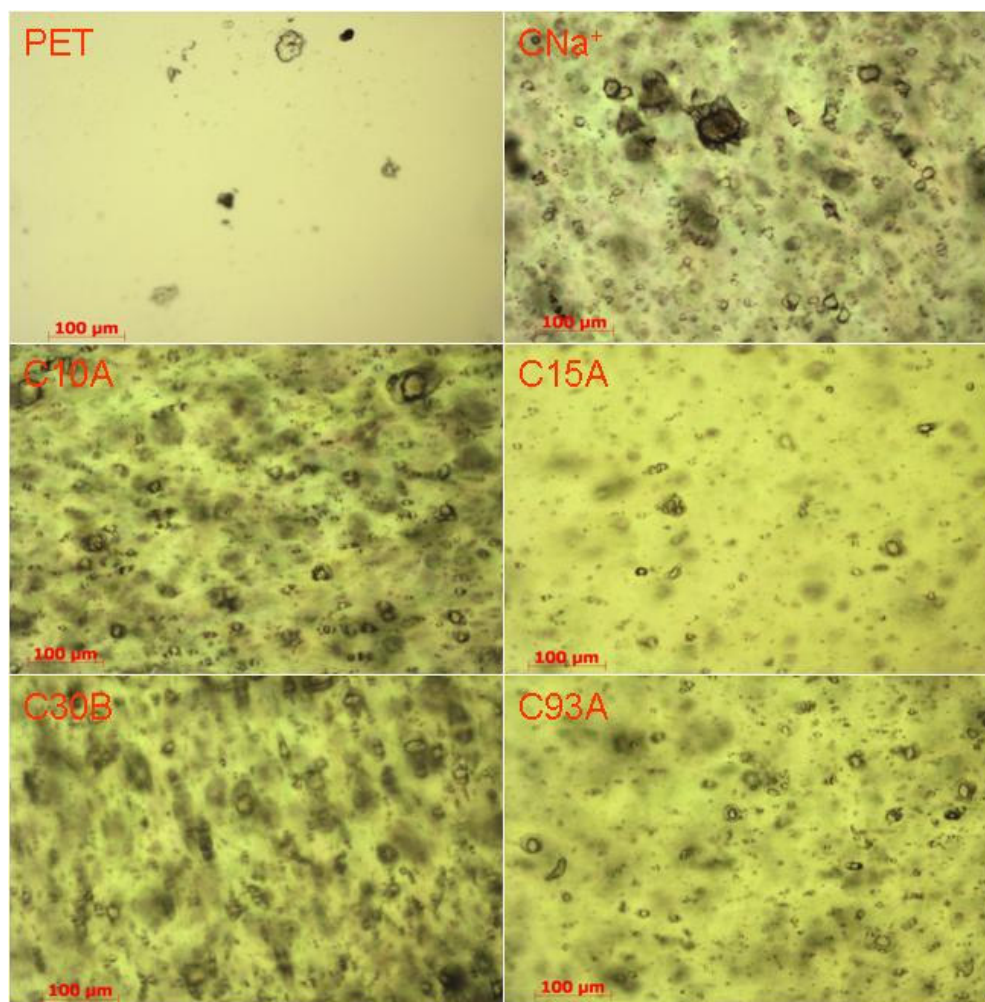
Figure 6.2.1.1–2 Optical micrographs of bottle wall section of PET and PET with Cloisite organoclays with 100μm scale bar.

The DSC initial heating scans for the clays obtained from alternative suppliers (i.e. N2, N3010, B2010 and I28) are shown in Figure 6.2.1.1-3. The cold crystallisation temperature behaviour of the nanocomposites produced from alternative organoclay suppliers was found to be fairly typical of what had been observed previously with Cloisite clays with varied T_c dependant on the clay used. As per the Cloisite clays it would be expected that the presence of the clay would have minimum impact on the blowing behaviour of the composites. The T_m was also found to deviate very little to that of PET control after the addition of clay. This is in line with expectations based on the results obtained for Cloisite clays. The overall crystallinity values of these materials was found to be

generally lower than that observed for the Cloisite clays (N2 6%, N3010 5%, B2010 6% and I28 7%). Based on the trends observed for the Cloisite clays it would be expected that these materials exhibit a similar level of dispersion to each other but inferior to that of C15A and C93A in particular. Micrographs of these materials are shown in Figure 6.2.1.1-4.
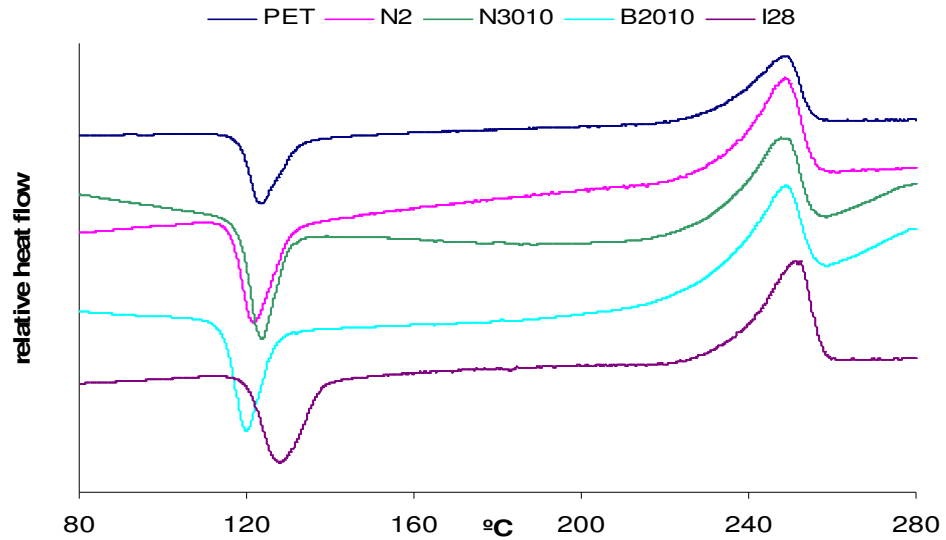
Figure 6.2.1.1–3 DSC initial heating for PET with Cloisite organoclays N2, N3010, B2010 and I28
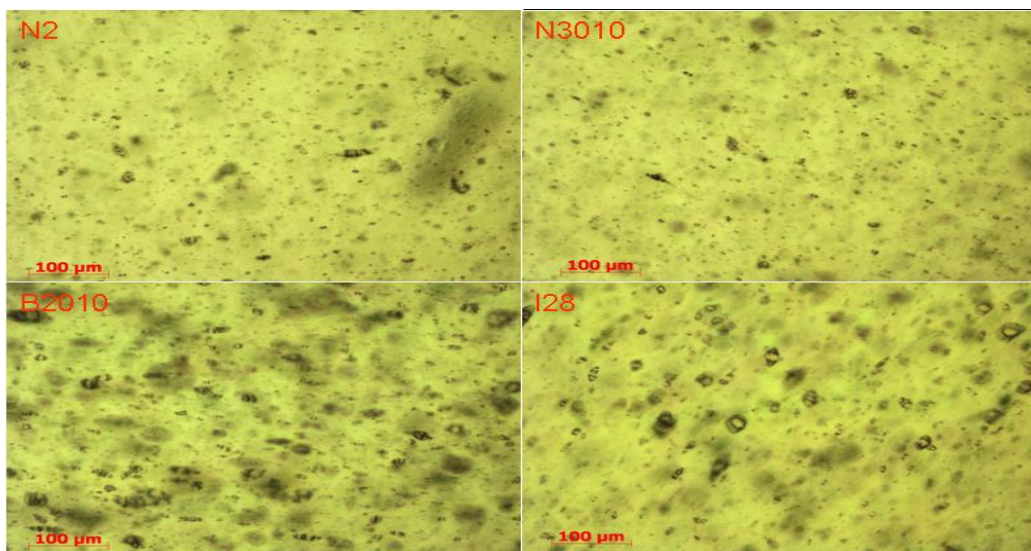
Figure 6.2.1.1–4 Optical micrographs of bottle wall section of PET and PET with organoclays N2, N3010, B2010 and I28 at 100µm scale bar.

Contrary to the expected poor dispersion all the clays from other commercial suppliers showed relatively good dispersion. For instance N2 and N3010 had dispersion similar to C15A with reduced overall particle size while B2010 and I28 had dispersion similar to that observed for C93A, with comparable particle size. This indicates that although for the Cloisite clays the level of crystallinity act as an indicator for the level of dispersion this is not the case with clays sourced from alternative suppliers. This indicates that the differences in clay microstructure also play a part in the crystallisation behaviour of the nanocomposites.

6.2.1.2 Cooling and re-heating after normalisation of heat history

After the initial heating scan and removal of heat history a further cooling cycle is carried out in order to determine the effect of the clays under controlled conditions of cooling and heating. Table 6.2.1.2 - 1 summarises the results.

Table 6.2.1.2 - 1 Summary table for DSC cooling from melt and crystal melting stages

Sample	$T_{c\ on}$	T_c	$T_{m\ end}$	ΔH_c j/g	$T_{m\ on}$	T_m	$T_{m\ end}$	ΔH_m j/g
PET	204	195	180	45.273	236	247	253	46.973
CNa^+	205	200	194	19.275	231	249	255	18.640
C10A	201	194	186	38.241	247	253	255	35.675
C15A	197	186	176	36.293	237	250	255	38.391
C30B	203	193	185	37.703	241	250	257	38.497
C93A	205	197	190	39.341	239	249	255	38.781
N2	207	201	185	35.681	230	250	257	25.368
N3010	203	196	188	37.824	236	249	254	33.937
B2010	205	199	192	39.370	238	250	255	34.545
I28	211	205	198	53.754	238	251	256	45.987

The data in the table suggests that for the Cloisite clays the presence of clay has only a slight effect on the T_c i.e. within 2ºC of the PET control (T_c 195ºC). The two clays which produce the most significant difference to the control are CNa^+

189

and C15A. In the case of CNa$^+$ there is little interaction between the PET and clay and there are large agglomerations of clay materials which can readily nucleate the PET explaining the elevated T_c of 200ºC. In the case of C15A intercalation of the clay has occurred hence there is significant interaction between the clay and PET. In addition from the POM the clay in the sample seems to be significantly better dispersed. This indicates when there is improved dispersion of the clay (i.e. the agglomerations are broken down and a greater number of clay particles exist in the matrix) that nucleation is hindered, in part due to restrictions on chain mobility due to the intercalation and interactions of the clay PET and clay and also partly due to the numerous clay particles acting as a physical barrier to crystallisation. The DSC cooling scans for the Closite clay nanocomposites are shown in figure 6.2.1.2–1.
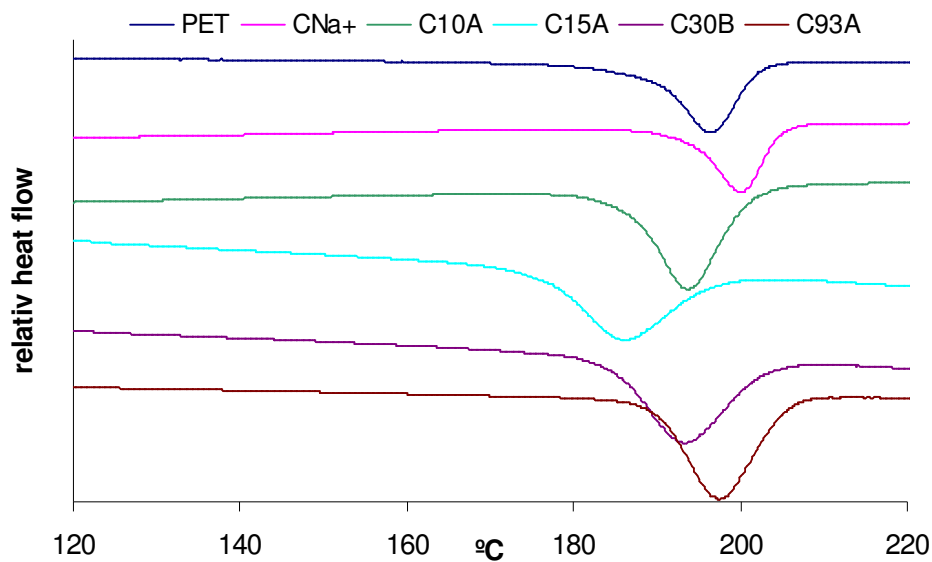
Figure 6.2.1.2–1 DSC cooling from the melt for PET and PET nanocomposites produced from Cloisite clays

Further DSC traces for the organoclays from other suppliers are shown in Figure 6.2.1.2-2. The clays produced by Sud Chemie (N2 and N3010) had thus far, in terms of XRD data, microscopy and initial heating scans had behaved very similarly, as would be expected given the similarity of the surfactants. On cooling from the melt quite a significant difference in the behaviour of the

nanocomposites produced has been noted. The N3010 composite has similar T_c to the PET control (196ºC cf 195º) while the N2 based nanocomposite has a significantly higher T_c of 201ºC. This result is interesting as the microstructure of the clay and the nanostructure of the composite are so similar and indicates that factors such as surfactant chain length can influence the final properties of the nanocomposite. In the case of the Elementis organoclay, B2010 there is a slight increase in the T_c value to 199ºC and in the case of the Nanocor I28 clay there was a more substantial increase in T_c to 205ºC. Overall for the clays from alternative manufacturers to Southern clays there appears to be a trend towards increased T_c and a nucleation effect on the PET on controlled cooling from the melt. This may, in part be due to the microstructure of the clays. In chapter 4.1.1 we have seen that the microstructure of the CNa^+ has a broad range of shapes and sizes with a notable angularity to the clay particles. In contrast when the raw clays from Sud Chemie, Elementis and Nanocor were examined the microstructure was found to be much more regular in terms of particle size and shape with a more rounded appearance for the clay particles. It is likely that the clay microstructure has significant influence on the crystallisation behaviour based on these results.
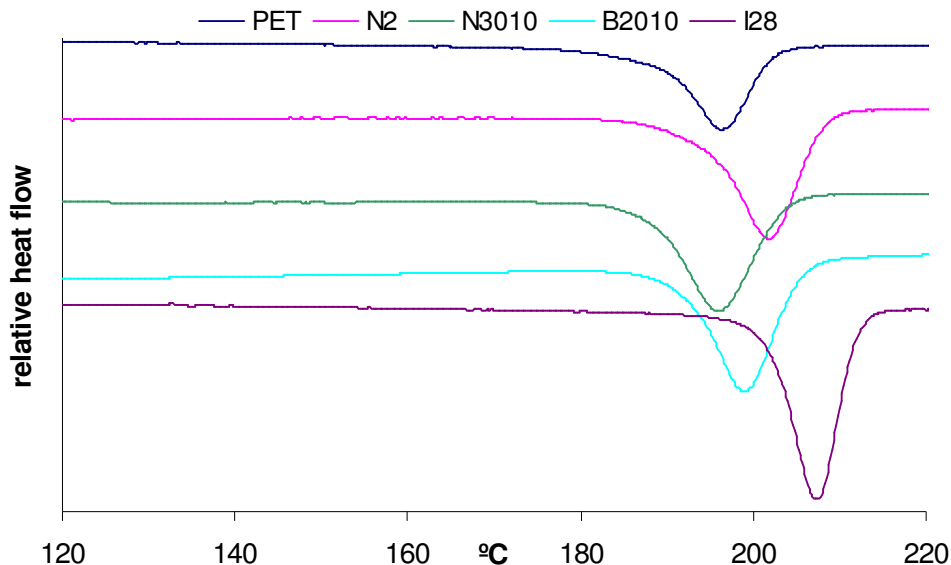
Figure 6.2.1.2-2 DSC cooling from the melt for PET and PET nanocomposites produced from N2, N3010, B2010 and I28 organoclays

The melting behaviour of the nanocomposites after controlled cooling also reveals some interesting behaviour. The DSC scans for crystal melting of nanocomposites containing Cloisite clays is shown in Figure 6.2.1.2–3.
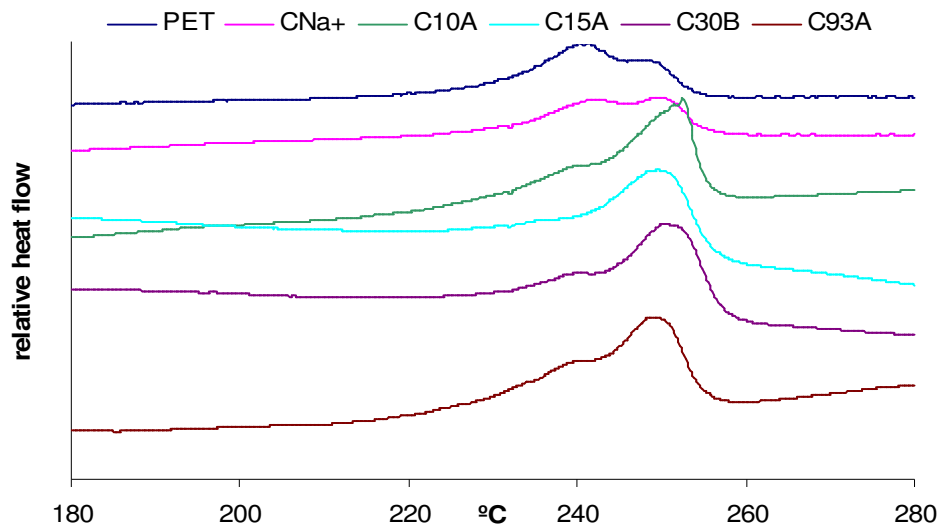
Figure 6.2.1.2–3 DSC crystal melting behaviour for PET and PET Cloisite organoclay nanocomposites

From the data it is evident that a double melting peak is evident for all the materials tested, with peaks at approximately 241ºC and 251ºC. This indicates either, the formation of two distinct crystal forms in PET on cooling from the melt or that a significant amount of re-crystallisation of the PET occurs during heating with the resultant formation of 2 crystal phases with different melting temperatures. In the case of PET control material the predominant peak is at 241ºC with the secondary peak at 251ºC. In the case of PET/CNa$^+$ nanocomposite where there is little interaction between the PET and the clay and intercalation has not occurred the two peaks are split approximately equally between 241ºC and 251ºC whereas in the case of the organoclays where intercalation has occurred and there is greater interaction of the PET and clay the primary peak is clearly that at 251ºC with the lower temperature peak diminished to a small shoulder within the larger peak. The melting scans for the other

commercial clays tested are shown in Figure 6.2.1.2-4 and observe a similar trend.

Overall, this indicates that the presence of organoclay in PET, when intercalated nanocomposites or those with favourable polymer clay interactions (C30B) are formed results in the preference for higher melting crystals compared to standard PET or PET with poorly interacting sodium form clay. This higher melting tendency appears to be a result of the clay polymer interactions.
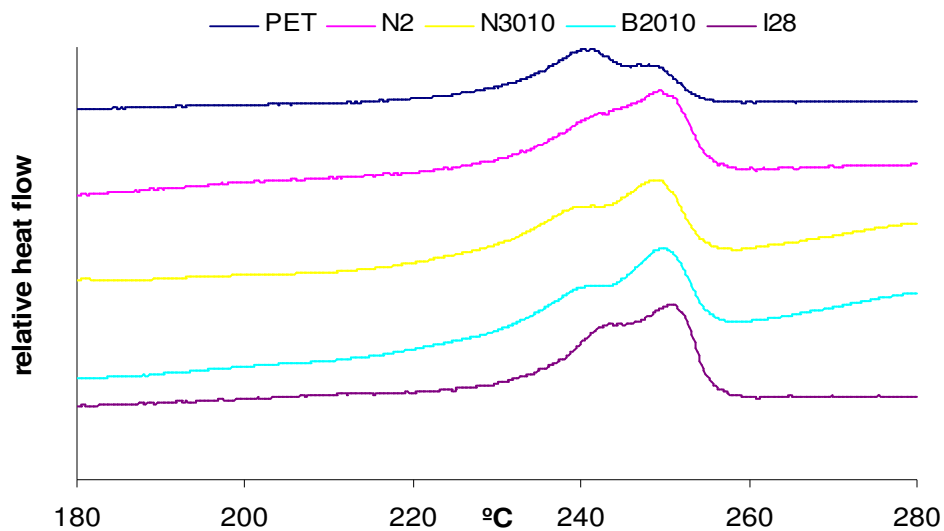
Figure 6.2.1.2–4 DSC crystal melting behaviour for PET and PET nanocomposites produced with N2, N3010, B2010 and I28 nanocomposites

6.2.2 In house modified clays

6.2.2.1 1st heat – behaviour on cooling from the extruder

The in house modified clays initial heating scans are shown in Figure 6.2.2.1-1. For the cetyl pyridinium modified clays it is evident that some nucleation has occurred for cold crystallisation as the T_c has reduced slightly from 125ºC for the PET to 119ºC (CPBr) and 123ºC (CPCl). In contrast the epoxy modified C30B and PVP modified clay show a slight increase in the cold crystallisation temperature to 128ºC and 126ºC respectively. Overall these differences are quite small and would not be expected to significantly affect the bottle blowing

193

process. The crystal content of these samples has been determined as 14% (PET), 9.5% (CPBr), 7% (CPCl), 9.5% (C30BE) and 7.5% (PVP) indicating that the clays cause a barrier to the crystallisation of the PET on cooling from the melt.
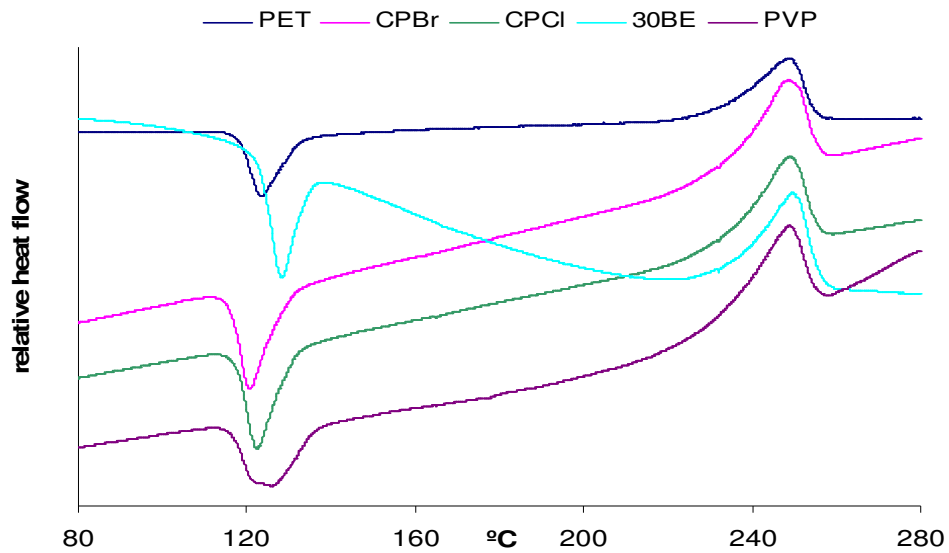
Figure 6.2.2.1-1 DSC initial heating for PET with in-house modified clays NaPVP, NaCPBr, NaCPCl and 30BE
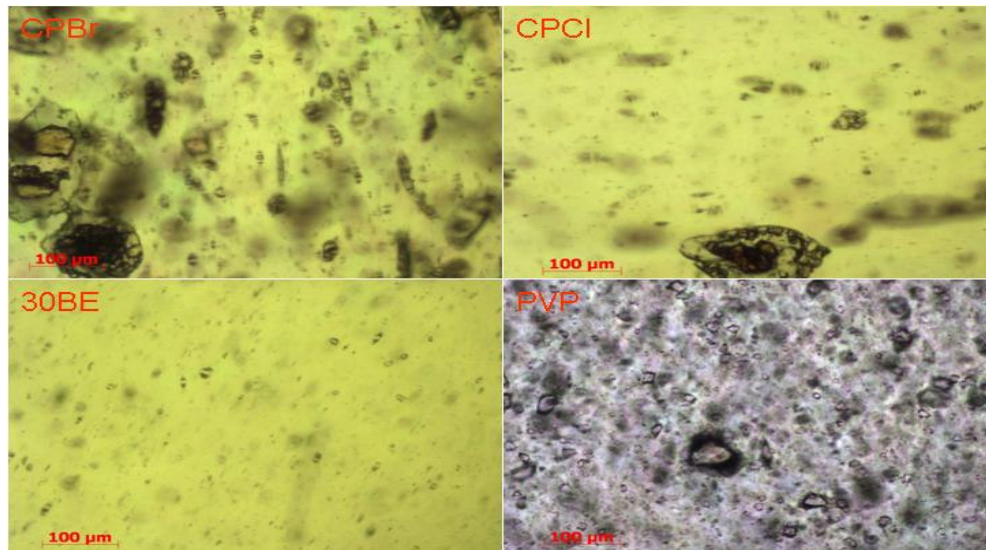
Figure 6.2.2.1–2 Optical micrographs of bottle wall section of PET and PET in-house modified organoclays with 100μm scale bar.

Micrographs taken from bottle wall samples to investigate the overall dispersion of filler are shown in Figure 6.2.1.1-2. From the micrographs it is evident that large agglomerations still exist for the CPBr. The CPCl sample is also similar with large agglomerations present but the overall dispersion is much improved. This would indicate that the better dispersed clay has a more significant impact on reducing the crystallinity as there are a larger number of clay particles acting as physical barriers to crystallisation. For the C30BE composite the dispersion of the clay can be seen to be very good and is an improvement to that seen for the commercial clays, particularly C30B, the parent clay. It appears that the use of epoxy has improved dispersion by both improving thermal stability and improving compatibility. Finally the PVP clay has an even but somewhat large particle size dispersion of clay as would be expected considering no intercalation has occurred hence clay PET interaction is of a minimal level.

6.2.2.2 Cooling and re-heating after normalisation of heat history.

Similar to the commercial clays a cooling and heating scan where heat history has been removed were also recorded and the data is tabulated (Table 6.2.2.2 - 1) below.

Table 6.2.2.2–1 Summary table of DSC cooling from the melt and crystal melting behaviour for in-house modified organoclays

Sample	$T_{c\ on}$	T_c	$T_{m\ end}$	ΔH_c j/g	$T_{m\ on}$	T_m	$T_{m\ end}$	ΔH_m j/g
PET	204	195	180	45.273	236	247	253	46.973
CPBr	202	194	184	39.599	239	250	255	33.233
CPCl	200	192	183	37.891	238	249	255	36.033
30BE	201	194	187	43.746	238	250	255	32.064
PVP	201	193	182	36.837	229	248	254	31.405

From the data and the DSC scans (Figure 6.2.2.2-1) it is clear that the crystallisation from the melt is not greatly affected by the in house modified clays despite the differences in the level of clay dispersion.
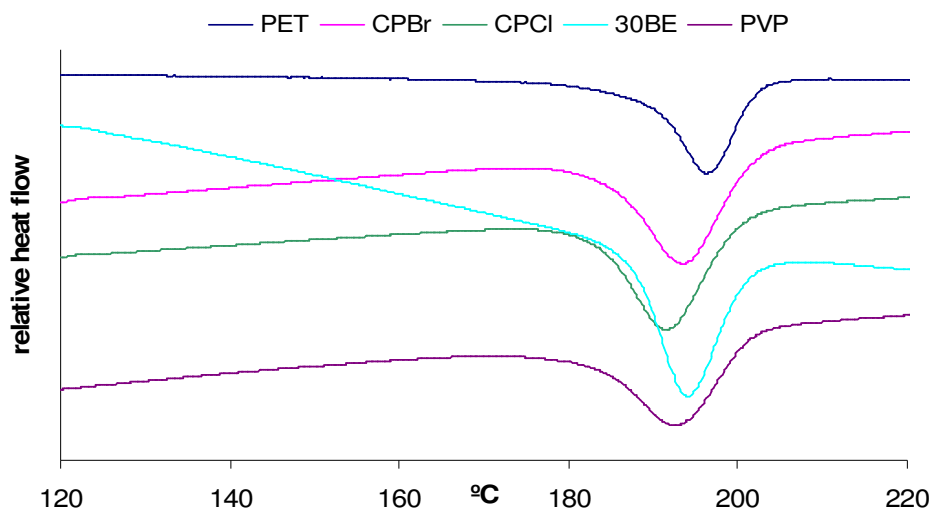
Figure 6.2.2.2–1 DSC cooling from the melt of in-house modified organoclay/PET nanocomposites
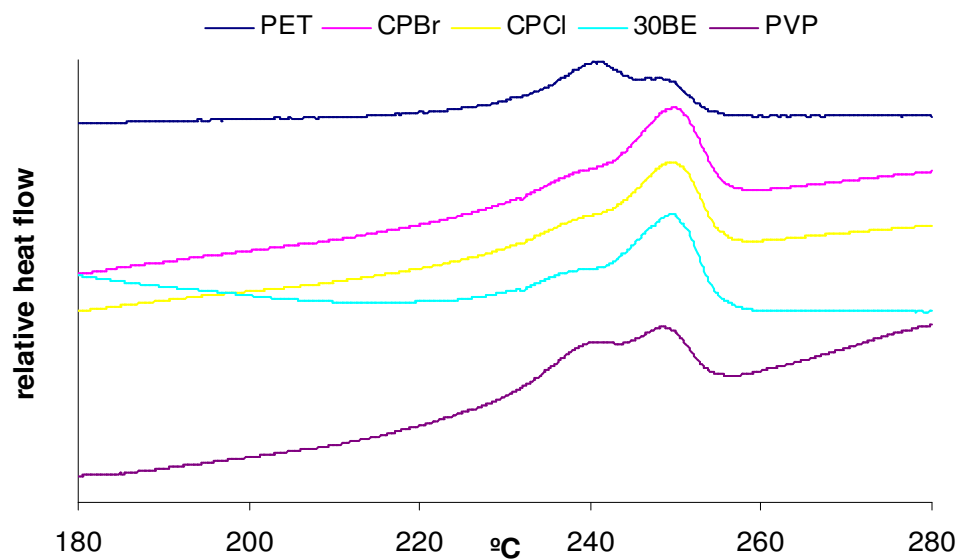
Figure 6.2.2.2–2 DSC crystal melting of PET nanocomposites with in-house modified organoclays

The melting behaviour of the nanocomposites (Figure 6.2.2.2-2) follows a similar pattern to that observed for the commercial clay based nanocomposites in that for PET and poorly interacting nanocomposite (i.e. PVP clay

nanocomposite) the predominant peak is at 241°C whereas for the more highly interacting nanocomposites the peak is shifted considerably to 251°C as per the commercial organoclay nanocomposites.

6.3 Gas barrier properties of PET nanocomposites

6.3.1 Commercial organoclays

The gas barrier properties to CO_2 were determined as per previous testing using 1l bottles. The results are quoted as BIF compared to the control PET material. Figure 6.3.1-1 shows the CO_2 egress behaviour of PET/CNa^+ nanocomposite.
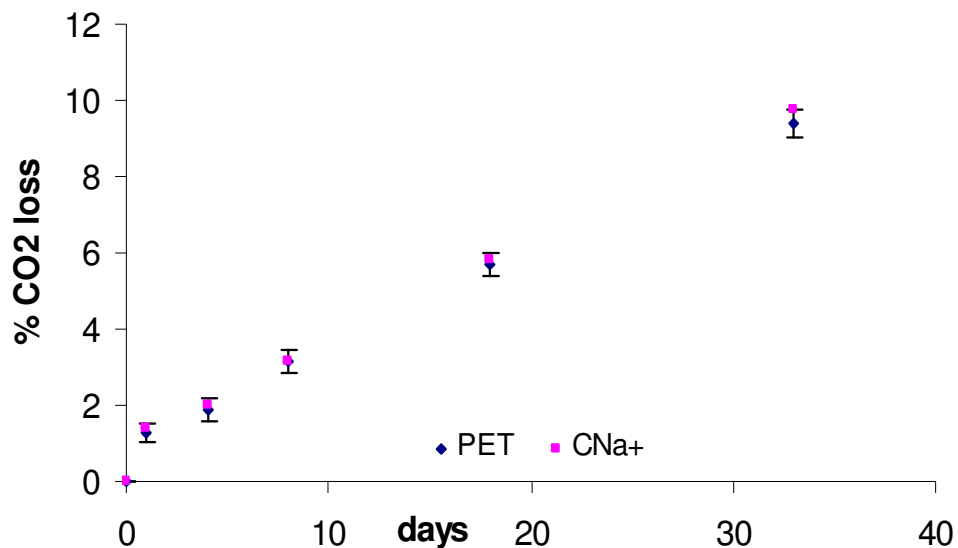
Figure 6.3.1–1 Comparison of CO_2 loss from PET and PET/0.75wt% CNa^+ nanocomposite

From the chart it is evident that no improvement in CO_2 barrier is obtained through the addition of unmodified clay to PET. This result is not unexpected as the nanocomposite does not exhibit good polymer clay interaction and the microscopy conducted shows large agglomerations of clay therefore the effect of the clay on barrier and its ability to form tortuous pathways to gas diffusion is limited.

For the nanocomposite produced with Cloisite 10A an intercalated nanostructure was obtained although the overall dispersion of the clay in the bottle wall was found to be poor with some large agglomerations present (up to approximately 50μm). It would be therefore expected that the overall improvement in barrier would be limited. This is shown to be true (Figure 6.3.1-2) with a BIF of 1.025 recorded.
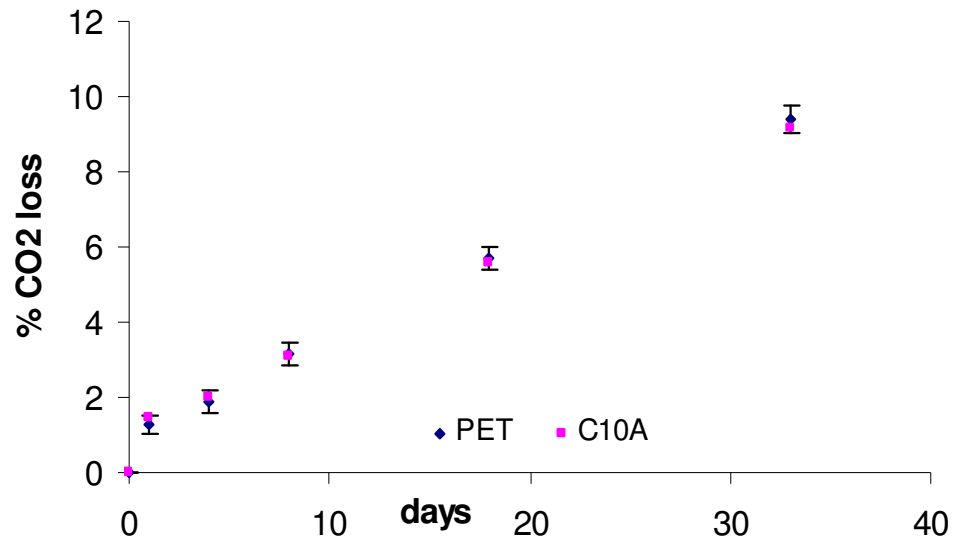
Figure 6.3.1–2 Comparison of CO_2 loss from PET and PET/0.75wt% C10A nanocomposite

Therefore for the PET/C10A nanocomposite it can be stated that no improvement in the barrier property has been obtained. The PET/C15A nanocomposite was also intercalated in nature and therefore would not be expected to exhibit a large improvement in CO_2 barrier (i.e. BIF 2). The CO_2 loss chart is shown in Figure 6.3.1–3. From the chart it can be seen that there is a significant improvement in the CO_2 retention corresponding to a BIF of 1.19 or a 20% improvement. This is due to the improved dispersion of the clay as seen in Figure 6.2.1.1-2 although the actual increase is still somewhat lower than would be expected of an exfoliated nanocomposite.
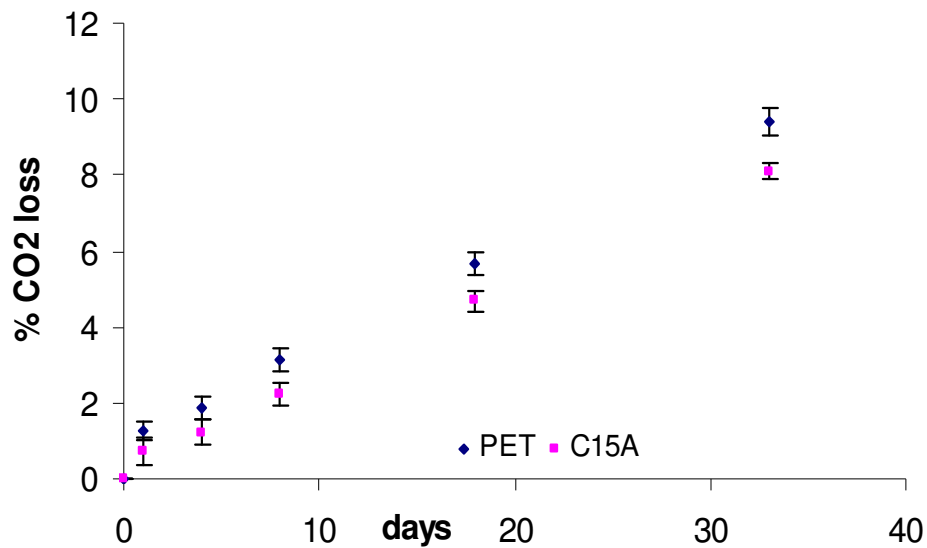
Figure 6.3.1–3 Comparison of CO_2 loss from PET and PET/0.75wt% C15A nanocomposite

The nanocomposite produced using C30B did not intercalate and there was a slight reduction in the (001) spacing of the clay that indicated some degradation of the clay may have occurred. The microscopy showed that the dispersion was relatively poor even though the predicted compatibility was expected to be good. The gas barrier was found to be similar to the PET within error of one standard deviation as shown in Figure 6.3.1-4
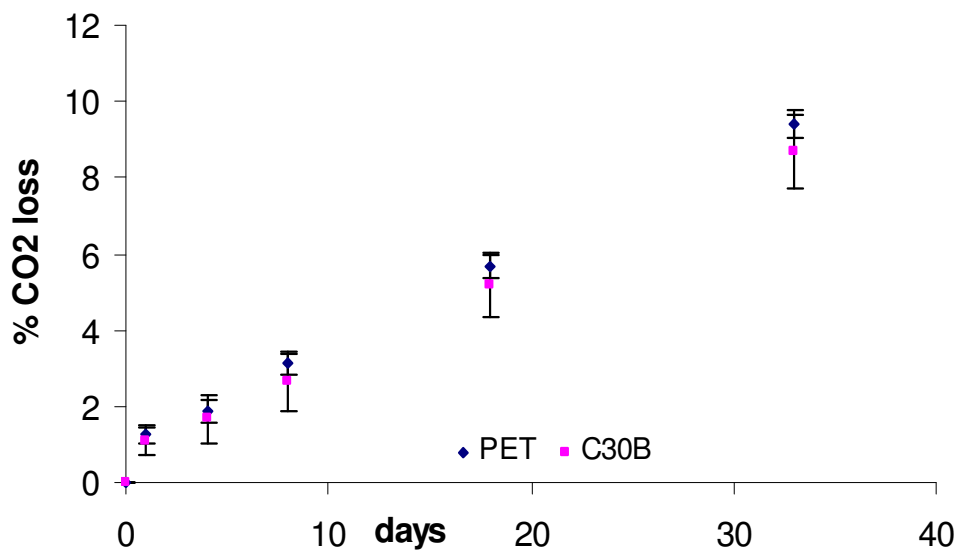
Figure 6.3.1–4 Comparison of CO_2 loss from PET and PET/0.75wt% C30B nanocomposite

The final Southern clays material, C93A exhibited an intercalated nanostructure and therefore interaction of polymer and clay can be expected. The microscopy showed good dispersion of the clay compared to CNa^+, C10A and C30B but was slightly inferior to that observed for C15A. The CO_2 loss chart is shown in Figure 6.3.1–5. The BIF was determined to be 1.16 and is similar to that observed for C15A within error.

Figure 6.3.1–5 Comparison of CO_2 loss from PET and PET/0.75wt% C93A nanocomposite

Figure 6.3.1–6 Comparison of CO$_2$ loss from PET and PET/0.75wt% N2 nanocomposite

Figure 6.3.1–7 Comparison of CO$_2$ loss from PET and PET/0.75wt% N3010 nanocomposite

Of the clays provided by alternative suppliers to Southern clays two were provided by Sud Chemie, N2 and N3010. These two materials have very similar organic modification and CO$_2$ loss charts are shown in Figures 6.3.1-6 and 6.3.1-

7. For these organoclays BIF of 1.17 and 1.20 for N2 and N3010 respectively were recorded. Both nanocomposites were determined to be intercalated in nature and were found to exhibit very good clay dispersion from microscopy with a low particle size (less than 30μm). Overall this indicates that very small changes in the nature of the surfactant have little effect on the overall barrier properties of the nanocomposite if the morphology remains largely unchanged. In addition to this finding it appears that the type of clay and its microstructure also has little impact on the overall barrier properties if the nanocomposite structure is similar. Overall these results are similar to those obtained for C15A and C93A Closite clay nanocomposites.

Elementis provided samples of B2010 organoclay with an unknown quarternary ammonium based surfactant. The resultant nanocomposite was shown to have an intercalated structure similar to the other organoclays, with the exception of C30B. The BIF of this material was determined to be 1.25 and the CO_2 loss chart is shown in Figure 6.3.1-8.

Similar to the Elementis material the Nanocor clay I28 also contains an unknown quarternary ammonium surfactant and an intercalated nanostructure. The CO_2 loss chart is shown in Figure 6.3.1-9 and a BIF of 1.16 was recorded. Both the I28 clay and the B2010 clay exhibited a similar level of dispersion from microscopy work (and this was similar to C93A).
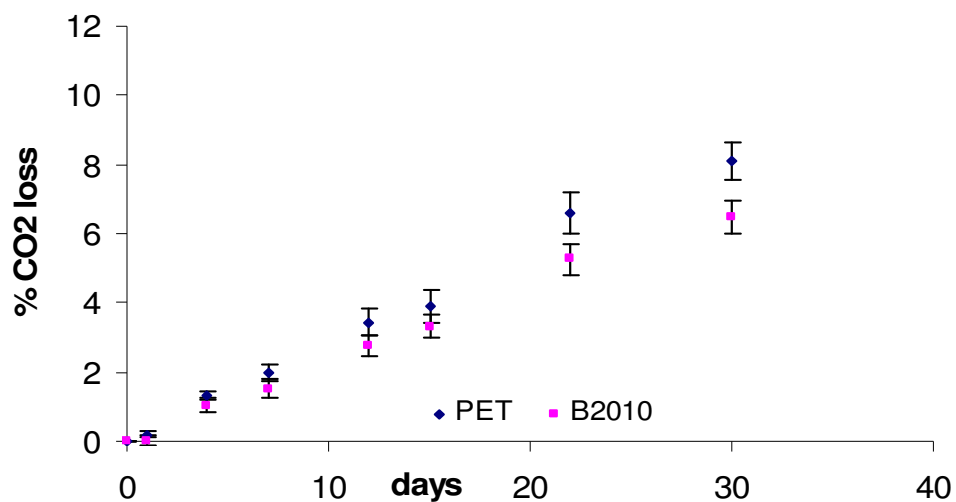
Figure 6.3.1–8 Comparison of CO_2 loss from PET and PET/0.75wt% B2010 nanocomposite
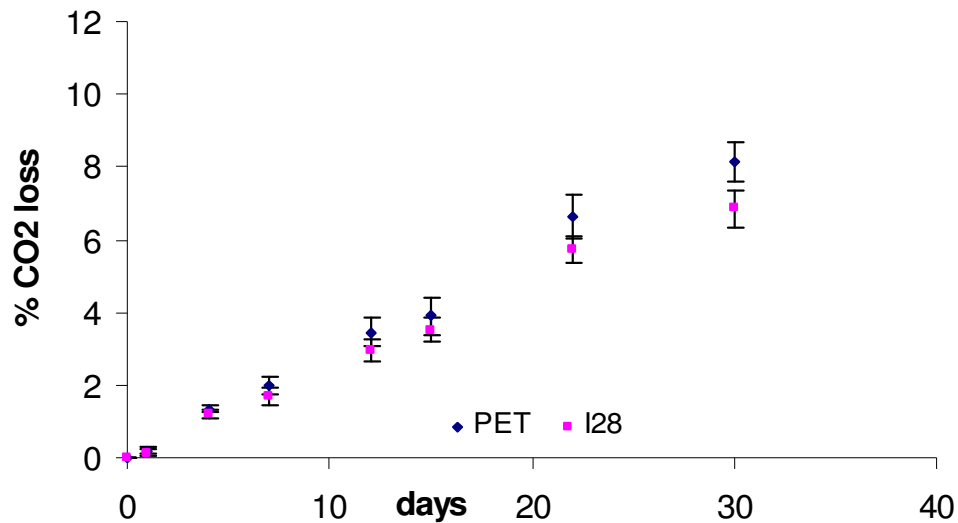
Figure 6.3.1–9 Comparison of CO_2 loss from PET and PET/0.75wt% I28 nanocomposite

Overall the CO_2 loss data indicates that an improvement in the CO_2 barrier property of PET is achievable through the incorporation of commercial organoclays but that the extent of improvement is restricted to about BIF 1.2 due to the difficulty in producing exfoliated nanocomposites.

6.3.2 In house modified clays

The CO_2 loss data for the cetyl pyridinium modified clays is shown in Figures 6.3.2-1 and 6.3.2-2. From the results a BIF of 1.13 and 1.06 was recorded for the CPBr and CPCl respectively. Both these composites showed poor dispersion of the organoclay with large agglomerations (up to 100μm in size) of clay evident in addition to a nanocomposite nanostructure indicating that intercalation of PET into the clay layers had not occurred, only degradation of the surfactant and hence collapse of the layered structure. This result implies that the best results for CO_2 are observed with the intercalated nanocomposites.
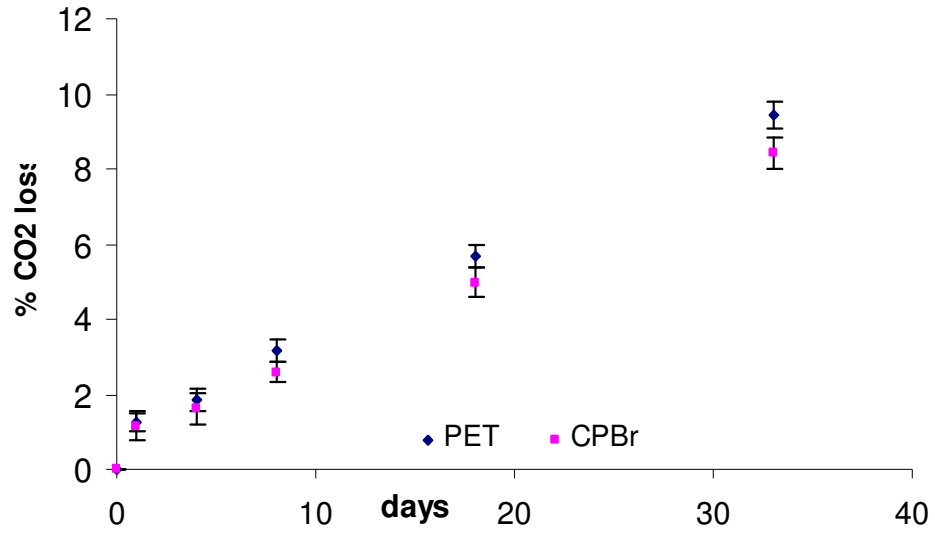
Figure 6.3.2–1 Comparison of CO_2 loss from PET and PET/0.75wt% NaCPBr nanocomposite

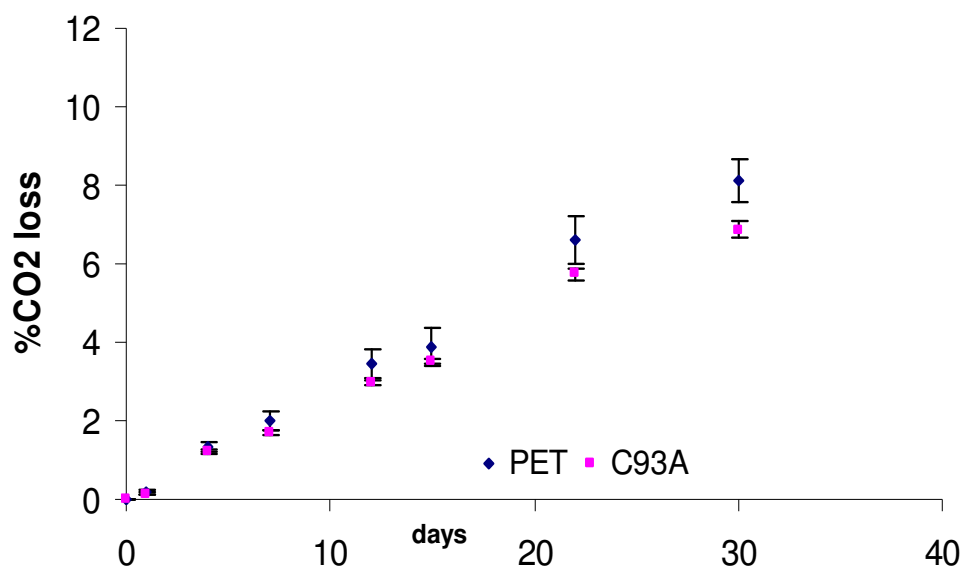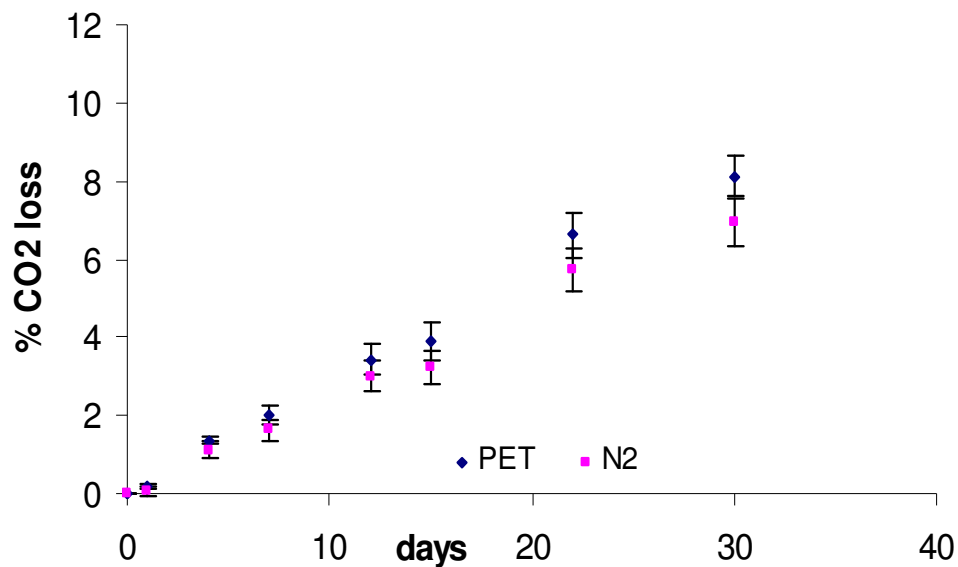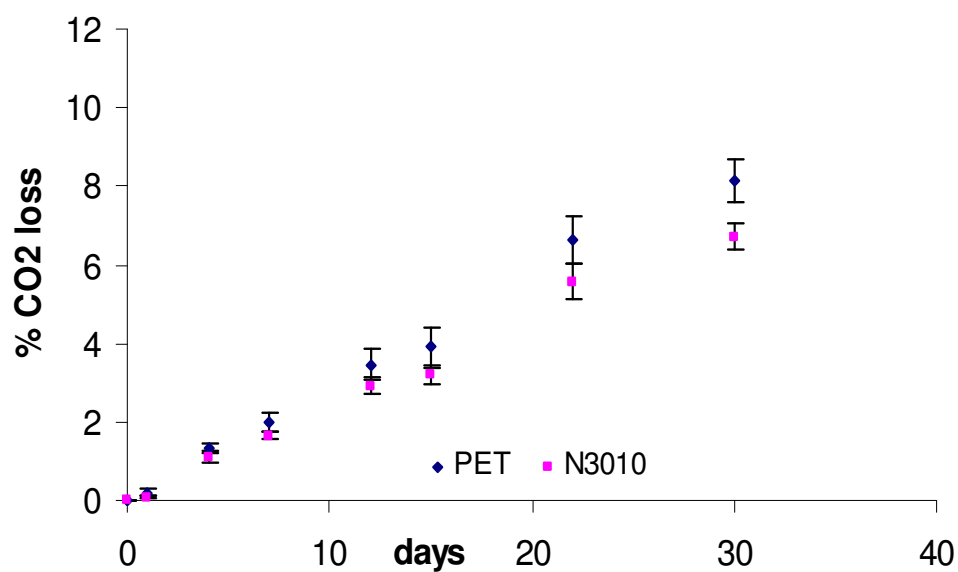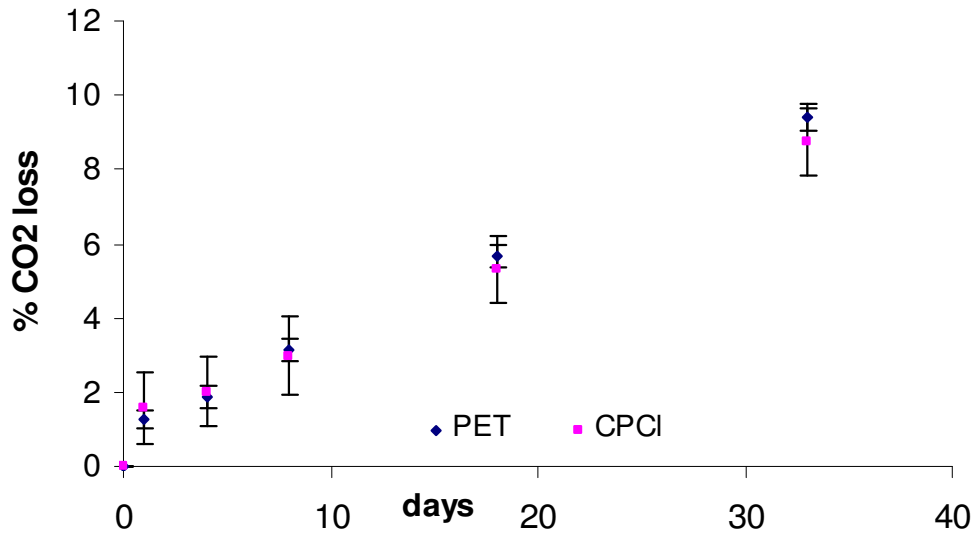**Figure 6.3.2 – 2 Comparison of CO_2 loss from PET and PET/0.75wt% NaCPCl nanocomposite**

For the C30BE nanocomposite material intercalation of the polymer into the clay was observed and the resultant dispersion of the clay appears very good compared to all the other nanocomposites yet the gas barrier property was poor (Figure 6.3.2-3) with a BIF of 1.05 recorded.
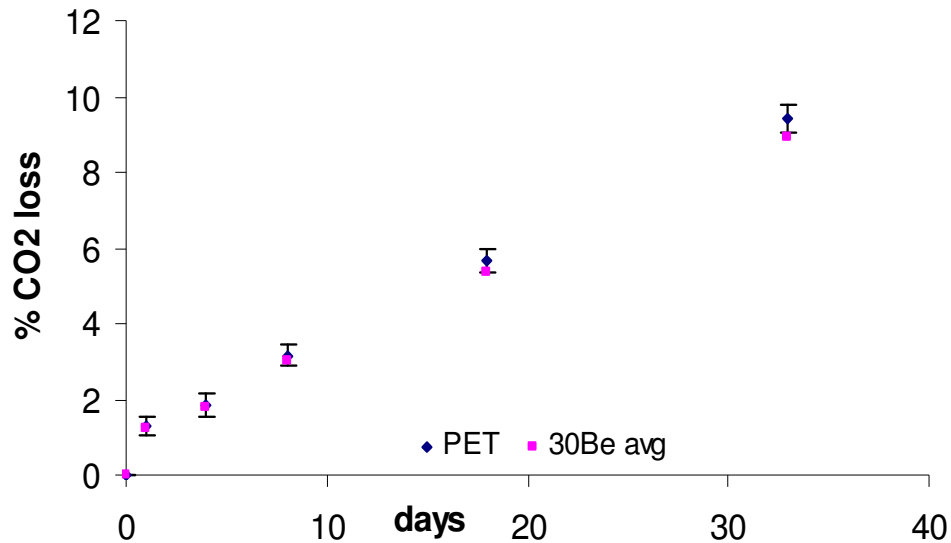
Figure 6.3.2–3 Comparison of CO$_2$ loss from PET and PET/0.75wt% C30BE nanocomposite

The compatibility of this clay was expected to be the best of all the organoclays tested yet only an intercalated nanocomposite with CO$_2$ retention similar to the base polymer was obtained. This may indicate that some of the clay polymer functionality was lost due to possible cross-linking of the hydroxyl surfactant by the epoxy.

The CO$_2$ loss for the final clay, modified with PVP is shown in Figure 6.3.2-4
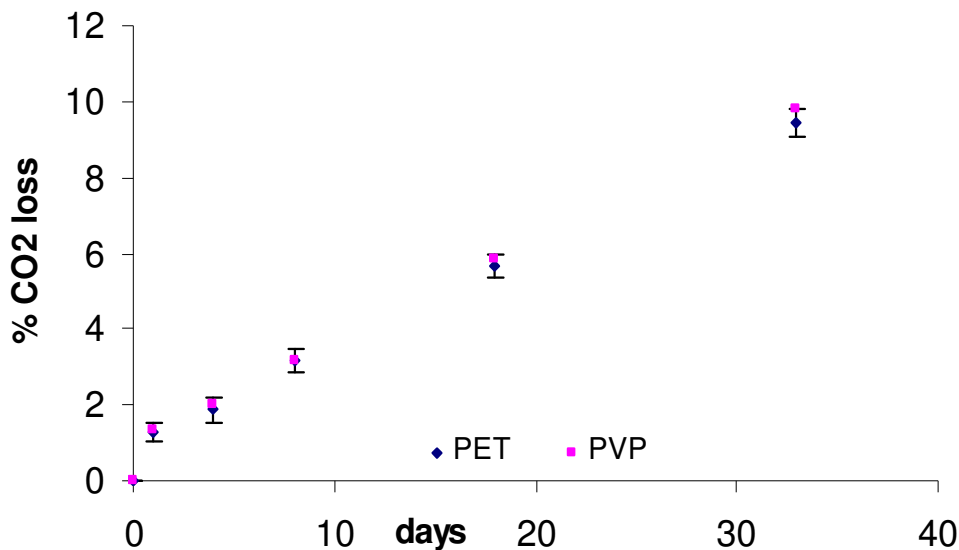
Figure 6.3.2-4 Comparison of CO$_2$ loss from PET and PET/0.75wt% PVP nanocomposite

For this nanocomposite it was found that PET was not able to intercalate the clay due to the very stable intercalated structure formed with the PVP. In essence this resulted in clay with similar properties to the CNa$^+$ base clay and as a result the gas barrier was similar (BIF 0.96).

6.4 Summary of PET nanocomposite behaviour

The nanocomposites produced with both the commercial clays and the in house modified clays all failed to exhibit an exfoliated morphology. For the commercial organoclays, with the exception of CNa$^+$ and C30B an intercalated nanocomposite with (001) spacing of approximately 3.1nm was formed regardless of the initial spacing (i.e. greater or less than 3.1nm) due to the clay surfactant. This indicates that the surfactant may be entirely replaced in the interlayer during processing with PET resulting in an interlayer with consistent spacing due to the presence of the PET in a stable configuration. For the CNa$^+$ material no intercalation of the clay galleries occurred as would be expected given its hydrophilic nature hence the resultant composite was in fact micro-disperse, rather than nano-disperse in nature. Finally of the commercial clays,

C30B also failed to produce an intercalated nanocomposite. This was a somewhat surprising result as this organoclay exhibits the best compatibility with PET based on the solubility parameter data. In this case there was actually a decrease in the (001) spacing of the nanocomposite indicating degradation of the surfactant had occurred. It is possible that due to the reactivity of surfactant hydroxyl groups degradation and chain scission reaction have occurred which have resulted in a lower molecular weight polymer unable to generate sufficient shear to open the interlayer spacing. This result also indicates that the direct compatibility of the polymer and clay surfactant may not perform such an important role as often suggested and that rather direct interactions between the polymer and clay surface are more important in defining the type of nanocomposite produced.

Of the in-house modified clays a more mixed series of results were obtained. For PVP modification no intercalation of the interlayer was observed nor any degradation of the interlayer. This indicates that the PVP is both thermally stable and also capable of significant interaction with the clay surface. This result further indicates the importance of direct interaction of polymer and clay and further indicates that the interactions of PVP and clay are much greater than those of PET and clay hence intercalation is thermodynamically unfavourable. The cetyl pyridinium based clays behaved somewhat similarly to C30B in that there was no intercalation of PET into the clay galleries and that there was a slight reduction in the (001) spacing indicating some surfactant degradation. This degradation was also particularly visible in the yellow/brown colour of the bottles produced. Although there was a significant difference in the thermal stability of the Bromide variant compared to the chloride variant (the chloride being the more thermally stable variant) no difference in the composite formation behaviour was observed. The final clay produced in house was epoxy modified C30B. This clay PET combination resulted in an intercalated nanocomposite despite the good polymer clay compatibility determined from Hansen solubility parameters. The final spacing was similar to that observed for the commercial clays (i.e. ~3.1nm) indicating that despite good surfactant/polymer compatibility it is not possible to form exfoliated nanocomposites without sufficient direct clay surface to polymer interactions.

From the DSC data it can be shown that the presence of clay does not have a great impact on the cold crystallisation behaviour that could affect the bottle blowing process and that the T_c temperatures are similar for all the clays. There are however some differences in the overall level of crystallinity of the as extruded composites. From the Cloisite clays it is evident that the type of surfactant influences the dispersion of clay and this impacts the level of crystallinity. Overall the level of crystallinity for the Cloisite organoclays is lower due to the clay layers and particles forming a barrier to the formation of larger more perfect crystals. The greater the dispersion the more significant the effect appears. When non Cloisite clays are used the effect on cold crystallisation and crystallinity and are less predictable indicating that the type of clay and its micro structure also significantly affect the crystallisation behaviour. The melting behaviour of the as extruded composites is relatively unaffected and similar behaviour is observed for the in house modified materials.

On cooling from the melt under controlled conditions most of the materials tested either have little effect on T_c or slightly retard crystallisation with the exception of N2 and I28. For these materials a combination of good dispersion and the clay microstructure has resulted in a considerable nucleating effect. On heating from a controlled cooling process a double melting point is observed. For PET and composites with poor polymer clay compatibility the predominant peak is the lower of the two but the addition of organoclay results in the predominant peak shifting to the higher temperature due to either the formation of an alternative, more stable crystal structure due to the clay or significant re- crystallisation of the PET during melting due to the presence of stable clay nucleation sites.

The resultant barrier properties of the nanocomposites were not as great as expected from theoretical considerations. This was due to the nanocomposites produced having an intercalated or even a micro dispersion hence the full surface area of the clay platelets available to act as barrier is significantly reduced compared to the exfoliated situation.

7 Non-clay nano-fillers for barrier modification of PET

Due to the difficulties in the approaches to CO_2 barrier improvement reported in chapter 6 and chapter 7 new and novel fillers to improve the barrier properties of PET are examined in this chapter.

7.1 Nano-silica flake enhanced PET

It is well known that layered nano-fillers such as clay can be used to enhance the barrier properties when exfoliated into discrete single layers. Chapter 7 has effectively demonstrated that for PET this is exceptionally difficult due to poor compatibility of polymer and surfactant, lack of direct interactions between the polymer and the clay surface and poor thermal stability of many surfactants employed. In order to overcome this problem novel flake shaped silica fillers will be investigated which possess a single layer structure. The advantage of employing such filler is that exfoliation problems associated with clays can be avoided and conventional processing techniques can be used to disperse the filler.

7.1.1 Morphology of Nano-silica flakes.

Nano enhanced silica flakes of 100nm and 350nm thickness are to be investigated and the properties determined. Initially SEM is used to investigate the nanostructure and a low resolution image is shown in Figure 7.1.1-1From the micrograph the plate-like structure of the silica flakes is clearly evident. In addition it can be seen that the flakes are essentially individual and not agglomerated and that there is a very wide range of particle size (some particles appear to be approaching 1000μm in length).
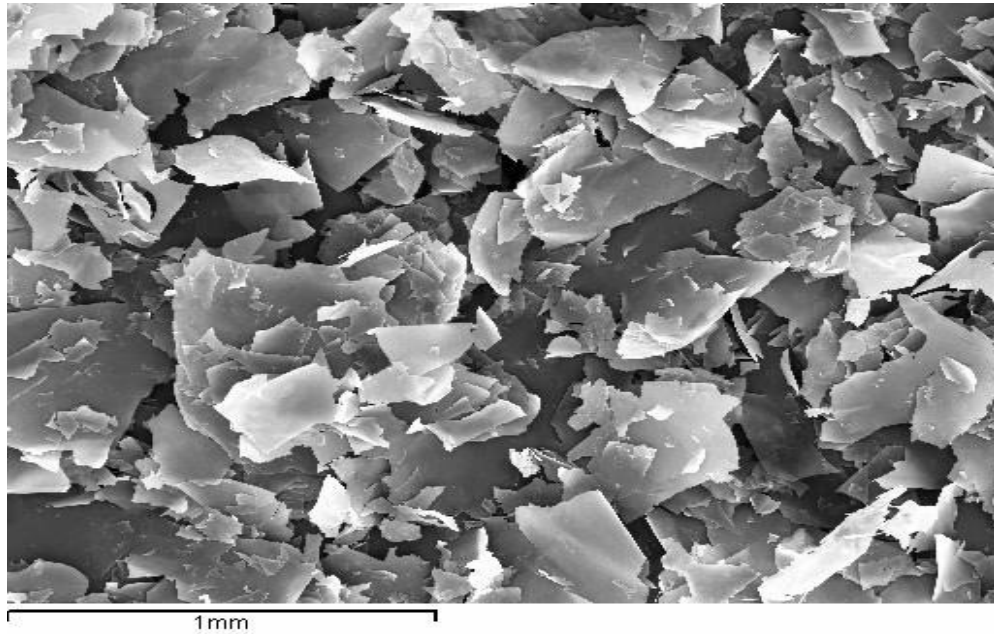
Figure 7.1.1–1 Typical low magnification SEM micrograph of 100nm nano-silica flakes (1mm scale bar).

Increasing the magnification (Figure 7.1.1-2) shows greater detail in the silica flakes and confirms that there is a loose association of particles rather than strong agglomeration. There is also a better indication of the very wide range of particle sizes in the materials with particles as small as 20-30μm clearly evident. In addition to this the transparent nature of the nano-silica flakes is clearly evident.
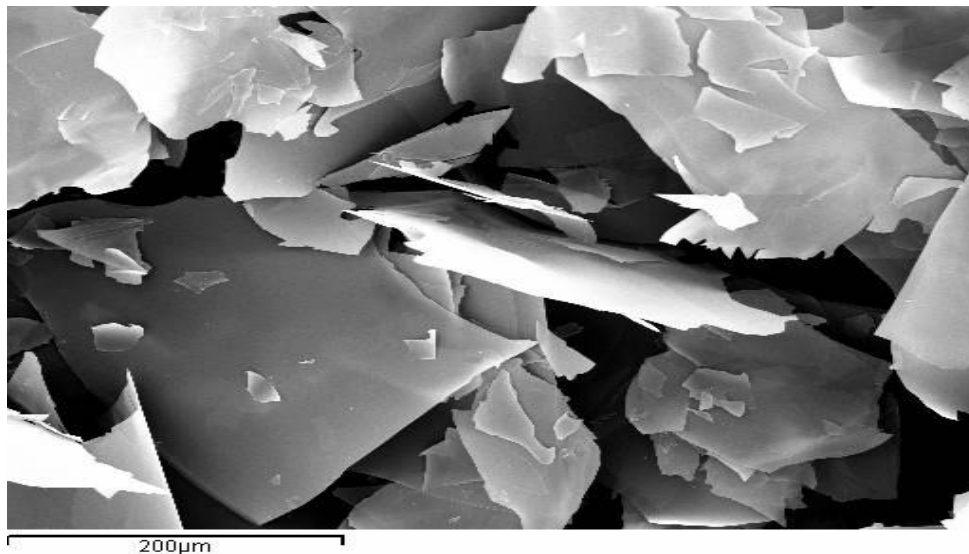
Figure 7.1.1–2 Typical high magnification SEM micrograph of 100nm nano-silica flakes (200μm scale bar)
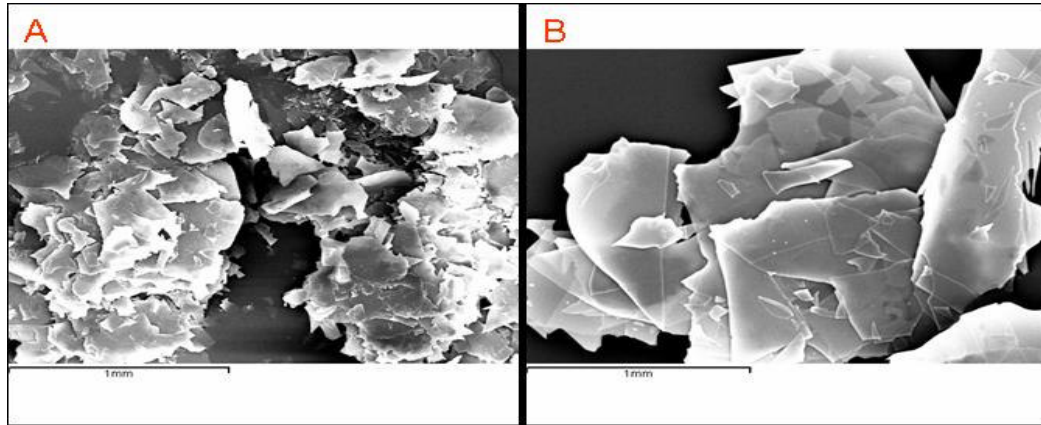
Figure 7.1.1–3 Typical SEM micrographs of 350nm nano-silica flakes at (A) low magnification and (B) higher magnification (1mm scale bar)

The structure of the 350nm flakes is very similar to that observed for 100nm flakes and is confirmed in the SEM micrographs (Figure 7.1.1-3).

7.1.2 Dispersion of nano-silica flakes in PET

To check the dispersion of nano-silica flakes in PET. POM was used on samples cut from the bottle wall for 100nm and 350nm thickness flakes at loadings of 1wt% and 2wt%. Micrographs of the 100nm flakes are shown in Figure 7.1.2 - 1.
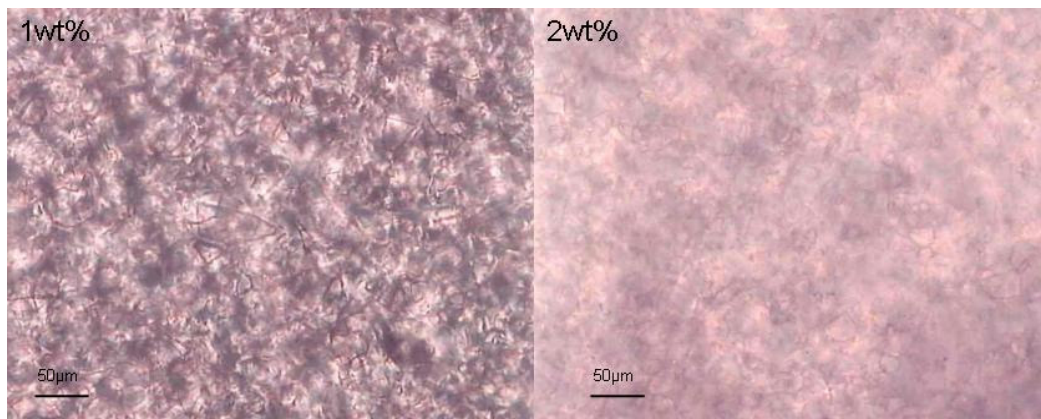
Figure 7.1.2–1 POM micrograph of 100nm silica flakes in PET bottle wall with 50μm scale bar

It is evident that there has been a significant reduction in the overall particle size compared to the original un-processed flakes with the maximum new particle size only approximately 70μm. In addition for 1wt% loading there does not

appear to be significant overlapping of the nano-silica platelets thus significant improvement in barrier would not be expected.

A similar pattern was observed for the 350nm nano-silica flakes, which is illustrated in the micrographs in Figure 7.1.2-2
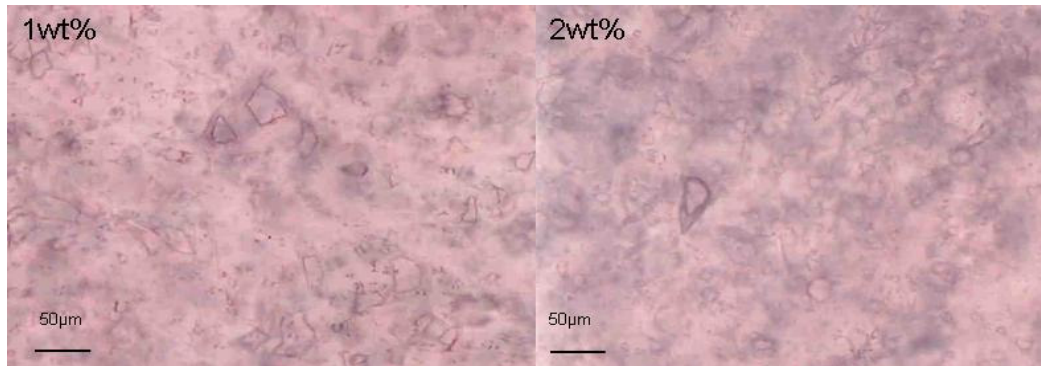
Figure 7.1.2–2 POM micrograph of 350nm silica flakes in PET bottle wall with 50μm scale bar
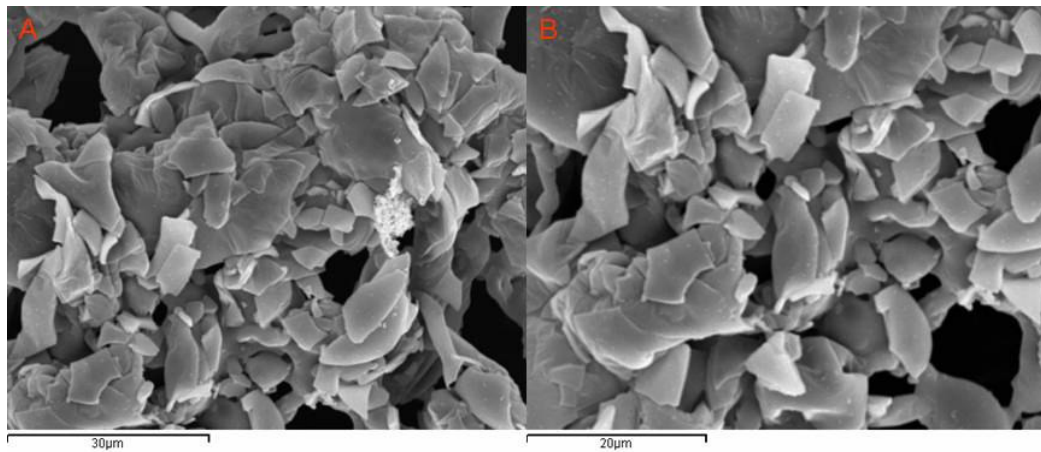
Figure 7.1.2–3 SEM micrographs of 100nm nano-silica flake residues at high magnification (30 and 20μm scale bars)

A more detailed investigation of the effect using SEM was undertaken in order to obtain a clearer picture of the extent of damage to the filler particles. Figure 7.1.2-3 shows the silica flake residue for 100nm flakes (2wt% loading) after removal of the polymer by treatment in a furnace at high temperature. The pictures clearly show that the particle size has been smashed to less than 10μm in

most cases with a few particles of 10 - 30μm also remaining. A similar situation is also observed for the 350nm flakes (2 wt%) as shown in Figure 7.1.2 - 4.
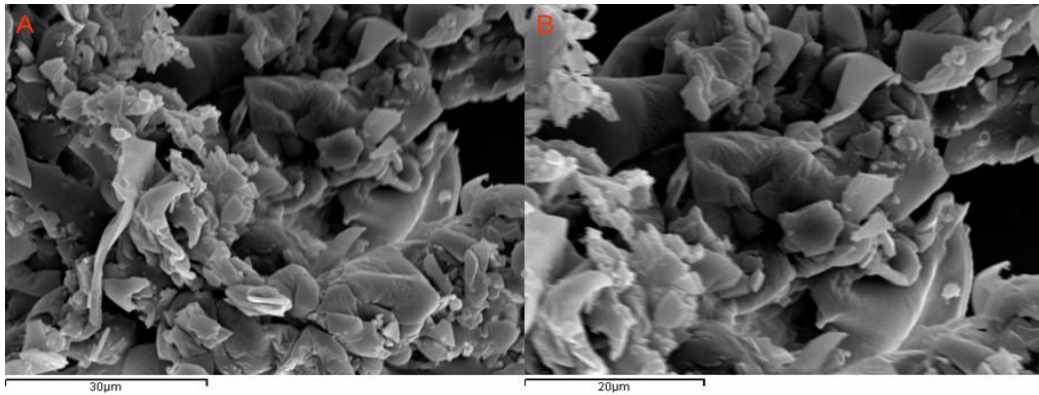
Figure 7.1.2 – 4 SEM micrographs of 100nm nano-silica flake residues at high magnification (30 and 20μm scale bars)

Overall it appears that the nano-silica flakes have potential for barrier enhancement due to their plate like shape and high aspect ratio (1750 for 100nm flakes and 500 for 350nm flakes based on a particle size of 175μm i.e. the mid point of the bulk of the distribution as obtained from the material data sheet) but processing via twin-screw extruder results in significant breakage of the silica flakes and reduction in the aspect ratio. Estimating the particle size from the POM and SEM a value of 10μm has been chosen and new values of aspect ratio of 100 and 30 have been calculated for 100nm and 350nm flakes respectively. This indicates that barrier may be less than predicted based on the initial particle size of the pristine nano-silica flakes.

7.1.3 Crystallisation behaviour of Nano-silica flake composites

The composite pellets produced were analysed by DSC to investigate the effect of the nano-silica flakes on the crystallisation behaviour. Table 7.1.3-1 summarises the behaviour on the initial heating scan and Figure 7.1.3-1 shows the scans.

Table 7.1.3–1 Summary of behaviour of nano – silica composites in the initial heating scan

Sample	Tc on	Tc	Tc end	ΔHc	Tm on	Tm	Tm end	ΔHm	χ%
PET	116	125	137	21.436	230	250	257	41.325	14.196
1% 100nm	110	117	135	26.524	232	249	256	39.586	9.323
2% 100nm	113	120	133	25.211	232	248	256	38.898	9.769
1% 350nm	117	122	130	26.019	229	250	260	34.7	6.196
2% 350nm	120	125	133	26.454	231	250	258	35.688	6.591

From the data it can be seen that the initial crystallisation onset temperature is reduced by the presence of 100nm thickness flakes to 110ºC and 113ºC respectively for 1wt% and 2wt% composites indicating that the flakes are acting as a nucleating agent. This new temperature is quite low and indicates care will be required to ensure no crystallisation of the bottle preforms occurs prior to blowing. For the 350nm thickness flakes the crystallisation onset temperature is slightly raised and is probably due to the less plate like shape (as indicated in section 8.1.2.) leading to less nucleation. The crystallisation peak temperature is slightly lower for 100nm flakes as would be expected as they act as a nucleating agent while temperature is similar for 350nm flakes. The end of crystallisation temperature is lower for all samples compared to PET but it is of note that the range of temperature over which crystallisation occurs is less (13ºC) for 350nm flakes than for the PET control and the 100nm flake samples (20 – 25ºC approximately) indicating that the 350nm flakes have an inhibiting effect on the crystallisation.
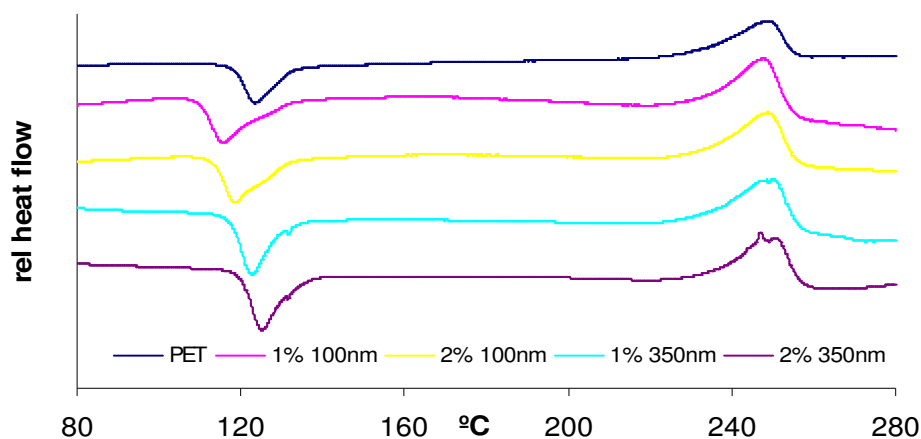
Figure 7.1.3–1 DSC initial heating scans for nano-silica flake composites

214

The melting behaviour of the nanocomposites is not greatly affected by the presence of glass flakes in the polymer matrix regardless of thickness or loading indicating this factor is governed by the crystals rather than the filler.

The overall crystallinity of the samples shows that the incorporation of the filler reduces the overall level of crystallinity. This indicates that the nano-silica flakes act as a physical barrier preventing the formation of the largest crystals hence resulting in an overall reduction in the level of crystallinity. Interestingly the amount of reduction appears to be dependant on the thickness of the flakes rather than the loading hence a reduction to ~9% for 100nm and ~6% for 350nm from 14% for the unmodified material indicating that the shape of the resultant silica flakes is important (i.e. that 100nm flakes remain more plate like than the 350nm flakes).
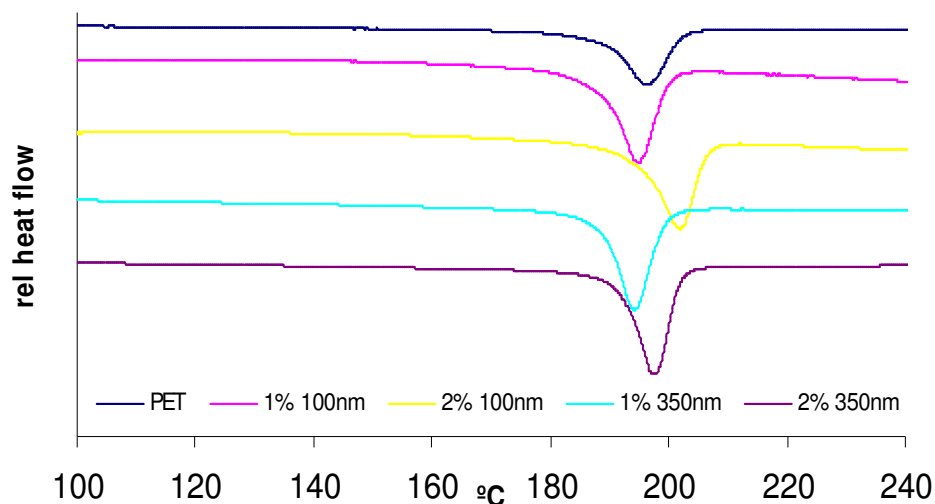
Figure 7.1.3–2 DSC cooling from the melt for nano-silica composites

On cooling from the melt (Figure 7.1.3-2) the most important factor is the loading of nano-silica flakes followed by the flake thickness. The T_{con} and T_c temperatures for PET are 204ºC and 195ºC respectively. The addition of 1wt% 100nm flakes results in little change in T_{con} and T_c (203º and 196ºC) but the T_{cend} temperature is increased to 188ºC therefore the range of temperature over which crystallisation has occurred is reduced indicating nucleation and a more rapid rate of crystallisation. When the loading is increased to 2wt% the whole

215

crystallisation process occurs over the range 208ºC – 196ºC indicating a very significant nucleation effect which is strongly related to the loading of nano-silica. When the 350nm flakes are used for both loadings the crystallisation occurs over a more narrow temperature range (20ºC) but the temperature of onset and peak crystallisation is lower than that observed for PET (199ºC and 194ºC for 100nm and 202ºC and 198ºC for 350nm) indicating that there is a nucleating effect but also an inhibition of the crystallisation onset.

The scans obtained in the second heating scan after controlled cooling are shown in Figure 7.1.3-3. It is evident that there are two main melting peaks present after cooling as previously observed for PET and PET with organoclays. In the case 1wt% 100nm nano-silica flakes two clear and well defined peaks are observed at 240ºC and 249ºC. Given their considerable separation it can be surmised that the presence of the flakes has led to the formation of two distinct crystal structures rather than re-crystallisation and re-melting processes. A similar situation can also be observed for both 350nm thickness flake loadings. The major difference is observed for 2wt% 100nm silica flakes. For this composite an entirely new peak is observed at 244ºC indicating the formation of a new crystal structure.
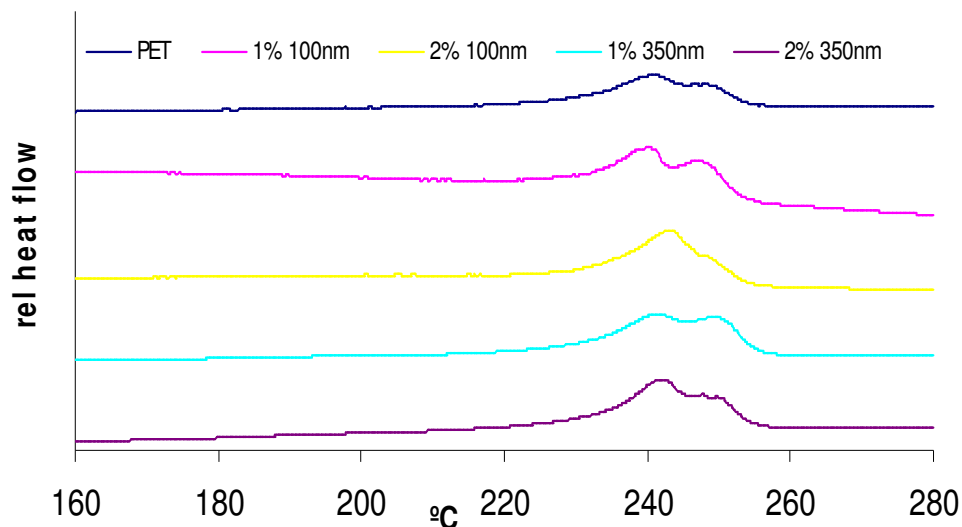
Figure 7.1.3–3 DSC crystal melting behaviour of nano-silica composites

Overall, the presence of the glass flakes affects the crystallisation of the composite through a strong nucleating effect. This is due to the plate-like nature of the filler providing crystal nucleation surfaces. The presence of the platelets also prevent the formation of the largest most perfect crystal structures hence the overall level of crystallinity is reduced. The behaviour is similar to that observed in the presence of organoclay.

7.1.4 Gas barrier properties of nano-silica flake enhanced PET

The gas barrier properties of the PET/nano-silica flakes composites were measured in bottle form as per previous materials except the material was a compound rather than a masterbatch (i.e. material was directly prepared via twin-screw extrusion with the required filler loading). For 100nm thickness flakes at 1wt% loading (Figure 7.1.4-1) there is a slight improvement (BIF 1.11) but overall the result can be considered similar to PET due to the overlapping of error bars.
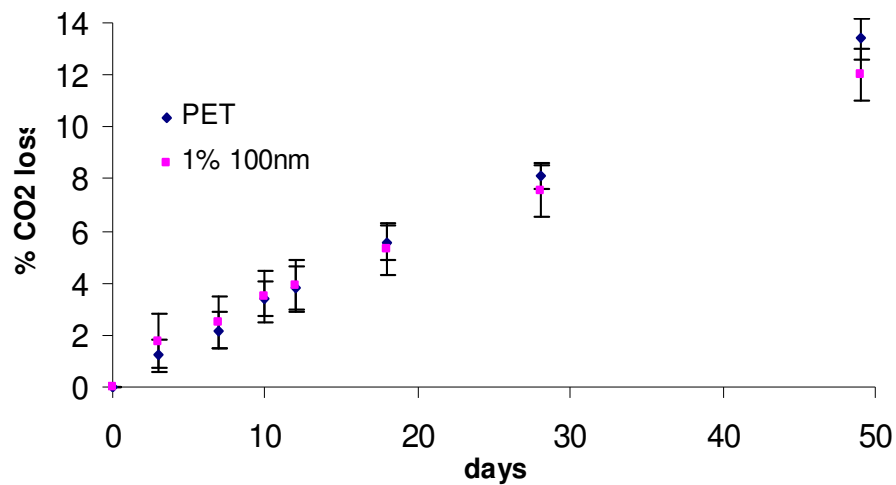
Figure 7.1.4–1 Comparison of CO_2 loss of PET and PET/1wt% 100nm nano-silica composite

When the loading of nano-silica flakes is increased to 2wt% the improvement observed for 100nm thickness flakes increases to 1.27 BIF (Figure 7.1.4-2). Overall this indicates that a critical volume fraction for overlapping of the nano-

silica flakes is between 1wt% and 2wt% loading. If the flakes had not suffered such extensive damage during extrusion processing it is likely that even greater improvements in CO_2 barrier would have been obtained.
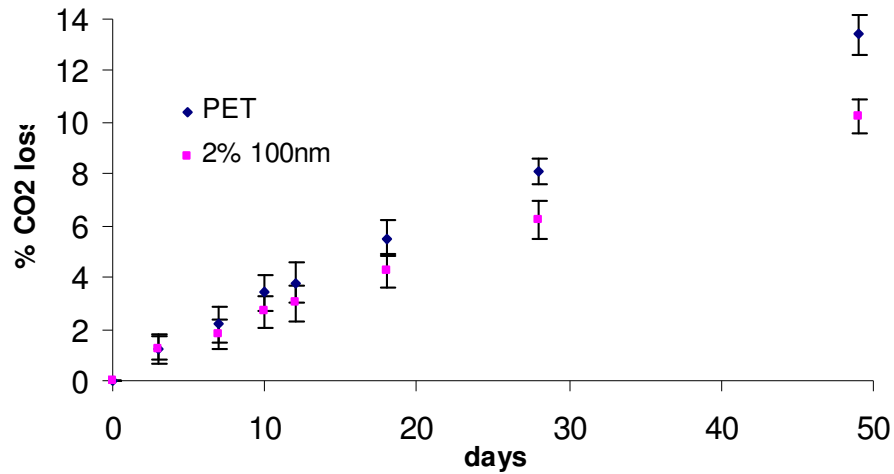
Figure 7.1.4–2 Comparison of CO_2 loss of PET and PET/2wt% 100nm nano-silica composite

In the case of 350nm thickness nano-silica flakes no major improvement is observed with 1wt% or 2wt% loading (Figure 7.1.4-3 & 7.1.4-4) within error. From the microscopy the particle size after the extrusion process is similar to that observed for the 100nm flakes but due to the increased platelet thickness the overall aspect ratio is reduced hence a level of silica flakes likely to improve the CO_2 barrier is likely to have been reached.
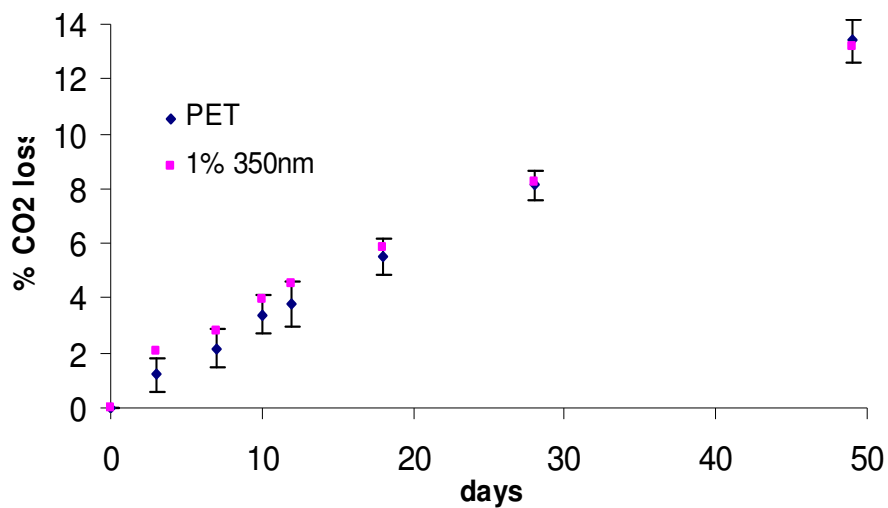
Figure 7.1.4–3 Comparison of CO$_2$ loss of PET and PET/1wt% 350nm nano-silica composite
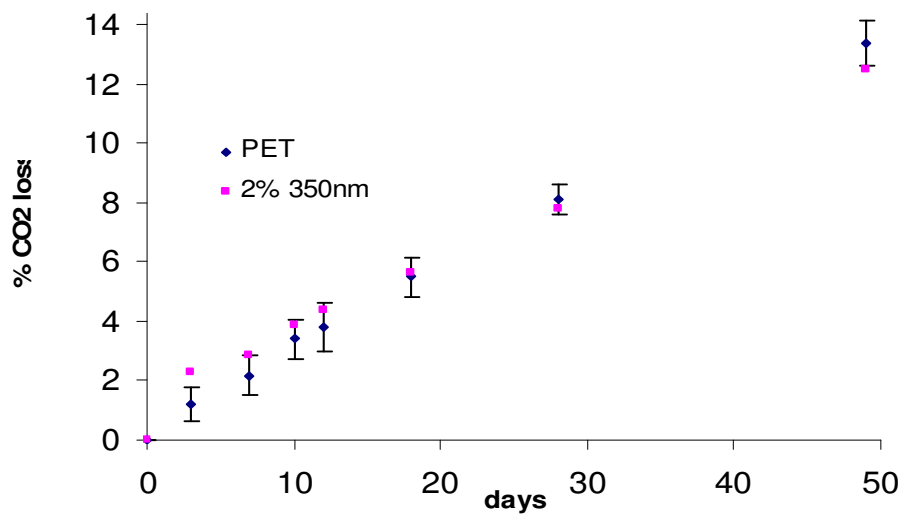
Figure 7.1.4–4 Comparison of CO$_2$ loss of PET and PET/2wt% 350nm nano-silica composite

One further factor that may have influenced the permeability of the bottles is the overall level of crystallinity in the bottle wall but this was measured using DSC and found not to vary greatly (PET 31.26%, 1% 100nm 35.78%, 2% 100nm 33.33%, 1% 350nm 32.34% and 2% 350nm 35.75%) indicating that the most

important factor in the barrier improvement was the presence of the nano-silica flakes forming tortuous pathways.

7.1.5 Summary of nano-silica enhanced PET

Overall the use of the nano-silica flakes shows considerable potential for utilisation as a gas barrier enhancing additive. The result effectively demonstrates that the CO_2 barrier property can be enhanced even after considerable breakage of the nano-silica flakes during processing.

7.2 Divalent metal layered phosphonates (DMLP)

DMLP are a relatively new material for use in nanocomposite applications and are limited to a few reports and patents. The materials produced for investigation as possible barrier additives are zinc phosphate-co-phenylphosphite (ZPcP), calcium phosphate-co-phenylphosphite (CPcP), calcium phenylphosphite (CP) and magnesium phosphate-co-phenylphosphite (MPcP).

7.2.1 Characterisation of DMLP

The materials produced were analysed using XRD and POM to gain an insight into the morphology of the materials. In addition TGA was used to investigate the thermal stability of the materials with particular attention to the stability at the PET processing temperature.

7.2.1.1 Morphological characterisation

7.2.1.1.1 Zinc Phosphate-co-phenylphosphonate (ZPcP)

The XRD data for the ZPcP sample is shown below in Figure 7.2.1.1.1-1. The resultant (001) peak is observed at 6.11° 2 theta and corresponds to a (001) spacing of 1.45nm between the layers. The peak is sharp and well defined indicating a highly regular spacing between the layers.
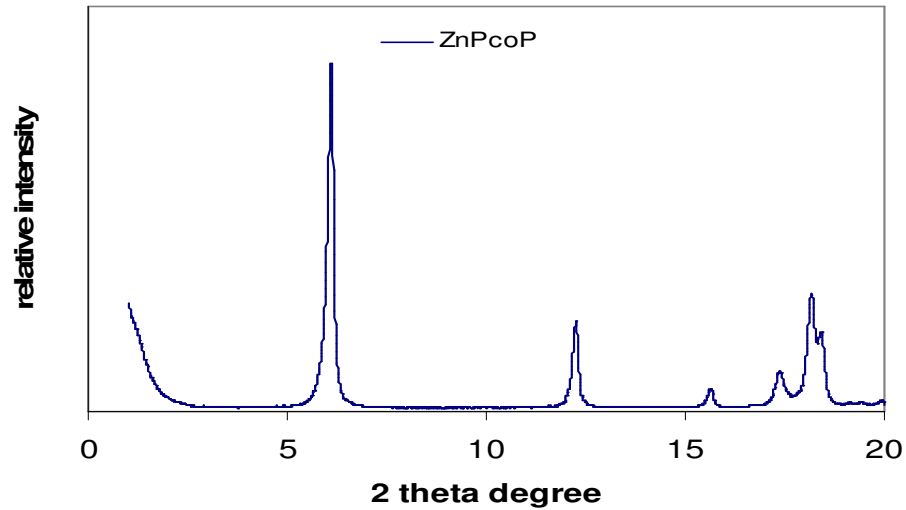
Figure 7.2.1.1.1-1 XRD pattern for ZPcP

Micrographs taken at X100 and X200 magnification are shown in Figure 7.2.1.1.1-2
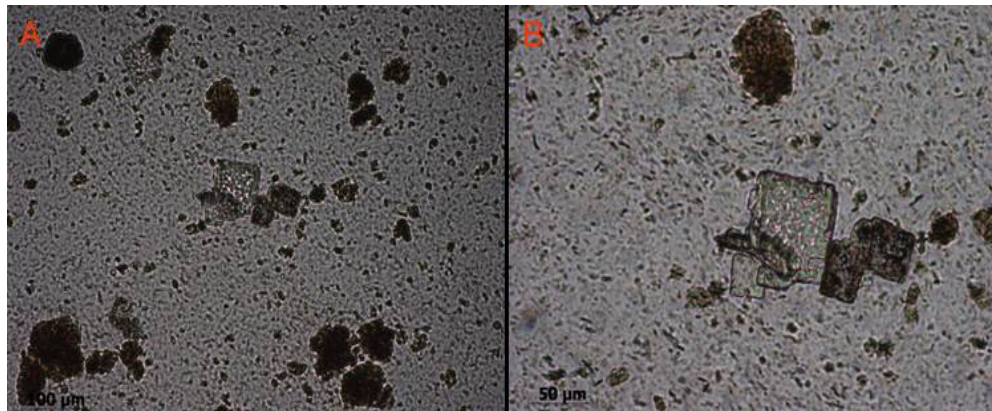
Figure 7.2.1.1.1-2 Micrographs of ZPcP at (A) low and (B) high magnification (50μm scale bars)

From the micrographs it is evident that there are some large particles greater than 50μm in size that appear flat and rectangular in nature. In addition to these large particles there are clearly a large number of smaller particles, some less than 5μm, many of which appear to be acicular in nature. In summary the results obtained from XRD indicating that the nanostructure of the ZPcP is regularly layered but

there is considerable variation in particle size and shape based on the microscopy which may hinder dispersion and resultant barrier properties.

7.2.1.1.2 Calcium Phosphate-co-phenylphosphite (CPcP)

The XRD scan of CPcP (Figure 7.2.1.1.2-1) shows a sharp and clear (001) peak centred at 5.78° 2 theta. This corresponds to a regular interlayer (001) spacing of 1.53nm.

Microscopic examination of the CPcP sample (Figure 7.2.1.1.2-2) shows that there is less variation in the particle size (typically 50μm). The particles appear flat and rounded in shape and there is clear evidence of agglomerations (up to ~170μm in size). On close examination the layered structure of the filler is clearly discernable.
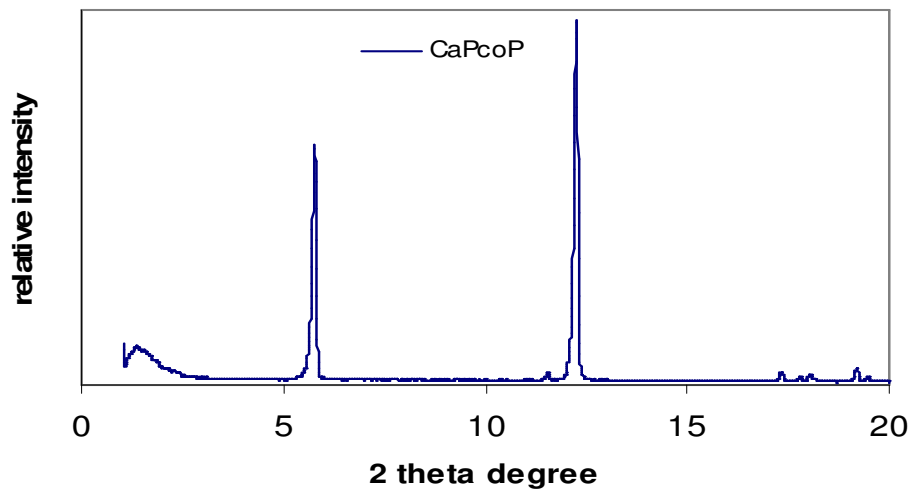
Figure 7.2.1.1.2-1 XRD pattern for CPcP
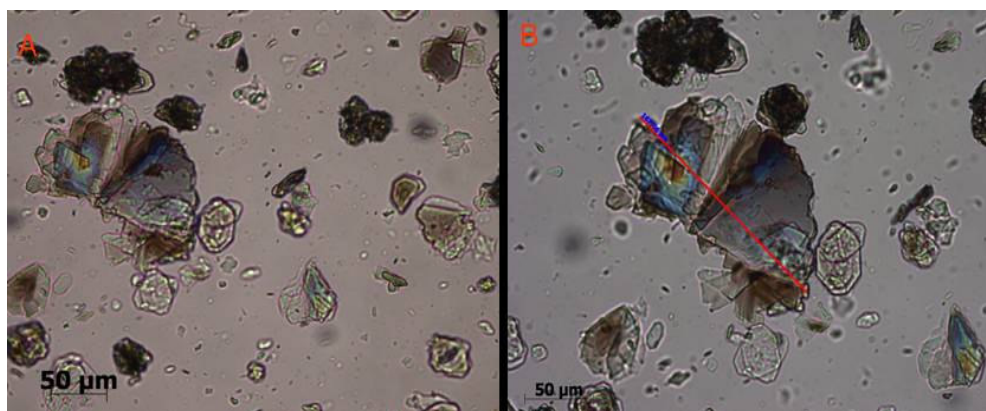
Figure 7.2.1.1.2-2 Micrographs of CPcP at (A) low and (B) high magnification (50µm scale bars)

7.2.1.1.3 Calcium Phenylphosphite (CP)

Examination of CP by XRD (Figure 7.2.1.1.3-1) revealed a sharp narrow (001) peak at 5.79° 2 theta which corresponds to an interlayer spacing of 1.53nm. The sharp peak indicates a very regular layered structure.
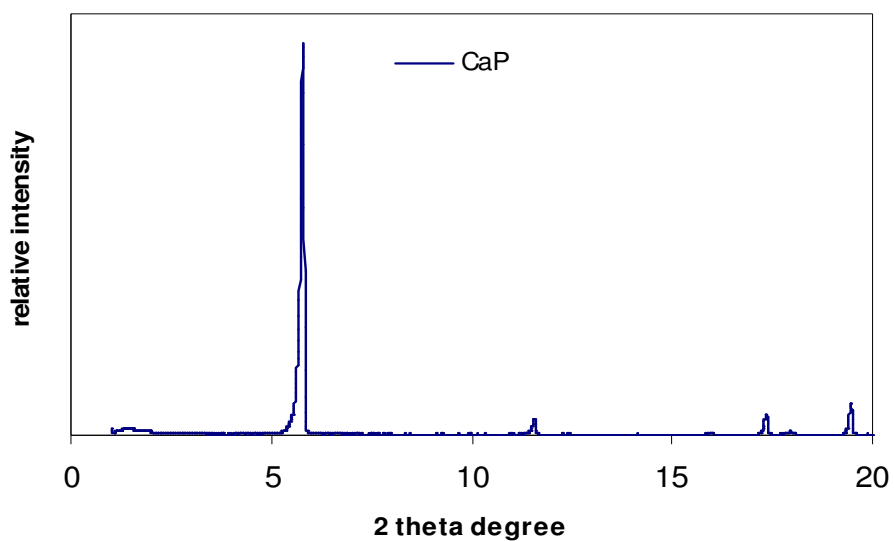
Figure 7.2.1.1.3-1 XRD pattern for CP
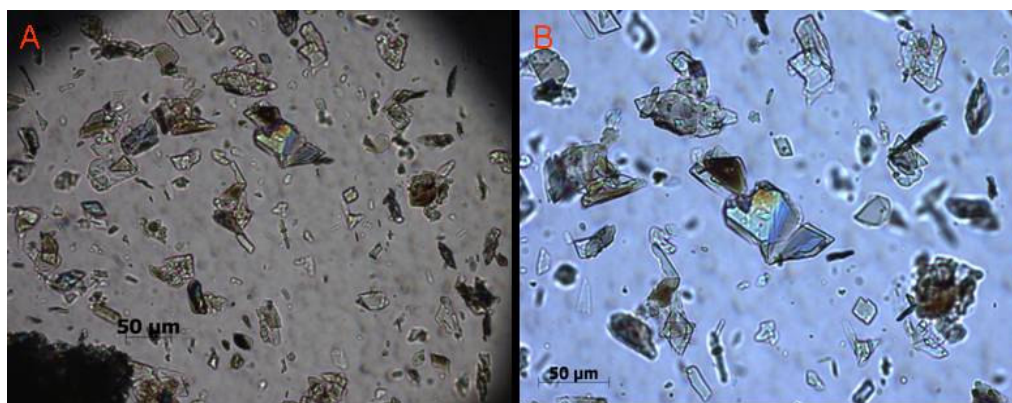
Figure 7.2.1.1.3-2 Micrographs of CP at (A) low and (B) high magnification (50µm scale bars)

In addition, the microscopy (Figure 7.2.1.1.3-2) reveals a range of particle sizes with many over 50µm in addition to a layered structure to the particles.

7.2.1.1.4 Magnesium phosphate-co-phenylphosphite (MPcP)

The XRD pattern of the MPcP shown in Figure 7.2.1.1.4-1 has a sharp (001) peak at 6.35° 2 theta which corresponds to an interlayer spacing of 1.39nm.
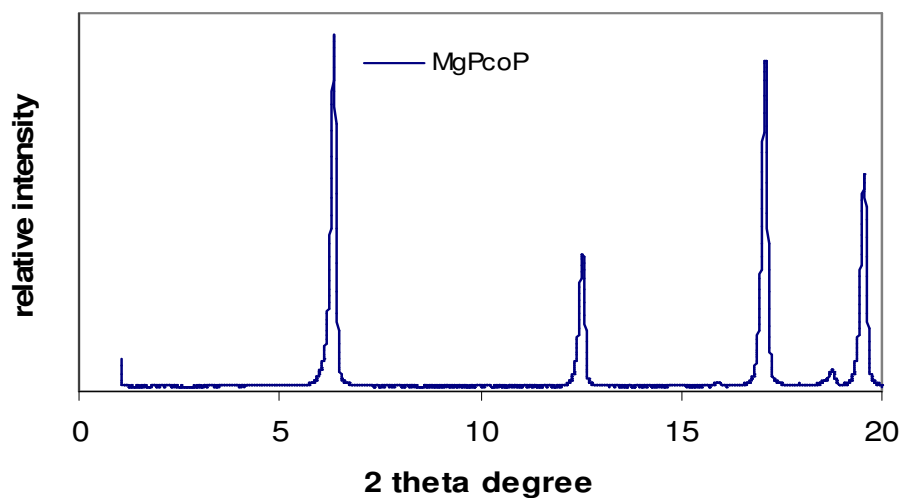
Figure 7.2.1.1.4-1 XRD pattern for MPcP

The supporting microscopy (Figure 7.2.1.1.4-2) indicates much larger agglomerations than seen for the previous materials (particularly the calcium

based phosphonates) with sizes in the range of several hundred microns. In addition the particles appear much more acicular in nature rather than plate like.
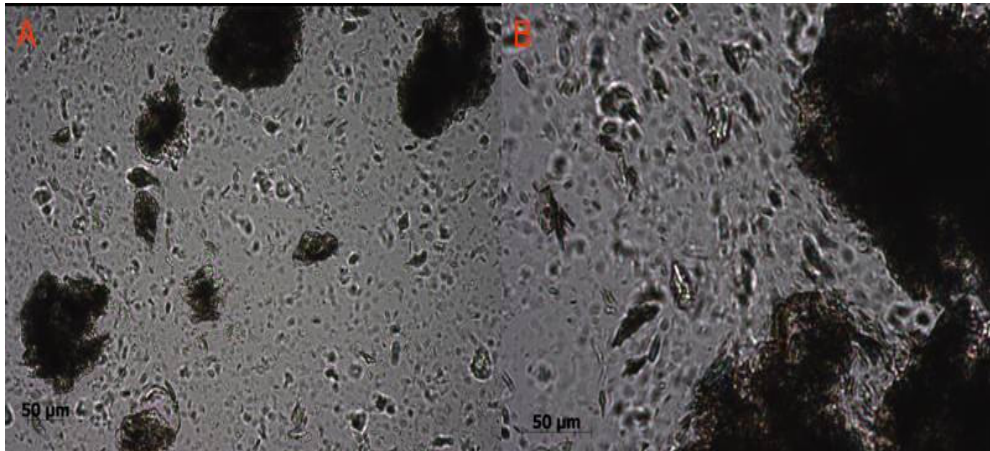
Figure 7.2.1.1.4-2 Micrographs of MPcP at (A) low and (B) high magnification (50μm scale bars)

7.2.1.2 Thermal stability of DMLP's

The TGA traces shown in Figures 7.2.1.2-1 – 7.2.1.2-4 illustrate one of the main potential benefits for these phosphonate materials compared to more traditional organically modified clays in that they are overall more thermally stable over a greater temperature range, in particular the PET processing range (270º - 300ºC).
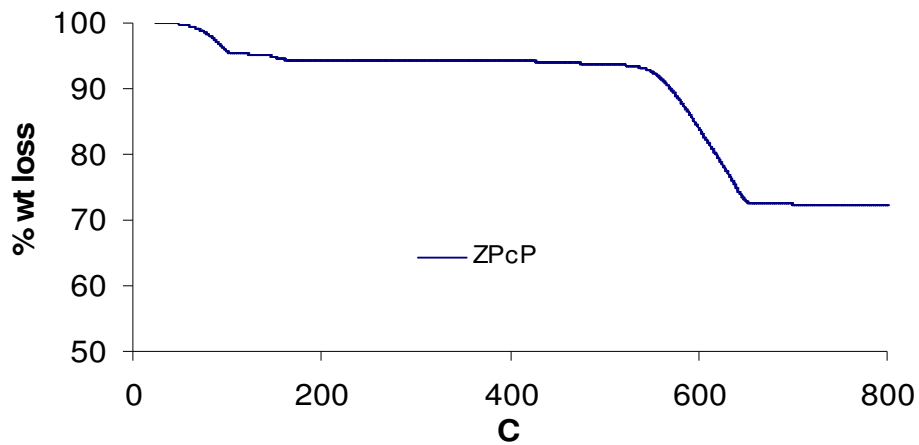
Figure 7.2.1.2-1 TGA data for ZPcP
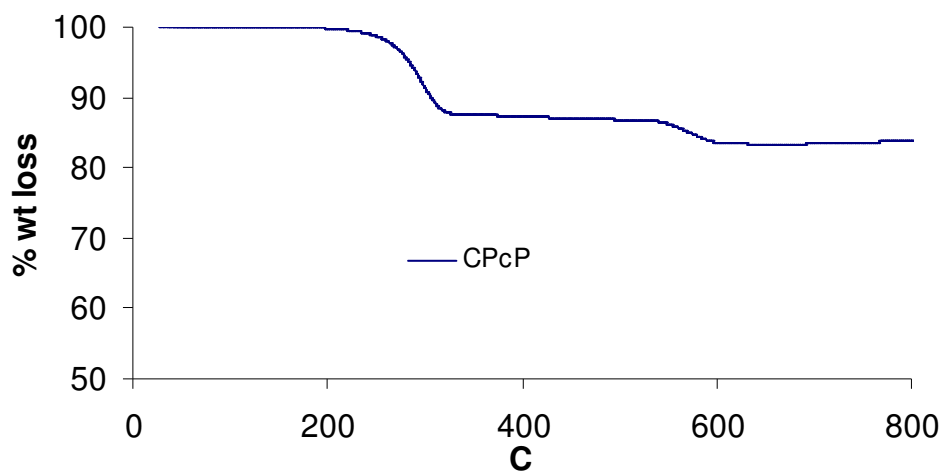
Figure 7.2.1.2-2 TGA data for CPcP
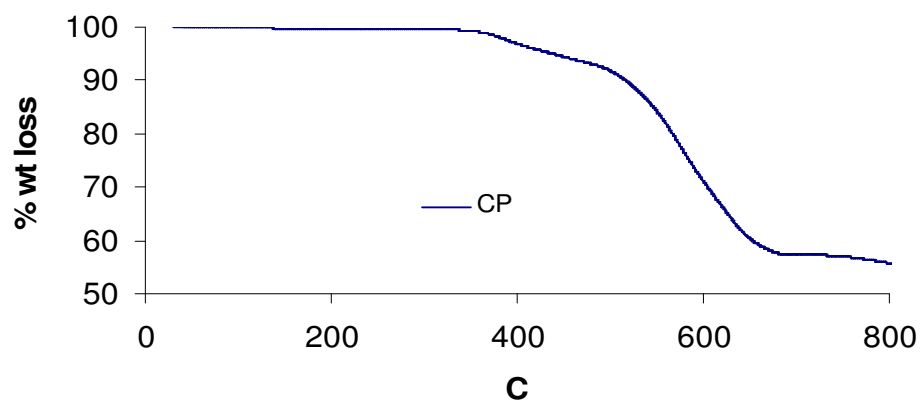
Figure 7.2.1.2-3 TGA data for CP
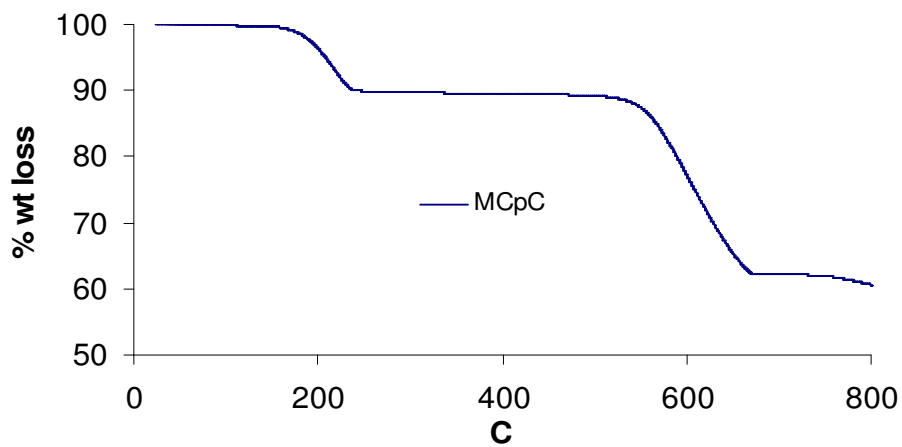
Figure 7.2.1.2-4 TGA data for MPcP

For the ZPcP layered phosphonate there is 5wt% loss at the relatively modest temperature of 146°C. This loss is associated with loosely bonded water and hydroxyl groups at the platelet edges and no significant degradation of the clay layers is observed until 541°C. This indicates that ZPcP has sufficient thermal stability for the PET processing temperature. The CPcP layered phosphonate exhibits even greater stability with 5wt% loss only occurring at 282°C and the next stage of degradation not occurring until 549°C again indicating good thermal stability at the PET processing temperature. CP layered phosphonate exhibits the greatest thermal stability with 5wt% loss only occurring at 437°C with no degradation at all occurring in the PET processing temperature range. The final layered phosphonate MPcP has a similar degradation profile to ZPcP with initial degradation of 5wt% occurring at 207°C with no further degradation until 530°C.

7.2.1.3 Summary of DMLP properties

In summary it has been shown that all the materials produced have a layered structure based on the very clear (001) peaks observed in XRD analysis. Microscopy has revealed some differences in the particulate shapes and sizes and has revealed the calcium based phosphonates to have the most obvious plate like shape and also to clearly show layered structure. In combination with TGA data indicating the calcium based materials have the best thermal stability it is expected that these materials have the greatest potential to improve the gas barrier properties.

7.2.2 Morphology of DMLP nanocomposites

XRD data (Figure 7.2.2-1) taken from the moulded samples of the nanocomposites pellets indicates that intercalation did not occur in any of the DMLP. It is possible that the phenyl group that is situated within the clay layers did not offer sufficient compatibility with PET to encourage intercalation. In addition the (001) interlayer spacing of the DMLP were all similar (~1.45nm – 1.53nm) due to the same interlayer spacing group (i.e. phenyl). This spacing is

slightly larger than that observed for unmodified clays but less than that observed for organically modified clays and this may indicate that the initial layer opening is too small to allow diffusion of PET chains into the phosphonate layers. The new peak positions were 6.13° (ZPcP), 6.17° (CPcP), 5.69° (CP) and 6.32° (MPcP) which correspond to (001) values of 1.44nm, 1.43nm, 1.55nm and 1.40nm respectively. The intensity and sharpness of the obtained peaks indicates that no significant disruption to the layered structure has occurred.
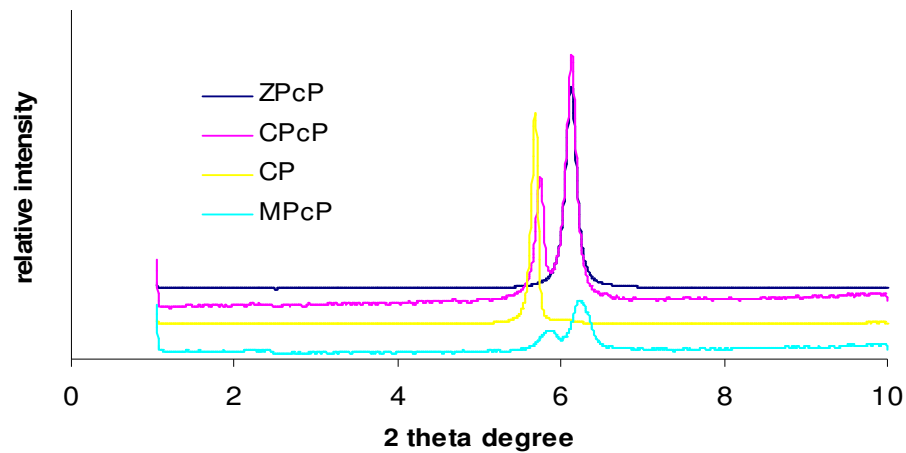
Figure 7.2.2-1 XRD Spectra of DLMP/PET nanocomposites

Microscopy was conducted on bottle wall samples prepared using both a solid and liquid masterbatch route to examine if any major differences in dispersion of the DMLP occurred. A comparison of the microscopy for ZPcP is shown in Figure 7.2.2-2.
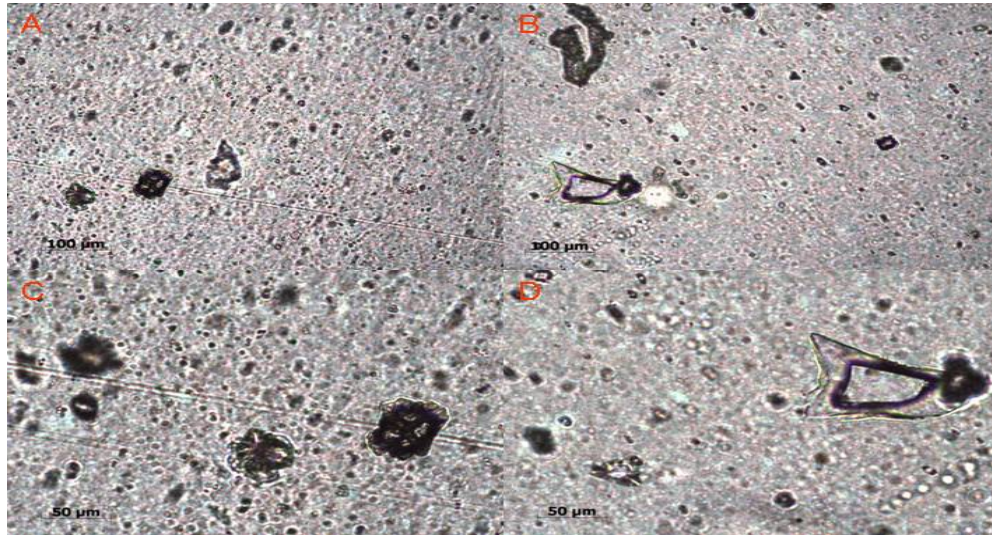
Figure 7.2.2-2 Optical micrographs of (A) ZPcP liquid low magnification, (B) ZPcP solid low magnification (100μm scale bar), (C) ZPcP liquid high magnification and (D) ZPcP solid high magnification (50μm scale bar)

Figure 7.2.2-2 A and B show the dispersion of the liquid masterbatch compared to the extrusion masterbatch at one hundred times magnification and indicate that the additional shear employed in the extrusion process results in improved dispersion. The general particle size (i.e. the background) is about 10μm for the liquid masterbatch with larger particles present up to a maximum of almost 100μm. In comparison the extrusion masterbatch has a smaller background of about 5μm with a smaller portion of large particles although the largest particle present is greater than 100μm in length. Increasing the magnification (Figure 7.2.2-2 C and D) confirms the improved dispersion of the extrusion masterbatch compared to the liquid masterbatch and also provides further detail on the composite morphology by illustrating the layered structure of the larger agglomerates. Figures 7.2.2-3 – 7.2.2-5 show the microscopy for the phosphonates CPcP, CP and MPcP and reveal a similar pattern i.e. that the dispersion of the liquid based masterbatch is inferior to that observed for the extrusion masterbatch.

w the dispersion of the liquid masterbatch compared to the extrusion masterbatch at one hundred times magnification and indicate that the additional shear employed in the extrusion process results in improved dispersion. The general particle size (i.e. the background) is about 10μm for the liquid masterbatch with

larger particles present up to a maximum of almost 100µm. In comparison the extrusion masterbatch has a smaller background of about 5µm with a smaller portion of large particles although the largest particle present is greater than 100µm in length. Increasing the magnification (Figure 7.2.2-2 C and D) confirms the improved dispersion of the extrusion masterbatch compared to the liquid masterbatch and also provides further detail on the composite morphology by illustrating the layered structure of the larger agglomerates. Figures 7.2.2-3 – 7.2.2-5 show the microscopy for the phosphonates CPcP, CP and MPcP and reveal a similar pattern i.e. that the dispersion of the liquid based masterbatch is inferior to that observed for the extrusion masterbatch.

Figure 7.2.2-3 Optical micrographs of (A) CPcP liquid low magnification, (B) CPcP solid low magnification (100µm scale bar), (C) CPcP liquid high magnification and (D) CPcP solid high magnification (50µm scale bar)
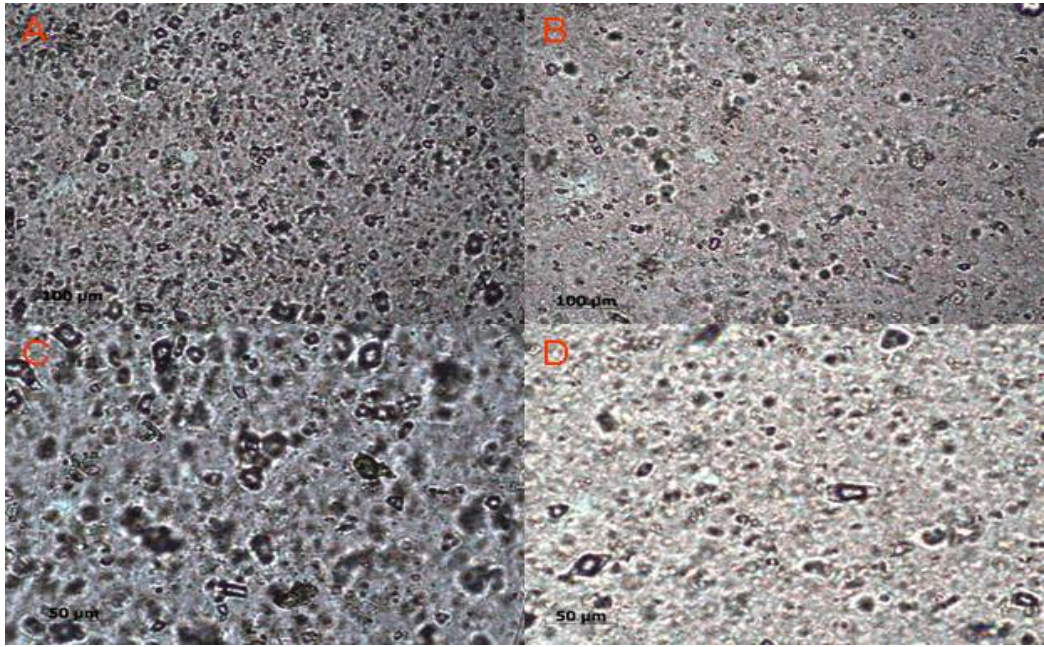
Figure 7.2.2-4 Optical micrographs of (A) CP liquid low magnification, (B) CP solid low magnification (100μm scale bar), (C) CP liquid high magnification and (D) CP solid high magnification (50μm scale bar)
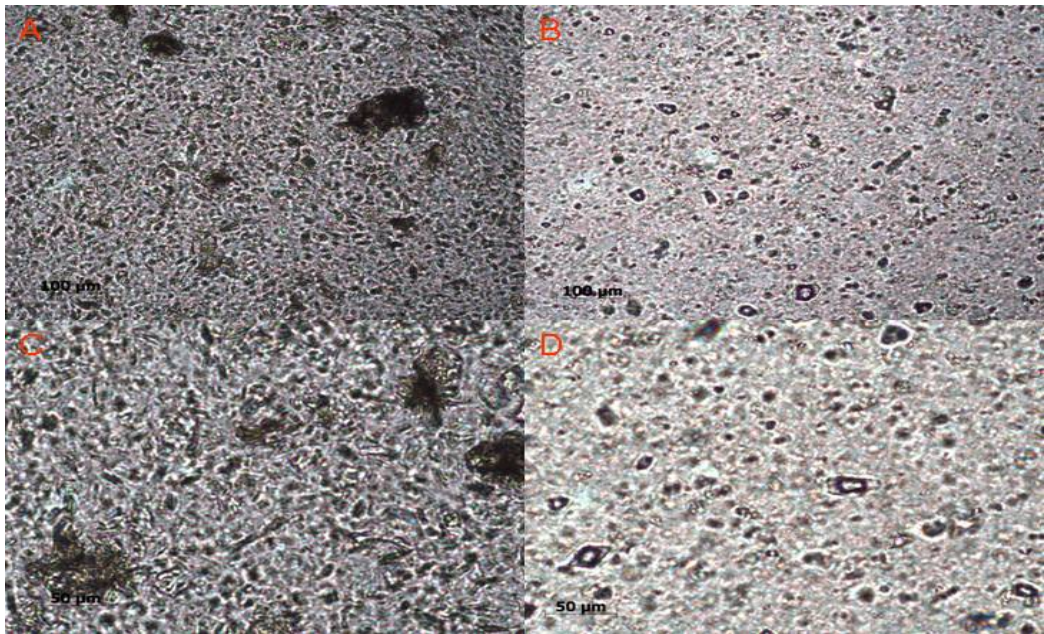
Figure 7.2.2-5 Optical micrographs of (A) MPcP liquid low magnification, (B) MPcP solid low magnification (100μm scale bar), (C) MPcP liquid high magnification and (D) MPcP solid high magnification (50μm scale bar)

The DMLP have produced microcomposites rather than true nanocomposite due to the failure of the PET to intercalate the layered structure. As such a micro – dispersion of the DMLP would be expected and this is confirmed through the microscopy conducted on the bottle wall samples. Using an extrusion masterbatch approach as opposed to a liquid one resulted in improved micro-dispersion but a true nanocomposite was still not produced. Based on these results significant improvements in CO_2 barrier would not be expected although, given the large size of the DMLP particles some improvement may still be obtained through increased tortuosity.

7.2.3 Crystallisation behaviour of DMLP nanocomposites

Then DSC behaviour for the DLMP nanocomposite pellets on initial heating is summarised in Table 7.2.3-1 and Figure 7.2.3-1.

Table 7.2.3-1 Summarised first heat data for DLMP

Sample	Tc on	Tc	Tc end	ΔHc	Tm on	Tm	Tm end	ΔHm	χ%
PET	116	125	137	21.436	230	250	257	41.325	14.2
ZPcP	114	120	130	25.692	233	248	253	40.178	10.3
CPcP	113	119	129	25.183	233	249	256	43.436	13
CP	116	121	128	24.981	233	248	255	40.649	11.2
MPcP	110	117	128	24.943	235	251	257	48.24	16.6
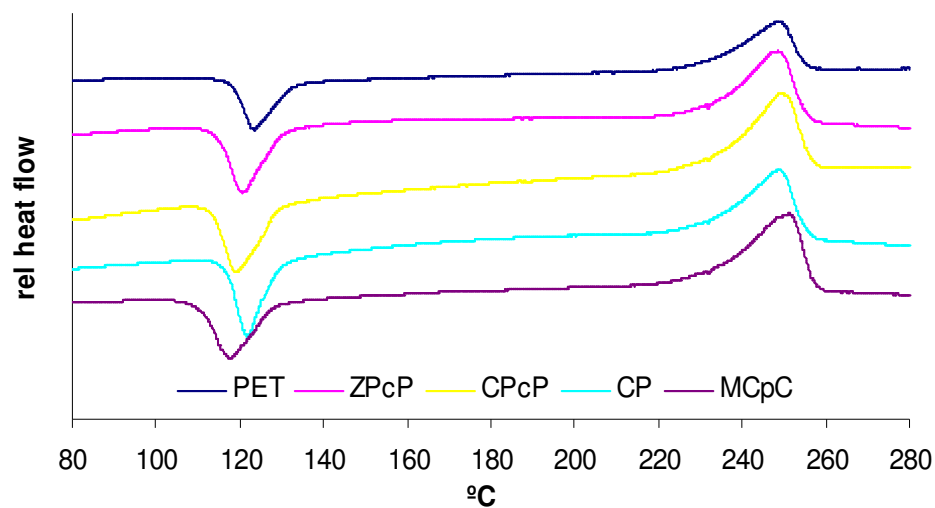
Figure 7.2.3-1 DSC initial heating scans for DLMP

232

From the table and chart it can be seen that the onset of crystallisation occurs at a lower temperature for the DLMP than for PET as does the T_c and crystallisation end. Overall this indicates that sufficient crystal nuclei (i.e. small crystallites) are present after the processing stage that re ordering around the nuclei can occur as soon as the polymer chains have sufficient mobility at temperature above T_g. The T_c temperature occurring at a reduced temperature and crystallisation occurring over a more narrow temperature range indicates faster crystallisation.

From the table and chart it is evident that the melting behaviour and the overall level of crystallinity remain largely unaffected by the presence of the DLMP.

After removal of the thermal history and subsequent cooling from the melt (Figure 7.2.3-2) a significant nucleating effect can be observed resulting in crystallisation occurring at significantly elevated temperature compared to the PET control.
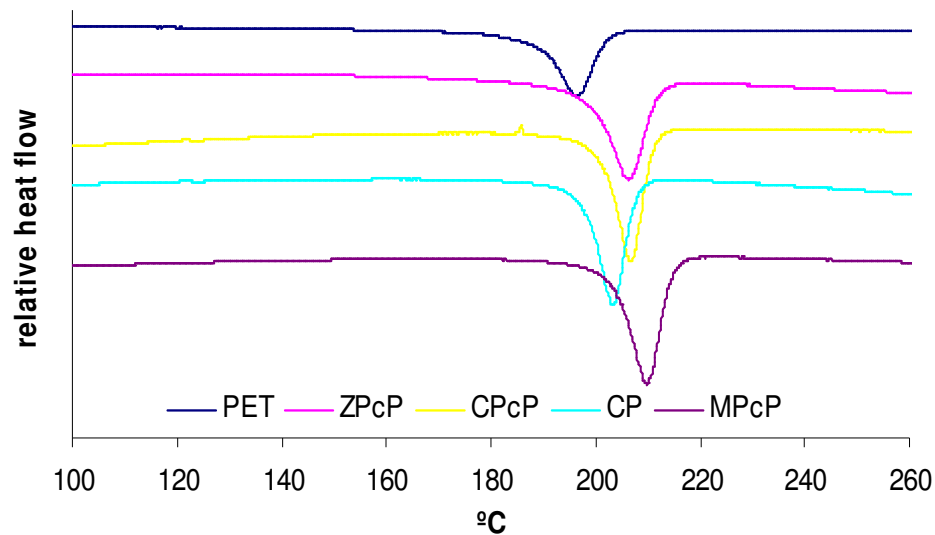
Figure 7.2.3-2 DSC cooling from the melt for DLMP

In the case of the PET control the T_{con} and T_c are 204ºC and 195ºC respectively while the incorporation of the DLMP results in increases in the T_{con} temperature to 212º, 211º, 207º and 214ºC for ZPcP, CPcP, CP and MPcP and increase in the T_c to 207º, 207º, 203º and 210º respectively. In addition, the temperature range

over which crystallisation occurs is reduced by the presence of the DMLP indicating both increased nucleation and an increase in the crystallisation rate.

The heating scans after controlled cooling are shown in figure 7.2.3-3. The chart shows a double peak for PET at 242ºC and 250ºC as seen previously for PET which is indicative of the melting of crystals with differing levels of perfection or re-crystallisation during melting due to the presence of stable nuclei. In contrast the systems filled with the DMLP exhibit a strong peak at 245ºC (247º) for the MPcP DMLP and a weak shoulder at 250ºC. The intense nature of this peak may be indicative of the formation of an alternative crystal form of PET with a different melting point.
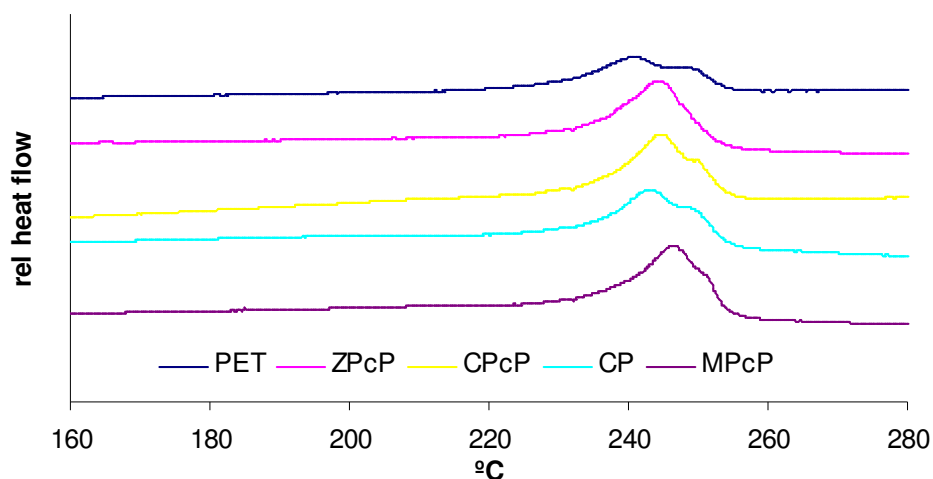
Figure 7.2.3-3 DSC crystal melting behaviour of DMLP nanocomposites

7.2.4 Gas barrier properties of DMLP nanocomposites

The gas barrier properties to CO_2 were measured on bottle samples as per the previous methods described. For the DMLP the filler loading in the bottle was 0.15wt% and samples were produced using a liquid masterbatch system and also a polymer masterbatch. The results for the ZPcP DMLP are shown in figure 7.2.4-1. Overall, there is very little difference between the nanocomposite materials and the PET control indicating that either the loading of DMLP was insufficient to significantly enhance the gas barrier properties or that the

dispersion of the DMLP was insufficient to develop a tortuous pathway. A similar pattern was also observed for the CPcP, CP and MPcP DMLP with the results shown in figure 7.2.4-2, -3 and -4 respectively.
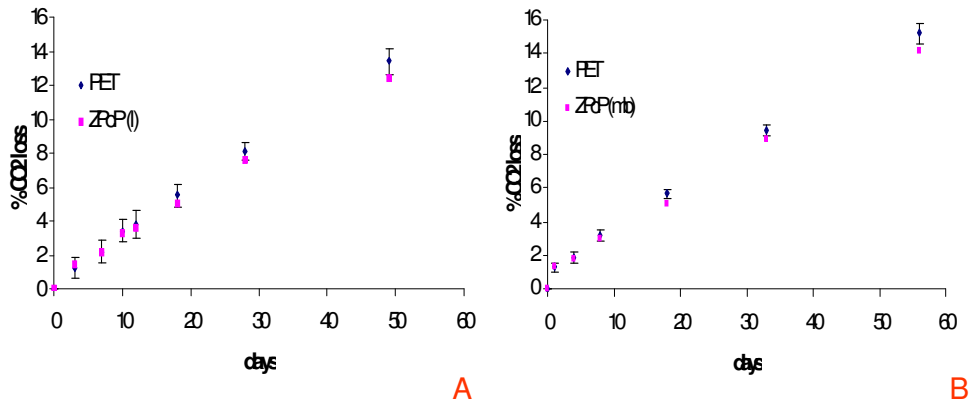
Figure 7.2.4-1 CO_2 loss data for ZPcP in (A) liquid masterbatch and (B) polymer masterbatch
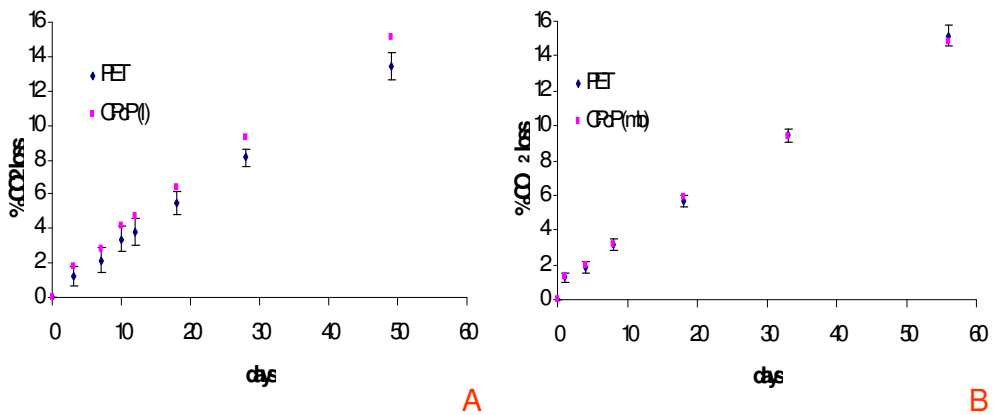
Figure 7.2.4-2 CO_2 loss data for CPcP in (A) liquid masterbatch and (B) polymer masterbatch

Despite the poor results exhibited there does appear to be a slight improvement when the material is added as a polymer masterbatch indicating that the high shear mixing environment in the twin-screw extruder is beneficial in generating good dispersion of the DMLP. Overall the results indicate that significantly

higher loadings or improved dispersion of the DMLP through exfoliation of the individual platelets would be required in order to give a significant improvement in the gas barrier properties.
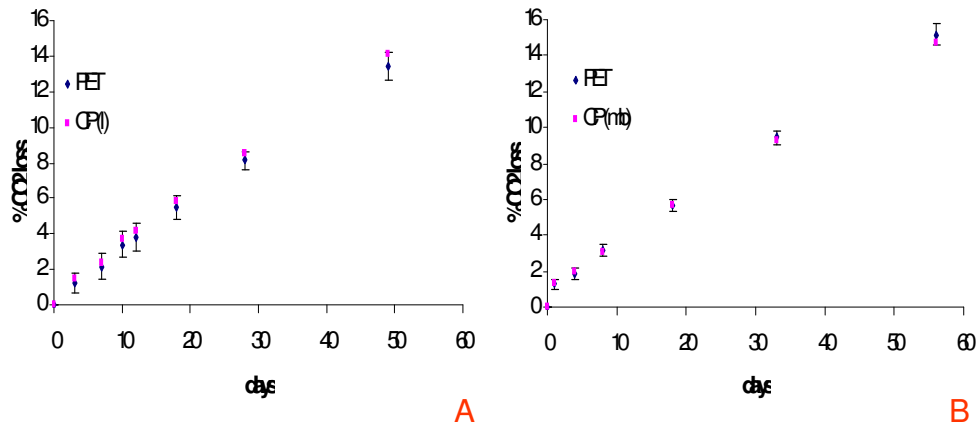
Figure 7.2.4-3 CO$_2$ loss data for CP in (A) liquid masterbatch and (B) polymer masterbatch
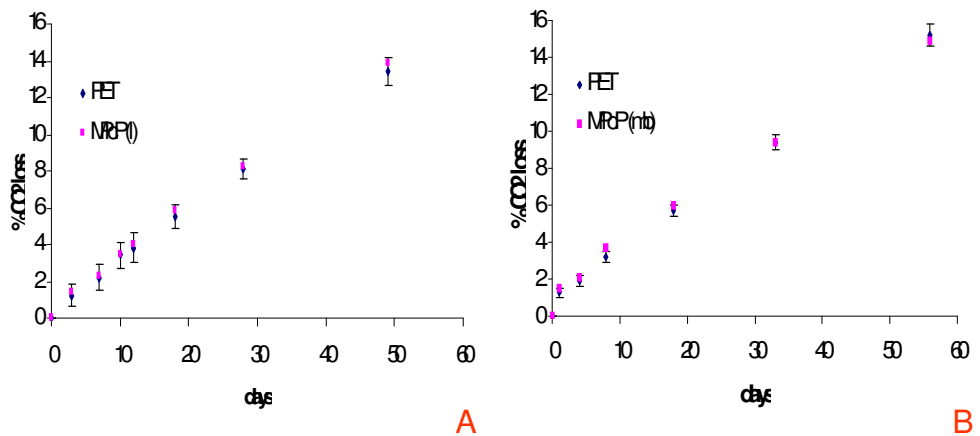
Figure 7.2.4-4 CO$_2$ loss data for MPcP in (A) liquid masterbatch and (B) polymer masterbatch

7.2.5 Summary of DMLP as gas barrier additive

From the results obtained from these materials it is evident that obtaining de-lamination of the DMLP layers is difficult hence if significant improvements in the barrier properties are to be achieved further investigation will be required.

8 Comparison of gas barrier results with model predictions for PET based nanocomposites

The permeability coefficient (P/P_o) i.e. the reduction in permeation due to the presence of filler can be effectively modelled to predict the maximum improvement in gas barrier for a given polymer/filler system. The following sections compare the model predictions to experimental results and discuss similarities and discrepancies in those results.

8.1 PET/Clay nanocomposites

It is generally accepted that the aspect ratio of MMT is 300 and it has been calculated that 0.75wt% gives a volume fraction clay content of 0.4%. The batches were adjusted for organoclay content in order to give 0.75wt% inorganic content hence the density of raw sodium form clay was used in the calculation of volume fractions. Table 8.1-1 summarises the permeation coefficient of the PET clay nanocomposites and also shows the theoretical values calculated using the models of Nielsen [153], Cussler [154], Fredrickson [155] and Gusev [156].

Table 8.1-1 Table of theoretical and experimentally derived permeability coefficients for clay

Sample	P/Po	Sample	P/Po
PET/CNa$^+$	1.035	PET/CPBr	0.883
PET/C10A	0.975	PET/CPCl	0.936
PET/C15A	0.853	PET/30BE	0.947
PET/C30B	0.912	PET/PVP	1.033
PET/C93A	0.86	Nielsen	0.6225
PET/N2	0.854	Cussler	0.5402
PET/N3010	0.831	Fredrickson	0.7265
PET/B2010	0.802	Gusev	0.6247
PET/I28	0.86		

The first feature of note is that all the models predict a significant reduction in permeation that is not reflected in the experimental results. In chapter 7 it was observed that for PET/CNa$^+$ and PET/PVP nanocomposites intercalation of the clay by the polymer was not achieved and that the overall the dispersion of the clay was very poor with large agglomerates. The morphology produced is essentially a micro-composite and the particulates do not exhibit a plate like shape but rather a more cubical shape (i.e. aspect ratio 1). If aspect ratio of 1 is used (as per samples exhibiting only micro-scale dispersion of clay) in the models values of 0.994, 0.999, 1.009 and 0.992 for permeability coefficient are obtained for the models of Nielsen, Cussler, Fredrickson and Gusev respectively. These values are much closer to the observed experimental values and indicate that use of the correct inputs is essential in obtaining good data from the models. From the other results the general trend is of reducing permeation with improved dispersion of the organoclay in the polymer despite all the nanocomposites exhibiting a predominantly intercalated morphology. These results indicate that the size of the clay platelet stacks has reduced thus resulting in an aspect ratio less than 300 but greater than 1 (e.g. if stacks of five platelets remained the new aspect ratio would be 60 resulting in permeation coefficient of 0.889 for Nielsen, 0.998 for Cussler, 0.90 for Fredrickson and 0.861 for Gusev). On the other hand it is also possible that large stacks remain in combination with a smaller volume fraction of exfoliated platelets with aspect ratio 300. In this case a volume fraction of 0.1% exfoliated platelets would give permeation coefficients of 0.867 for Nielsen, 0.996 for Cussler, 0.914 for Fredrickson and 0.839 for Gusev models respectively. Overall it is likely that a situation exists where there is a non uniform mixture of tactoid sizes in addition to some individual clay layers.

From the model predictions and results it is evident that the morphology of the nanocomposite in terms of the clay particle size is crucial in terms of applying the correct data to the model but the model can interpret and predict complex behaviour if the morphology is adequately understood.

8.2 PET/Nano-silica flake composites

The nano-silica flakes used in this study exhibit a wide range of particle sizes (as illustrated in 3.1.3) hence it was necessary to estimate an average particle size of 175µm in order to calculate aspect ratios of 1750 and 500 for 100nm thickness and 350nm thickness nano-silica flakes respectively. Due to the known brittle nature of silica flakes high loadings of 1wt% and 2wt% were selected as it was expected that the aspect ratio would be reduced on processing hence the barrier effect would be reduced. Based on the density supplied by the manufacturers of 2.6g/cm^3 volume fractions of 0.55% and 1.1% were determined. In Table 8.2-1 model predictions based on Nielsen, Cussler, Fredrickson and Gusev are again used to predict the permeation behaviour of the nanocomposites and compared to the experimental data. In addition new aspect ratios based on the examination of residues from the bottle walls were used to estimate the actual aspect ratio of the silica flakes after processing (found to be 100 and 28 for 100nm and 350nm flakes respectively) and these values are also compared to the experimental results.

Table 8.2-1 Permeation coefficient data for nano-silica flakes and comparison with model data for pristine and post processing flakes

Sample		1% 100nm	2% 100nm	1% 350nm	2% 350nm
Experimental results		*0.897*	*0.792*	*0.957*	*0.929*
Nielsen	Pristine	0.1712	0.0931	0.4187	0.2637
	Processed	0.78	0.66	0.9222	0.8665
Cussler	Pristine	0.1473	0.0823	0.0799	0.1798
	Processed	0.9727	0.7569	0.9994	0.9967
Fredrickson	Pristine	0.3013	0.1811	0.5601	0.4091
	Processed	0.8191	0.7133	0.9152	0.8558
Gusev	Pristine	0.127	0.0427	0.4284	0.2736
	Processed	0.7631	0.643	0.895	0.844

From the results presented in the table it is clearly evident that the experimentally recorded permeation is much greater than predicted by the models for both 100nm and 350nm thickness flakes due to significant breakage of the silica flakes in processing (as shown in Section 8.1.2). When new aspect ratios are estimated from the microscopy it can be seen that the model predictions are quite close indicating that the behaviour of a nanocomposite can be predicted well when the particulate morphology is well characterised (i.e. the filler exists as single layers). The differences between the model predictions and the experimental results indicate that different systems may be better characterised by a certain model and also estimating the aspect ratio introduces some error. Overall it has been shown that permeation models can effectively predict the properties of nano-silica flakes based PET nanocomposites.

8.3 PET/DLMP nanocomposites

For the DLMP, based on our microscopic evaluation and material presented by Rule [ref] the platelet size was determined to be 5μm for ZPcP, 40μm for CPcP, 30μm for CP and 10μm for MPcP. Based on XRD interlayer spacing and the layer structure it is assumed that the layer thickness is 1nm hence aspect ratios of 5000, 40000, 30000 and 10000 were estimated for ZPcP, CPcP, CP and MPcP respectively. The aspect ratio of these materials is very large and hence low loadings of filler can be expected to give large improvements in the gas barrier properties. Table 8.3-1 gives the model predictions for these materials after Nielsen, Cussler, Fredrickson and Gusev in addition to the experimental results for permeation coefficient.

In comparing the experimental results and the model predictions it is evident that the predicted improvement in gas barrier properties has not occurred. Based on the microscopic evidence it is clear that the particle size of the DLMP has remained the same after processing and XRD has shown that no intercalation structure has been achieved further indicating that detailed information on the composite morphology is required in order to realise properties predicted by these common models of gas permeation.

Table 8.3-1 Table of theoretical and experimentally derived permeability coefficients for DLMP

Sample	Experimental	Nielsen	Cussler	Fredrickson	Gusev
ZPcP (l)	0.932	0.1663	0.1438	0.3256	0.12
CPcP (l)	1.085	0.0243	0.0136	0.0472	0
CP (l)	1.033	0.0624	0.0502	0.1502	0
MPcP (l)	1.135	0.0623	0.1047	0.2371	0.05
ZPcP (mb)	0.949	0.1663	0.1438	0.3256	0.12
CPcP (mb)	0.976	0.0243	0.0136	0.0472	0
CP (mb)	0.965	0.0624	0.0502	0.1502	0
MPcP (mb)	0.985	0.0623	0.1047	0.2371	0.05

9 Summary, Discussion, Conclusions and future work

9.1 Summary and discussion

In chapter 4 the properties of clays were investigated in detail. The commercially available organoclays were found to exhibit a wide range of thermal stabilities and compatibilities towards the polymers under investigation. In general C30B was found to have the best compatibility towards the polyamides and the PET while the other materials where more hydrophobic in nature. Although offering the best compatibility the C30B was found to have poor thermal stability and hence it would be expected that significant degradation of the surfactant would occur at the polymer processing temperature (especially for the MXD6, G21, T5000 and PET which are all processed at temperatures of 250ºC or above) potentially inhibiting the formation of highly exfoliated nanocomposites. In order to resolve the problem of combined compatibility and thermal stability several novel clay modifications were identified and it was demonstrated that improved compatibility (particularly towards PET) in conjunction with thermal stability in excess of the PET processing temperature (270ºC) could be achieved thus increasing the hope that PET nanocomposites with a highly dispersed nature could be produced.

In evaluating the different polyamide materials much was learned about the mechanism of clay dispersion in different types of polymer. In the case of PA6 it was observed that molecular weight has an influence on the ability of the clay to be highly dispersed in the polymer. It was observed that the high molecular weight polymers were more readily able to disperse the clay due to the higher shear generated in the twin screw extruder. In addition, it was also observed that the surfactant also influences the level of dispersion but is not directly related to the compatibility (as defined by the Hansen solubility parameter). In PA6 all the clays investigated produced highly dispersed (exfoliated) nanocomposites with the exception of C15A which is the most hydrophobic of the clays examined due to the presence of two long alkyl chains in contrast to C93A with only one long

alkyl chain. Based on fractional solubility parameter data these materials exhibit the same compatibility towards the PA6 but it is not possible to produce a highly dispersed/exfoliated nanocomposite only one with an intercalated nature for C15A while C93A nanocomposite is highly dispersed. Thus overall the indication is that for the readily exfoliated PA6 system the nature of the surfactant has a significant role in determining the outcome of the nanocomposite formation process, particularly the thermal stability (i.e. C93A is greater than C15A).

For MXD6 a similar range of clays produced significantly different results compared to the PA6. In this case only the C93A organoclay produced a nanocomposite with considerable dispersion/exfoliation despite C30B exhibiting the best compatibility toward the polymer based on the solubility parameter data. This result indicates that the thermal stability of the organoclay also plays a role in determining if the morphology of the resultant nanocomposite in conjunction with the compatibility of the surfactant.

For the final two PA's investigated (G21 and T5000) it was only possible to produce nanocomposites with an intercalated morphology with compatibility and thermal stability having little influence on the final morphology. When considering the results obtained for the PA's collectively it is evident that there is an order of polarity (i.e. amide group concentration) with PA6 having the greatest polarity followed by MXD6, G21 and T5000 with the least polarity. This indicates that overall the polarity of the polymer (and hence its ability to directly interact with the clay platelet surface) has greater significance in determining the final nanocomposite morphology than issues of surfactant/polymer compatibility, surfactant thermal stability and polymer molecular weight.

In addition to obtaining information on the mechanisms and factors influencing nanocomposite morphology the investigation of PA based nanocomposites was undertaken in order to assess the potential of the different PA/clay combinations for use as a PA based nanocomposite masterbatch for PET packaging. Based on our results PA6 nanocomposites (with the exception of the C15A clay) and the MXD6/C93A combination have the best potential for this application. Despite this an initial investigation was conducted into the compatibility of the Pa's and their effect on the permeation of the PET as it was thought these factors may also influence the final decision on the best way forward for the PA based

nanocomposite masterbatch approach. From the solubility parameter data PA6 followed by MXD6 and G21 would be expected to exhibit the best compatibility but based on the transparency of the mouldings both PA6 and G21 appear incompatible due to considerable haze while in contrast both MXD6 and T5000 (unexpectedly based on the solubility parameter data) appear very compatible with excellent transparency when added to PET at 5%. When it was attempted to produce bottles it was found that the PA6 nucleated the PET in the preform preheating stage prior to blowing to such an extent that bottles could not be blown. Of the remaining materials MXD6 exhibited the best permeation properties and transparency with both G21 and T5000 having inferior gas barrier and significant discolouration and haze in the bottles. Based on all the available data the best route forward for a PA masterbatch approach to improving the gas barrier properties of PET was determined to be the MXD6/C93A combination.

The initial investigation of the MXD6/C93A nanocomposite for masterbatch application immediately raised issues as it was observed that the incorporation of clay in MXD6 had a significant nucleating effect when added to PET. The loading of clay in MXD6 was reduced from 5wt% to 1wt% (0.1wt% clay in the bottle) and with this loading it was possible to produce bottles with 5wt% of MXD6 nanocomposite in the PET. The barrier properties of these bottles were found to be similar to a simple PET 5wt% MXD6 blend indicating that the clay had not had a significant effect because it is either confined to the MXD6 phase and has not been dispersed throughout the full polymer matrix or the loading is insufficient to expect significant improvements in the gas barrier from the clay alone.

In order to address this problem novel processing techniques were developed as described in detail in chapter 6. When materials were produced as a compound (i.e. all the final bottle components pre-extruded together prior to injection moulding) the gas barrier (BIF ~1.6 cf ~2) dropped considerably compared to a simple blend of PET and MXD6 mixed in injection moulding. In addition the compound materials also exhibited significant discolouration (amber coloured bottles) and haze indicating that significant degradation had taken place. The addition of a catalyst to promote ester amide interchange interactions and improve the compatibility of PET with clay had little effect as did the pre-blending of the polymers by twin-screw extrusion prior to addition of clay again

with the intention of improving the compatibility of PET and clay. A second approach to make a master-batch both with and without pre-blending of the clay and with and without catalyst produced slightly better BIF (~1.75) compared to the compound approach. The discolouration was less than that associated with the compound due primarily to the incorporation of a large amount of pristine PET in the masterbatch approach during processing to form bottles. The overall barrier improvement is disappointing as was that achieved when an MXD6 nanocomposite was blended with PET both with and without catalyst. In this case the bottles exhibited the least yellowing but the increase in BIF (~1.4) was poor. Overall the blending approaches investigated illustrate the significant effect of degradation on the gas barrier properties and the difficulty in transferring exfoliation from PA into the whole polymer matrix. The use of catalyst to improve the compatibility of PET and MXD6 by the synthesis of in-situ block copolymers was not successful and the presence of catalyst may have led to further degradation although the barrier properties of catalysed and non catalysed materials within the same process group are not significantly different. In summary to progress the PA based masterbatch approach to improving barrier properties the effect of degradation of the polymer during twin-screw extruder processing needs to be addressed and understood as this appears to be the main factor limiting the barrier properties of the novel blends.

Chapter 7 of this thesis covered the direct intercalation of clays by PET. From the results it is evident that it is not possible to exfoliate the current commercial organoclays in PET. It is believed that the primary limiting factor in the development of PET/clay nanocomposites is the lack of polymer/surfactant affinity and the poor thermal stability of the organoclays but our studies have shown that even when novel surfactants are used with improved compatibility and thermal stability exfoliation can still not be achieved.

The nanocomposites produced with PET and the clays investigated were always intercalated in nature with an interlayer spacing of approximately 3.15 – 3.35nm with the exception of C30B, CPBr, CPCl, PVP and CNa$^+$ clay. In the latter cases C30B, CPBr and CPCl all had a reduced interlayer spacing after processing with PET. All these polymer/clay combinations exhibited considerable discolouration, particularly in the bottles and microscopy revealed very poor dispersion of the clay indicating that degradation of the clay surfactant had resulted in a collapsing

of the clay interlayer. It is likely that this collapse of the interlayer has prevented initial diffusion of polymer chains into the clay galleries due to insufficient space. It appears that the high compatibility of PET and C30B surfactant is less of a factor than thermal stability of the organoclay surfactant in facilitating initial intercalation of the clay galleries. For the case of PVP clay it appears that a very thermally stable interlayer modifier with significant affinity for the clay is very difficult to replace with PET due to unfavourable thermodynamics. Finally no intercalation of the clay was observed for the PET/CNa$^+$ system due to the hydrophilic nature of the unmodified clay interlayer and in all likelihood insufficient interaction of the PET chains with the clay surface. Based on these observations it would appear that the other commercial and in house modified clays exhibited sufficient thermal stability to allow initial penetration of the polymer chains into the clay galleries to allow an intercalated nanocomposite to form. The XRD results for these materials are, as stated all very similar at approximately 3.15 – 3.35nm for interlayer spacing regardless of the initial surfactant and interlayer spacing. This indicates that the surfactant is replaced in the interlayer by PET as if both surfactant and PET were present the interlayer spacing would be different for different clays depending upon the size of the surfactant molecule. In the literature [170] the c dimension of the unit cell (i.e. along the chain) for PET is quoted as 1.075nm thus three repeats of this would give an interlayer spacing of 3.225nm. It is possible that with some tilt from the perpendicular a fourth unit with δ^+ charge on the carbonyl carbon forms the fold in the polymer chain resulting in a lamellae of 3 unit cells thickness as depicted schematically in Figure 9.1-1.

This consistent interlayer spacing is also observed regularly in the literature (section 1.9) and it is believed that this is the first time this behaviour has been considered. Further to this effect a similar observation can also be made for PBT nanocomposites. For PBT the c dimension of the unit cell is given as 1.159nm or 1.295nm dependant on the crystal form in the literature [171] and typical interlayer spacing with various clays were found to range between 3.42nm and 3.94nm [172-174] these values are again similar to three multiples of the unit cell c dimension. In addition, similar behaviour has also been observed by Okamoto [175] for PLA/clay nanocomposites.
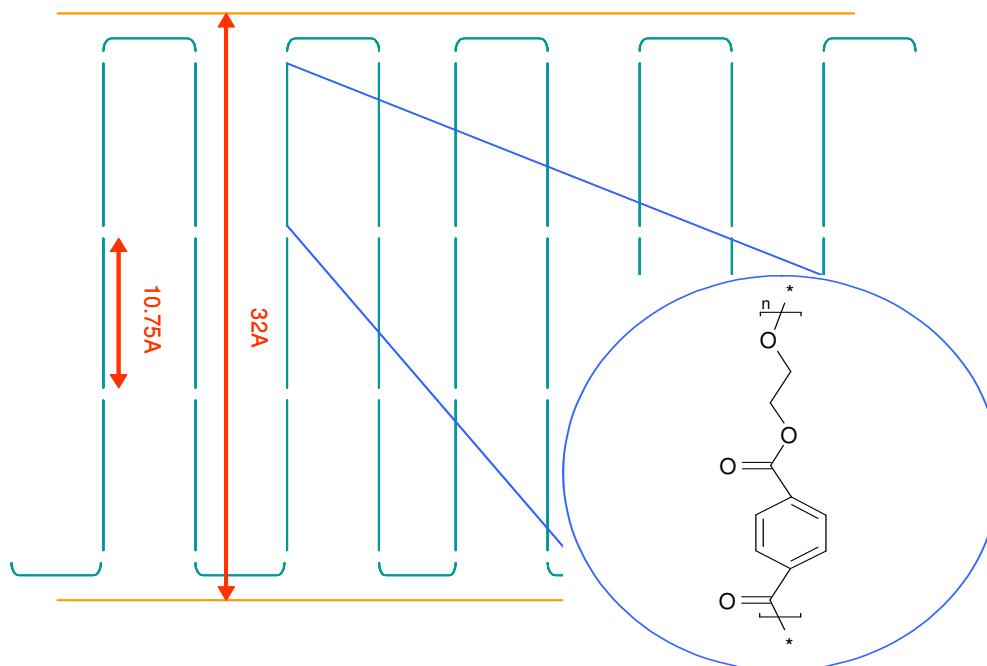
Figure 9.1-1 Schematic representation of possible crystalline PET structure in clay interlayer.

Mechanistic theories thus far proposed such as those of Giannelis and Via [176-178] indicate exfoliation is most likely in situations where polar interactions between the polymer and clay are maximised while apolar interactions between the polymer chains and surfactant alkyl chains are minimised. This would suggest that increased polarity of the polymer is beneficial in order for a high level of exfoliation to occur and explains the efficacy of PA6 compared to the other PA's studied in the formation of exfoliated nanocomposites. In the case of PET the change from amide linkage to ester linkage results in reduced polarity and it appears that polar attractions although significant are not sufficient for the PET to peel apart the individual layers. It would appear that to increase the extent of exfoliation of clay in PET the polarity of the polymer should be increased rather than development of surfactants with increased compatibility and thermal stability.

The final aspect of this thesis investigated the use of novel fillers for the improvement of PET CO_2 barrier. The nano-silica flakes were found to be effective in overcoming the problem of delamination of clay layers due to their single layer morphology and as such significant improvements were made to the

CO_2 barrier but these were not as great as expected due to significant breakage of the filler platelets during processing. In contrast it was found that the DMLP were very difficult to disperse and as a result did not significantly affect the gas barrier properties of the PET.

9.2   Conclusions

From our studies aimed at improving the gas barrier properties of PET packaging using nanocomposites technology several useful conclusions can be drawn. From the work conducted on PA based nanocomposites we can conclude that the most significant factor in determining the morphology of the nanocomposite is the polarity of the polymer. The most polar of the polyamides i.e. PA6 in this study produced nanocomposites much more readily than the other less polar polymers studied. In addition for PA6 the surfactant polymer interactions are also of some importance as is the molecular weight of the polymer, but these factors remain secondary to the polarity which allows direct interaction with polar groups on the surface of the clay.

When considering PA materials for a masterbatch application for PET we have found that despite its ability to effectively exfoliate clay, PA6 is a poor choice due to its rapid crystallisation rate which results in the PA6 nucleating crystallisation in the PET. Based on this we concluded that MXD6 would make the best material and found as per previous authors that MXD6 is indeed very effective in enhancing the barrier properties of PET. Based on all the MXD6 nanocomposite blending work, including the use of novel processing techniques and catalyst it has been shown that the transfer of exfoliation from the MXD6 phase to the PET phase is very difficult due to the tendency of the MXD6 to form discrete domains in the PET.

From our investigations of direct intercalation of clays by PET we have found that the clay thermal stability and compatibility of surfactant of PET are of little consequence in the synthesis of highly exfoliated nanocomposites. Rather it has been shown that the polarity of the polymer is of much more consequence and that the polarity of PET is insufficient to produce high levels of exfoliation. In addition we have been able to conclude that in processing the surfactant is lost

from the clay interlayer resulting in crystallisation of the PET in the clay layer with a lamellae thickness of approximately 3.2nm (i.e. three times the c dimension). Due to these inherent difficulties in obtaining PET/clay nanocomposites with a high degree of delamination of clay layers other fillers have been investigated. To this end we have been able to show that the use of single layered uncharged fillers such as nano-silica flakes enables us to neatly avoid the problem of delamination and produce bottles with improved CO_2 barrier. The barrier improvements obtained were less than hoped but we have confirmed that this is due to breakage of the filler in processing and the data adequately fits model predictions indicating exceptional barrier properties could be achieved if the initial platelet size could be retained. In addition we have observed poor properties of DMLP in terms of barrier performance and we can conclude this is due to poor compatibility of the interlayer as thermal stability is excellent. In addition we have also been able to show that DMLP offer excellent potential due to their tendency not to discolour the PET in processing.

Overall these studies have enabled us to gain much greater understanding of the difficulties in using clay/polymer nanotechnology for the enhancement of PET gas barrier properties and provide clear indications of areas for further development in future studies.

9.3 Future work

The work conducted in this study has provided many interesting insights into the mechanisms of clay exfoliation in polyamides and PET. In addition we have been able to learn a great deal about different fillers and how they behave in nanocomposite formation. Despite gaining these new insights many new questions have been raised. To more fully evaluate the effect of polymer polarity on the ability of PA's to exfoliate clay more work is required on different polyamides. To this end an investigation of other aliphatic linear PA's such as PA6,6, PA10 and PA6,10 would prove useful. In addition this would give us further data to compare the effect of aliphatic nature versus aromatic nature and how this influences the delamination of the clays in PA's. In addition, it would be interesting to further evaluate the influence of viscosity on the exfoliation

process, in particular for MXD6 where lower and higher molecular weight material is readily available but as yet untried for nanocomposites formation.

From the perspective of a master-batch approach it has been shown that MXD6 gives the best improvements in gas barrier but the transfer of clay exfoliation to the PET phase has proven problematic and yellowing has been an issue. To improve this situation further work to investigate the synthesis if PET/PA block copolymers for the compatibilisation of PET and MXD6 could be undertaken as this may assist the transfer of the exfoliated clay from the MXD6 phase to the whole polymer matrix. Other experiments worth considering would be to look at the use of stabilisers and antioxidants in order to reduce the discolouration of the blend materials and potential chain extenders in order to reduce the effect of molecular weight loss.

Future work to investigate PET/clay nanocomposites would consist primarily of investigating ways of improving the compatibility of the polymer and clay surface directly. Rather than look at the clay surfactant future work could consist of efforts to directly modify the polymer to increase its polarity. PET ionomers have shown partial success in this area and it is possible that by modifying both clay and polymer with ionomers sufficient compatibility could be achieved to de-laminate clay platelets. Other possible techniques could be to graft highly polar groups onto the backbone chain of PET or to include more polar-co monomers in the polymerisation process.

The final area where further work could significantly contribute to the search for a viable PET monolayer barrier material is in the development of non-clay nanofillers. For nano-silica flakes the potential is clear to see and further work should revolve around the use of low shear mixing processes in order to reduce the breakage of the filler. Such techniques could include polymerisation reactor addition of the nano silica flakes or the use of single screw extrusion to reduce shear in processing. For the DMLP as the interlayer is uncharged the use of phosphonic acids with functional groups such as carboxylic acid or hydroxyl may significantly improve the compatibility with PET and enable improved dispersion of the filler.

10 References

[1] J.R. Whinfield, J.T. Dickinson, UK Patent No. 578079 (1946).

[2] N. Wyeth, A. Roseveare UK Patent No. 1341845-8 (1973).

[3] Anon www.sba-cci.com

[4] W.H. Carothers, J. Am Chem. Soc., 51, 2548, (1929).

[5] W.H. Carothers, J. Am Chem. Soc., 51, 2560, (1929).

[6] W.H Carothers, US Patents No. 2,130,947 and No. 2,130,948 (1938).

[7] P. Schlack, German Patent No. 748253 (1938).

[8] F.G. Lum, E.F. Carlston, J.C. Butler, US Patent No. 2766211 (1956).

[9] E.F. Carlston, F.G. Lam, Ind. Engin. Chem., 49, 1239, (1957).

[10] Anon www.mgc-a.com/Pages/MXD6/hist-mxd6.html.

[11] K. Matsunami, K. Furukawa, K. Hachiboshi, US Patent No. 3847479 (1974).

[12] T. Okudaira, Y. Hama, US Patent No. 4398642 (1983).

[13] M.A Cochran, R. Folland, J.W. Nicholas, M.E.R. Roberts, US Patent No 5021515 (1991)

[14] Y.s.Hu, V. Prattipati, S. Mehta, D.A. Schiraldi, A. Hiltner, E. Baer, Polymer, 46, 2685, (2005).

[15] Y. Liang, Proceedings of 'Nanocomposites 2006', Brussels, Mar 14-15 2006.

[16] J.A. Grande, www.ptonline.com/articles/200508fa1.html

[17] S. Schaaf 'Polyamides – Thermoplastic materials for high-tech applications and modern life', Verlag Moderne Industrie (1997), Ch2.

[18] Technical Data Sheet 'Grivory G21' www.emsgrivory.com

[19] Anon, 'Trogamid materials brochure' www.degussa-hpp.com

[20] H. Ludewig, 'Polyester fibres chemistry and technology', Wiley Interscience, New York (1971)

[21] F. Villain, J. Coudane, M. Vert, J. Appl. Polym. Sci., 52, 55 (1994)

[22] F. Villain, J. Coudane, M. Vert, Polym. Deg. Stab., 43, 431 (1994)

[23] E. Schaaf , H. Zimmerman, W. Dietzel, P Lohmann, Acta Polymerica, 32, 250 (1981)

[24] K. Ravindranath, R.A. Mashelkar, Chem. Eng. Sci., 41, 2197 (1986)

[25] S. Chen, F. Chen, J. Polym. Sci: Part A: Polym. Chem., 25, 533 (1987)

[26] B. Duh, J. Appl. Polym. Sci., 83, 1288 (2002)

[27] E. Marechal, In: S. Fakirov 9editor), Polyesters: synthesis and chemical aspects. Handbook of thermoplastic polyesters, vol. 1. New York: Wiley; 2002. p. 1.

[28] K.M. Jones, 'Plastic South Africa' Presentation given to the Plastic Institute, South Africa, 18, (1992)

[29] C. Bonnebat, G. Roullet, A.J. de Vries, SPE 37th Annual Conference, New Orleans, 273 (1979)

[30] S.A. Jabarin, Polymer Eng. ScL, 24, 376 (1984)

[31] A.B. Thompson, I. Marshall, J. Appl. Chem., 4, 145 (1954)

[32] C.J. Heffelfinger, R.G. Schmidt, Appl. Polymer ScL, 9, 2661 (1965)

[33] C. Bonnebat, J. Beautemps, A.J. de Vries, Polymer ScL, 58, 109 (1977)

[34] S.A.Jabarin, E.A. Lofgren, Polymer Eng. ScL, 26, 620 (1986)

[35] G. Le Bournelle, L. Monnerie, J.P. Jarry, Polymer, 27, 856 (1986)

[36] W. Fuller, A. Mahendrasingen, C. Martin, Polymer, 40, 5553 (2000)

[37] H. Yasuda, Y. Stannett, Polymer ScL, 57, 907 (1962)

[38] Light, R.R. and Seymour, R.W (1982) Polymer Eng. ScL, 22, 857.

[39] L. Monnerie, A.S. Maxwell, F. Laupretre, I.M. Ward, Polymer, 39, 6835 (1998)

[40] M. Zanetti, S. Lomakin, G. Camino, Macromol. Mater. Eng. 279, 1 (2000)

[41] P. Balia, B.K. Samantary, S.K. Srivastana, Mater. Res. Bull, 35, 1717 (2000)

[42] W. Xiao, M. Zahn, Z. Li, Materials and Design, 24, 455 (2003)

[43] W.H. Awad, J.W Gilman, M. Nyden, R.H. Harris, Jr., T.E. Sutto, J. Callahan, P.C. Trulove, H.C. Delong, D.M. Fox, Thermochimica Acta, 409, 3 (2004)

[44] H. He, J. Duchet, J Galy, J.F. Gerard,. J. Colloid and Interface Sci., 288, 171 (2005)

[45] S. Letaief, A.M. Luengo, P. Aranda, E. Ruiz-Hitzky, Adv. Func. Mater., 16, 401 (2006)

[46] L.A.S de a Prado, C.S. Karthikeyan, K. Schulle, S.P. Nunes, I.I. de Torriani, J. Non-cryst. Solids, 351, 970 (2005)

[47] C.W. Francis, Soil Sci., 115, 40 (1973)

[48] P. Aranda, E. Ruiz-Hitzky, Chem. Mater., 4, 1395 (1994)

[49] D. Mason 'New applications for coatings containing glass flakes',

www.ngfeurope.com/docs/european_coatings_show_flake.pdf

[50] Anon, GlassFlake Ltd Technical literature,

www.glassflake.com/pages/Revised%20Glassflake%20Brochure%200308.pdf

[51] P. Franklin, D. J. Wood, N. L. Bubb, Dental Materials, 21, 365 (2005)

[52] Anon, presented at 'Functional fillers', Brussels, Feb 2006

[53] A. Clearfield, Progress in Inorganic Chemistry, 47, 371 (1998)

[54] A.H. Mahmoudkhani, V. Langer, Solid State Science, 3, 519 (2001)

[55] G.B. Hix, K.D.M. Harris, J. of Mat. Chem., 8, 579 (1998)

[56] P. Grebier, C. Guerin, B. Henner, J. Unal, J. of Mat. Chem, 9, 2559 (1999)

[57] J. Wang, Y. Hu, B. Li, Z. Gui, Z. Chen, Ultasonics Sonochemistry, 11, 301 (2004)

[58] H. Sue, K.T. Gam, N. Bestaoui, A. Clearfield, M. Miyamoto, N. Miyatake, Acta Materialia, 52, 2239 (2004)

[59] W.J. Boo, L.Y. Sun, J. Liu, A. Clearfield, H. Sue, M.J. Mullins, H. Pham, Composites Sci. and Tech., 67, 262 (2007)

[60] G. Alberti, M. Casciola, M. Pica, WO Patent No 03/081691 (2003)

[61] M. Rule, WO Patent No 05/111131 (2005)

[62] H. Loye, T. Hansen, J. Stone, B. Zhang, WO Patent No 06/012581 (20060

[63] R. Deguchi, T. Nisho, A. Okado, US Patent 5102948 (1992)

[64] M. McRae, B.R. Christiano, S.N. Murthy, H. Tuller, US Patent 5385776 (1995)

[65] P. Arnada, E. Ruiz-Hitzky, Chem. Mater., 4, 1395 (1992)

[66] D.J. Greenland, J. Colloid Sci., 18, 647 (1963)

[67] C.W. Francis, Soil Sci., 115, 40 (1973)

[68] H.G. Joen, H.T. Jung, S.W. Lee, S.D. Hudson, Polym Bull., 41, 107 (1998)

[69] C. Tseng, J. Wu, H. Lee, F. Chang, Polymer, 42, 10063 (2001)

[70] R. Magaraphan, W. Lilayuthalert, A. Sirivat, J.W. Schwank, Comp. Sci. Tech, 61, 1253 (2001)

[71] S.D. Burnside, E.P. Giannelis, Chem. Mater., 7, 1597 (1995)

[72] A. Usuki, A. Koiwai, Y. Kojima, M. Kawasumi, A. Okada, Y.T. Kurauchi, O. Kamigaito, J. Appl. Polym. Sci., 55, 119 (1995)

[73] M. Kawasumi, M. Hasegawan, A.Usuki, A. Okada, Macromolecules, 30, 6333 (1997)

[74] A. Kiersnowski, J. Piglowski, Eur. Polym. J., 40, 1199 (2004)

[75] L. Biasci, M. Aglietto, G. Ruggeri, F. Ciardelli, Polymer, 35, 3296 (1994)

[76] H.R. Dennis, D.L. Hunter, D. Chang, S. Kim, J.L. White, J.W. Cho, D.R. Paul, Polymer, 42, 9513 (2001)

[77] T.D. Fornes, P.J. Yoon, D.L. Hunter, H. Keskkula, D.R. Paul, Polymer, 42, 9929 (2001)

[78] K. Chavarria, R.K. Shah, D.L. Hunter, D.R. Paul, Polym. Eng. Sci., 47, 1847 (2007)

[79] F. Gao, Materials Today, 7, 50 (2004)

[80] M. Alexandre, P. Dubois, Mater. Sci. Eng. Rep., 28, 1 (2000)

[81] C. Edser, Plastics Additives and Compounding, 4, 30 (2002)

[82] H. Cox et al, presented at: 4th World Congress in Nanocomposites, EMC, San Francisco, 1-3 September (2004)

[83] F. Patterson presented at: 4th World Congress in Nanocomposites, EMC, San Francisco, 1-3 September (2004)

[84] T. Abujoudeh, F. Patterson, presented at Nanocomposites 2004, Brussels, 17-18 March (2004)

[85] C.F. Ou, M.T. Ho, J.R. Lin, J. Polym. Res., 10, 127 (2003)

[86] C.F. Ou, M.T. Ho, J.R. Lin, J. Appl. Polym. Sci., 91, 140 (2004)

[87] G.D. Barber, C.M. Carter, R.B. Moore, ANTEC Vol 3: Special Areas, 301 (2000)

[88] G.D. Barber, R.B. Moore, Polym. Mater. Sci. and Eng., 82, 241 (2000)

[89] C.M. Carter, ANTEC Vol 3: Special Areas, 973 (2001)

[90] J. Chang, D. Park, J. Polym. Sci.: Part B: Polym. Phys., 39, 2581 (2001)#

[91] W. Liu, X. Tian, P. Cui, Y. Li, K. Zheng, Y. Yang, J. Appl. Polym. Sci., 91, 1229 (2004)

[92] W. Hahm, H. Myung, S.S. Im, Macromol. Res., 12, 85 (2004)

[93] J. He, H. Li, X. Wang, Y. Gao, European Polym. J., 42, 1128 (2006)

[94] M.L. Di Lorenzo, M.E. Errico, M. Avella, J. of Mater. Sci., 37, 2351 (2002)

[95] M. Qu, Y. Wang, C. Wang, X. Ge, D. Wang, Q. Zhou, European Polym. J., 41, 2569 (2005)

[96] P. Bhimaraj, D. Burris, W.G. Sawyer, C.G. Toney, R.W. siegel, L.S. Schadler, Wear, 264, 632 (2008)

[97] G. Zhang, T. Shichi, K. Takagi, Materials Letters, 57, 1858 (2003)

[98] Z. Ke, B. Yongping, Materials Letters, 59, 3348 (2005)

[99] Y. Ke, C. Long, Z. Qi, J. of Appl. Polym. Sci., 71, 1139 (1999)

[100] Y. Ke, Z. Yang, C. Zhu, J, J. Appl. Polym. Sci., 85, 2677 (2002)

[101] Y. Imai, S. Nishimura, E. Abe, H. Tateyama, A. Abiko, A. Yamaguchi, T. Aoyama, H. Taguchi, Chem. Mater., 14, 477 (2002)

[102] C. Saujanya, Y. Imai, H. Tateyama, Polymer Bulletin, 51, 85 (2003)

[103] Y. Imai, Y. Inukai, H. Tateyama, Polymer Journal, 35, 230 (2003)

[104] J. Chang, S. Kim, Y. Joo, S. Im, Polymer, 45, 919 (2004)

[105] T. Tsai, C. Hwang, S. Lee, ANTEC Vol 2: Materials, 248 (2000)

[106] T. Tsai, C. Li, C. Chang, W. Cheng, C. Hwang, R. Wu, Adv. Mater. 17, 1769 (2005)

[107] T Tsai, Presented at: Asia PETnology, Shanghai, 30-31st Oct (2006)

[108]S. Kim, S. Park, S-C. Kim, Polymer Bulletin, 53, 285 (2005)

[109] J. Hao, X. Lu, S. Liu, S. Lau, Y. Chua, J. Appl. Polym. Sci., 101, 1057 (2006)

[110] S. Lee, Y. Ma, H. Rhee, J. Kim, Polymer, 46, 2201 (2005)

[111] W. Choi, H. Kim, K. Yoon, O. Kwon, C. Hwang, J. Appl. Polym. Sci., 100, 4875 (2006)

[112] A. Sanchez-Solis, A. Garcia-Rejon, O. Manero, Macromol. Symp. 192, 281 (2003)

[113] L.F. Boesel, L.A. Pessan, J. Meta. and Nanocryst. Mater., 14, 89 (2002)

[114] S. Pendse, A. Ranade, N. D'Souza, J.A. Ratto, ANTEC Vol 2: Materials 2343 (2204)

[115] I.Y. Phang, K.P. Pramoda, T. Liu, C. He, Polym. Int., 53, 1282 (2004)

[116] C.I.W. Calcagno, C.M. Mariani, S.R. Teixeira, R.S. Mauler, Polymer, 48, 966 (2007)

[117] Y. Wang, J. Gao, Y. Ma, U.S. Agarwal, Composites Part B: Eng., 37, 399 (2006)

[118] D.C. McConnel, P.R. Hornsby, C.Y. Lew, E.H. Qua, ANTEC Vol. 3: Special areas, 387 (2006)

[119] S. Pendse, N. D'Souza, J.A. Ratto, ANTEC Vol. 3: Special areas, 3492, (2005)

[120] A. Pegoretti, J. Kolarik, C. Peroni, C. Migliaresi, Polymer, 45, 2751 (2004)

[121] A. Garcia-Rejon, Y. Sinard, C. DeGrandpre, ANTEC Vol 1: Processing, 372 (2001)

[122] L.K. Sahu, N.A. D'Souza, B. Gnade, ANTEC 2006, 1554 (2006)

[123] M.D. Sanchez-Garcia, E. Gimenez, J.M. Lagaron, J. of Plastic Film and Sheeting, 23, 133 (2007)

[124] F. Gao, Z. Han, S. Chen and J.B. Hull, In Proc. Organic-Inorganic Hybrids II, PRA, Guildford, 28-29 May (2002)

[125] J.M. Cervantes-Uc, J.V. Cauich-Rodriguez, H. Vazques-Torres, L.F. Garfias-Mesias, D.R. Paul, Thermochimica Acta, 457, 92 (2007)

[126] C.B. Hedley, G. Yuan, B.K.G. Theng, Appl. Clay. Sci., 35, 180 (2007)

[127] R.D. Davis, J.W. Gilman, T.E. Sutto, J.H. Callahan, P.C. Trulove, H.C. De Long, Clays and Clay Minerals, 52, 171 (2004)

[128] W. Xie, R. Xie, W. Pan, D. Hunter, B. Koene, L. Tan, R. Vaia, Chem. Mater., 14, 4837 (2002)

[129] J. U. Calderon, B. Lennox, M.R. Kamal, Appl. Clay Sci., 40, 90 (2008)

[130] H.A. Patel, R.S. Somani, H.C. Bajaj, R.V. Jasra, Appl. Clay. Sci., 35, 194 (2007)

[131] W.H. Awad, J.W. Gilman, M. Nyden, R.H. Harris, jr., T.E. Sutto, J. Callahan, P.C. Trulove, H.C. Delong, J. of Polym. Sci: Part B: Polym. Phys., 40, 2661 (2002)

[132] C.H. Davis, L.J. Mathias, J.W. Gilman, D.A. Schiraldi, J.R. Shields, P. Trulove, T.E. Sutto, H.C. Delong, J. of Polym. Sci: Part B: Polym. Phys., 40, 2661 (2002)

[133] M.C. Costache, M.J. Heidecker, E. Manias, C.A. Wilkie, Polym. For Adv. Tech., 17, 764 (2006)

[134] K. Stoeffler, P.G. Lafleur, J. Denhault, Polym. Deg. and Stab., 93, 1332 (2008)

[135] M. Lai, K. Chang, W. Huang, S. Hsu, J. Yeh, J. of Phys. And Chem. of Solids, 69, 1371 (2008)

[136] J.W. Chung, S. Son, S. Chun, T.J. Kang, S. Kwak, Polym. Deg. and Stab., 93, 252 (2008)

[137] C. Thellen, C. Orroth, D. Froio, J. Lucciarini, J.A. Ratto, ANTEC Vol 2: Materials, 2130 (2004)

[138] M. Yuan, X. Pan, C. Wan, Polymers and Polymer Composites, 12, 619 (2004)

[139] M. Lai, J. Kim, Polymer, 46, 4722 (2005)

[140] G.D. Barber, S.P. Bellman, R.B. Moore, ANTEC Vol 2: Materials, 1369 (2003)

[141] G.D. Barber, B.H Calhoun, R.B. Moore, Polymer, 46, 6706 (2005)

[142] A. Ammala, C. Bell, K. Dean, Comp. Sci. and Tech., 68, 1328 (2008)

[143] C. Koning, M. Van Duin, C. Pagnoulle, R. Jerome Prog. Polym. Sci., 23, 707 (1998)

[144] C.W. Mackosko, H.K. Jeon, T.R. Hoye, Prog. Polym. Sci., 30, 939 (2005)

[145] L.A. Utracki, 'Commercial Polymer Blends', Chapman and Hall, ch17, 361 (1998)

[146] S. Bandi, S. Mehta, D.A. Schiraldi, A. Hiltner, E. Baer, Polym. Deg. and Stab., 88, 341 (2005)

[147] Y.S. Hu, V. Prattipati, A. Hiltner, E. Baer, S. Mehta, Polymer, 46, 5202 (2005)

[148] A.S. Michaels, H.J. Brixler, J. Polym. Sci, 50, 393 (1961)

[149] A.S. Michaels, W.R. Vieth, J.A. Barrie, J. of Appl. Phys., 34, 1 (1963)

[150] A.S. Michaels, W.R. Vieth, J.A. Barrie, J. of Appl. Phys., 34, 13 (1963)

[151]E.A. McGonigle, J.J. Liggat, R.A. Pethrick, S.D. Jenkins, J.H. Daly, D. Hayward, Polymer, 42, 2413 (2001)

[152] W.R. Vieth, Diffusion in and through polymers: Principles and applications, Munich: Hanser (1990).

[153] L.E. Nielsen, J. Macromol. Sci. (Chem.), A1 (5), 929 (1967)

[154] E.L. Cussler, S.E. Hughes, W.J. Ward III, R. Arris, J. Membr. Sci., 38, 161 (1988)

[155] G.H. Fredrickson, J. Bicerano, J. Chem. Phys., 110, 2181 (1999)

[156] A.A. Gusev, H.R. Lusti, Adv. Mater., 13, 1641 (2001)

[157] R.M. Barrer, J.A. Barrie, N.K. Raman, Polymer, 3, 605 (1962)

[158] R.K. Bharadwaj, Macromolecules, 34, 9189 (2001)

[159] B. Xo, Q. Zheng, Y. Song, Y. Shangguan, Polymer, 47, 2904 (2006)

[160] C. Lu, Y. Mai, Comp. Sci. and Tech., 67, 2895 (2007)

[161] Anon, PET 9221W technical data sheet, www.eastman.com

[162] Anon, MXD6 technical data sheet, www.mgc-a.com/eng

[163] C.M. Hansen, J. Paint Tech., 39, 511 (1967)

[164] N. Kasai, M. Kakudo, X-Ray Diffraction by Macromolecules, Springer/Kodansha Scientific Ltd (2005).

[165] G.W.H. Hohne, W.F. Hemminger, H.-J, Flammersheim, Differential Scanning Calorimetery, Springer (2003)

[166] T.R. Compton, Polymer Reference Book, ChemTec Publishing (2006)

[167] F. Gao, Oral Communication (2004)

[168] T. Jiang, Y. Wang, J. Yeh, Z. Fan, European Polymer Journal, 41, 459 (2005)

[169] K. Bouma, G.M.M Groot, J. Feijen, R.J, Gaymans, Polymer, 41, 2727 (2000)

[170] R. P. Daubeny, C.W. Bunn, Proc. Of the Royal Society A, Mathematical and Physical, 226, 531 (1954)

[171] M. UYokouchi, Y. Sakakibara, YVhakani. H. Tadokoro, T. Tanaka, K. Yado, Macromolecules, 9, 226 (1976)

[172] D. Wu, C. Zhou, Z. Hong, D. Mao, Z. Bian, European Polymer Journal, 41, 2199 (2005)

[173] J. Chang, M.K. Mun, J. Appl. Polym. Sci., 100, 1247 (2001)

[174] J. Xiao, Y. Hu, Z. Wang, Y. Tang, Z. Chen, W. Fan, European Polymer Journal, 41, 1030, (2005)

[175] O. Yoshida, M. Okamoto, J. of Polym. Eng., 26, 919 (2006)

[176] E.P. Giannelis, R. Krishnamoorti, E. Manias, Advances in Polymer Science, 138, 107 (1999)

[177] R.A. Vaia, E.P. Giannelis, Macromolecules, 30, 7990 (1999)

[178] R.A. Vaia, E.P. Giannelis, Macromolecules, 30, 8000 (1999)